Immunité, Immunodéficience et Protéines Membranaires

Franck Fieschi

Mémoire pour l'obtention de l'Habilitation à Diriger des Recherches.

Franck FIESCHI
Maître de Conférence, section 64 du CNU

Membres du Jury

Dr. Jacqueline Cherfils	Rapporteuse
Dr. Fernando Arenzana-Seisdedos	Rapporteur
Pr. Rob Ruigrok	Rapporteur
Pr. Marc Fontecave	Examinateur
Pr. Eva Pebay-Peyroula	Examinatrice

Institut de Biologie Structurale
Laboratoire des protéines membranaires
CEA/CNRS/UJF – UMR 5075

Remerciements

Les travaux présentés dans ce document ont bénéficié de l'environnement de plusieurs laboratoires et de l'interaction avec de nombreux collègues et amis scientifiques. Mes remerciements vont donc en premier lieu à Michel Lepoivre, Marc Fontecave, Britt-Marie Sjöberg et Eva Pebay-Peyroula pour l'accueil qu'ils m'ont fait dans leurs groupes respectifs aux différentes étapes de mon parcours. Doublement merci à Marc, pour le plaisir qu'il me fait en ayant accepté de faire partie de ce jury (*en souvenir du bon vieux temps*).

Je tiens ensuite à remercier chaleureusement Mme Jacqueline Cherfils, ainsi que Mrs Fernando Arenzana-Seisdedos et Rob Ruigrok pour l'honneur qu'ils me font et la confiance qu'ils me témoignent en acceptant de participer à ce jury.

Pour finir, ce travail est le résultat d'efforts en équipe avec de nombreuses personnes qui ont croisé ma route : compagnons d'armes, collaborateurs, étudiants. Sans les nommer tous, qu'ils soient tous assurés de ma profonde gratitude et de mon amitié. Toutefois, je souhaite faire une mention particulière, pour leur rôle, à mes "étudiants, post-docs et compagnons de labo" : Claire, Sylvie, Georges, Laure, Michel, les deux Corinne (H & V), Dominique, et Jacques.

Sommaire

Franck FIESCHI
né le 9 Juillet 1969 (36 ans), à Cannes - France
Français, Marié (à Christelle), 3 enfants (Théotime, Philémon et Fantine)

Adresse professionnelle:
Institut de Biologie Structurale
Laboratoire des Protéines Membranaires (LPM)
41 rue Jules Horowitz
38027 Grenoble Cedex 1
Tel. : (33) (0)4 38 78 91 77/ Fax : (33) (0)4 38 78 54 94
Email : franck.fieschi@ibs.fr

Titres Universitaires

2005 Habilitations à Diriger des Recherches –Université Joseph Fourier

1993-96 **Doctorat de Biologie Cellulaire et Moléculaire,** *mention Trés honorable et les Félicitations du jury* - Université Joseph Fourier, Grenoble - France.

1993 **D.E.A. de biologie cellulaire et moléculaire**, *mention très bien* - Université Joseph Fourier, Grenoble - France.

1991 **Maitrise de Biochimie,** *mention bien* - Université Paris Sud, Orsay - France.

1990 **Licence de Biochimie,** *mention assez bien* - Université Paris Sud, Orsay - France.

1989 **D.E.U.G B**, *mention bien* - Université des Sciences de Caen - France.

Expériences Professionnelles

Déc 97/… **Maître de Conférence** à l'Université Joseph Fourier de Grenoble. Laboratoire des Protéines Membranaires (directeur : Eva Pebay-Peyroula) à l'Institut de Biologie Structurale, CEA-CNRS-UJF (UMR 5075)
Programmes de recherche : Etude structurale du complexe membranaire de la NADPH Oxydase et des récepteurs du virus HIV. Methodologies d'expression de protéines membranaires recombinantes.

1997 **Séjour Post-doctoral dans le laboratoire du Pr. Britt-Marie Sjöberg** (1 an)- Université de Stockholm - Suède. Financement : **Bourse E.M.B.O.** puis **H.F.S.P.**
Programme de recherche : "Functionnal and structural characterization of ribonucleotide reductase from *Corynebacterium ammoniagenes*."

1992-96 **D.E.A. et THESE dans le laboratoire du Pr. Marc Fontecave** (3 ans) - Université Joseph Fourier, Grenoble - France.
Programme de recherche : "Etude structure-fonction de la NAD(P)H:flavine oxydoréductase de *E.coli*."

1990-91 **Stage sous la direction du Dr Michel Lepoivre** (6 mois) - Institut de Biochimie de l'Université Paris Sud, Orsay - France
Programmes de recherche : "Inactivation de la ribonucléotide réductase (RNR) par NO et sélection de cellules adhérentes de souris surexprimant la sous-unité R2 de la RNR."

Résumé de la production et communication scientifique

15 publications dans des revues internationales (**voir détail plus loin**).

4 publications dans des ouvrages et actes de congrès.

12 séminaires et conférences invités (dans des universités, centres de recherches ou colloques).

4 communications orales et **17** posters dans des congrès scientifiques.

Responsabilités universitaires et électives (1998 à 2005)

Correspondant de l'UFR de biologie pour l'antenne universitaire de Valence jusqu'à l'année 2003-2004.

Coordinateur mise en place du L1 dans le cadre de la réforme LMD sur le site de Valence, année 2003-2004.

Responsable de deux à quatre modules d'enseignement de DEUG à Valence (antenne universitaire de l'Univ. Joseph Fourier –Grenoble), de 1998 à 2004.

Participation à des jurys de thèse depuis 2000.

Membre élu de la commission de spécialiste de l'UFR de Biologie (section 64 à 69) de l'UJF de 2000 à 2003

Vice président Rang B de la commission de spécialiste de l'UFR de Biologie (section 64 à 69) de l'UJF depuis 2004

Membre nommé de la commission de spécialiste section 64 de l'Université Claude Bernard de Lyon depuis 2005.

Financements et Responsabilités de recherche

<u>Période Post-doc (1997) :</u>

1997 Obtention d'une Bourse EMBO

1997 Obtention d'une bourse et de subvention fonctionnement + équipement HFSP (Human Frontier Science Project)

<u>Période 1998-2002 (Maître de Conférence):</u>

1998 Subvention d'installation par la FRM (Fondation pour la recherche médicale)

1999 Pilotage de la construction et installation d'un nouveau laboratoire au sein de l'IBS, le LPM : installation d'une activité de Biologie moléculaire-Biochimie des protéines au sein d'un groupe de cristallographie des protéines.

2000 Conseil scientifique et expertise auprès de la start-up grenobloise "Protein eXpert" : réalisation d'une expertise (rédaction d'un rapport) pour Protein eXpert et la cellule UJF-Industrie.

2000 Coopération industrielle avec Roche : évaluation de la technologie RTS

2000 Subvention ANRS : réseau sur "l'étude des co-récepteurs CXCR4 et CCR5) du VIH (Phase 1). (Coordination Hugues Lortat-Jacob, Eva Pebay-Peyroula). Financement pour un CDD Ingénieur : Corinne Vivès.

2000 Subvention de la Ligue contre le cancer (coordinateur Franck Fieschi)

2001 Subvention Ensemble contre le SIDA (coordinateur Franck Fieschi et Anne Imberty)

2001 Bourse post-doctorale ANRS pour Corinne Houlès

2002 Subvention ACI physico-chimie de la matière complexe (coordinateur Laurent Davoust)

2002 Renouvellement bourse post-doctorale ANRS Corinne Houlès

2002 Subvention Ensemble contre le SIDA (coordinateur Franck Fieschi et Anne Imberty)

2003 Subvention ANRS : responsable et coordinateur d'un réseau de laboratoire sur l'étude structurale des co-récepteurs CXCR4 et CCR5 du VIH (Phase 2).
2004 Subvention pour un projet de 3 ans en réseau attribué par la "Bill et Melinda Gates Fondation" suite à un appel d'offres international. (coordinateur Félix Rey) : Programme PDVI (Pediatric Dengue Vaccine Initiative). Financement d'un Post-doc : Michel Thépaut
2005 Programme ANRS : Surexpression et renaturation des co-récepteurs CXCR4 et CCR5 du VIH : coordinateur d'un réseau de 3 laboratoires.

Encadrements scientifiques (jeunes chercheurs) :

Période Post-doc (1997) :

1997 Encadrement d'une étudiante démarrant sa thèse sur mon sujet de stage post-doctoral (pendant 5 mois) (Stockholm University) : Yasmin Huque. (thèse soutenue le 8/6/2001)

Période 1998-2002 (Maître de Conférence):

1998 - Janvier : Participation à l'encadrement d'un étudiant en thèse - **Sylvestre Grizot** (soutenu le 22/06/2001)
- Octobre : Co-direction de thèse - **Massenet Claire** (soutenance décembre 2002)

2000 Encadrement d'une stagiaire post-doctorale (collaboration Hugues Lortat-Jacob, IBS) dans le cadre d'un contrat ANRS : **Corinne Vivès**

2000 Maître de stage d'une étudiante en D.E.A. de Biochimie Structurale et fonctionnelle **: Sylvie Chenavas**.

2001 - Codirection de thèse **: Sylvie Chenavas**.
- Encadrement d'une stagiaire Post-Doctorale (collaboration avec Anne Imberty, CERMAV et Fernando Arenzana, Institut Pasteur) dans le cadre d'un double contrat solidarité SIDA et ANRS : **Corinne Houlès (2 ans)**

2002 Maître de Stage de **Bertrand Arnou**, étudiant en DEA de Biochimie structurale et Fonctionnelle.

2005 Maître de stage de **Georges Tabarani**, étudiant en M2 de Biochimie.

2005 Encadrement d'un Stagiaire Post-doctoral (collaboration réseau "Pediatric Dengue Vaccine Initiative") : **Michel Thépaut**

Publications dans des revues internationales

Parues

P15. Massenet C., Chenavas S., Cohen-Addad C., Dagher M.C., Brandolin, G., Pebay-Peyroula, E. and **Fieschi F**. (**2005**) *J. Biol. Chem.* 2005 280, 13752-13761. ◆

"Effects of p47^{phox} C-terminus phosphorylations on binding interactions with p40phox and p67phox : structural and functional comparison of p40^{phox} and p67^{phox} SH3 domains."

P14. Navarro-Sanchez E., Altmeyer R., Amara A., Schwartz O., **Fieschi F.**, Virelizier JL., Arenzana-Seisdedos F, Despres P. (**2003**) *EMBO Rep*. 2003 4, 723-728.

"Dendritic-cell-specific ICAM3-grabbing non-integrin is essential for the productive infection of human dendritic cells by mosquito-cell-derived dengue viruses."

P13. Lozach P.Y., deLacroix de Lavalette A., Lortat-Jacob H., Staropoli, I., Foung S., Amara A., Houlès C., **Fieschi, F.**, Schwartz, Virelizier, J.L., Arenzana-Seisdedos, F., and Altmeyer R. **(2003)** *J. Biol. Chem.* 278, 20358-66

"High affinity interaction of Hepatitis C virus envelope glycoprotein E2 with C-type lectins L-SIGN and DC-SIGN depends on oligomerisation of the carbohydrate recognition domain"

P12. Halary, F, Amara A, Lortat Jacob H, Messerle, M, Delaunay, T, Houlès, C, **Fieschi, F**, Arenzana-Seisdedos, F, Moreau, JF and Dechanet-Merville, J. **(2002)** *Immunity* 17, 653-654.

"Human cytomegalovirus binding to DC-SIGN is required for dendritic cell infection and target cell trans-infection."

P11. Royant, A, Grizot, S, Kahn, R, Belrhali, H, **Fieschi, F**, Landau, E, and Pebay-Peyroula E **(2002)** *Acta crystallographica D* 58, 784-791.

"Detection and characterisation of merohedral twinning in two protein crystals : bacteriorhodopsin and p67phox"

P10. Grizot S, Fauré J, **Fieschi F**, Vignais, P.V., Dagher MC, Pebay-Peyroula, E **(2001)** *Biochemistry* 40, 10007-13

"Crystal structure of the Rac1-RhoGDI complex involved in NADPH oxidase activation"

P9. Grizot S, **Fieschi F**, Dagher MC, Pebay-Peyroula E. **(2001)** *J Biol Chem.* 276, 21627-21631.

"The active N-terminal region of p67^{phox}: structure at 1.8 Å resolution and biochemical characterizations of the A128V mutant implicated in chronic granulomatous disease. "

P8. Grizot, S, Grandvaux, N, **Fieschi, F,** Fauré, J, Massenet, C, Andrieu, J-P, Fuchs, A, Vignais, P.V., Timmins, P A, Dagher, M-C and Pebay-Peyroula, E **(2001)** *Biochemistry* 40, 3127-33.

"Small angle neutron scattering and gel filtration analyses of the neutrophil NADPH Oxydase cytosolic factors higlights the role of the C-terminal end of p47phox in the association with p40phox"

◆ Cet article a été sélectionné par des membres de l'editorial board de *J.Biol.Chem.* comme "Paper of the Week". Ci dessous un extrait du mail de l'éditeur.

"...The Papers of the Week is a feature of JBC Online. We ask our Editorial Board members and our Associate Editors to select papers that rank in the top 1% of papers they will review in a year in significance and overall importance. We expect that about 50-100 papers will be selected each year from the over 6600 we publish. Once selected, the paper is highlighted in the Table of Contents (TOC) of the issue of JBC Online in which it appears. There is a link from the TOC to a summary that explains why the work was selected for this honor. The paper is also included in a cumulative collection of JBC Papers of the Week that can be accessed directly from the home page of JBC Online. .."

Herbert Tabor, Editor

P7. Huque, Y, **Fieschi, F**, Torrents, E, Gibert, I, Eliasson, R, Reichard, P, Sahlin, M and Sjöberg B-M **(2000)** *J. Biol. Chem.* 275, 25365-25371.
"The active form of the R2F protein of class Ib ribonucleotide reductase from *Corynebacterium ammoniagenes* is a diferric protein"

P6. Nivière, V, **Fieschi, F**, Décout, J-L and Fontecave M. **(1999)** *J. Biol. Chem.* 274, 18252-18260.
"The NAD(P)H :Flavin oxidoreductase from *Escherichia coli* : Evidence for a new mode of binding for reduced pyridine nucleotides"

P5. Fieschi, F, Torrents, E, Toulokhonova, L, Jordan, A, Hellman, U, Gibert, I, Barbe, J., Karlsson, M and Sjöberg, B-M. (**1998**) *J. Biol. Chem.* 273, 4329-4337.
"The Manganese-containing ribonucleotide reductase of *Corynebacterium ammoniagenes* is a class Ib enzyme"

P4. Nivière,V, **Fieschi, F**, Décout, J-L, and Fontecave, M. **(1996)** *J. Biol. Chem.* 271, 16656-16661.
"Is the NAD(P)H : flavin oxidoreductase from *Escherichia coli* a member of the ferredoxin-$NADP^+$ reductase family ? Evidence for the catalytic role of serine 49 residue."

P3. Fieschi, F, Nivière, V, and Fontecave, M. **(1996)** *Eur. J. Biochem* 237, 870-875.
"Cys-5 and Cys-214 of NAD(P)H:flavin reductase from *Escherichia coli* are located in the active site"

P2. Fieschi, F, Nivière, V, Frier, C, Décout, J-L, and Fontecave, M. **(1995)** *J. Biol. Chem.* 270, 30392-30400.
"Mechanism and substrate specificity of the NAD(P)H:flavin oxidoreductase of *Escherichia coli* "

P1. Lepoivre, M, **Fieschi, F**, Covès, J, Thelander, L, and Fontecave, M. **(1991)** *Biochem. Biophys. Res. Comm.* 179, 442-448.
"Inactivation of ribonucleotide reductase by nitric oxide"

Soumises

P16. Chenavas, S, Simorre, JP, Dubosclard, V, Pebay-Peyroula, E, Gans, P, Brutscher, B, and **Fieschi, F**. **(2005)** Submitted to *Febs Journal*
"NMR characterization of free and complexed $p67^{phox}$ and $p40^{phox}$ PB1 domains in solution"

P17. Tabarani, G, Reina, J. J., Vivès, C., Lortat-Jacob, H., Rojo, J., and **Fieschi, F. (2005)** Submitted to *Angewandte Chemie*.
" Mannose Hyperbranched Dendritic Polymers Interact with Clustered Organization of DC-SIGN and Inhibit gp120 Binding"

En préparation

P18. Durand, D, Cannella, D, Dubosclard, V, Pebay-Peyroula, E, Vachette, P, and **Fieschi, F. (2005).**
"The auto-inhibitory state of $p47^{phox}$ highlighted by small angle X-ray scattering."

P19. Li, XJ, Paclet, MH, **Fieschi, F,** Grunwald, D, Campion, Y, Morel, F and Stasia, MJ (**2005**)
"Leu505 of neutrophil Nox2 is crucial in the NADPH binding process during NADPH oxidase activation"

Publications dans des ouvrages et actes de congrès.

PO4. Chenavas, S, Brutscher B, Gans, P, JP Simorre, Pebay-Peyroula, E and **Fieschi F. (2004)** In Congrès international de Biochimie, Marrakech, Maroc 3-6 Mai. p 118-122.
"Etude structurale en solution du complexe $PB1^{p67phox}$/$PB1^{p40phox}$ de la NADPH oxidase".

PO3. Nivière, V, Fontecave, M, Vanoni, M, **Fieschi, F.(1999)** In : "Flavins and flavoproteins 1999", Editors : S. Ghisla, P. Kronek, P. Macheroux, H. Sund. Rudolf Weber agencies for scientific publication, Berlin 1999, p 289-292
" Flavin reductase Fre from *Escherichia coli* : Identification of reaction Intermediates and Evidence for a new mode of Binding for Reduced Pyridine Nucleotides."

PO2. Nivière, V, **Fieschi, F**, Frier, C., Décout, J-L, and Fontecave, M. **(1996)** In : "Flavins and Flavoproteins 1996", Editors : Stevenson, K. J., Massey, V., and Williams, C. H. Jr. University of Calgary press. In press.
"Is the NAD(P)H:flavin oxydoreductase a member of the ferredoxin-NADP+ reductase family ? Identification of residues essentials for substrate binding and catalysis."

PO1. Lepoivre, M, **Fieschi, F**, Covès, J, and Fontecave, M. **(1992)** In : "The Biology of Nitric Oxide" - Enzymology, Biochemistry and Immunology -. Editeurs : Moncada, S., Marletta, M.A., Hibbs, J.B., Higgs, E.A., Portland Press, London and Chapel Hill, vol. 2, 95-98
"Inhibition of ribonucleotide reductase by nitric oxide donors"

Conférences et Séminaires sur Invitation

C12. "DC-SIGN : a break in the wall (of the immune system)"
22 avril 2005, Instituto de Investigaciones Quimicas, CSIC, Sevilla - Spain

C11. **<u>Conférence pleinière d'ouverture</u>** des $4^{ème}$ rencontres francophones "NADPH Oxydases".[1]
"Assemblage et activation de la NADPH oxydase des neutrophiles : une perspective structurale"
17 Mars 2005, $4^{ème}$ Rencontre Francophone "NADPH oxydases".CRSSA, La Tronche - France

C10. "Récepteurs du VIH : Approches méthodologiques de l'expression vers la caractérisation fonctionnelle"
2 juin 2004, Invitation pour un séminaire à la Faculté de pharmacie, Meylan –France

C9. " Structure cristallographique du complexe SH3$p40^{phox}$/$p47^{phox}$C-ter"
Mai 2003, 3ème rencontre Francophone de la NADPH oxidase, Institut Albert Bonniot, Grenoble – France

C8. "Etude structurale et fonctionnelle du complexe de la NADPH oxydase des neutrophiles"
Décembre 2002, Journée Recherche de l'UFR de Biologie de l'Univ. Joseph Fourier, Grenoble - France

C7. "Etude structurale et fonctionnelle du complexe de la NADPH oxydase des neutrophiles"
Novembre 2002, Conférence dans le cadre des séminaires hebdomadaires de l'IBS, Grenoble – France.

---

[1] Ces rencontres ont à leur début concerné les groupes grenoblois uniquement. Leur intérêt et succès n'a fait que croître. Le "club oxydase" est passé de régional à national puis depuis la troisième fois est devenu les "rencontres francophones NADPH oxydases" rassemblant des groupes Français, Suisses, Luxembourgeois et Belges. Depuis le début, ce congrès a été organisés sur Grenoble pour des raisons historiques (grâce à l'énergie de Mme le Pr. F. Morel). Lors de la dernière édition, des Anglais et américains sont venus assistés à ce congrès francophone qui a compté une centaine de participants.

C6. "Expression de facteurs cytosoliques de la NADPH Oxydase**"**
Décembre 2001, First RTS-Roche meeting, Institut Pasteur, Paris – France

C5. "La synthèse de protéine sans cellules : une première évaluation du 'Rapid Translation System'.**"**
Novembre 2001, Invitation pour un séminaire au CERMO, Université Joseph Fourier, Grenoble –France

C4. "Etude structurale de p67phox"
Septembre 2001, 2ème réunion du Club NADPH oxydase, IBS, Grenoble - France

C3. "Les relations structure-fonction dans le complexe de la NADPH oxydase. Approche cristallographique"
Janvier 1998, Séminaire CERLIB (comité d'étude des radicaux libres), Institut Albert Bonniot, Grenoble – France

C2. "Structure-function study of the NAD(P)H:flavin oxidoreductase from *Escherichia coli* "
May 97, Department of Molecular Biology, Stockholm University – Suède.

C1. "Structure-function study of the NAD(P)H:flavin oxidoreductase from *Escherichia coli* : prototype of a new class of flavin dependent enzymes"
Septembre 96, Séminaire donné au Bijvoet Center, Utrecht University - Pays bas.

Communications orales

CO4. "The NADPH Oxydase : Stratégie pour l'étude structurale d'un complexe membranaire"
Novembre 1999, Journée CEA "Structure et fonction des membranes biologiques", Sassenage – France**.**

CO3. " The NADPH oxydase complex : a structural approach to unravel the process"
Juin 1998, EMBO course " Current Methods in Membrane Protein Research ", EMBL, Heidelberg – Allemagne.

CO2. "La NAD(P)H:flavine oxydoréductase de *E.coli* : une dérive des flavoprotéines à FAD ? Les réponses apportées par la mutagénèse dirigée et les études cinétiques."
Juillet 1995, XXIIème Forum des jeunes chercheurs de la Société Francaise de Biochimie et Biologie Moléculaire, Grenoble - France.

CO1. "La NAD(P)H:flavine oxydoréductase de *Escherichia coli* : caractérisation du site flavinique."
Mai 1995, XIème Rencontre Interdisciplinaire de Biochimie, Saint-Agnan - France.

Communications par affiches

CA18. "Optimisation of HIV co-receptor expression"26 june-1 july 29th 2004. FEBS Congress. Warsaw, Poland
Vives, C, Mouillac, B, Baneres, JL, Pebay-Peyroula E, et **Fieschi F.**

CA17. "Characterisations of viral glycoproteins - DC-SIGN interactions : defining the importance of the DC-SIGN oligomerisation domain" 6-11 July 2003. 12th European Carbohydrate Symposium, Grenoble – France.
Houles, C, Lortat-Jacob, H., Imberty, A., **Fieschi, F.**

CA16. "Structural studies of cytosolic factors of the NADPH oxidase". 30 avril - 3 Mai 2002, 1st International Conference on NADPH Oxidases, Rauischholzhausen Castle, Germany

Grizot S, Massenet C, Cohen Addad C, Dagher MC, **Fieschi F**, Pebay-Peyroula E.

CA15. " Expression of cytosolic factors of the NADPH Oxidase complex using the Rapid Translation System : a prospective approach to the direct synthesis of a protein complex". 20 décembre 2001, First RTS meeting, Institut Pasteur, Paris - France
Ayala, I, Chenavas, S, Courtial, S, **Fieschi, F**

CA14. "Expression of cytosolic factors of the NADPH Oxidase complex using the Rapid Translation System", 11-14 avril 2000, Analytica 2000 (congrés pour l'analyse, la biotechnologie et les techniques de laboratoires), Munich - Allemagne
Ayala, I, Pebay-Peyroula, E, **Fieschi, F**

CA13. "The NADPH : oxydase complex. Alternatives to the cristallization of modular proteins", 21 Février-1 Avril 2000, 10ème session de HERCULES "Neutron and synchrotron radiation for biomolecular structure and dynamics", Grenoble – France.
Massenet, C, **Fieschi, F**, Pebay-Peyroula, E.

CA12. "Flavin reductase of Escherichia coli. Structure-Activities Studies.", 29Août- 4 Septembre 99, 13th International Congress Flavins and Flavoproteins, Konstanz – Allemagne.
Nivière V, Vanoni M A, **Fieschi F**, Fontecave M

CA11. "The metal cofactor in the classIb RNR from Corynebacterium ammoniagenes", 11-16 juillet 99, "9th International Conference on Biological Inorganic Chemistry (IBIC 9), Minneapolis, Minnesota – USA.
Huque Y, **Fieschi F**, Torrents E, Eliasson R, Reichard P, Sahlin M and Sjöberg BM

CA10. "Characterisation of the metal cofactor in the Class Ib Ribonucleotide Reductase from Corynebacterium ammoniagenes", 8-12 mai 99, Chemistry of metals in biological systems, Tomar – Portugal.
Huque Y, **Fieschi F**, Torrents E, Eliasson R, Reichard P, Sahlin M and Sjöberg BM

CA9. "The NADPH : oxydase complex ", 21 Février-1 Avril 99, 9ème session de HERCULES "Neutron and synchrotron radiation for biomolecular structure and dynamics", Grenoble – France.
Grizot S, **Fieschi, F**, Pebay-Peyroula, E.

CA8. " Characterisation of the manganese containing Class Ib Ribonucleotide Reductase from Corynebacterium ammoniagenes", 6-19 juillet 98, école d'été "spectroscopy and engineering of metalloproteins" at "Fourth European Biological Inorganic Chemistry Conference (EUROBICS 4)", Oeiras – Portugal.
Huque Y, **Fieschi F**, Sahlin M and Sjöberg BM

CA7. "The ribonucleotide reductase of *Corynebacterium ammoniagenes* is related to the class Ib type of ribonucleotide reductases", 28 Aout - 2 Septembre 97, 46ème Harden Conference "Structure and Mechanism of Oxidases and Related Systems", Plymouth - Angleterre.
Fieschi, F, Torrents, E, Toulokhonova, L, Jordan, A, Hellman, U, Gibert, I, Karlsson, M and Sjöberg, BM

CA6. "Flavin reductase of *Escherichia coli* : Identification of essential residues involved in flavin binding and catalysis", 30 Juin - 6 Juillet 96, 12th International Symposium on Flavins and Flavoproteins, Calgary - Alberta - Canada
Nivière, V, **Fieschi, F**, Décout, J-L, Frier, C, Fontecave, M.

CA5. "Réactivation de la ribonucléotide reductase : études structure function de la NAD(P)H:flavine oxydoréductase of *E.coli*", 27-29 Mars 96, 3ème rencontre du GDR Metalloprotéines et analogues synthetiques, Giens - France.
Nivière, V, **Fieschi, F**, Fontecave, M.

CA4. "Synthesis and study of enzymatically activable antisense or antigene oligonucleotide-flavin conjugates", 11-14 Septembre 95, NATO Workshop : "DNA cleavers and chemotherapy of cancer or viral diseases", Toulouse - France.
Frier, C, **Fieschi, F**, Décout, J.L., and Fontecave, M.

CA3. "Oligonucléotides activables enzymatiquement et capables de générer des radicaux oxygénés :une nouvelle stratégie pour la coupure d'ADN et la thérapie antisens.", Juin 95, 4ème Journée CRSSA-CERLIB "Nitric oxyde and others free radicals", Grenoble - France.
Frier, C, **Fieschi, F**, Decout, J.L., and Fontecave, M.

CA2. "Flavin reductase of *E.coli* : Identification of essential residues involved in flavin binding and catalysis.", Mai 95, First european symposium of the Protein Society, Davos - Suisse.
Nivière, V, **Fieschi, F**, and Fontecave, M.

CA1. "Synthesis of enzymatically activable antisense oligonucleotides tethered to the flavin ring.", Avril 95, International conference "Therapeutic Oligonucleotides from Cell to Man", Seillac - France.
Frier, C, **Fieschi, F**, Décout, J-L, Niviere, V, and Fontecave, M.

Collaborations Scientifiques

Collaborations transversales à mes différents projets :

Hugues Lortat-Jacob
LEM-GAG, IBS
Grenoble

Patrice Vachette et Dominique Durand,
Université Paris XI,
Orsay.

Projet NADPH Oxydase :

Marie-Claire Dagher
BBSI-DRDC
CEA, Grenoble

Françoise Morel et Marie Jose Stasia
GREPI, CHU-Michalon
LaTronche

Bernhardt Brutscher
LRMN-IBS
Grenoble

Jan Willew de Gier
Svante Arrhenius lab, Biochemistry dept,
Stockholm, Sweden.

Projet co-récepteur, CXCR4 et CCR5, du VIH :

Fernando Arenzana-Seisdedos
Institut Pasteur
Paris

Françoise Baleux
Institut Pasteur
Paris

Jean-Louis Banères
Montpellier

Bernard Mouillac
Montpellier

Projets Lectine de type C des cellules dendritiques :

Anne Imberty
CERMAV
Grenoble

Javier Rojo
Instituto de Investigaciones Quimicas-CSIC
Sevilla – Spain.

Le Réseau Dengue :
Les groupes de Félix Rey, Fernando Arenzana-Seisdeidos et Philippe Després (Institut Pasteur)

Formation professionnelle

1. Currents Methods in Membrane Protein Resarch.
   Embo Practical Course, June 17-26, 1998. Heidelberg, Allemagne.

2. Biacore Basics.
   Biacore International SA training organism, 21-22 Octobre 2004, Paris

3. Kinetics and Affinity Analysis using Biacore, Level I.
   Biacore International SA training organism, 23 Mars 2005, Paris

4. Kinetics and Affinity Analysis using Biacore, Level II
   Biacore International SA training organism, 24 Mars 2005, Paris

Activités d'enseignement

Malgré l'objectif très "recherche" d'un mémoire d'HDR, je me permets de prendre le temps de présenter mes activités d'enseignement. En tant que Maître de Conférence, celles-ci activité sont indissociables de ma vie de chercheur. Il est donc, de mon point de vue, important que l'évaluation du dossier recherche d'un maître de conférence se fasse à la lumière de la connaissance de l'importance de cette composante. Elle est forcément à l'origine d'une dispersion et de dossier scientifique, comparativement à celui d'un agent CNRS, forcément moins étoffé.

Service d'enseignement :

Le service plein d'un maître de conférence est de 192 h équivalent TD par an.
Voici un récapitulatif des heures effectuées sur les huit années écoulées à ce poste. Sur **8 ans** je n'ai qu'un déficit de **12 h.** Ceci correspondant simplement à un écart classique obtenu du fait des contingences horaires sur une année. J'ai donc parfaitement rempli les obligations d'enseignements demandées. Les enseignements dispensés l'ont été sous forme de Cours Magistraux, TD et TP, et cela au niveau des 1er, 2ème, 3ème et 4ème années de cycle universitaire.

Année scolaire	Service effectué en eq TD	Service en heures réelles (h Cours +h Td + h TP)
1997-1998	174	226
1998-1999	215	246
1999-2000	159	206
2000-2001	237	263
2001-2002	185	230
2002-2003	172	215
2003-2004	174	203
2004-2005	16 h (année de délégation)	16 h
	Total effectué : **1316 h eq TD**	Total : **1605 h réel**
	Total à faire : **1344 h**	
	Déficit sur 8 ans : **12 h**	

Investissement et réalisations pédagogiques à l'UJF – Grenoble 1.

Outre des responsabilités universitaires énoncées en page 2 (*correspondant UFR à Valence, vice-président de la commission de spécialistes et responsabilité de 2 modules de DEUG première année*). Je me suis investi ponctuellement dans divers projets pédagogiques qui ont demandé un investissement en temps additionnel à celui normalement consacré pour effectuer le service normal d'un maître de conférence. Ces différents points sont détaillés ci-dessous.

1. Mise en place du module DEB (année 99-00)

Sous la direction de Jean-Gabriel Valay, initiateur du projet (MCF en génétique à l'UJF et maintenant Directeur de l'UFR de Biologie), *j'ai participé au montage d'un module de TP innovant de 150 heures pour les Maîtrises de Biochimie et de Biologie Cellulaire-Physiologie*. Ce module, nommé DEB pour Démarche Expérimentale en Biologie, est centré sur l'étude du stress oxydant conduit les étudiants, au travers d'un travail personnel et de séances de tutorat, à élaborer les expériences qu'ils mènent ensuite pendant 3 semaines de TP, ceci au travers de 4 approches : génétique, physiologie, biochimie et biologie cellulaire. En tant que biochimiste, *j'ai mis au point et testé, avec Hélène Jouve, les différentes expériences de Biochimie "envisageables" et/ou "proposées" pour les étudiants. Nous avons également rédigé la partie Biochimie du polycopié destiné aux étudiants ainsi qu'un polycopié Biochimie destiné aux autres enseignants non biochimistes du module.*

2. Développement d'un document pédagogique multimédia pour le DEUG : "Introduction à la Biologie Structurale".

Sous ma direction, un moniteur de 3ème année, Gurvan Michel, s'est attaqué à la construction d'un site : "Introduction à la biologie structurale". Appréhender le repliement tridimensionnel d'une protéine et les interactions dans l'espace entre les acides aminés qui la composent n'est pas facile pour les étudiants de premier cycle. Au travers de ce site, les étudiants peuvent visualiser et faire tourner les molécules à l'écran, choisir les modes de représentation (représentation éclatée ou compacte, boules et tiges ou structure secondaire, etc…) et peuvent ainsi se bâtir une représentation plus juste de l'organisation des protéines dans l'espace**.** *Ce site a été installé sur les machines dans les salles informatiques libres services, accessibles pour les étudiants. Il est utilisé pour des manipulations de molécules dans certains enseignements de Biochimie.*

3. Création d'un nouveau module d'option libre en DEUG, "Initiation à la Biologie Structurale" avec le Pr Marc Jamin (en 2001)

Les TD de ce module utilisent comme outil et source d'exercices le site multimédia mentionné ci-dessus. De plus, des cours de présentation générale des techniques de la biologie structurale ont été mis en place, ainsi que des visites des différents sites technologiques grenoblois importants dans ce champ disciplinaire (ESRF, ILL, EMBL et Albert Bonniot).

Dans le cadre de la réforme LMD, ce module a disparu en tant que tel mais à servi de base pour le nouveau module de L3 qui porte le même nom "Initiation à la Biologie Structurale".

4. J'ai été tuteur de deux moniteurs en thèse : Christophe Desprez et Cécile Dahout.

5. Participation à l'animation d'expositions et d'ateliers scientifiques ouvert au public au Muséum d'Histoire Naturelle de Grenoble ou place Victor Hugo à l'occasion de la semaine "Science en fête" (en 98 et 99 et 2003).

Préambule

Dans ce document présenté en vue de l'obtention de l'habilitation à diriger des recherches, je rappellerai l'historique de mon parcours scientifique et le contexte de mon arrivée au sein du groupe qui m'héberge toujours actuellement, celui fédéré par Eva Pebay Peyroula au sein de l'IBS. Dans cette unique partie, je me laisserai aller à un style plus personnel, notamment en mettant en lumière l'état d'esprit dans lequel j'ai traversé ces années. Je profiterai de ce cadre aussi pour remercier ou rendre hommage aux personnes qui ont jalonné ce parcours.

Puis j'aborderai la partie recherche proprement dite. L'objectif de l'HDR est d'évaluer la capacité de l'impétrant à diriger des recherches, ce que l'on pourrait tenter de définir, au delà de qualités scientifiques nécessaires pour tout chercheur, par l'acquisition de certaines, voire l'ensemble, des compétences suivantes : la recherche de financement, la mise en place de projet, l'encadrement d'étudiants, la gestion de collaborations, la capacité à faire vivre des sujets au sein d'un laboratoire et à s'intégrer dans une logique de groupe. Ainsi, dans ce document, je prendrai le parti de ne pas rédiger une deuxième thèse accumulant une description dans le détail des résultats obtenus au cours de mon activité, mais plutôt un document où l'ensemble des travaux que j'ai réalisés, encadrés, ou auxquels j'ai collaboré seront répertoriés.

Cette présentation sera découpée en chapitres thématiques correspondant aux différents sujets dont j'ai la responsabilité scientifique. Chaque partie présentera de manière aussi brève que possible le contexte biologique de l'étude et définira les objectifs poursuivis, de manière générale pour le thème. En général, les travaux réalisés ne seront pas développés mais seront illustrés ensuite par les publications (introduites par un court résumé). Certaines, plus importantes à mes yeux, seront mises en avant par la présentation de l'article intégral correspondant. Les autres seront simplement rappelées par la première page, contenant "l'abstract" des articles (afin de ne pas alourdir ce document). Les travaux non encore publiés, soumis et en préparation (quand une version presque finalisée est disponible) seront, eux, systématiquement présentées en intégralité du fait de leur non-accessibilité dans les bases de données bibliographiques.

Après une courte introduction générale, un premier chapitre sera consacré au système d'étude sur lequel j'ai le plus travaillé depuis mon arrivée au sein du groupe (8 ans), le complexe de la NADPH oxydase.

Dans une deuxième partie, je présenterai les deux projets que j'ai démarrés plus récemment au sein du laboratoire (4 ans) et qui vont représenter les deux axes principaux de mon investissement dans les prochaines années. Ces deux projets touchent, notamment, à l'infection au VIH et plus particulièrement à la caractérisation structurale et fonctionnelle des récepteurs membranaires impliqués dans la reconnaissance du virus à différentes étapes du processus d'infection. Ce sont, d'une part, les co-récepteurs CXCR4 et CCR5 indispensables dans le processus d'infection des lymphocytes T, et d'autre part, les récepteurs lectiniques DC-SIGN et Langerine, des cellules dendritiques, impliqués dans la dissémination et le convoyage du virus vers les organes lymphoïdes.

Pour finir, dans un troisième chapitre, je rappellerai très brièvement les autres sujets d'études sur lesquels j'ai été amené à travailler au cours de ma courte carrière, c'est-à-dire mes sujets de stage post-doctoral, de thèse et de second cycle universitaire.

Historique d'un parcours.
(pour le plaisir des souvenirs)

Itinéraire d'un enfant gâté.

Une des joies de ma fonction est d'être constamment confronté à des étudiants. Dans le contexte de la 4e année universitaire (dorénavant nommée Master 1), on peut être amené à vivre, à leur contact, les moments initiaux qui vont décider d'un choix de carrière : l'angoisse de la recherche du premier stage en labo et parfois l'exaltation, consécutive à cette première expérience, et la naissance d'une passion que l'on voit briller dans le regard de certains étudiants.

Pour moi, comme pour d'autres, c'est ainsi que commença mon parcours. Après ce que l'on appelait encore un DEUG B dans un passé pas si vieux, mais qui prend déjà des accents poussiéreux, c'est en licence à Paris XI que j'ai pu avoir ma première expérience de recherche dans le cadre d'un stage d'été au sein du groupe du Dr. MICHEL LEPOIVRE. Au cours de ces deux mois, dont le thème était l'étude de l'inactivation de la ribonucléotide réductase par l'oxyde nitrique, le goût pour les métiers de la recherche s'est imposé à moi avec force. C'est donc tout naturellement que j'ai poursuivi cette expérience de labo en maîtrise, aux côtés de Michel Lepoivre. Je veux profiter de l'occasion qui m'est donnée ici pour rendre hommage à Michel qui a su en ces moments particuliers de ma jeune vie d'adulte, à la lisière des choix d'une vie, me transmettre son goût du travail expérimental et d'une certaine rigueur scientifique. Ces deux périodes de stages (6 mois au total) ont contribué très modestement à un travail, à l'époque en collaboration, avec un Professeur de chimie fraîchement nommé au LEDSS à Grenoble. À ma grande surprise, je fus alors associé comme auteur au sein d'un article issu de ce travail. Ceci fut pour moi le plus grand élan qui me fut donné au cours de ma vie et qui m'a poussé jusqu'ici.

Après un service militaire musclé, s'est posée la question du stage de DEA. À l'époque je fus tiraillé par un choix difficile pour un jeune homme passionné d'une part, et amoureux de l'autre. D'un côté, le laboratoire de Michel Lepoivre m'ouvrait ses portes en DEA à Paris XI, de l'autre celle qui allait devenir ma femme avait quitté Orsay (et Paris XI) pour l'INPG à Grenoble. Finalement, le nom du co-auteur du premier article auquel j'étais associé devint pour moi une évidence, "MARC FONTECAVE professeur à Grenoble". C'est ce choix confortable qui m'a conduit à contacter Marc sans me poser la moindre question sur la qualité de ce choix (ou presque), je ne savais rien sur lui et son groupe[2]. Il s'est avéré par la suite que j'avais une fois de plus beaucoup de chance. C'est ainsi, que de Octobre 92 à Octobre 96, j'ai fait mon DEA et ma thèse chez Marc, au LEDSS, sous la direction de Vincent Nivière. J'y ai étudié le mécanisme enzymatique et mené une caractérisation structurale et fonctionnelle d'une flavine réductase impliquée, entre autres choses, dans l'activation de la ribonucléotide réductase et le métabolisme du Fer. Sous la direction conjointe de Vincent et de Marc, j'ai acquis ce qui représente une part importante de mes compétences actuelles : la biochimie, l'enzymologie, l'ingénierie des protéines, et un goût pour les interfaces disciplinaires. En effet, la thèse dans cet environnement pluridisciplinaire rassemblant des biochimistes, biologistes moléculaires, chimistes organiciens et inorganiciens fut une période d'échanges et d'enrichissement intenses. Toutes ces spécialités rassemblées dans un groupe, tout jeune à l'époque, a conduit à une ambiance de travail extraordinaire, stimulante et inoubliable. Les souvenirs de cette période sont joyeux et chaleureux.

[2] Si ce n'est que Michel Lepoivre le tenait en haute estime (c'était plutôt bon signe).

En janvier 97, je suis ensuite parti en Stage Post-Doctoral en Suède chez BRITT-MARIE SJÖBERG pour approfondir mes compétences en biologie moléculaire et aborder l'étude d'une ribonucléotide réductase supposée jusqu'alors d'une nouvelle classe fonctionnelle (avec un centre métallique à Manganèse). Une dizaine de jours avant mon départ pour Stockholm, un coup de fil de Marc m'a alerté de la publication des postes de MCF à Grenoble en attirant mon attention sur un profil de recherche pouvant être en très bonne adéquation avec le mien. Sur ses conseils et malgré la jeunesse de mon dossier d'alors (à 15 jours du début de mon post doc.), j'ai candidaté sur ce poste de "Biochimiste-Biologiste moléculaire avec une expérience des flavoprotéines et interessé par les approches structurales". Ce poste était affiché chez EVA PEBAY-PEYROULA, un nom qu'à l'époque (j'ose le dire) je n'avais jamais entendu[3] (chose totalement improbable aujourd'hui à Grenoble). J'ai donc démarré mon post-doc en Janvier en plein concours MCF avec, au bout de mes 15 premiers jours à Stockholm, un aller retour Suède-France pour les auditions. Le concours passé, j'ai pu pleinement m'investir dans mon stage postdoral. Une fois de plus, je suis arrivé dans un environnement privilégié, un laboratoire où les nationalités étaient multiples (francais, indien, allemand, russe, américain, suèdois,…) et dans une ville à la luminosité magique, Stockholm, où les scientifiques étrangers sont soignés au petit oignons. Ce séjour postdoctoral en Suède représente, pour moi et mon épouse, une sorte de parenthèse enchantée. Tout s'est orchestré de manière parfaite : un support financier exemplaire[4], la naissance de notre fils ainé, des relations humaines de grandes qualités, un dépaysement total, et un sujet ou tout fonctionnait à merveille. Enfin, conduire son travail post-doctoral en se sachant classé premier à un concours MCF est sans doute la cerise sur le gâteau à l'origine de ce sentiment de félicité. Il fut presque dur de penser au retour au bout de seulement 11 mois de post-doc (reprise en décembre et non pas en octobre après arrangement avec l'UJF et Eva pour ma prise de fonction). Ce séjour aura, malgré sa brièveté, permis d'aboutir à deux publications dans *J. Biol. Chem* avec réception de la lettre d'acceptation du premier article pour mon dernier jour de labo. La boucle fut bouclée avec ce final inespéré tel qu'on oserait en rêver sans y croire.

Mon arrivée dans le groupe d'Eva, en décembre 97, est évidemment un tournant majeur dans mon parcours. Tout d'abord bien sûr le statut de maître de conférence a apporté un changement important. Il a fallu apprendre à intégrer à mon activité recherche, outre l'enseignement, toutes les responsabilités qui vont avec et l'investissement nécessaires dans la communauté universitaire pour que vive et fonctionne les institutions. Lors de ma prise de fonction à l'IBS, Eva n'avait pas encore son propre groupe. Elle venait d'être nommée à l'Institut Universitaire de France et représentait l'émergence d'un sous-groupe au sein d'un laboratoire plus vaste, le LCM, dirigée par Otto Dideberg. Autour d'Eva, un petit noyau de personnes, Claudine Cohen-Addad et Valérie Biou, toutes deux chercheuses CNRS. Dans cette petite communauté de femmes physiciennes (où soufflait parfois une brise revendicatrice), j'étais donc le premier et seul biologiste. À cela, il faut tout de même ajouter deux étudiants, qui démarraient leur thèse avec Eva, mais qui étaient externalisés dans d'autres laboratoires grenoblois pour des raisons de place et d'équipements. Après avoir dû évoluer à l'interface Chimie-Biologie durant ma thèse, l'interface Physique-Biologie devait devenir mon quotidien. Eva m'a tout de suite témoigné une confiance et une liberté tout à fait étonnantes envers un si jeune maître de conférence (28 ans à l'époque). J'ai d'abord eu la

[3] Dans mon questionnement sur la pertinence de ma candidature, je me souviens avoir demandé à Marc, en parlant du groupe d'Eva, "Est ce que c'est un bon groupe ? Scientifiquement et humainement est-ce quelqu'un de bien ?". Marc m'avait répondu avec la précision et la concision dont il est capable: "c'est ce qui se fait de mieux"

[4] J'ai obtenu coup sur coup deux bourses internationales : un financement EMBO que j'ai abandonné au bout de trois mois pour un financement Human Frontier Science Project bien plus juteux.

charge de mettre en place une activité de Biologie moléculaire et de Biochimie au sein du groupe et, pour cela, la tâche de faire mes premières demande de fonds, de subventions. D'un point de vue scientifique, je me suis vu engagé sur la partie membranaire de la NADPH Oxydase puis, ensuite, également sur les facteurs cytosoliques. L'installation de la biologie moléculaire et des outils nécessaires à la purification des protéines a permis le retour de Sylvestre Grizot, un des thésards jusqu'alors "exilé" au BBSI, chez nos collaborateurs sur le projet "Oxydase". À cette occasion j'ai pu, au côté d'Eva, participer à l'encadrement de cet étudiant tout à fait exceptionnel. J'ai eu ensuite l'opportunité de pouvoir co-diriger de manière officielle ma première étudiante en thèse, Claire Massenet, sur les facteurs cytosoliques $p40^{phox}$ et $p47^{phox}$.

Puis un nouveau challenge et un nouveau cadeau s'est présenté à nous (année 1999, encore Bravo Eva). Nous avions la possibilité d'aménager le fond de l'aile 3 de l'IBS (qui servait de vaste grenier où tous les groupes de l'Institut entassaient leurs cadavres…) pour en faire un labo tout neuf pour notre futur groupe en voie d'émancipation. Ce fut une expérience tout à fait privilégiée, pendant plusieurs mois, semaine après semaine, nous avons tous ensemble, avec les différents corps de métier, travaillé à l'élaboration de notre futur laboratoire. Rares sont ceux qui ont ce privilège de commander sur plan leur futur espace de travail, jusqu'à choisir l'emplacement des lampes, la couleur des meubles, et le design des bureaux. Une fois de plus j'ai eu le sentiment d'être comme cet enfant gâté à qui l'on donne plus qu'il n'aurait espéré. Bien sûr, ce fut du travail, du temps mais cet investissement en équipe a été une belle expérience. Le résultat fut à la hauteur de nos espérances : un endroit fonctionnel, ou l'on se sent bien, presque chez soi. Tout d'abord BSCM puis ensuite LPM[5], le laboratoire d'Eva était né. C'est à partir de cette période que, grâce à Eva, j'ai fait des rencontres scientifiques importantes qui ont conditionné les orientations majeures de mon activité jusqu'à aujourd'hui.

En 2000, Eva avait été sollicitée, avec Hugues Lortat-Jacob, pour initier à l'IBS un projet de longue haleine avec en ligne de mire, la structure des co-récepteurs du virus HIV (des GPCRs). Ce projet structural devait partir de zéro, c'est à dire sans source de protéine disponible. Tout devait être fait : la mise au point d'un système de surexpression de ces protéines membranaires, leurs stabilisation et purification, …jusqu'à la cristallogenèse et la structure. C'est dans ce contexte et à l'occasion de la création d'un réseau ANRS sur ce projet que j'ai fait deux rencontres importantes, Fernando Arenzana-Seisdedos (de l'Institut Pasteur) et Corinne Vivès. Fernando était à l'origine du projet co-récepteur dans lequel nous nous sommes engagés avec d'autres et sur lequel nous avons beaucoup sué et souffert[6]. Mais c'est aussi lui, avec son énergie et son enthousiasme, qui m'a encouragé peu de temps après à démarrer un travail sur les lectines membranaires de cellules dendritiques et plus particulièrement DC-SIGN. Il est donc à l'origine de deux des projets dont j'ai la responsabilité scientifique maintenant dans le labo et je l'en remercie. Ces deux sujets ont été l'occasion de nombreuses ouvertures, nouvelles collaborations et rencontres pour moi. La première d'entre elles est celle de Corinne Vivès. Elle est arrivée au sein du groupe, sur un CDD financé par l'ANRS, pour travailler à mes côtés sur le projet co-Récepteur. Elle n'est jamais repartie[7]. Avoir à gérer trois projets assez différents, dont un très "membranaire" et à caractère très méthodologique, quand on a la disponibilité d'un maître de conférence n'est pas à priori raisonnable. Si je n'avais pas eu la présence de Corinne, comme soutien et relais, je pense pouvoir dire honnêtement que les choses n'en seraient pas là aujourd'hui. En effet, elle s'est peu à peu impliquée et a apporté son soutien dans mes deux autres projets (Lectines

[5] BSCM pour Biologie Structurale des Complexes Membranaires, LPM pour Labo. des Prot. Membranaires.
[6] et c'est loin d'être fini...mais on aime ça.
[7] Elle a été recrutée dans l'équipe, comme Ingénieur de Recherche, au CEA.

membranaires et maintenant NADPH Oxydase). Merci à toi, Corinne pour ta confiance, ta simplicité et ta bonne humeur toujours égale (ne change rien).

Puis est venue l'année 2001, avec une nouvelle thèse en co-direction, celle de Sylvie Chenavas, et le début du projet DC-SIGN au laboratoire avec l'arrivée d'une stagiaire post doctorale, Corinne Houlès, en collaboration avec Anne Imberty. Durant les deux ans qui suivirent, beaucoup d'énergie fut consacrée à la mise au point des outils de surexpression, protocole de purification et tests fonctionnels sur les deux projets co-récepteurs et DC-SIGN. Avec plus de succès immédiat sur DC-SIGN où nous sommes parvenus à produire différentes formes tronquées de la protéine. Nous avons valorisé ces outils et ces efforts au travers de collaborations avec, notamment, le groupe de Fernando Arenzana.

C'est en 2003, que j'ai ensuite fait la connaissance de trois personnes avec lesquelles de nombreux projets en commun vont être engagé dans les années à venir. Tout d'abord, Patrice Vachette et Dominique Durand avec lesquels nous abordons maintenant l'étude en solution de nos facteurs cytosoliques entiers par SAXS. Leur gentillesse transforme chacune de nos manips et discussions en grand moment de plaisir scientifique. En ce qui concerne le troisième, Javier Rojo, c'est lors du congrès Eurocarb 12 (à Grenoble) que j'ai finalement fait sa rencontre. Javier, me ramène un peu maintenant à l'interface Chimie-Biologie. Ce chimiste des sucres développait alors des molécules dendritiques avec pour cibles DC-SIGN. Dès ce moment, nous avons eu la volonté de travailler ensemble. Cela a conduit à un premier travail actuellement soumis, un sujet pour une 3^{e} thèse au labo sous ma direction (qui démarre en septembre, Georges Tabarani) et une amitié franco-espagnole qui sera, je l'espère sincèrement, durable et productive.

Nous voilà donc arrivé en 2005. Si l'on regarde, les sujets sur lesquels je travaille maintenant, ils sont très loin de ceux sur lesquels j'ai démarré ma carrière. J'ai démarré, dans un environnement chimie-biologie, sur des enzymes catalysant des réactions rédox provenant d'un contexte bactérien. Et maintenant, malgré le fait que je n'ai pas du tout été formé pour cela, j'ai entre les mains des projets centrés sur des protéines membranaires, ou associées aux membranes, appartenant au système immunitaire. J'ai encore beaucoup de chemin à faire pour rattraper mes lacunes en immunologie, mais la route est belle et enthousiasmante. L'interface avec la physique, malgré parfois aussi le sentiment d'atteindre mes limites, est également une source d'enrichissement permanente.

Je terminerai donc cette mini "bio" par un grand merci reconnaissant à Eva pour l'accueil qu'elle m'a fait, la confiance qu'elle m'a offerte, son regard positif et son volontarisme.

Merci pour ces 8 dernières années.

Introduction Générale.

Immunité, Immunodéficience et Protéines Membranaires.

NADPH oxydase, CXCR4, CCR5 et DC-SIGN : des protéines membranaires représentatives des différentes missions du système immunitaire.

L'organisme humain doit sans cesse lutter contre divers pathogènes tels que des bactéries, des virus ou encore des parasites. Cette défense est assurée par de nombreux mécanismes qui constituent l'immunité. Celle-ci est composée schématiquement de l'immunité spécifique (IS) et de l'immunité non spécifique (INS).

L'immunité spécifique, comme son nom l'indique, est une réponse adaptée à chaque agent pathogène. Cette voie du système immunitaire nécessite une reconnaissance préalable de l'agresseur, d'où une phase de latence de la réaction « primaire ». Cependant, il existe une mémoire de la première agression. Les infections futures par le même pathogène seront alors plus vite neutralisées, avec une réponse immunitaire plus affine et plus intense. C'est la réaction dite « secondaire ». Les acteurs principaux de cette immunité sont d'une part les lymphocytes B, producteurs d'anticorps, responsables de la réponse immunitaire spécifique humorale et d'autre part les lymphocytes T qui, une fois activés ou sensibilisés, remplissent différentes fonctions et constituent l'immunité spécifique cellulaire.

Par contre, l'immunité non spécifique se caractérise par la présence permanente de ses acteurs, même en absence de pathogènes. Cela lui confère une capacité de contre-attaque immédiate. Quel que soit l'agent infectieux, son mode d'action face à l'agression est toujours le même : la cascade du complément, la phagocytose et/ou la dégranulation. Les principaux responsables de cette immunité sont donc les cellules phagocytaires, comprenant les macrophages et les leucocytes polynucléaires neutrophiles.

Une défaillance des acteurs clé de chacun de ces deux versants de l'immunité conduit à un état de fragilité, voire de danger de mort pour l'individu. Une telle défaillance sera parfois acquise, comme c'est le cas dans l'infection au VIH où c'est principalement le système immunitaire spécifique qui est visé. D'autre fois, cette immunodéficience sera innée et donc le résultat de l'invalidation d'un composant important, du fait de mutation génétique, comme dans le cas de la Granulomatose Septique Chronique où c'est l'immunité non spécifique qui est cette fois atteinte. Ainsi, au travers des trois projets sur lesquels je suis engagé, je suis amené à appréhender à la fois le système spécifique et non spécifique dans un contexte "d'immunodéficience".

Plus que tout autre tissu, le système immunitaire devra, pour coordonner l'ensemble de ses nombreux acteurs cellulaires de fonctions différentes, utiliser une pléthore d'agents de signalisation et de régulation. Il sera donc essentiel que chacun de ces messages soit détectés par les cellules immunitaires. De plus, par essence, certaines de ses cellules devront pouvoir interagir avec les organismes pathogènes à détecter et éliminer. Et enfin, pour cette dernière tâche de destruction de l'ennemi, la production d'espèce toxique devra pouvoir se faire de manière orientée, c'est-à-dire hors de la cellule immunitaire, elle-même sensible, mais vers

l'extérieur (à proximité du pathogène) ou bien dans des vésicules de capture à l'environnement contrôlé (phagosomes). Toutes ces fonctions, qui sont à la base même des missions du système immunitaire, peuvent être résumées ainsi :

1. Perception et transduction des signaux de chimiotactisme, d'activation, etc…
2. Interaction hôtes-pathogènes
3. Production orientée d'agents toxiques, bactéricides

À cet énoncé, il apparaît comme une évidence que les protéines membranaires vont avoir une position centrale dans le dispositif (même si elle n'est pas exclusive, bien sûr). Les différents projets dont j'ai la charge concernent des protéines, ou des complexes de protéines, localisées à la membrane de différentes cellules composant ce tissu complexe et circulant qu'est le système immunitaire. Chacune de ces protéines est concernée par une ou plusieurs des catégories fonctionnelles évoquées ci-dessous. Ainsi, CXCR4 et CCR5 sont des récepteurs chimiotactiques mais également des récepteurs clés du VIH. DC-SIGN joue un rôle important dans les phénomènes d'activation des lymphocytes T mais également dans l'interaction avec de nombreux pathogènes. Enfin, le complexe de la NADPH oxydase produit, hors de la cellule, des espèces réactives de l'oxygène pour détruire les bactéries, et son activation est le point final d'une voie de signalisation complexe initiée par la perception de signaux externes par des récepteurs semblables aux susmentionnés CCR5 et CXCR4.

Cette apparente cohérence d'ensemble cache des différences importantes dans la nature des compétences et connaissances à déployer pour l'étude de chacunes de ces protéines. Ainsi, les co-récepteurs font appel pour leur étude structurale à une nécessité de développement méthodologique important (surexpression protéine membranaire et physico-chimie de la renaturation des protéines). DC-SIGN nécessite un rapprochement avec la glycobiologie (notamment la chimie des sucres et la biochimie des lectines). Et la NADPH oxydase et son activation demande un investissement important dans la biologie de la transduction du signal (voie de transduction, biologie des protéines modulaires et des changements conformationnels, …) et à terme l'enzymologie des réactions rédox. Enfin, pour chacun de ces projets, qui comportent tous une perspective structurale, l'interface avec les méthodes bio-physiques d'études (de la cristallographie des protéines à la résonnance plasmonique de surface en passant par le RMN ou le SAXS) revêt une importance grandissante.

Dans la suite de ce rapport, je vais tenter de vous présenter, de la manière la plus claire possible, chacun des projets évoqués en espérant vous faire sentir la richesse et la diversité que m'apporte chacun d'entre eux.

Chapitre I.

Le complexe de la NADPH oxydase des neutrophiles

I. La NADPH oxidase : une arme de destruction massive

Suite à une blessure ou à une lésion produite par un agent pathogène, il se produit une réaction inflammatoire au cours de laquelle les cellules de l'immunité sont recrutées. Contrairement aux macrophages qui résident dans les tissus, les leucocytes et les monocytes sont circulants, leur deplacement sur le site de l'infection est médié par les macrophages résidants. Ceux-ci sécrètent des chimioattractants (cytokines et chimiokines), éléments essentiels au processus d'alerte et de signalisation. Il en résulte une accumulation de leucocytes puis de monocytes sur le site de l'infection. La destruction des pathogènes se déroule alors, notamment, à l'aide de la phagocytose.

Parmi les cellules phagocytaires, ce sont les polynucléaires neutrophiles qui représentent 95 % des granulocytes (leucocytes et macrophages) circulants. Après la phagocytose, leur action anti-infectieuse se réalise par deux types de mécanismes : ceux dépendant de l'oxygène, grâce au complexe enzymatique de la NADPH Oxydase situé au niveau de la membrane cytoplasmique du phagosome, et la dégranulation qui permet la dégradation du pathogène mort.

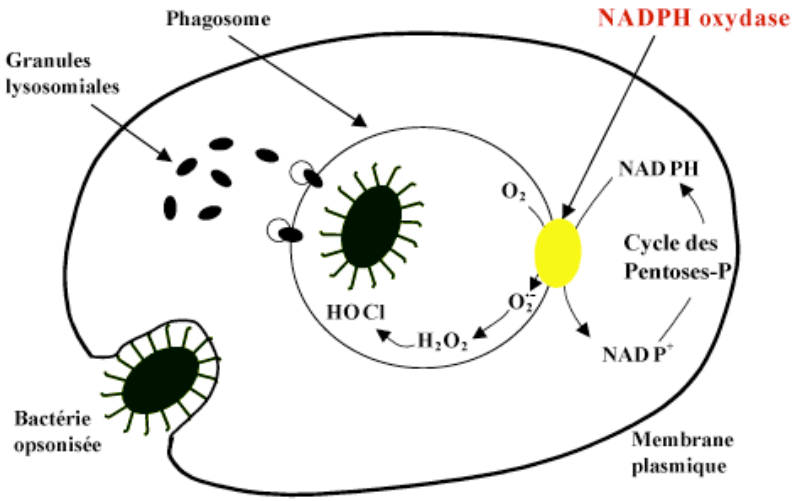

Figure 1 : Explosion respiratoire et dégranulation liées à la phagocytose. Après internalisation du pathogène (ici une bactérie) et formation du phagosome, deux évènements se produisent : la formation d'espèces réactives de l'oxygène, amorcée par la NADPH Oxydase, et la dégranulation, c'est-à-dire le déversement du contenu des granules cytoplasmiques dans le phagosome.

Un défaut de la NADPH oxydase se traduit par la création de foyers d'infection chronique, c'est le cas chez les patients atteints de CGD (chronic granulomatous disease), maladie génétique rare. Elle est due à une ou plusieurs mutations dans l'un des gènes codant pour les constituants du complexe. Les patients atteints de ce syndrome n'arrivent plus à lutter contre les infections bactériennes. C'est une forme d'immunodéficience innée et non pas acquise. Suite à l'internalisation des micro-organismes, la NADPH oxydase est activé, assemblée afin de déclencher le transfert d'électrons du NADPH vers O_2. Cet événement doit être régulé très finement afin d'éviter la production de radicaux oxygénés intempestive dans les cellules. En effet, une dérégulation de cette activité hautement toxique peut conduire à des troubles importants comme des inflammations de type arthrite.

II. Un enzyme membranaire à multiple composants.

Le complexe de la NADPH Oxydase des neutrophiles humains est constitué du flavocytochrome b_{558} membranaire, de trois facteurs cytosoliques ($p67^{phox}$, $p47^{phox}$ et $p40^{phox}$) et d'une petite protéine G localisés dans le cytoplasme du neutrophile au repos.

a) le flavocytochrome b558

Le flavocytochrome b_{558}, composé des protéines $gp91^{phox}$ et $p22^{phox}$, phox pour phagocyte oxidase, est situé dans la membrane des neutrophiles (figure 2). Il contient tout l'équipement redox nécessaire au transfert d'électron du NADPH à l'oxygène moléculaire, mais n'est pas actif en l'absence des composants solubles du complexe.

Figure 2 : Topologie des composants membranaires du flavocytochrome b_{558} de la NADPH Oxydase. D'après les prédictions de structures, $gp91^{phox}$ est composé de 6 hélices α transmembranaires et $p22^{phox}$ de 3 hélices α transmembranaires. $gp91^{phox}$ possède un site de liaison au NADPH, un site de liaison au FAD et deux hèmes (Fe). $p22^{phox}$ possède dans sa région C-terminale cytosolique une séquence riche en prolines.

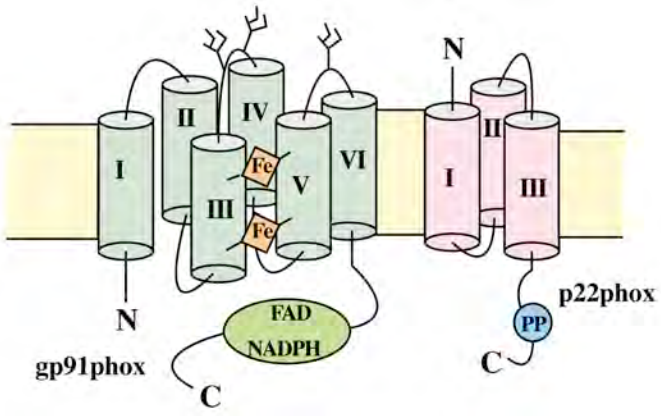

b) La petite protéine G, Rac

Rac, rac1 ou rac2, possède une chaîne hydrophobe qui induit une localisation membranaire. Cette chaîne hydrophobe peut être masquée par une protéine appelée GDI (Guanine nucleotide Dissociation Inhibitor) qui permet ainsi la solubilisation de la protéine G et l'inhibition de la réaction d'échange GDP/GTP. Dans le cas de la famille Rho, la protéine de type GDI est appelée RhoGDI (figure 3). Ainsi, dans la cellule au repos, Rac est essentiellement localisé dans le cytoplasme, associé à RhoGDI. Suite à l'activation, Rac se dissocie de RhoGDI. Il rejoint alors la membrane où il participera à l'activation du flavocytochrome b_{558}.

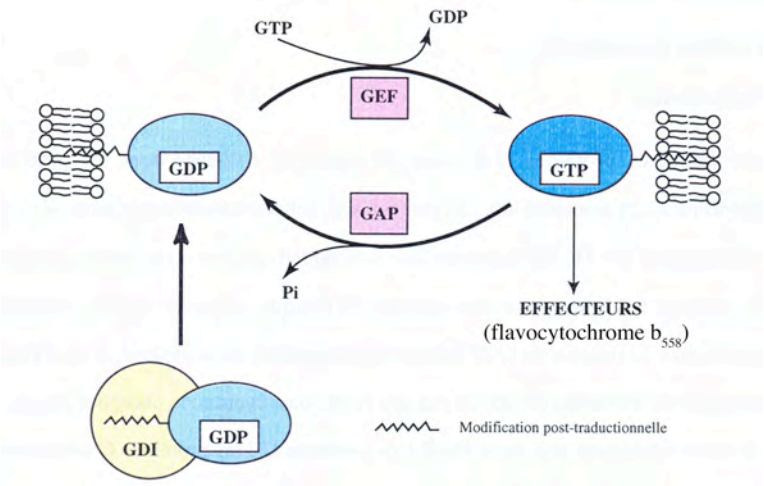

Figure 4 : Schéma général du cycle des petites protéines G. La petite protéine G est représentée en bleu et la protéine GDI (Guanine nucleotide Dissociation Inhibitor) en jaune. GEF : Guanine nucleotide Exchange Factor ; GAP : GTPase Activating Protein ; Pi : phosphate inorganique

c) Les facteurs cytosoliques, p47^{phox}, p67^{phox} et p40^{phox}

Les facteurs cytosoliques sont des protéines modulaires, c'est à dire constituées de segments de séquences peptidiques dont la structuration fonctionelle est indépendante du reste de la protéine. L'enchaînement de modules différents au sein d'une protéine va lui conférer des propriétés et une fonction particulières. Ces modules structuraux permettent le plus souvent des interactions de type protéine/protéine. Ainsi, dans le neutrophile au repos, les facteurs cytosoliques peuvent interagir entre eux par le biais de leurs domaines structuraux.

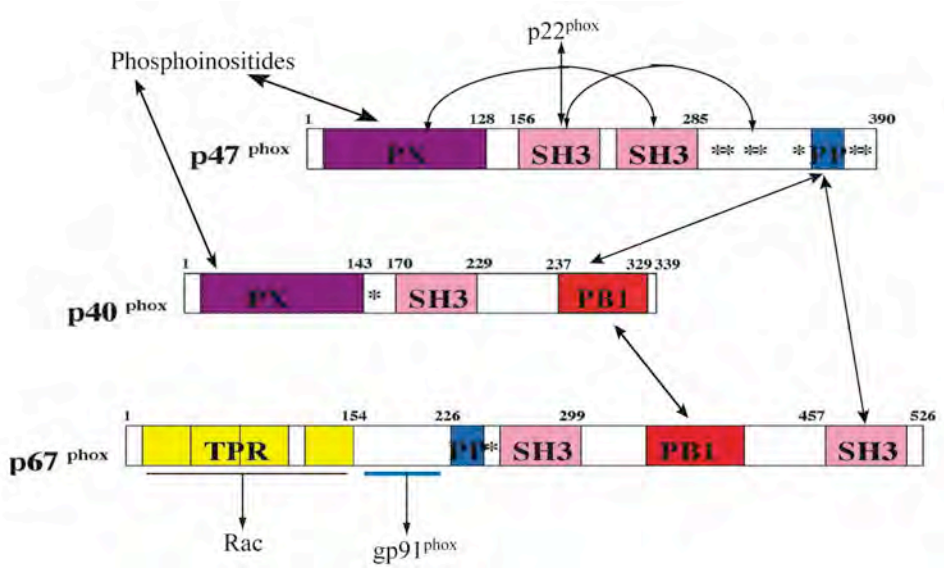

Figure 5 : Interactions possibles des facteurs cytosoliques. Il existe, au sein de l'ensemble des facteurs cytosoliques, 5 types de modules différents : le motif TPR (TetratricoPeptide Repeat), le motif PP (Poly-Proline), le domaine PX (PhoX), le domaine SH3 (Src Homology 3) et le domaine PB1 (Phox Bem1p). La région de p67^{phox} soulignée en bleu correspond au domaine d'activation (199-210) et les * correspondent aux sites de phosphorylation.

La protéine p47^{phox} est la protéine qui va diriger l'assemblage du complexe et "sentir" le signal d'activation par le biais de phosphorylations multiples sur ses sérines. p67^{phox} a un rôle direct dans l'activation du transfert d'électron, c'est le facteur d'activation moléculaire qui fonctionne de concert avec la petite protéine G Rac. p40phox a un rôle de régulateur global de l'activité qui est encore mal défini à ce jour.

III. Activation de la NADPH oxydase

a) Voies de signalisation conduisant à l'activation de La NADPH oxydase

Les voies de transmission du signal d'activation sont nombreuses et complexes et passent principalement par des molécules activatrices, chimioattractants, produites sur le lieu de l'infection. Ces composés vont se lier à des récepteurs à 7 hélices transmembranaires présents à la surface des neutrophiles. Différentes voies de transduction du signal sont déclenchées et conduisent à la phagocytose, la dégranulation et l'activation de la NADPH oxydase (figure 6).

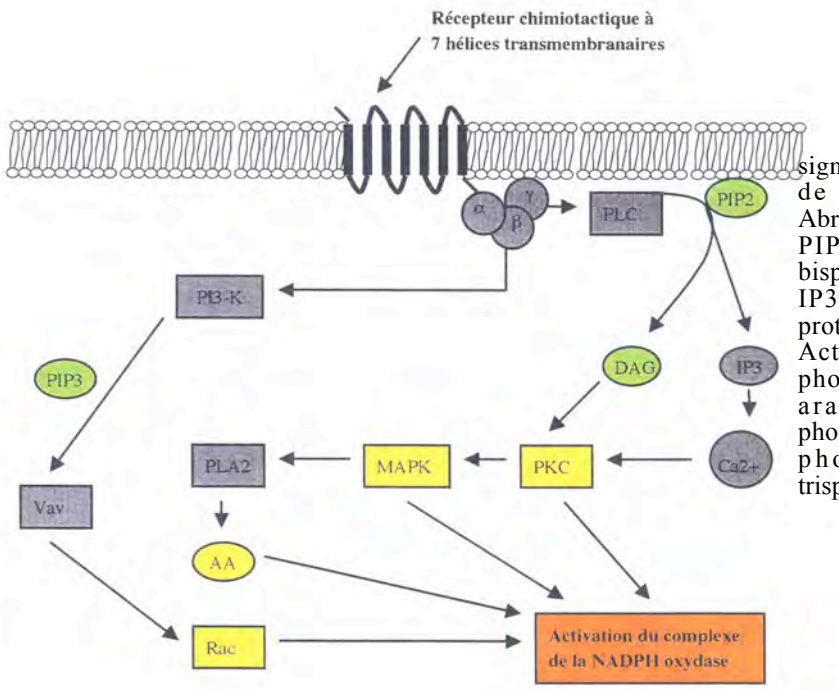

Figure 6 : Voies de signalisation conduisant à l'activation de la NADPH Oxydase. Abréviations : PLC, phospholipase C ; PIP2, phosphatidylinositol 4,5 bisphosphate ; DAG, diacylglycerol ; IP3, inositol trisphosphate, PKC, protéine kinase C; MAPK, Mitogen-Activated Protein kinase, PLA2, phospholipase A2 ; AA, acide arachidonique ; PI3-K , phosphatidylinositol 3-kinase ; PIP3, phosphatidylinositol 3,4,5 trisphosphate

b) Activation de la NADPH Oxydase : assemblage à la membrane

Dans la cellule au repos, les composants solubles $p67^{phox}$, $p47^{phox}$, $p40^{phox}$ et la petite protéine G Rac sont dans le cytoplasme. Il est généralement admis qu'*in vitro*, les facteurs cytosoliques recombinants forment un complexe de stoechiométrie 1 :1 :1. La petite protéine G, quant à elle, se trouve à l'état soluble par son interaction avec le GDP Dissociation Inhibitor (GDI) (Figure 6).

Figure 6 : Schéma de l'activation du complexe de la NADPH Oxydase.

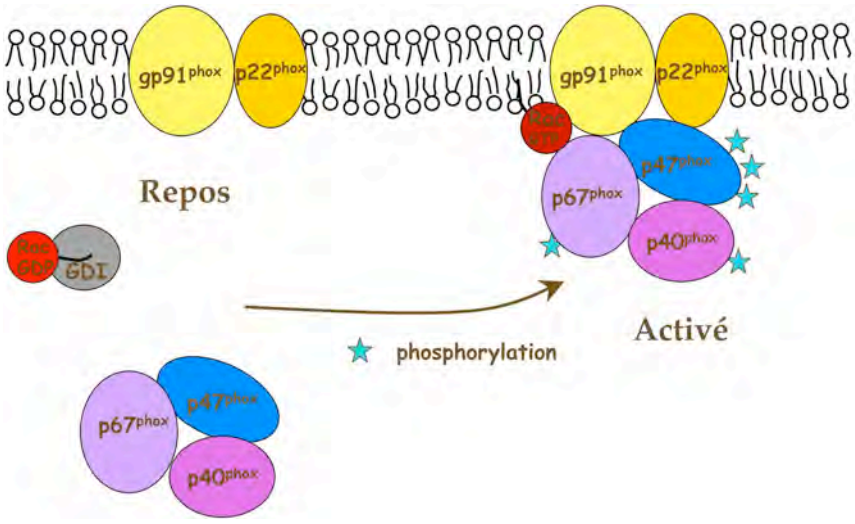

L'activation est initiée par des séries de modifications structurales de $p47^{phox}$ (induite par phosphorylation), elle entraîne la translocation des facteurs cytosoliques à la membrane. De manière indépendante, Rac est également transféré à la membrane. Puis les différents composants sont assemblés, le flavocytochrome b558 activé permettant ainsi le transfert d'électrons.

IV Questions, objectifs, difficultés et stratégies dans l'étude structurale de la NADPH oxydase.

Lorsque ce projet a démarré dans l'équipe, la nature des évènements moléculaires qui président à l'activation du complexe, son assemblage et le transfert d'électrons n'étaient pas ou peu connus. Comment interagissent les différents composants au repos ? Quelles modifications structurales les phosphorylations entraînent elles ? Comment se réalise l'assemblage final ? Quel est le rôle de chaque composant dans la plasticité structurale de l'ensemble ? Quelles sont les éléments de structures et les modifications qui enclenchent un état de compétence du flavocytochrome b_{558} ? Comment se fait le transfert d'électrons au travers de la membrane ? Voilà une liste non exhaustive des questions d'ordre moléculaire, structural et mécanistique que nous voulions aborder sur ce système d'une grande complexité.

Pour ce faire le laboratoire s'est engagé (déjà avant mon arrivée) dans l'étude de ce système avec la volonté de caractériser d'un point de vue structurale les différents composants du système aussi bien cytosolique que membranaire et dans leurs différents états : seul ou en complexe, au repos ou dans un état d'activation (phosphorylation).

Nous nous sommes confrontés à deux difficultés majeures :

- L'accès à la partie membranaire
- La flexibilité intrinsèque des facteurs cytosoliques de nature modulaire.

La partie membranaire :

À mon arrivé dans le labo, je me suis dans un premier temps fortement investi sur la partie membranaire au travers de deux approches : la purification du flavocytochrome b558 à partir de neutrophiles de bœuf (sang obtenu en abattoir) en collaboration avec Jacques Doussière (BBSI, DRDC, CEA-Grenoble), et la production de manière recombinante des protéines ou de régions tronquées du flavocytochrome b_{558} (en fait $p22^{phox}$ et la région C-ter de $gp91^{phox}$). Malgré un effort important, aucune de ces deux approches n'a permis un accès à des protéines qui soient en qualité et quantité compatibles avec des études de nature structurales.

Les facteurs cytosoliques :

Les facteurs cytosoliques ont pu être produits de manière recombinante. Mais malgré des efforts importants (notamment sur $p47^{phox}$ et $p67^{phox}$), ces protéines sous leur formes entières ne se sont pas révélées accessibles à la cristallisation. L'organisation modulaire, avec des domaines de structure autonome reliée par des linkers, semble entraîner une flexibilité globale incompatible avec la formation de cristaux.

APPROCHES UTILISEES ET RESULTATS :

Nous sommes engagés dans une approche de dissection moléculaire des facteurs cytosoliques pour contourner le problème de flexibilité. Nous avons ainsi entrepris des études structurales en solution (diffusion de neutrons) avec les protéines entières et des approches

hautes résolutions (cristallographie aux rayons X ou une étude en RMN lorsque cela était nécessaire) sur des domaines structuraux isolés (sauf pour Rac et RhoGDI qui ne sont pas de nature modulaire). D'un point de vue plus fonctionnel, conjointement à ces études structurales au sens strict, nous avons reproduit lorsque cela était possible des mutations qui conduisent à des phénotypes CGD pour expliquer l'origine moléculaire de la déficience et mener des études d'interactions entre domaines partenaires avec ou sans les phosphorylations lorsque cela se justifiait et était possible.

L'ensemble des résultats que nous avons obtenus sont présentés ci–après, de manière anti-chronologique, sous la forme d'articles à paraître (soumis ou en préparation) ou parus (dans leur intégralité ou simplement l'abstract).

Perspective : Nos résultats et ceux produits par d'autres équipes (ce sujet est le cadre d'une compétition internationale très forte) ont contribué à faire progresser notablement les connaissances moléculaires des différents composants du système (principalement cytosoliques) mais pour l'essentiel les questions posées au début de ce paragraphe peuvent toujours l'être dans presque les mêmes termes. Afin de repousser plus loin ce que l'on connait de la NADPH oxydase et de son mécanisme d'activation et de fonctionnement, il faut maintenant revenir aux difficultés initiales :

- l'organisation structurale des facteurs cytosoliques entiers et leur dynamique au cours de la phosphorylation
- l'accés à la partie membranaire pour son étude structurale et fonctionnel.

Dans l'objectif de répondre à la première difficulté, nous avons entamé une collaboration avec le groupe de Patrice Vachette et Dominique Durand pour leur expertise dans l'utilisation de la diffusion de rayons X aux petits angles. L'objectif est d'obtenir uen enveloppe dans laquelle nous replacerons la structure haute résolution des différents modules et ainsi apréhender les relations internes entre modules au sein des facterus cytosoliques ou de complexe de ceux-ci. Un premier travail en cours de rédaction est présenté juste après.

En ce qui concerne, la partie membranaire, et principalement $gp91^{phox}$, nous allons contourner le problème. Cette protéine humaine ne pouvant être ni-produite de façon recombinante, ni purifiée à partir d'échantillons sanguin, nous allons nous concentrer sur une protéine de séquence et de structure analogue. Il existe une protéine membranaire, YedZ, à 6 segments transmembranaires chez *E.coli* qui présente des similitudes de séquences avec la région à 6 segment transmembranaire de $gp91^{phox}$. Cette protéine à été découverte par Jan Willem de Gier avec qui nous avons établi une collaboration. YedZ présente les

caractéristiques d'un flavocytochrome et l'énorme avantage de se surexprimer dans la membrane bactérienne. Sur la base d'une structure de Yed Z, une modélisation de $gp91^{phox}$ pourrait être envisagé.

Publications issues de ce projet : P15, P11, P10, P9, P8, et PO4 (voir page 7 et 8)
P15 et P9 sont présentés en intégralités ci après, et juste l'abstract pour les autres.

Publication à venir :

P19 (en préparation, non présenté),
P18 (en préparation),
P16 (soumis à *Febs Journal*)

Les manuscripts P18 et P16 sont présentés ci-après.

Articles présentés en intégralité

Article P15 : Massenet *et al.* (2005) *J.Biol.Chem. Paper of the week*
La structure du domaine SH3 de p40-phox seul et en complexe avec le peptide-Cterminal de p47-phox.

Nous avons produit, cristallisé et résolu la structure du module SH3 de la protéine p40^{phox} seul et en complexe avec sa cible potentielle, une séquence polyproline en Cterminal de la protéine p47^{phox}. Par spectroscopie de fluorescence, nous avons caractérisé l'évolution de l'affinité de ce module pour sa cible, la séquence polyproline de p47^{phox}, en fonction de l'état de phosphorylation des sérines encadrant le motif d'interaction. Ce travail a permis de conclure sur les conséquences liés aux phosphorylations. Ainsi, des échanges de partenaires d'interactions possibles au sein du complexe au cours de l'activation du fait de modification d'affinités consécutives aux phosphorylations étaient suggérés ; nous montrons que de tels échanges n'existent pas dans ce contexte. De plus ce travail apporte de nouvelles informations structurales sur la protéine p40^{phox} et les modalités d'interaction avec la séquence polyproline C-terminale de p47^{phox}.

Article P9 : Grizot *et al.* (2001) *J.Biol.Chem.*
La structure de la partie N-terminale de p67

Nous avons produit une forme tronquée de p67 (résidus 1 à 213), la plus petite forme active de cette protéine, et obtenu des petits cristaux qui diffractent à plus de 1.8 Å à l'ESRF. Les phases ont été déterminées à 2.8 Å par la méthode SAD puis étendues à 1.8 Å par aplatissement du solvant. La structure est constituée de 4 motifs répétitifs de type TPR (tetratricopeptide repeat), la succession de ces 4 motifs crée un sillon hydrophobe dans lequel se loge l'extension C-terminale de la protéine. En parallèle à la protéine native, nous avons étudié une protéine mutante (A128V) responsable de la CGD. Nous avons montré par des mesures de dichroïsme circulaire que le mutant est très instable au-dessus de 30°C ce qui expliquerait le non-fonctionnement de la NADPH oxydase chez les patients présentant cette mutation.

Article P16 : Chenavas *et al.* (2005) soumis à *Febs Journal.*
Etude structurale en solution de la zone de dimérisation entre p67^{phox} et p40^{phox} :

Les domaines PB1 de p67^{phox} et p40^{phox} responsable de la complexation constitutive de ces deux protéines ont été surproduites avec marquages isotopiques. Une collaboration avec le groupe de RMN de l'IBS a permis d'avoir accés à la structure du module PB1 de p67^{phox}, la topologie du module PB1 de p40^{phox} et de définir, par des expériences de chemical shift mapping, les sites d'interaction sur chacune des deux protéines. Le comportement des modules PB1 isolés en solution et des aspects de la dynamique de l'interaction sont discutés.

Article P18 : *Durand et al.* (2005) en préparation.
Détermination de l'enveloppe moléculaire de p47^{phox} au repos :

Par diffusion de rayons X au petits angles, nous avons déterminé l'enveloppe moléculaire de p47phox entier. Dans cette enveloppe nous avons replacé les structures hautes résolutions des différents modules consituants p47^{phox}. Ce travail jette les premières bases structurales pour appréhender le mécanisme de l'activation dépendante de p47^{phox}.

THE JOURNAL OF BIOLOGICAL CHEMISTRY
Vol. 280, No. 14, Issue of April 8, pp. 13752–13761, 2005

Printed in U.S.A.

Effects of p47^{phox} C Terminus Phosphorylations on Binding Interactions with p40^{phox} and p67^{phox}

STRUCTURAL AND FUNCTIONAL COMPARISON OF p40^{phox} and p67^{phox} SH3 DOMAINS*♦

Received for publication, November 15, 2004, and in revised form, January 5, 2005
Published, JBC Papers in Press, January 18, 2005, DOI 10.1074/jbc.M412897200

Claire Massenet‡§¶, Sylvie Chenavas‡§¶, Claudine Cohen-Addad‡, Marie-Claire Dagher‖, Gérard Brandolin‖, Eva Pebay-Peyroula‡, and Franck Fieschi‡**

From the ‡Institut de Biologie Structurale, UMR 5075 CEA/CNRS/Université Joseph Fourier, Laboratoire des Protéines Membranaires, 41 rue Jules Horowitz 38027 Grenoble cedex 1, France and the ‖Département Réponse et Dynamique Cellulaire, BBSI, UMR 5092 CEA/CNRS/UJF, 17 avenue des Martyrs, 38054 Grenoble cedex 9, France

The neutrophil NADPH oxidase produces superoxide anions in response to infection. This reaction is activated by association of cytosolic factors, p47^{phox} and p67^{phox}, and a small G protein Rac with the membranous flavocytochrome b_{558}. Another cytosolic factor, p40^{phox}, is associated to the complex and is reported to play regulatory roles. Initiation of the NADPH oxidase activation cascade has been reported as consecutive to phosphorylation on serines 359/370 and 379 of the p47^{phox} C terminus. These serines surround a polyproline motif that can interact with the Src homology 3 (SH3) module of p40^{phox} (SH3^{p40}) or the C-terminal SH3 of p67^{phox} (C-SH3^{p67}). The latter one presents a higher affinity in the resting state for p47^{phox}. A change in SH3 binding preference following phosphorylation has been postulated earlier. Here we report the crystal structures of SH3^{p40} alone or in complex with a 12-residue proline-rich region of p47^{phox} at 1.46 Å resolution. Using intrinsic tryptophan fluorescence measurements, we compared the affinity of the strict polyproline motif and the whole C terminus peptide with both SH3^{p40} and C-SH3^{p67}. These data reveal that SH3^{p40} can interact with a consensus polyproline motif but also with a noncanonical motif of the p47^{phox} C terminus. The electrostatic surfaces of both SH3 are very different, and therefore the binding preference for C-SH3^{p67} can be attributed to the polyproline motif recognition and particularly to the Arg-368^{p47} binding mode. The noncanonical motif contributes equally to interaction with both SH3. The influence of serine phosphorylation on residues 359/370 and 379 on the affinity for both SH3 domains has been checked. We conclude that contrarily to previous suggestions, phosphorylation of Ser-359/370 does not modify the SH3 binding affinity for both SH3, whereas phosphorylation of Ser-379 has a destabilizing effect on both interactions. Other mechanisms than a phosphorylation induced switch between the two SH3 must therefore take place for NADPH oxidase activation cascade to start.

The neutrophil NADPH oxidase is a central component of the nonspecific host resistance against microbial infection. The critical role of this enzyme is illustrated by a genetic disease, chronic granulomatous disease (CGD),[1] in which mutations in genes coding for NADPH oxidase components impair the ability of the patient to fight against infection. The NADPH oxidase is composed of several proteins, a membrane-bound heterodimeric flavocytochrome *b* (gp91^{phox} and p22^{phox}), cytosolic proteins (p40^{phox}, p47^{phox}, p67^{phox}), and a small GTP-binding protein (Rac1 or Rac2) (for review, see Ref. 1). Upon exposure to specific stimuli, activation of the enzyme takes place through multiple phosphorylation events of the cytosolic components (2–5). Phosphorylations rearrange the protein-protein interactions among the cytosolic proteins ending with their translocation, simultaneously with Rac-GTP, to the membrane embedded flavocytochrome *b*. The resulting activated complex catalyzes the electron transfer from NADPH to O_2 leading to the production of superoxide anions, thus generating highly reactive oxygen species (ROS) in the phagocytic vacuole. For many years these ROS have been designated as the main actors in the neutrophil killing activity. Recent work suggests that in addition to its role in ROS formation, O_2^- generation leads to phagosomal Cathepsin G and Elastase mobilization in the microbicidal process (6).

The three cytosolic proteins p47^{phox}, p67^{phox}, and p40^{phox} are modular proteins formed by various domains, such as SH3, PX, PB1, and TPR, usually found in signal transduction cascades. Numerous possible interactions within these proteins have been reported and are summarized in Fig. 1*A*. p47^{phox} and p67^{phox} are known to be essential for activation. In CGD patient lacking p47^{phox}, p67^{phox} is not translocated to the membrane. In contrast p67^{phox} is not essential to p47^{phox} translocation (7). In the activation process, p47^{phox} is the sensor of the activation signal through multisite phosphorylations and secondly the scaffolding protein conducting translocation of the other cytosolic factors to the membrane component of the oxidase. p67^{phox} is an activating factor in the electron transfer reaction (8). In contrast to p47^{phox} and p67^{phox}, nowadays no CGD related to p40^{phox} is known. p40^{phox} was first identified as a p67^{phox}-associated protein in resting neutrophils (9–11). p40^{phox} translocates to the membrane upon stimulation in a p47^{phox}-dependent manner (12). The protein comprises the fol-

* The costs of publication of this article were defrayed in part by the payment of page charges. This article must therefore be hereby marked "*advertisement*" in accordance with 18 U.S.C. Section 1734 solely to indicate this fact.

♦ This article was selected as a Paper of the Week.

The atomic coordinates and structure factors (codes 1W6X (for SH3^{p40}) and 1W70 (for SH3^{p40}/polyPro^{p47} complex) have been deposited in the Protein Data Bank, Research Collaboratory for Structural Bioinformatics, Rutgers University, New Brunswick, NJ (http://www.rcsb.org/).

§ Both authors were supported by Ministère de l'Education Nationale de la Recherche et de la Technologie and Association pour la Recherche sure le Cancer fellowships.

¶ These authors contributed equally to this work.

** To whom correspondence should be addressed. Tel.: 33-438-789-177; Fax: 33-438-785-494; E-mail: fieschi@ibs.fr.

[1] The abbreviations used are: CGD, chronic granulomatous disease; SH3, Src homology 3; PX, Phox homology; PB1, Phox-Bem1p homology; SH3^{p40}, SH3 domain of p40^{phox}; C-SH3^{p67}, C-terminal SH3 domain of p67^{phox}; p47^{phox}-Cter, p47^{phox} C terminus (residues 358–390); polyPro^{p47}, polyproline motif of p47^{phox} (residues 358–372); PDB, Protein Data Bank; HPLC, high performance liquid chromatography.

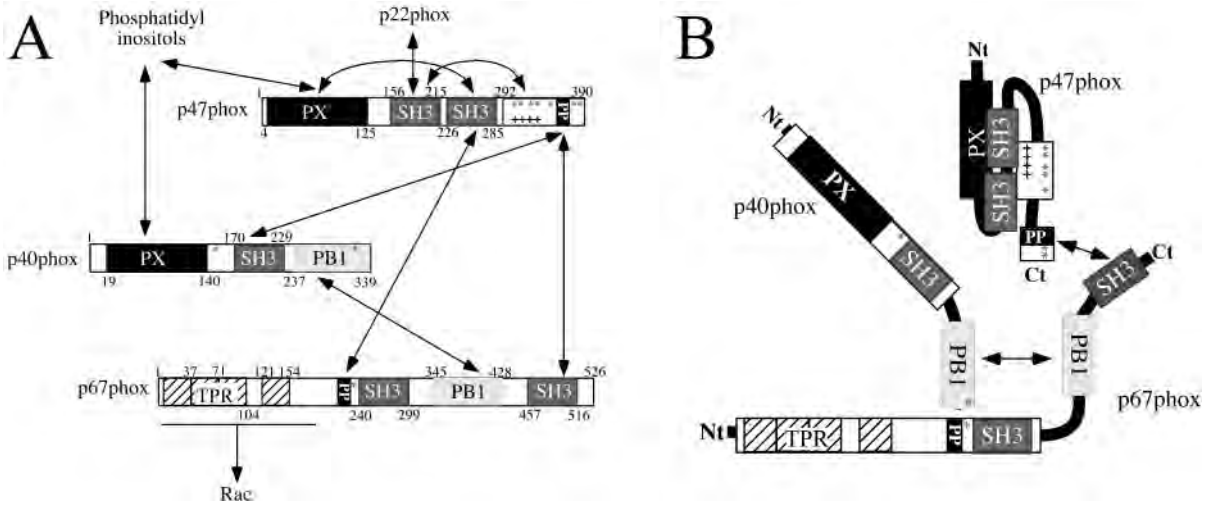

FIG. 1. **Schematic representations of the cytosolic factors and their domains.** *A*, *arrows* indicate all possible interactions that have been shown experimentally (17, 18, 31, 37, 60–65). *B*, interactions existing *in vitro*, in a resting state model, between nonphosphorylated recombinant cytosolic factors (20, 27).

lowing domains, PX, SH3, and PB1 (Fig. 1*A*) (13). These modules confer to p40^{phox} the ability to interact respectively with phosphatidylinositol 3-phosphate (14–16), p47^{phox} C terminus (17–19), and p67^{phox} PB1 domain (20). The physiological role of p40^{phox} is still a matter of debate. It has been postulated to modulate superoxide production, either positively (21–23) or negatively (18, 24–26). In the last couple of years, an increasing body of structural and biochemical data shed light on the organization of the cytosolic complex in the resting state and on some events consecutive to p47^{phox} phosphorylation. In the resting state p47^{phox}, p67^{phox}, and p40^{phox} are thought to exist as a 1:1:1 ternary complex (27) as shown with purified proteins. Although p40^{phox} and p67^{phox} are both able to interact with the C-terminal polyproline region of p47^{phox}, the p47^{phox}/p67^{phox} complex is favored (19, 27). A ternary complex can be achieved by the association of p40^{phox} with p67^{phox} (28) through their respective PB1 domain (20, 27–29) (Fig. 1*B*). However, it has been recently shown (30) that, *in vivo*, p47^{phox} is dissociated from the p67^{phox}/p40^{phox} complex, as suggested previously (31).

Activation initiated by the binding of chemotactic substances to neutrophil receptors leads, through signaling pathways, to primary phosphorylation of Ser-359 and/or Ser-370 of p47^{phox} (5). Additional phosphorylations can occur among the seven other C-terminal serines of p47^{phox}. Among them, Ser-303, Ser-304, Ser-328, and Ser-379 have been identified as important for membrane translocation, interaction with p22^{phox}, and the activation of the complex as shown by several mutagenesis studies (4, 32, 33).

It is now well established that these phosphorylations modify p47^{phox} binding properties. From the resting to the activated state, p47^{phox} is proposed to change from a closed to an open conformation where the PX domain is either masked by the internal C-terminal SH3 of p47^{phox} or free for interaction with lipids of the membrane (34, 35). In addition, the two p47^{phox}-SH3 domains have been shown to be either buried or accessible to the p22^{phox} polyproline (32, 36). Interactions with lipids and p22^{phox} are believed to account for the association of p47^{phox} with the membrane (37, 38). Despite these new insights on p47^{phox}, there is almost no information concerning the reorganization of p67^{phox} and p40^{phox} in the cytosolic complex upon phosphorylation. When examining the extended possibilities of interactions between cytosolic factors (Fig. 1*A*) and the limited panel of those present in the resting state (Fig. 1*B*), a rearrangement involving the three proteins has been suggested (24, 27). At the present stage, several structures of individual domains or of complexes made by two domains are available (16, 29, 34–36, 39–41). It has been proposed that the phosphorylation of p47^{phox} could modulate its interaction with p67^{phox} or p40^{phox}, respectively (17, 24, 27). To understand the structural rearrangements occurring upon activation, structural information on the effect of nonphosphorylated and phosphorylated serines is needed. We addressed this question, characterizing at a molecular level the interaction of the SH3 domain of p40^{phox} (SH3^{p40}) with the polyproline region of p47^{phox}.

We report the three-dimensional structure of SH3^{p40} with and without the C-terminal polyproline of p47^{phox} at 1.46 and 2 Å resolution, respectively. Comparison with the structure of the C-terminal SH3 domain of p67^{phox} (C-SH3^{p67}) complexed to the p47^{phox} C terminus (41) highlights a strong difference between both SH3 domains. We compare the dissociation constants of both SH3^{p40} and C-SH3^{p67} with polyproline peptides by fluorometric techniques. The effect of phosphorylation on Ser-359, Ser-370, and Ser-379 on the binding of both SH3 toward p47^{phox} is also investigated.

EXPERIMENTAL PROCEDURES

Protein Expression and Purification

SH3^{p40}—A DNA fragment encoding the p40^{phox} SH3 module, from Arg-174 to Lys-228, was amplified by PCR using the full-length p40^{phox} sequence (31) as a template. The PCR fragment was cloned into the pCRscript Amp SK(+) cloning vector according to the manufacturer's protocol (Stratagene). The resulting pCRscript-SH3^{p40} plasmid was cleaved with NdeI and XhoI and the 168-base fragment containing the SH3^{p40} sequence was subcloned in pIVEX 2.4 (Roche Applied Science). The resulting vector named pIVEX-SH3^{p40} was transformed and amplified in *Escherichia coli* BL21(DE3) strain. The sequence of the construct was checked by sequencing.

The His-SH3^{p40} was overexpressed as described for p40^{phox} (19). After 3 h, cells were harvested and resuspended in chilled lysis buffer (20 mM Hepes, pH 7.5, 0.4 M NaCl supplemented with 40 mM imidazole and 5% glycerol). All of following operations were carried out at 4 °C. Cells were disrupted by sonication then centrifuged at 40,000 rpm for 40 min in a Beckman 45 Ti rotor. The supernatant was loaded at 2 ml/min on 4 ml of Ni^{2+}-nitrilotriacetic acid column equilibrated in the previous buffer. Proteins were eluted with a 50-ml linear imidazole gradient (40–300 mM) at 2 ml/min. Fractions containing His-SH3^{p40} were pooled, concentrated to 6 mg/ml, and subjected to overnight digestion at 20 °C with 2.4 units of factor Xa/mg of protein in the presence of 2.5 mM $CaCl_2$. Digestion products were loaded at a flow rate of 1 ml/min onto the Hiload 16/60 Superdex 75 gel filtration column (Amersham Biosciences) equilibrated in 20 mM Hepes, pH 7.5, 150 mM NaCl. The

TABLE I
Data collection and refinement statistics

Data statistics	Free SH3^{p40}	SH3^{p40}/polyP^{p47} complex
Data collection details		
Space group	$P2_1$	$P2_12_12_1$
Cell dimensions (Å, degree)	a = 35.2; b = 45.2; c = 35,1; β = 111.4	a = 39.6; b = 50.5; c = 68.2
SH3 per asymmetric unit	2	2
Data collection statistics		
Resolution range (Å)	20–2	23.7–1.46
Unique reflections	6876	23,423
Redundancy	3.4 (2.8)[a]	5.0 (4.0)[b]
Completeness (%)	98.1 (90.9)[a]	94.3 (83.7)[b]
I/σ (I)	3.7 (2.4)[a]	13 (3.1)[b]
R_{merge} (%)	10.8 (26.9)[a]	2.9 (20.4)[b]
Refinement statistics		
R factor (R_{cryst}/R_{free})	24.7/25.0	18.1/20.7
No. of atoms per asymmetric unit	943	1396
No. of protein atoms	882 (33) [c]	1135 (16) [c]
No. of water molecules	61 (41) [c]	227 (30) [c]
Root mean square deviation		
Bond length (Å)	0.007	0.009
Bond angle (°)	1.3	1.5

[a] Values in parentheses indicate the highest resolution shell: 2.04–2.10 Å.
[b] Values in parentheses indicate the highest resolution shell: 1.46–1.54 Å.
[c] Values in parentheses indicate the average B-factors (Å^2).

resulting protein fractions containing SH3^{p40} were concentrated to 14 mg/ml. The final recombinant protein comprised 5 N-terminal residues (LIKHM) from the previous linker, as determined by N-terminal sequencing.

C-SH3^{p67}—The sequence encoding residus 455–516, the C-terminal SH3 domain of p67^{phox} (C-SH3^{p67}), was amplified by PCR and cloned into pET15b (Novagen). The sequence of the resulting vector named, pET-CSH3^{p67}, was checked by sequencing. The protein was expressed in *E. coli* BL21(DE3) strain and first enriched by affinity chromatography on a Ni^{2+}-nitrilotriacetic acid column equilibrated in 20 mM Hepes, pH 7.5, 150 mM NaCl, 20 mM imidazole and eluted with a linear gradient of imidazole (20–300 mM). The His tag was cleaved with thrombin (Sigma) overnight at 20 °C with 2.4 units thrombin/mg of protein, and further purification was carried out by gel filtration on Superdex 75 (Amersham Biosciences) equilibrated with 150 mM NaCl, 20 mM Hepes, pH 7.5, 2 mM dithiothreitol.

Proline-rich region of p47^{phox}

The peptide KPQPAVPPRPSAD (residues 360–372 of p47^{phox}) was synthesized using conventional technology. The peptide was purified by HPLC using a C18 column and a linear gradient of 5–60% CH_3CN in water with 0.1% trifluoroacetic acid. The peptide was lyophilized prior to resuspension in water (50 mg/ml) for crystallization. Peptide concentration was determined by amino acids analysis. The six other peptides were synthesized by Neosystem (Table II). They were repurified by HPLC using a C18 column and a linear gradient of 5–60% CH_3CN in water with 0.1% trifluoroacetic acid. The purity of the peptides was higher than 95%.

Tryptophan Fluorescence Spectroscopy

Fluorescence measurements were performed at 20 °C in a Fluoromax (Jobin-Yvon) spectrofluorometer. The excitation wavelength was set at 290 nm, and the fluorescence emission was recorded between 295 and 450 nm. Increasing amounts of peptide were added to a fluorescence cuvette containing 100 μl of a SH3^{p40} solution. The resulting shift of maximal emission wavelength ($\Delta\lambda$) was monitored over a large range of p47^{phox} peptide concentration. The equilibrium dissociation constant (K_d value) characterizing the SH3/polyproline interaction was determined according to Equation 1 under the assumption that the fluorescence shift $\Delta\lambda$ was proportional to the concentration of the SH3/polyproline complex.

Considering $\Delta\lambda = \Delta\lambda_{max}([exp]/[SH3t])$,

$$K_d = [SH3t]\left(\frac{\Delta\lambda}{\Delta\lambda_{max}} - 1\right) + [pept]\left(\frac{\Delta\lambda_{max}}{\Delta\lambda} - 1\right) \qquad \text{(Eq. 1)}$$

where [SH3t] = total SH3^{p40phox} concentration, [pept] = total peptide concentration, [cpx] = complex concentration, $\Delta\lambda = \lambda_{SH3} - \lambda$, and $\Delta\lambda_{max} = \lambda_{SH3} - \lambda_{cpx}$.

Crystallization

Crystals were grown by hanging-drop vapor diffusion by mixing equal volumes of protein and reservoir solutions. The best diffracting crystals of free SH3^{p40} were obtained at 14 °C from a protein solution at 14 mg/ml in 20 mM Hepes, pH 7.5, 150 mM NaCl, and a reservoir solution containing 200 mM sodium acetate, pH 4.6, 100 mM ammonium sulfate, 40% polyethylene glycol monomethyl ether 2000. Crystals grew up within 2 months. Crystals of SH3^{p40}/polyPro^{p47} were grown at 20 °C with a reservoir containing 100 mM sodium citrate/citric acid, pH 5, 2.4 M ammonium sulfate. To obtain the complex, SH3^{p40} at 14 mg/ml in 20 mM Hepes, pH 7.5, and 150 mM NaCl was mixed at 1:5 molar ratio to the polyproline peptide solution (50 mg/ml in water). This ratio was determined from the dissociation constant extrapolated from fluorescence measurements and corresponds to the presence of roughly 90% complexed SH3^{p40}/polyPro^{p47}. Crystals were obtained within two or 3 weeks. Their size and quality were improved by macro-seeding with a reservoir solution containing 100 mM citrate/citric acid, pH 5, and 2.2 M ammonium sulfate to a final size of 200 × 50 × 20 μm.

Prior to x-ray diffraction experiments crystals were flash frozen in liquid nitrogen. Free SH3^{p40} crystals were frozen directly from the mother liquor and SH3^{p40}/polyPro^{p47} crystals were soaked in a cryobuffer (reservoir solution containing 15% glycerol) prior to freezing.

Data Collection, Structure Determination, and Refinement

Free SH3^{p40}—Free SH3^{p40} crystals cooled at 100 K diffracted to 2 Å on a rotating anode (Nonius) using a MARCCD detector (Mar 345, X-ray Research). Crystals diffracted anisotropically and were highly mosaic; several crystals were screened to obtain the best diffracting crystal. Data were processed with DENZO and SCALEPACK (42) and reduced with the CCP4 package (43). Statistics are shown in Table I. The space group is pseudo-orthorhombic and R_{sym} values are 11.5 and 10.8% in $C222_1$ or $P2_1$ space groups, respectively. The structure of SH3^{p40} was solved by molecular replacement using the program AMORE (44). The search model was a superposition of eight SH3 structures: SEM (PDB code 1SEM), spectrin (PDB code 1SHG), tyrosine kinase Abl (PDB code 1ABQ), tyrosine kinase Fyn (PDB code 1FYN), Eps8 (PDB code 1I0C), Crk (PDB code 1B07), amphiphysin 2 (PDB code 1BB9), Hck (PDB code 1BU1), restricted to main chain atoms. These SH3 domains share 38, 33, 15, 20, 22, 24, 22, and 18% sequence identity with SH3^{p40}, respectively. Molecular replacement using each structure individually as a starting model failed. The model of SH3^{p40} was refined using CNS (45), and 5% of the data (randomly selected reflections) was excluded from refinement as free R-flagged reflections. The refinement was initially tried in both space groups $C222_1$ and $P2_1$; the R_{cryst} values clearly excluded the orthorhombic form. The asymmetric unit contains two SH3^{p40} domains, which were refined by constraining the core of the monomers (*i.e.* β-strands excluding the loops) with a 2-fold symmetry.

SH3^{p40}/PolyPro^{p47}—The crystals flash frozen to 100 K diffracted poorly only showing elongated spots to 3.5 Å and a very high mosaicity

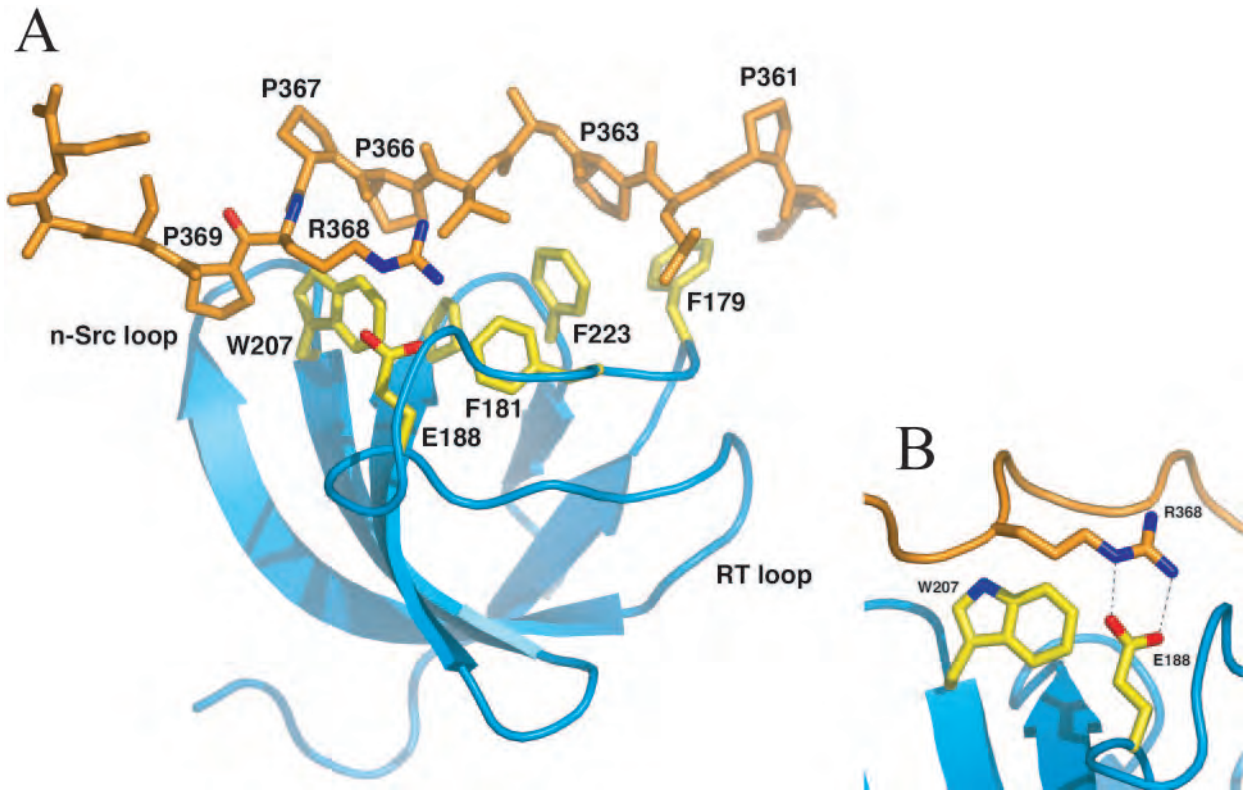

FIG. 2. **The structure of SH3^{p40} in complex with the polyproline motif of p47;phox.** *A*, overall fold of the complex. The figure highlights the core SH3^{p40} structure formed by two β-sheets (in *blue*). The p47^{phox} polyproline peptide (residues 360–372) is depicted in *orange*. The main SH3^{p40} residues interacting with the polyPro^{p47} peptide are shown in *yellow* and labeled. *B*, a close-up view of R368^{p47}. The figure shows p40^{phox} residues that interact with R368^{p47} through van der Waals contacts (Trp-207^{p40}) or electrostatically (Glu-188^{p40}). The figure was drawn with the program PyMol (www.pymol.org).

that prevented data integration, despite the fact that no crystalline ice was formed in the liquid surrounding the crystal. To improve the diffraction, the crystal temperature was raised by blocking the cryostream for a few seconds and rapidly dropped back to 100 K. After a few cycles of annealing, crystals cooled to 100 K diffracted to high resolution. A complete data set to 1.46 Å was collected on beamline BM30A, European Synchrotron Radiation Facility-Grenoble, using a Mar CCD detector and a wavelength of 0.98 Å. The same programs as for the free SH3^{p40} were used for data treatment; statistics are shown in Table I. The space group is $P2_12_12_1$ with a unit cell of a = 39.6 Å, b = 50.5 Å, c = 68.2 Å. Free SH3^{p40} was used as a search model to solve the structure of SH3^{p40}/polyPro^{p47} by molecular replacement. SH3^{p40}/polyPro^{p47} crystals contain two 1:1 complexes in the asymmetric unit. After a few cycles of refinement with CNS, the polyproline peptide was build automatically using the program ARP (46). During the refinement, no constraints between the molecules in the asymmetric unit were applied.

Both structures, free SH3^{p40} and SH3^{p40}/polyPro^{p47}, were refined by iterative cycles of manual corrections with O (47) and energy minimization or simulated annealing followed by *B*-factor refinements using CNS. The models were refined to final R_{cryst} and R_{free} of 24.7 and 25.0% at 2 Å resolution for the SH3^{p40} and R_{cryst} and R_{free} of 18.1 and 20.7% at 1.46 Å resolution for SH3^{p40}/polyPro^{p47}. The quality of the final models was analyzed with Procheck (48) and Whatcheck (49).

RESULTS

SH3^{p40} Structures—The crystalline arrangement of SH3^{p40} crystals consists of tightly packed protein layers with weak connections in between layers that involve mainly C-terminal Lys-228^{p40} from one monomer interacting with a symmetry related Lys-228^{p40} from the second monomer. The weak connections in one direction (which is parallel to a–c) probably explain the anisotropy. The crystal packing for SH3^{p40}/polyPro^{p47} is different and more compact. In both crystal forms, the two molecules present in the asymmetric unit are very similar with root mean square deviations on main chain atoms of 0.06 and 0.3 Å for SH3^{p40} and SH3^{p40}/polyPro^{p47}, respectively.

The free SH3^{p40} structure comprises residues 174–228 for both monomers present in the asymmetric unit and 61 water molecules. The SH3^{p40}/polyPro^{p47} structure consists of residues 169–228 for both SH3^{p40} (chains A and B) and of residues 360 to 372 (chain C) and 360–369 (chain D) for the polyPro^{p47} peptides associated to monomers A and B, respectively. PolyPro^{p47} peptides are acetylated in their N-terminal end. In addition to the protein, four sulfate ions, two trifluoroacetic acid molecules and 227 water molecules per asymmetric unit were located from the electron density maps and refined. The two SH3^{p40} structures, free or in complex with polyPro^{p47}, are very similar even in the peptide binding site. Because of the much higher resolution of SH3^{p40}/polyPro^{p47} crystals, this structure is discussed below.

The general topology of SH3^{p40} is very similar to that of other SH3 domains (50–53) and consists of five β-strands arranged as two orthogonal β-sheets, forming a compact antiparallel β-barrel (Fig. 2*A*). The binding site located at the surface of the barrel is flanked by the RT and n-Src loops. These loops are variable among SH3 domains and contribute to the specificity of polyproline binding.

Polyproline Binding Site—Residues 360–369 of polyPro^{p47} (360^{p47} to 369^{p47}) are well determined in both molecules present in the asymmetric unit. They adopt a polyproline helix of type II (PPII) conformation with three residues per turn. The peptide is located in a groove formed by hydrophobic residues highly conserved among SH3 domains and negative electrostatic patches on the SH3^{p40} surface (Figs. 2*A* and 3*A*). Residues 360^{p47} to 369^{p47} interact with SH3^{p40} mainly via van der Waals contacts involving Phe-179^{p40}, Asn-184^{p40}, Asp-206^{p40}, Trp-207^{p40}, Pro-220^{p40}, and Phe-223^{p40} located in the hydrophobic pocket of SH3^{p40} (Fig. 4). A few hydrogen bonds are also involved, in particular between the indole nitrogen of

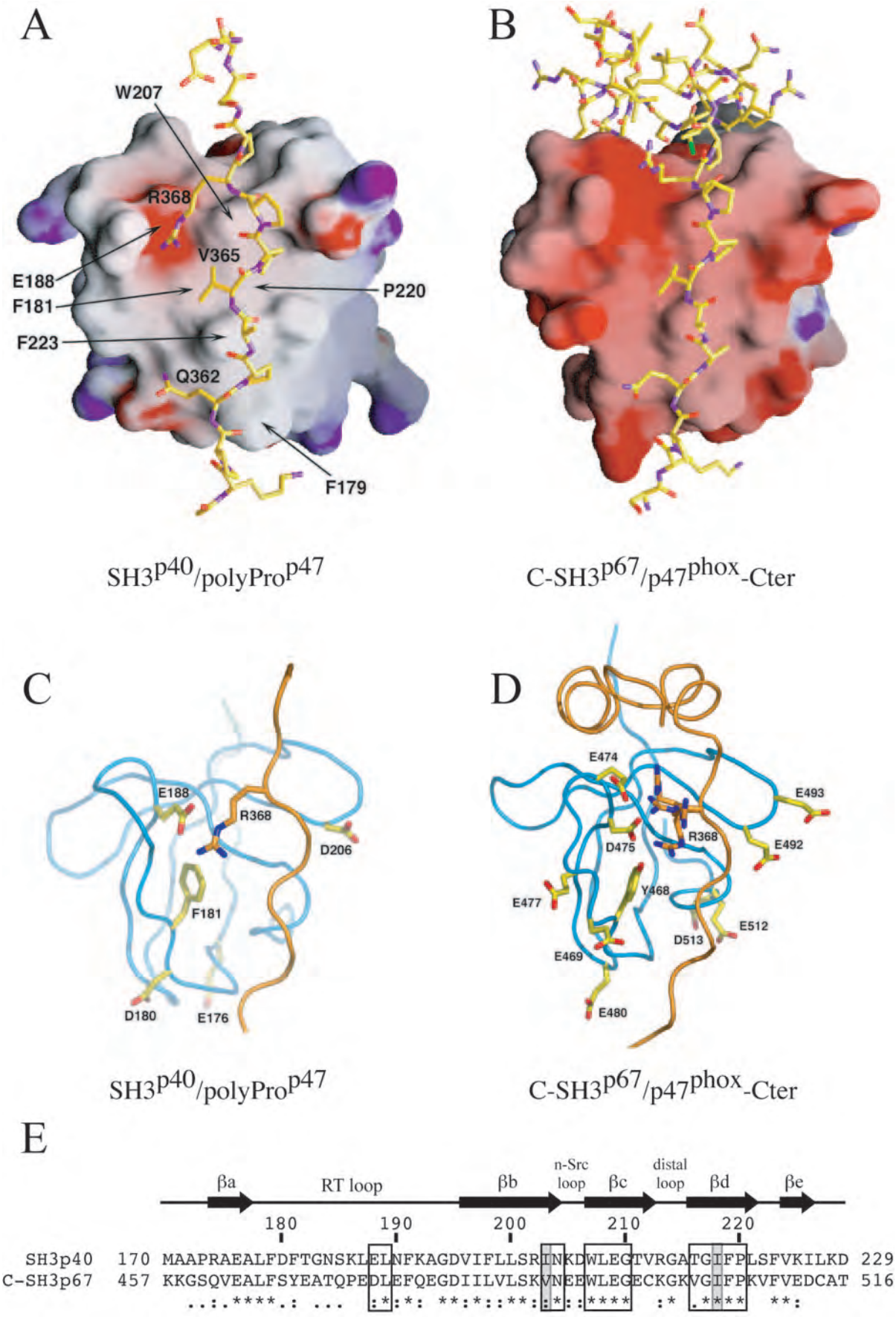

FIG. 3. **Comparison of SH3^{p40}/polyPro^{p47} and C-SH3^{p67}/p47^{phox}-Cter.** The C-SH3^{p67}/p47^{phox}-Cter structure shown in the figure is the most representative NMR structure (PDB code 1k4u). In *A* and *B* the electrostatic potential surfaces are compared. Positive and negative surfaces are shown in *blue* and *red*, respectively. *A*, SH3^{p40}. The surface shows a negative patch in the vicinity of Glu-188^{p40} interacting with Arg-368^{p47}. *B*,

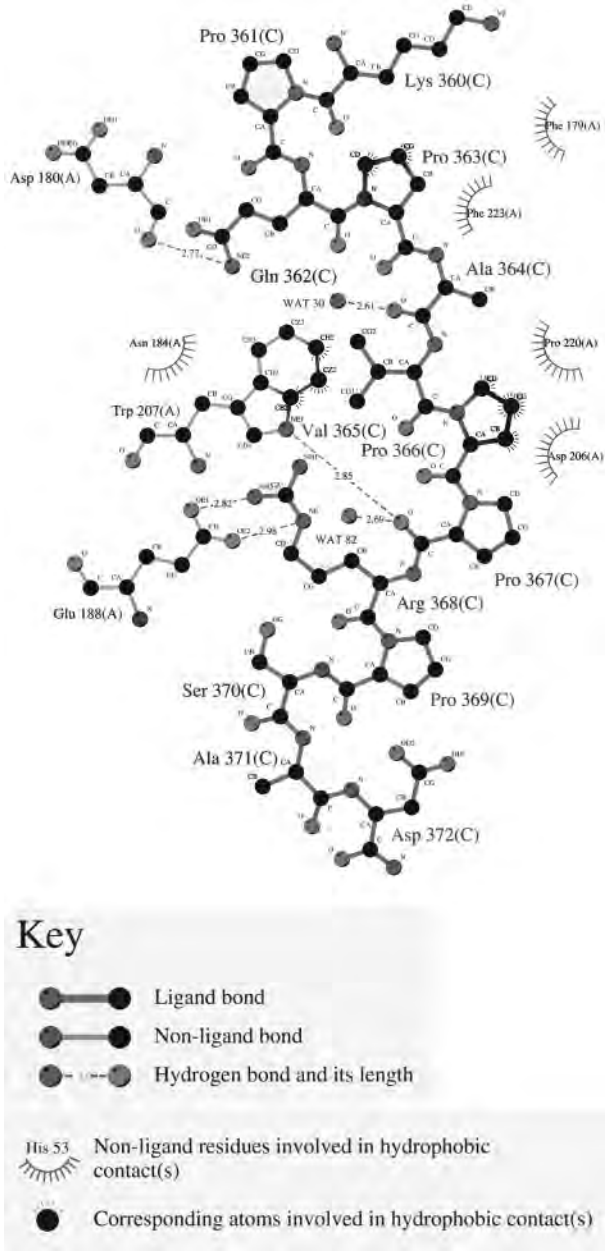

FIG. 4. **Interaction between polyPro^{p47} and SH3^{p40}.** The plot shows the p47^{phox} polyproline motif (residue Cys (*C*)) surrounded by interacting residues of SH3^{p40} (residue Ala (*A*)). p40^{phox} residues at hydrogen bond distances from polyPro^{p47} are indicated (distances in Å), and residues within van der Waals distances are labeled. The figure was drawn with LIGPLOT (59).

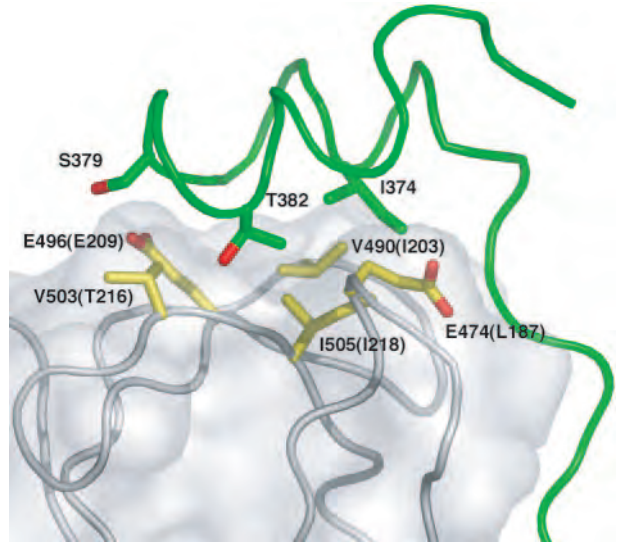

FIG. 5. **Interaction interface of the non-P*XXP* motif of p47^{phox}-Cter with C-SH3^{p67}.** The surface of C-SH3^{p67} is drawn in *white* and p47^{phox}-Cter in *green*. The complex used is the most representative structure from PDB file 1k4u (41). Side chain residues of C-SH3^{p67} are in *yellow*. The corresponding residues of SH3^{p40} are indicated in *parentheses*. The figure was drawn with PyMol.

Trp-207^{p40} and the carbonyl oxygen of Pro-367^{p47} or between the Nϵ of Gln-362^{p47} and the carbonyl oxygen of Asp-180^{p40}. Arg-368^{p47} seems to play a key structural role in the complex as it is involved in several interactions: an electrostatic bonding with Glu-188^{p40} located in the RT loop of SH3^{p40} and van der Waals contacts involving the aliphatic side chain of Arg-368^{p47} and Trp-207^{p40} (Fig. 2*B*). Two water molecules are also involved in the peptide binding and bridge Ser-222^{p40} to Ala-364^{p47} and Asn-204^{p40} to Pro-367^{p47}. As a result of the complex formation, Trp-207^{p40} is buried and hidden from the solvent in SH3^{p40}/polyPro^{p47} in contrast to the free SH3^{p40}.

Comparison of SH3^{p40}/PolyPro^{p47} and C-SH3^{p67}/p47^{phox}-Cter—SH3^{p40} shares 44% sequence identity with C-SH3^{p67} (Fig. 3*E*), and the structures superimpose with root mean square deviations on main chain atoms of less then 1 Å. The structure of C-SH3^{p67} was solved by NMR in complex with the C-terminal end of p47 (residues 359–390, PDB code 1k4u) (41). Fig. 3 compares the electrostatic surfaces of both SH3s showing the large negative surface for C-SH3^{p67} due the presence of many acidic residues. In our structure the side chain of Arg-368^{p47} has a low *B*-factor indicative of a very well defined position in the complex, in line with a strong electrostatic interaction with Glu-188^{p40}. Negatively charged surfaces are limited to Glu-188^{p40} located in the SH3^{p40} RT loop (Fig. 3, *A* and *C*). On the contrary, in C-SH3^{p67}/p47^{phox}-Cter (41), the side chain of Arg-368^{p47} has multiple conformations as seen from the various NMR structures. In contrast, other residues in the vicinity of Arg-368^{p47} presented only one side chain conformation. The C-SH3^{p67} RT loop contains up to five acidic amino acids responsible for a strong negatively charged surface and allowing multiple positioning of the Arg-368^{p47} side chain (Fig. 3, *B* and *D*). The superposition of both SH3 structures also highlights possible interactions of SH3^{p40} with the C-terminal end of p47^{phox} beyond polyPro^{p47} residues present in our structure. Previously some residues of C-SH3^{p67} were identified as part of the binding surface using NMR cross-saturations experiment (41). As seen in sequence alignment of both SH3 (*boxes* in Fig. 3*E*), all these residues are highly conserved (77% identity) or closely related in SH3^{p40}. Ile-505^{p67} and Val-490^{p67} were identified as being particularly important in the interaction (*gray boxes* in Figs. 3*E* and Fig. 5).

Several serine residues in p47^{phox}-Cter have been shown to be critical in NADPH oxidase activation. Among the serine

C-SH3^{p67}. The surface is highly negative. The difference of Arg-368^{p47} binding mode is highlighted in *C* and *D*. SH3 side chains of mainly acidic residues are shown in *yellow* and Arg-368^{p47} is in *orange*. *C*, SH3^{p40}/polyPro^{p47} (this work). *D*, a sample of various orientations from the different NMR structures is shown for Arg-368^{p47}. *E*, sequence alignment between SH3^{p40} and C-SH3^{p67}. Residues of C-SH3^{p67} involved in the p47^{phox}-Cter interaction (41) are *boxed*. Moreover, *gray boxes* underline residues Ile-505^{p67} and Val-490^{p67} directly in contact with non-P*XXP* motif of p47^{phox}-Cter. Residues are referred as identical (*), strongly similar (:), or weakly similar (.). Surfaces *A* and *B* were drawn with GRASP (66). *C* and *D* were drawn with PyMol.

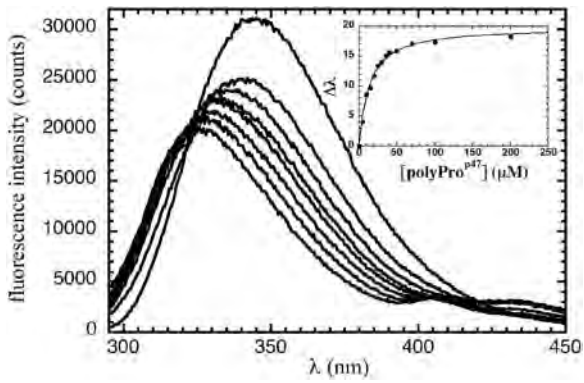

FIG. 6. **Intrinsic tryptophan fluorescence of C-SH3^{p67} *versus* polyproline concentration.** Binding of the P*XX*P wild type peptide to a 5 μM C-SH3^{p67} solution is followed by the λ_{max} shift, and the fluorescence intensity decreases. Fluorescence was recorded after gradual addition of peptide from 0 to 200 μM (the highest fluorescence intensity corresponding to 0 μM). The *inset* shows the variation of λ_{max} as a function of peptide concentration.

residues studied herein, only Ser-370^{p47} is present in our structure. Its side chain points toward the solvent and is clearly not involved in the interaction with SH3^{p40}. From 1k4u coordinates, the same observation is made for C-SH3^{p67}. Ser-359^{p47} and Ser-379^{p47} are not present in our peptide, their interaction is extrapolated from the superposition of 1k4u coordinates with our structure. Ser-359^{p47} is located at the N-terminal end of the peptide, its location is close to Glu-480^{p67} equivalent to Ala-193^{p40}. Ser-379^{p47} interacts with Glu-496^{p67} (conserved in SH3^{p40}) and from our extrapolated structure is likely to interact also with SH3^{p40}.

Interaction between p47^{phox} and p40^{phox} or p67^{phox} Characterized by Fluorescence Measurements—We have measured the dissociation constants of a series of peptides corresponding to the P*XX*P motif (358–372) or the whole p47^{phox}-Cter (358–390) with SH3^{p40} or the C-SH3^{p67} (Fig. 6 and Table II). Both types of peptides (short or long) are almost identical to the peptides used for the structural studies and therefore they will be denoted in the following text polyPro^{p47} and p47^{phox}-Cter, respectively. The entire proteins, p47^{phox} and p40^{phox}, interact with an estimated K_d of 5 μM (19, 27). This value is 40 times lower than the K_d between SH3^{p40} and polyPro^{p47}, suggesting that the interaction between the two proteins involves other regions in addition to the SH3/polypro couple. The K_d of p47^{phox}-Cter toward SH3^{p40} is 380 times lower than that of PolyPro^{p47} alone. Thus, our measurements show that the binding between SH3^{p40} and p47^{phox}-Cter implicates both the P*XX*P motif and a non-P*XX*P region of p47^{phox}-Cter. Interestingly, it corresponds to the same interacting regions for p47^{phox} with C-SH3^{p67} as identified by Kami *et al.* (41). In addition, our K_d value for the C-SH3^{p67}/p47^{phox}-Cter interaction (Table II) is consistent with their results. Although the same regions of p47^{phox} seem to be involved in the interaction with both SH3, it is clear from Table II that the complex with C-SH3^{p67} is favored (K_d ratio of 11, line 4 in Table II). The preference for C-SH3^{p67} is already observed for the short polyPro^{p47} peptide (K_d ratio of 20, line 1 in Table II), and the additional residues of p47^{phox}-Cter do not modify significantly the difference in affinity toward SH3^{p40} and SH3^{p67} (comparison of line 1 and line 4 in Table II). Therefore, the contribution of the strict P*XX*P motif by itself induces the preference for p67^{phox}. The difference in affinities of p47^{phox}-Cter for both SH3 domains obtained from our fluorescence measurements is consistent with our structural data. Indeed, the comparison of the structures highlights a strong difference in the electrostatic potential surface between the two SH3 along the polyPro binding site that enhances the binding of polyPro^{p47} to C-SH3^{p67}, whereas only few differences are present among the interactions with the extra C-terminal residues.

Effect of Ser-359/Ser-370 or Ser-379 Phosphorylation on the Binding of p47^{phox} to SH3^{p40} and C-SH3^{p67}—Table III summarizes data from the literature on the specific role of each serine phosphorylation. We have investigated the role of the phosphorylatable serines surrounding polyPro^{p47} on SH3 recognition. Various peptides have been synthesized, in which Ser-359^{p47} and Ser-370^{p47} are either substituted by aspartates or phosphorylated (Table II). Both modifications (mutation or phosphorylation), in either short or long peptide, do not affect significantly the binding to SH3^{p40}. Therefore, as a first approximation, our observations validate the Ser-to-Asp mutation approach which has been widely used to mimic serine phosphorylations (4, 5, 32). The affinity of C-SH3^{p67} for short polyPro^{p47} peptides is moderately reduced by aspartate mutations and slightly more by phosphorylations. Even in the absence of a direct interaction of Ser-359^{p47} and Ser-370^{p47} with C-SH3^{p67}, the higher electronegative character of additional phosphates compared with Asp residues, added to the strong electronegative surface of C-SH3^{p67}, might explain this effect. However, even if phosphorylation reduces the K_d ratios toward both SH3 from 20 to 5 (comparison of lines 1 and 3 in Table II), C-SH3^{p67} still has a stronger affinity than SH3^{p40}. With p47^{phox}-Cter, in a native form or with Ser-to-Asp mutations, no major differences are observed, probably because the increase of binding interface with the addition of the non-P*XX*P region of p47^{phox} masks the small differences in affinity observed among the short peptides.

To address the question of the role of Ser-379^{p47} during activation, binding properties of p47^{phox}-Cter, with Ser-379^{p47} phosphorylated or not, have been investigated. Upon phosphorylation, the K_d ratios of the two peptides toward both SH3s increase by a factor of 5 and 30 for SH3^{p67} and SH3^{p40}, respectively (comparison of lines 4 and 6 in Table II), denoting an important modification of the interaction between p47^{phox}-Cter and both SH3.

We show herein that phosphorylations of Ser-359^{p47} and Ser-370^{p47} have no significant impact neither on the binding of p47^{phox}-Cter to both SH3s nor in modifying the binding preference between SH3^{p67} and SH3^{p40}. The side chain orientation of the two serines in the structures explains the low effect of the phosphorylation of Ser-359^{p47} and Ser-370^{p47}; both side chains point away from the interaction. In contrast, the phosphorylation of Ser-379^{p47} destabilizes SH3^{p40}/p47^{phox}-Cter and C-SH3^{p67}/p47^{phox}-Cter with a stronger effect for SH3^{p40}.

DISCUSSION

Structural Determinants of the Interaction between p47^{phox}-Cter and SH3^{p40}

Two possible SH3 interacting partners have been identified for the polyproline motif of the p47^{phox} C terminus: SH3^{p40} and C-SH3^{p67} (Fig. 1*A*). Various models for the cytosolic complex in the resting state have been proposed, arguing for polyPro^{p47} complex with either SH3^{p40} or C-SH3^{p67} (10, 12, 31). Several studies based on the respective affinities of both p40^{phox} and p67^{phox} for p47^{phox} (19, 27, 54, 55) led to the accepted model of a trimeric organization (Fig. 1*B*) in which C-SH3^{p67} interacts with polyPro^{p47}, while p40^{phox} and p67^{phox} are held together via a PB1/PB1 interaction (27). Despite the importance of SH3-polyproline interactions in the NADPH oxidase complex, no high resolution structural information is available to explain the favored interactions occurring within the p47^{phox}/p67^{phox}/p40^{phox} complex. Previous NMR-based structure of C-SH3^{p67}/polyPro^{p47} highlighted the contribution of the whole p47^{phox}

TABLE II

Dissociation constants comparison of p47^{phox} C-terminal peptides towards SH3^{p40} and C-SH3^{p67}

The dissociation constants of the various p47^{phox} C-terminal peptides were determined by tryptophan fluorescence as described under "Experimental Procedures". Standard deviations were calculated from fits to individual data sets.

p47^{phox} peptides	SH3^{p40}	C-SH3^{p67}	K_d^{p40}/K_d^{p67}	p40^{phox}	p67^{phox}
	μM	μM		μM	μM
p47^{phox} (1–390)			250	5[a,b]	0.02[b]
PolyPro^{p47} (358–372)					
1. RSKPQPAVPPRPSAD	200 ± 20	10 ± 0.7	20		
2. RDKPQPAVPPRPDAD	270 ± 27	31 ± 1.9	8.7		
3. RS(PO_3H_2)KPQPAVPPRPS(PO_3H_2)AD	268 ± 13	61 ± 4.3	4.4		
p47^{phox}-Cter (358–390)					
4. RSKPQPAVPPRPSADLILNRCSESTKRKLASAV	0.52 ± 0.11	0.047 ± 0.030	11		
5. RDKPQPAVPPRPDADLILNRCSESTKRKLASAV	1.17 ± 0.28	0.060 ± 0.030	20		
6. RSKPQPAVPPRPSADLILNRCS(PO_3H_2)ESTKRKLASAV	14.4 ± 0.60	0.290 ± 0.037	50		

[a] From Ref. 19.
[b] From Ref. 27.

TABLE III

Review of effects of some mutations on p47^{phox} serines susceptible to phosphorylations

All results reported in this table come from *in vivo*, whole cell systems, using EBV transform p47^{phox}-deficient B cells expressing different forms of p47^{phox} except for Ref. 32 where K562 cell systems have been used with the same results.

Serines	Mutants	Phosphorylations on other serines	Membrane transfer	NADPH oxidase activity	Ref.
	Wildtype	+	+	+	
Ser-303/304	S303A/S304A	+	+	−	4, 3, 32
	S303E/S304E	+	+	+	4
	S303D/S304D	+	+	−	4
Ser-328	S328A	ND[a]	ND[a]	−	3, 32
Ser-359/370	S359A/S370A	−	−	−	5, 3
	S359K/S370K	−	−	−	5
	S359D/S370D	+	+	−	5
	S359E/S370E	+	+	−	5
Ser-379	S379A	+	+/−	−	33

[a] ND, not determined.

C-terminal sequence, downstream the P*XX*P motif (41). Indeed, this additional non-P*XX*P sequence showed an extra interaction that results in high affinity and specificity. This suggested that the non-P*XX*P region can be responsible for stronger interactions with C-SH3^{p67} rather than SH3^{p40}. To discuss the role of the non-P*XX*P region of p47^{phox} in SH3^{p40}/p47^{phox}, we compared the binding properties of p47^{phox}-Cter to the SH3 modules of p67^{phox} and p40^{phox}, based on fluorometric results and three-dimensional structure analysis. Fluorescence measurements reveal three major points: 1) as for C-SH3^{p67}, SH3^{p40} is able to establish an additional interaction with the non-P*XX*P motif of p47^{phox}-Cter, 2) the stronger affinity for C-SH3^{p67} than for SH3^{p40} is due to the P*XX*P motif itself and more precisely the Arg-368^{p47} binding mode, and 3) the isolated SH3^{p40} module presents a higher affinity for p47^{phox}-Cter than the whole p40^{phox} protein for p47^{phox}.

p40^{phox} Interacts with a PXXP and a Non-PXXP Motif of p47^{phox}-Cter—SH3^{p40} exhibits a K_d of 0.52 μM for p47^{phox}-Cter, which is a high affinity compared with 10–50 μM for most SH3-peptide interactions. Using p47^{phox} peptides corresponding to the P*XX*P motif (residues 358–372) or corresponding to p47^{phox}-Cter (residues 358–390), we show that the C-terminal non-P*XX*P region is not responsible for the difference in affinities toward the two SH3 modules. Despite the fact that the C-terminal region allows in each case a much stronger affinity than with the P*XX*P motif alone, the specificity resides mainly within the P*XX*P motif recognition. Interaction of both SH3 with the non-P*XX*P motif of p47^{phox}-Cter seems to be identical, the residues of C-SH3^{p67} identified as part of the binding surface for this noncanonical interaction have been previously identified using NMR cross-saturation experiments (Fig. 3*E*) (41).

Stronger Affinity of p47^{phox}-Cter toward SH3^{p67} Is Explained by the Arg-368^{p47} Binding Mode—Interactions of polyPro^{p47} with both SH3 are mainly hydrophobic except for Arg-368^{p47}. A strong difference in the electrostatic potential surface of the two SH3 may be responsible for the stronger binding of P*XX*P motif to C-SH3^{p67}. Indeed, Arg-368^{p47} interacts only with Glu-188^{p40} in our structure, whereas it has multiple interacting mode with the RT loop of the C-SH3^{p67}. Previous experiments have focused on the importance of Arg-368^{p47} in the binding strength (41): (*i*) replacement of this arginine by an alanine decreases affinity for C-SH3^{p67} by a factor of 625 and (*ii*) binding of the isolated non-P*XX*P motif of p47^{phox} (residue 369^{p47} to 390^{p47}) is observed only when Arg-368^{p47} is added to the peptide. A much stronger negatively charged RT loop in C-SH3^{p67} than in SH3^{p40} can account for a higher association of the two binding partners and/or a stronger efficiency in keeping the protein complexed.

Modules Flanking SH3^{p40} Modulate Its Affinity for p47^{phox}—Our fluorescence measurements reveal that the affinity between p47^{phox} and p67^{phox} is identical to the affinity between p47^{phox} peptides and C-SH3^{p67} domain (Table II). This confirms that the p47^{phox}-p67^{phox} complex is completely determined by C-SH3^{p67} and p47^{phox}-Cter sequences. On the contrary, strong difference in affinity between p47^{phox} and p40^{phox} on one side and between p47^{phox}-Cter and SH3^{p40} on the other side is observed (Table II). The presence of PX and PB1 domains on each side of SH3^{p40} lowers the affinity toward p47^{phox} by 1 order of magnitude. Thus, in p40^{phox}, the binding properties of SH3^{p40} are tuned down by the flanking modules. Interestingly, Lopes *et al.* (26) have shown recently that phosphorylation of p40^{phox} on threonine 154 changes the conformation of the protein thus resulting in an inhibitory effect on NADPH oxidase. Thr-154^{p40} is located between the PX and the SH3 domains (26), and the authors proposed that, after its phosphorylation, SH3^{p40} could be exposed and compete with p67^{phox} for p47^{phox} binding. Moreover, Sathyamoorthy *et al.* (24) reported

that transient expression of the SH3^{p40} domain *in vivo* inhibits more efficiently the NADPH oxidase than the full-length p40^{phox}. Although the role of p40^{phox} (inhibitory or stimulatory) is still a matter of debate, these observations are in line with our results of an increased affinity toward p47^{phox} of SH3^{p40} alone with respect to the whole p40^{phox}. However, such an increase in affinity due to a possible exposure of SH3^{p40}, is not sufficient to compete with the strength of the p67^{phox}/p47^{phox} interaction (Table II). Additional effects have to occur that might be related to additional phosphorylations on p67^{phox} (56, 57), p40^{phox} (58), and particularly p47^{phox}, which is polyphosphorylated (2, 3).

Phosphorylation on p47^{phox} C Terminus; Consequences toward the SH3/PolyPro Interaction between Cytosolic Factors

Phosphorylation on Ser-359/370 of p47^{phox} Does Not Promote a Switch of p47^{phox} Binding from C-SH3^{p67} to SH3^{p40}—Data from numerous studies delineating the phosphorylation of p47^{phox} serine residues during the activation cascade are summarized in Table III. Globally they suggest (5) that Ser-359/370 are phosphorylated first, allowing subsequent phosphorylation of Ser-379 for an efficient membrane translocation and finally of Ser-303/304 to induce the activity of the complex. The effect of Ser-303/304 phosphorylation, in the activation mechanism, has been clearly unraveled and confirmed (4, 32, 36) and involves the phosphorylation of Ser-328^{p47} (32). Mutation of serines 359 and 370 to alanines abrogated completely the subsequent steps in the activation mechanism from consecutive phosphorylation on other serines to NADPH oxidase activation. In a cellular context, replacement of serines by glutamate or aspartate residues restored the phosphorylation events on other serines of p47^{phox} as well as membrane translocation of the cytosolic factors but not NADPH oxidase activity. Therefore prior phosphorylation of Ser-359/370 is necessary to allow subsequent phosphorylations and the activation cascade to take place (5). The presence of two phosphorylation sites, Ser-359/370, surrounding a polyproline motif crucial for the organization of the ternary complex suggested that phosphorylation may modify the interactions among the cytosolic factors during activation. Several groups suggested a possible switch from one SH3 to the other (24) during the phosphorylation process (17, 27, 58). At the molecular level, very little is known on the evolution of the interaction network between the cytosolic factors following phosphorylation. Until now studies have mainly focused on the phosphorylation consequences in the intramolecular organization of p47^{phox} itself. In our work, K_d measurements of p47^{phox} peptides, phosphorylated or not, reveal no significant modifications in the difference in affinity toward the isolated SH3 domains of p67^{phox} and p40^{phox}. Thus, the switch hypothesis of binding of p47^{phox} from C-SH3^{p67} to SH3^{p40}, as a direct effect of phosphorylations on SH3 affinities, can now be ruled out.

Recent work (30) has shown that in the resting state before any priming event, p47^{phox} was dissociated from the ternary complex in the cytoplasm. The ternary complex was seen only in phorbol 12-myristate 13-acetate-activated neutrophils. These results suggest that in a cellular context, despite a possible strong interaction of p47^{phox} with the p67^{phox}/p40^{phox} heterodimer as observed *in vitro* (27), phosphorylations are required for ternary complex formation. Here we show that such phosphorylations are fully compatible with the formation of p47^{phox}-Cter/C-SH3^{p67} complex, since they do not affect the dissociation constant. Thus, Ser-359/370 phosphorylation might promote the initial ternary complex formation in the neutrophil where the C terminus of p47^{phox} may not be accessible due to the cellular environment in contrast to recombinant cytosolic factors in solution.

Phosphorylation on Ser-379^{p47} Weakens Cytosolic Complex in Vitro—Finally we investigated consequences of phosphorylation on Ser-379^{p47} previously reported as a potential site of kinase action for NADPH oxidase regulation (2, 33). The C-SH3^{p67}/p47^{phox}-Cter structure solved by Kami *et al.* (41) shows that Ser-379^{p47} is accessible and can contribute to the binding of the non-P*XX*P motif. Depending on the various NMR structures, Ser-379^{p47} can establish an hydrogen bond with Glu-496^{p67}, one of the residues identified in the interaction interface (Figs. 3*E* and 5). As seen in Table II, phosphorylation of Ser-379^{p47} impairs the affinity of p47^{phox}-Cter for both SH3. This can be interpreted as a steric effect but more probably as a repulsive charge effect between the phosphorylated Ser-379^{p47} and the neighboring residues Glu-496^{p67} or Glu-209^{p40}. The consequence of this phosphate addition in p47^{phox}-Cter is not SH3 specific and weakens the cytosolic factor complex. Ser-379^{p47} was the first Ser whose mutation to Ala, reported in Table III, impaired oxidase activation and membrane translocation (33). The loss of affinity may be surprising for a translocation mechanism needing a tightly associated complex to co-migrate as a whole to the membrane for NADPH oxidase activation. However, upon Ser-379^{p47} phosphorylation the modification of affinity toward SH3^{p67} is moderate, contrary to the change of affinity toward SH3^{p40}. The only conclusion that can be drawn from our study is that Ser-379^{p47} phosphorylation will not promote SH3^{p40} binding. The clarification of the cellular role of this serine phosphorylation will have to await further studies.

In summary, the p47^{phox} binding preference toward p67^{phox} rather than p40^{phox} is attributable to a negative contribution of SH3^{p40} neighboring modules and the difference in the p47^{phox} polyPro binding properties is probably due to a strong difference in the negative net charge of the SH3 RT loops (Fig. 3). However, we show herein that SH3^{p40} is competent for p47^{phox} binding with a strong affinity and specificity involving both P*XX*P and the non-P*XX*P motif of p47^{phox}-Cter. The existence of a physiologic situation in the activation or regulation mechanism where a SH3^{p40}/p47^{phox} interaction takes place has not been evidenced so far. However, in light with the binding specificity of SH3^{p40} toward p47-Cter, the reported roles of p40^{phox} in oxidase activity regulation could arise from a possible p40^{phox}/p47^{phox} interaction occurring during the various steps of the NADPH oxidase activation/deactivation mechanism. Moreover, we have shown clearly that the phosphorylation event on Ser-359/370 cannot initiate the activation cascade through modification of the SH3 binding properties and therefore the molecular mechanism involved here has still to be deciphered. Finally, we have shown that a phosphate on Ser-379 has a deleterious effect on the strength of interaction of p47^{phox} with SH3^{p40} and C-SH3^{p67}.

In addition to a better understanding of the molecular basis of the polyproline-SH3 interactions within the cytosolic *phox* complex, and a clarification of the phosphorylation consequence in the complexes formation and their stabilities, this work provides the high resolution structure of the last p40^{phox} module not yet reported. Indeed, the crystal structures of PX and PB1 domains have been previously reported isolated (16) or in complex with p67^{phox} PB1 (29). Thus, the whole structure of p40^{phox} is now known as individual pieces. Deeper understanding in the structure-function relationship of p40^{phox} will have to await three-dimensional positioning of the different modules with respect to each others. Moreover, a clear and definitive view of the kinetics and order of the phosphorylation events on p47^{phox} but also on p40^{phox} and p67^{phox} will be es-

sential to solve the complete molecular puzzle of the activation cascade.

Acknowledgments—We are grateful to Dr. J. F. Hernandez for the synthesis of the p47^{phox} peptide 360–372, Corinne Vives for reading the manuscript, Philippe Frachet for help with HPLC purification of peptides, and Richard Kahn for his strong support in crystallographic data collection and treatment.

REFERENCES

1. Vignais, P. V. (2002) *Cell. Mol. Life Sci.* **59,** 1428–1459
2. el Benna, J., Faust, L. P., and Babior, B. M. (1994) *J. Biol. Chem.* **269,** 23431–23436
3. El Benna, J., Faust, R. P., Johnson, J. L., and Babior, B. M. (1996) *J. Biol. Chem.* **271,** 6374–6378
4. Inanami, O., Johnson, J. L., McAdara, J. K., Benna, J. E., Faust, L. R., Newburger, P. E., and Babior, B. M. (1998) *J. Biol. Chem.* **273,** 9539–9543
5. Johnson, J. L., Park, J. W., Benna, J. E., Faust, L. P., Inanami, O., and Babior, B. M. (1998) *J. Biol. Chem.* **273,** 35147–35152
6. Reeves, E. P., Lu, H., Jacobs, H. L., Messina, C. G., Bolsover, S., Gabella, G., Potma, E. O., Warley, A., Roes, J., and Segal, A. W. (2002) *Nature* **416,** 291–297
7. Heyworth, P. G., Curnutte, J. T., Nauseef, W. M., Volpp, B. D., Pearson, D. W., Rosen, H., and Clark, R. A. (1991) *J. Clin. Invest.* **87,** 352–356
8. Nisimoto, Y., Motalebi, S., Han, C.-H., and Lambeth, J. D. (1999) *J. Biol. Chem.* **274,** 22999–23005
9. Someya, A., Nagaoka, I., and Yamashita, T. (1993) *FEBS Lett.* **330,** 215–218
10. Wientjes, F. B., Hsuan, J. J., Totty, N. F., and Segal, A. W. (1993) *Biochem. J.* **296,** 557–561
11. Tsunawaki, S., Mizunari, H., Nagata, M., Tatsuzawa, O., and Kuratsuji, T. (1994) *Biochem. Biophys. Res. Commun.* **199,** 1378–1387
12. Dusi, S., Donini, M., and Rossi, F. (1996) *Biochem. J.* **314,** 409–412
13. Ponting, C. P., Ito, T., Moscat, J., Diaz-Meco, M. T., Inagaki, F., and Sumimoto, H. (2002) *Trends Biochem. Sci.* **27,** 10
14. Kanai, F., Liu, H., Field, S. J., Akbary, H., Matsuo, T., Brown, G. E., Cantley, L. C., and Yaffe, M. B. (2001) *Nat. Cell Biol.* **3,** 675–678
15. Ellson, C. D., Gobert-Gosse, S., Anderson, K. E., Davidson, K., Erdjument-Bromage, H., Tempst, P., Thuring, J. W., Cooper, M. A., Lim, Z. Y., Holmes, A. B., Gaffney, P. R., Coadwell, J., Chilvers, E. R., Hawkins, P. T., and Stephens, L. R. (2001) *Nat. Cell Biol.* **3,** 679–682
16. Bravo, J., Karathanassis, D., Pacold, C. M., Pacold, M. E., Ellson, C. D., Anderson, K. E., Butler, P. J., Lavenir, I., Perisic, O., Hawkins, P. T., Stephens, L., and Williams, R. L. (2001) *Mol Cell* **8,** 829–839
17. Fuchs, A., Dagher, M. C., Faure, J., and Vignais, P. V. (1996) *Biochim. Biophys. Acta* **1312,** 39–47
18. Ito, T., Nakamura, R., Sumimoto, H., Takeshige, K., and Sakaki, Y. (1996) *FEBS Lett.* **385,** 229–232
19. Grizot, S., Grandvaux, N., Fieschi, F., Faure, J., Massenet, C., Andrieu, J. P., Fuchs, A., Vignais, P. V., Timmins, P. A., Dagher, M. C., and Pebay-Peyroula, E. (2001) *Biochemistry* **40,** 3127–3133
20. Ito, T., Matsui, Y., Ago, T., Ota, K., and Sumimoto, H. (2001) *EMBO J.* **20,** 3938–3946
21. Tsunawaki, S., Kagara, S., Yoshikawa, K., Yoshida, L. S., Kuratsuji, T., and Namiki, H. (1996) *J. Exp. Med.* **184,** 893–902
22. Cross, A. R. (2000) *Biochem. J.* **349,** 113–117
23. Kuribayashi, F., Nunoi, H., Wakamatsu, K., Tsunawaki, S., Sato, K., Ito, T., and Sumimoto, H. (2002) *EMBO J.* **21,** 6312–6320
24. Sathyamoorthy, M., de Mendez, I., Adams, A. G., and Leto, T. L. (1997) *J. Biol. Chem.* **272,** 9141–9146
25. Vergnaud, S., Paclet, M. H., El Benna, J., Pocidalo, M. A., and Morel, F. (2000) *Eur. J. Biochem.* **267,** 1059–1067
26. Lopes, L. R., Dagher, M. C., Gutierrez, A., Young, B., Bouin, A. P., Fuchs, A., and Babior, B. M. (2004) *Biochemistry* **43,** 3723–3730
27. Lapouge, K., Smith, S. J., Groemping, Y., and Rittinger, K. (2002) *J. Biol. Chem.* **277,** 10121–10128
28. Nakamura, R., Sumimoto, H., Mizuki, K., Hata, K., Ago, T., Kitajima, S., Takeshige, K., Sakaki, Y., and Ito, T. (1998) *Eur. J. Biochem.* **251,** 583–589
29. Wilson, M. I., Gill, D. J., Perisic, O., Quinn, M. T., and Williams, R. L. (2003) *Mol. Cell* **12,** 39–50
30. Brown, G. E., Stewart, M. Q., Liu, H., Ha, V. L., and Yaffe, M. B. (2003) *Mol. Cell* **11,** 35–47
31. Fuchs, A., Dagher, M. C., and Vignais, P. V. (1995) *J. Biol. Chem.* **270,** 5695–5697
32. Ago, T., Nunoi, H., Ito, T., and Sumimoto, H. (1999) *J. Biol. Chem.* **274,** 33644–33653
33. Faust, L. R., el Benna, J., Babior, B. M., and Chanock, S. J. (1995) *J. Clin. Invest.* **96,** 1499–1505
34. Hiroaki, H., Ago, T., Ito, T., Sumimoto, H., and Kohda, D. (2001) *Nat. Struct. Biol.* **8,** 526–530
35. Karathanassis, D., Stahelin, R. V., Bravo, J., Perisic, O., Pacold, C. M., Cho, W., and Williams, R. L. (2002) *EMBO J.* **21,** 5057–5068
36. Groemping, Y., Lapouge, K., Smerdon, S. J., and Rittinger, K. (2003) *Cell* **113,** 343–355
37. Sumimoto, H., Hata, K., Mizuki, K., Ito, T., Kage, Y., Sakaki, Y., Fukumaki, Y., Nakamura, M., and Takeshige, K. (1996) *J. Biol. Chem.* **271,** 22152–22158
38. Ago, T., Kuribayashi, F., Hiroaki, H., Takeya, R., Ito, T., Kohda, D., and Sumimoto, H. (2003) *Proc. Natl. Acad. Sci. U. S. A.* **100,** 4474–4479
39. Grizot, S., Fieschi, F., Dagher, M. C., and Pebay-Peyroula, E. (2001) *J. Biol. Chem.* **276,** 21627–21631
40. Lapouge, K., Smith, S. J., Walker, P. A., Gamblin, S. J., Smerdon, S. J., and Rittinger, K. (2000) *Mol. Cell* **6,** 899–907
41. Kami, K., Takeya, R., Sumimoto, H., and Kohda, D. (2002) *EMBO J.* **21,** 4268–4276
42. Otwinowski, Z., and Minor, W. (1997) *Methods Enzymol.* **276,** 307–326
43. Collaborative Computational Project, No. 4 (1994) *Acta Crystallogr. Sect. D Biol. Crystallogr.* **50,** 760–763
44. Navaza, J. (1994) *Acta Crystallogr. Sect. A* **50,** 157–163
45. Brunger, A. T., Adams, P. D., Clore, G. M., DeLano, W. L., Gros, P., Grosse-Kunstleve, R. W., Jiang, J. S., Kuszewski, J., Nilges, M., Pannu, N. S., Read, R. J., Rice, L. M., Simonson, T., and Warren, G. L. (1998) *Acta Crystallogr. Sect. D Biol. Crystallogr.* **54,** 905–921
46. Perrakis, A., Harkiolaki, M., Wilson, K. S., and Lamzin, V. S. (2001) *Acta Crystallogr. Sect. D Biol. Crystallogr.* **57,** 1445–1450
47. Jones, T. A., Zou, J. Y., Cowan, S. W., and Kjeldgaard. (1991) *Acta Crystallogr. Sect. A* **47,** 110–119
48. Laskowski, R. A., MacArthur, M. W., Moss, D. S., and Thornton, J. M. (1993) *J. Appli. Crystallogr. Sect. D Biol. Crystallogr.* **26,** 283–291
49. Network, E.-D. V. (1998) *J. Mol. Biol.* **276,** 417–436
50. Musacchio, A., Noble, M., Pauptit, R., Wierenga, R., and Saraste, M. (1992) *Nature* **359,** 851–855
51. Musacchio, A., Saraste, M., and Wilmanns, M. (1994) *Nat. Struct. Biol.* **1,** 546–551
52. Wu, X., Knudsen, B., Feller, S. M., Zheng, J., Sali, A., Cowburn, D., Hanafusa, H., and Kuriyan, J. (1995) *Structure* (*Lond.*) **3,** 215–226
53. Liang, J., Chen, J. K., Schreiber, S. T., and Clardy, J. (1996) *J. Mol. Biol.* **257,** 632–643
54. Wientjes, F. B., Panayotou, G., Reeves, E., and Segal, A. W. (1996) *Biochem. J.* **317,** 919–924
55. Grandvaux, N., Grizot, S., Vignais, P. V., and Dagher, M. C. (1999) *J. Cell Sci.* **112,** 503–513
56. Benna, J. E., Dang, P. M., Gaudry, M., Fay, M., Morel, F., Hakim, J., and Gougerot-Pocidalo, M. A. (1997) *J. Biol. Chem.* **272,** 17204–17208
57. Dang, P. M., Morel, F., Gougerot-Pocidalo, M. A., and Benna, J. E. (2003) *Biochemistry* **42,** 4520–4526
58. Bouin, A. P., Grandvaux, N., Vignais, P. V., Fuchs, A., and Rabilloud, T. (1998) *J. Biol. Chem.* **273,** 30097–30103
59. Wallace, A. C., Laskowski, R. A., and Thornton, J. M. (1995) *Protein Eng.* **8,** 127–134
60. Sumimoto, H., Kage, Y., Nunoi, H., Sasaki, H., Nose, T., Fukumaki, Y., Ohno, M., Minakami, S., and Takeshige, K. (1994) *Proc. Natl. Acad. Sci. U. S. A.* **91,** 5345–5349
61. Leto, T. L., Adams, A. G., and de Mendez, I. (1994) *Proc. Natl. Acad. Sci. U. S. A.* **91,** 10650–10654
62. de Mendez, I., Homayounpour, N., and Leto, T. L. (1997) *Mol. Cell. Biol.* **17,** 2177–2185
63. Diekmann, D., Abo, A., Johnston, C., Segal, A. W., and Hall, A. (1994) *Science* **265,** 531–533
64. Leusen, J. H., Fluiter, K., Hilarius, P. M., Roos, D., Verhoeven, A. J., and Bolscher, B. G. (1995) *J. Biol. Chem.* **270,** 11216–11221
65. McPhail, L. C. (1994) *J. Exp. Med.* **180,** 2011–2015
66. Nicholls, A., Sharp, K. A., and Honig, B. (1991) *Proteins* **11,** 281–296

THE JOURNAL OF BIOLOGICAL CHEMISTRY
Vol. 276, No. 24, Issue of June 15, pp. 21627–21631, 2001

Printed in U.S.A.

The Active N-terminal Region of p67^{phox}

STRUCTURE AT 1.8 Å RESOLUTION AND BIOCHEMICAL CHARACTERIZATIONS OF THE A128V MUTANT IMPLICATED IN CHRONIC GRANULOMATOUS DISEASE*

Received for publication, January 30, 2001
Published, JBC Papers in Press, March 21, 2001, DOI 10.1074/jbc.M100893200

Sylvestre Grizot‡, Franck Fieschi‡, Marie-Claire Dagher§, and Eva Pebay-Peyroula‡¶

From the ‡Institut de Biologie Structurale, CEA-CNRS-UJF, UMR 5075, 41 rue Jules Horowitz, 38027 Grenoble cedex 1, France and the §Laboratoire Biochimie et Biophysique des Systèmes Intégre's/CEA-CNRS-UJF, UMR 5092/Département de Biologie Moléculaire et Structurale/CEA Grenoble, 17 Rue des Martyrs, 38054 Grenoble cedex 9, France

Upon activation, the NADPH oxidase from neutrophils produces superoxide anions in response to microbial infection. This enzymatic complex is activated by association of its cytosolic factors p67^{phox}, p47^{phox}, and the small G protein Rac with a membrane-associated flavocytochrome b_{558}. Here we report the crystal structure of the active N-terminal fragment of p67^{phox} at 1.8 Å resolution, as well as functional studies of p67^{phox} mutants. This N-terminal region (residues 1–213) consists mainly of four TPR (tetratricopeptide repeat) motifs in which the C terminus folds back into a hydrophobic groove formed by the TPR domain. The structure is very similar to that of the inactive truncated form of p67^{phox} bound to the small G protein Rac previously reported, but differs by the presence of a short C-terminal helix (residues 187–193) that might be part of the activation domain. All p67^{phox} mutants responsible for Chronic Granulomatous Disease (CGD), a severe defect of NADPH oxidase function, are localized in the N-terminal region. We investigated two CGD mutations, G78E and A128V. Surprisingly, the A128V CGD mutant is able to fully activate the NADPH oxidase *in vitro* at 25 °C. However, this point mutation represents a temperature-sensitive defect in p67^{phox} that explains its phenotype at physiological temperature.

The NADPH oxidase of phagocytic cells is responsible for the production of microbicidal superoxide anions. This enzymatic complex is activated at the onset of phagocytosis by association of its cytosolic factors p67^{phox}, p47^{phox}, and the small G protein Rac with a membrane-associated flavocytochrome b_{558} (1). Mutations in any of these components except Rac can lead to a severe immune defect known as Chronic Granulomatous Disease (CGD).[1] The cytosolic factors p47^{phox}, p40^{phox}, and p67^{phox} are modular proteins comprising a set of structural domains such as SH3 domains, proline-rich regions, and TPR motifs (2), all of which are prone to protein-protein interactions. Through these various domains, the cytosolic factors are able, upon stimulation, to associate, translocate to the membrane, and finally activate the electron transfer from NADPH to O_2 through the flavocytochrome b_{558}. Over the past few years, serious efforts have been made to delineate the nature and the succession of intra- and intermolecular interactions between the cytosolic factors leading to the activated complex (3, 4). Most, if not all, pairwise interacting protein domains have been identified, but the sequence of the molecular rearrangements as well as the structural modifications governing this cascade are still a matter of debate. It is known that Rac can interact in a GTP-dependent manner with the N-terminal region of p67^{phox} comprising amino acids 1–199 (5). Moreover, all known missense mutations in p67^{phox} responsible for CGD are localized in this N-terminal region (6). This region of p67^{phox} has been shown to contain four TPR motifs (2) that were first identified as degenerate 34 amino acid sequences present in a variety of proteins from bacteria to eukaryotes (7, 8). One TPR motif consisting of two antiparallel α helices termed A and B and a TPR domain (a succession of TPR motifs) adopts an overall superhelical fold (9). Using various binding assays, a first study suggested that p67^{phox} interacts with Rac only through 30 residues downstream of the TPR domain (10). A second study showed that Rac-p67^{phox} interaction involves the TPR domain itself (11). To unravel the properties and Rac binding sites on p67^{phox}, structures of the non-complexed p67^{phox} and of the Rac-p67^{phox} complex had to be deciphered. Recently, a first piece of the puzzle was achieved with the structure at 2.4 Å of the complex between the N-terminal region of p67^{phox} (residues 1–203) and Rac-GTP, showing an unusual interaction of a TPR domain with a partner protein (12).

In this study, we report the structure at 1.8 Å resolution of the catalytically active N-terminal region (residues 1–213) of p67^{phox} that contains four TPR motifs. We compared it to the Rac-p67^{phox} structure as well as to other TPR domain structures. We have also investigated the molecular and structural basis of the defects due to some of the CGD mutations. In particular, we report biochemical and biophysical evidence for the instability of the A128V mutant at physiological temperature, in agreement with our structural analyses.

EXPERIMENTAL PROCEDURES

Native and Selenomethionyl Protein Production—The cDNA for the N-terminal part of p67^{phox} corresponding to amino acids 1–213 was obtained by polymerase chain reaction and cloned into pET-15b (Novagen). The protein was expressed in *Escherichia coli* BL21 (DE3) and purified by affinity chromatography in two steps: first on a Ni^{2+}-column equilibrated in 20 mM Hepes, pH 7.5, 250 mM NaCl and eluted with a linear gradient of imidazole and second on an SP-Sepharose column equilibrated in 20 mM Hepes, pH 7.5 and eluted with a linear gradient

* This work was supported in part by the Association pour la Recherche sur le Cancer. The costs of publication of this article were defrayed in part by the payment of page charges. This article must therefore be hereby marked "*advertisement*" in accordance with 18 U.S.C. Section 1734 solely to indicate this fact.

The atomic coordinates and structure factors (code 1hh8) have been deposited in the Protein Data Bank, Research Collaboratory for Structural Bioinformatics, Rutgers University, New Brunswick, NJ (http://www.rcsb.org/).

¶ To whom correspondence should be addressed. Tel.: 33-0-4-3878-9583; Fax: 33-0-4-3878-5494; E-mail: pebay@ibs.fr.

[1] The abbreviations used are: CGD, chronic granulomatous disease; TPR, tetratricopeptide repeat; SAD, single wavelength anomalous dispersion; rmsd, root mean square deviation; GST, glutathione *S*-transferase; GTP-γ-S, guanosine 5′-3-*O*-(thio)triphosphate.

of NaCl. The protein was then concentrated to 5–6 mg/ml with Centricon10 (Amicon). Seleno-L-methionine (Se-Met)-labeled protein was produced in a similar way. The protein was expressed in *E. coli* B834 (DE3). A 50-ml preculture in Luria-Bertani medium was used to inoculate 2 liters of a defined medium prepared as reported before (13) supplemented with 20 mg/liter of Se-Met. The last purification step was done in the presence of 10 mM dithiothreitol and 1 mM EDTA to avoid oxidation of selenomethionines. High resolution electrospray ionization mass spectrometry was consistent with 100% selenium incorporation.

CGD Mutants of p67^{Nter}—Mutants G78E and A128V of p67^{phox}-(1–213) were constructed using site-directed mutagenesis (Stratagene kit) on the native cDNA cloned in the pET-15b vector. The mutant A128V was expressed in *E. coli* BL21 (DE3) at 15 °C for 16 h instead of the 3 h at 37 °C employed for the native protein. The first steps of the purification were the same as for the native protein, but an additional purification step was carried out by gel filtration on a Superdex 200 Hiload 16/60 column (Amersham Pharmacia Biotech) equlibrated in 20 mM Hepes, pH 7.5 and 200 mM NaCl. The protein was concentrated to 5 mg/ml with Centricon10.

Limited Proteolysis—Native p67^{phox}-(1–213) and the A128V mutant at a concentration of 0.6 mg/ml were submitted to limited proteolysis for one hour at 25 °C by trypsin (Roche Molecular Biochemicals) at a protease/protein ratio of 1:200 (w/w).

Circular Dichroism (CD)—CD spectra were recorded on a Jobin Yvon CD6 dichrograph from 190 to 260 nm with a 1-mm path length cell and a thermostated cell holder. The protein concentrations were 0.5 mg/ml. The spectra were recorded on one sample per protein from 15 to 35 °C by increments of 5 °C. At each temperature, the sample was incubated for 15 min.

NADPH oxidase activity—The NADPH oxidase activating potency was assessed in a semi-recombinant cell-free system (14) containing 3.5 μg of membrane protein, 20 pmol of recombinant p47^{phox}, 20–400 pmol of an N-terminal fragment of p67^{phox}, 2 mM $MgCl_2$ and 10 pmol of Rac in a final volume of 200 μl. Rac was loaded with GTP-γ-S in the presence of 4 mM EDTA, followed by addition of $MgCl_2$ to 20 mM. An optimal amount of arachidonic acid (5–20 nmol) was added with strong agitation. After a 10-min activation, the elicited oxidase activity was assessed using the superoxide dismutase inhibitable cytochrome *c* reduction in the presence of 250 μM NADPH and 100 μM cytochrome *c*, followed at 550 nm using a Labsystem IEMS microplate reader.

Assay of Rac Binding—Rac fused to GST or GST alone were immobilized on glutathione-Sepharose beads (Amersham Pharmacia Biotech). Rac was loaded with GTP-γ-S on the beads. The beads were washed and incubated for 2 h at 4 °C with a stoichiometric amount of p67^{phox}-(1–213) or the A128V mutant. After washing, proteins bound to the beads were analyzed by SDS-polyacrylamide gel electrophoresis.

Crystallization—Crystals of the native protein or the Se-Met protein were grown at 20 °C by vapor diffusion in hanging drops by mixing equal volumes of protein (5–6 mg/ml) and reservoir solutions (17% polyethylene glycol monomethyl ether 2000, 100 mM sodium citrate, pH 4.5, 10% glycerol, and 10 mM dithiothreitol in the case of the Se-Met protein). The crystals grew as thin needles ($20 \times 20 \times 200$ μm^3) and belong to the trigonal space group $P3_1$ ($a = b = 67.7$ Å, $c = 50.2$ Å) with one molecule in the asymmetric unit. Crystals exhibit various amounts of merohedral twinning; however, non-twinned crystals could be selected after analyzing the diffraction data.[2]

Data Collection and Processing—A native data set was collected (beamline ID14-EH1, ESRF-Grenoble) to 1.8 Å resolution (Table I), integrated with DENZO (15) and scaled with SCALA (16). A SAD data set was collected on a selenomethionyl-substituted crystal at the K absorption edge of selenium (beamline ID29, ESRF-Grenoble). Data were integrated and scaled with the DENZO/SCALEPACK programs. The program Shake and Bake (17) located 5 of 7 selenium atoms expected in the asymmetric unit.

Structure Determination and Refinement—Initial phases calculated with MLPHARE (16) using the 5 selenium sites allowed the location of a sixth selenium atom detected in an anomalous Fourier difference map. Final phases from MLPHARE resulted in a figure of merit of 0.37–2.8 Å resolution. Phases were extended to 1.8 Å on the native data set using the program DM (16) assuming a solvent content of 45% of the unit cell volume (Table I). 85% of the model was built automatically using the program wARP (18). Loop residues 151–158, residues 2–3 at the N terminus and 191–193 at the C terminus were added manually using the program O (19). The structure was refined with CNS (20) to a final crystallographic R_{factor} of 18.2% and an R_{free} of 20.5% at 1.8 Å resolution (Table II). The model consists of residues 2–193 of p67^{phox}, 160 water molecules, and one citrate anion, the citrate being essential for crystallization. All non-glycine residues are in the most favored or additionally allowed regions of the Ramachandran plot according to PROCHECK (21). The figures were prepared with MOLSCRIPT (22) and Raster3D (23).

[2] A. Royant, S. Grizot, F. Fieschi, E. M. Landau, R. Kahn, and E. Pebay-Peyroula, manuscript in preparation.

TABLE I
Data reduction and phasing statistics

	SAD data set	Native data set
Data collection		
wavelength (Å)	0.979	0.934
resolution (Å)	2.8	1.8
total reflections	50476	95808
unique reflections	6150	23850
redundancy	8.3	4.0
completeness (%)[a]	99.3 (99.3)	99.5 (99.5)
$I/\sigma(I)$[a]	7.8 (3.7)	12.4 (3.6)
R_{sym} (%)[a,b]	9.5 (18.6)	4.7 (19.8)
Phasing		
phasing power[a]	1.91 (1.68)	
R_{Cullis}[c] (ano)	0.73	
FOM[d] before solvent flattening (to 2.8 Å)	0.37	
FOM after solvent flattening (to 1.8 Å)	0.69	

[a] Values in brackets correspond to the highest resolution shell.
[b] $R_{sym} = \Sigma\Sigma|I_j(h) - \langle I(h)\rangle|/\Sigma\langle I(h)\rangle$.
[c] R_{Cullis} (anomalous) $= \Sigma|D_{ph} - D_{phc}|/\Sigma|D_{ph}|$.
[d] FOM, figure of merit.

TABLE II
Refinement statistics

resolution range (Å)	20 – 1.8
number of reflections	23707
R_{cryst}/R_{free}[a] (%)	18.3/20.5
rmsd bonds (Å)	0.005
rmsd angles (°)	1.05
Number of non-hydrogen atoms	
protein	1541 (16.3)[b]
water	160 (24.5)[b]
citrate anion	13 (17.9)[b]

[a] $R_{cryst} = \Sigma||F_{obs}| - |F_{calc}||/\Sigma|F_{obs}|$. R_{free} was calculated on 5% of data excluded from refinement.
[b] Values in brackets are the average B values in Å^2.

RESULTS AND DISCUSSION

Overview of the Structure and Physiological Relevance—The N-terminal region of p67^{phox} used in this study was shown to be fully competent in NADPH oxidase activation both *in vitro* and *in vivo* (24, 25). The electron density map obtained from SAD phasing was clearly interpretable (Fig. 1). p67^{phox}-(1–213) consists of four TPR motifs followed by an extended loop, which inserts into the hydrophobic groove formed by the helical organization of the TPRs (Fig. 2). The first three TPRs are contiguous and 16 residues (105 to 120) forming two antiparallel β-strands are inserted between TPR3 and TPR4. A comparison with other recently reported TPR domain structures (9, 26) highlights a remarkable conservation of the overall structure. For example, the TPR1 domain of Hop (PDB accession code 1ELW), composed of three TPR motifs, could be superimposed on three consecutive TPR motifs of p67^{phox} with rmsd values of 0.95 Å and 1.40 Å with the first three and the last three p67^{phox} TPRs, respectively. This indicates that the fold of TPR domains is highly conserved despite a rather small sequence identity; in addition, the insertion of amino acids 105–120 in p67^{phox} does not disrupt the superhelical structure of the TPR domain. Following TPR4, a helix (residues 156–166) terminates the TPR domain and an extended structure (residues 168–186) folds back into the internal hydrophobic groove of the superhelix. The structure ends with a short helix (residues 187–193),

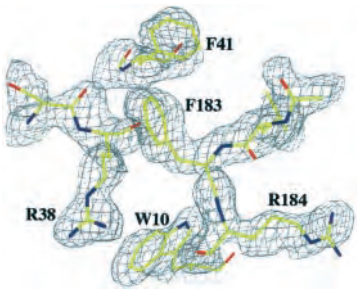

FIG. 1. **Experimental electron density.** The experimental map at 1.8 Å resolution (contoured at 1 σ) is clearly interpretable and side chains are easily identified.

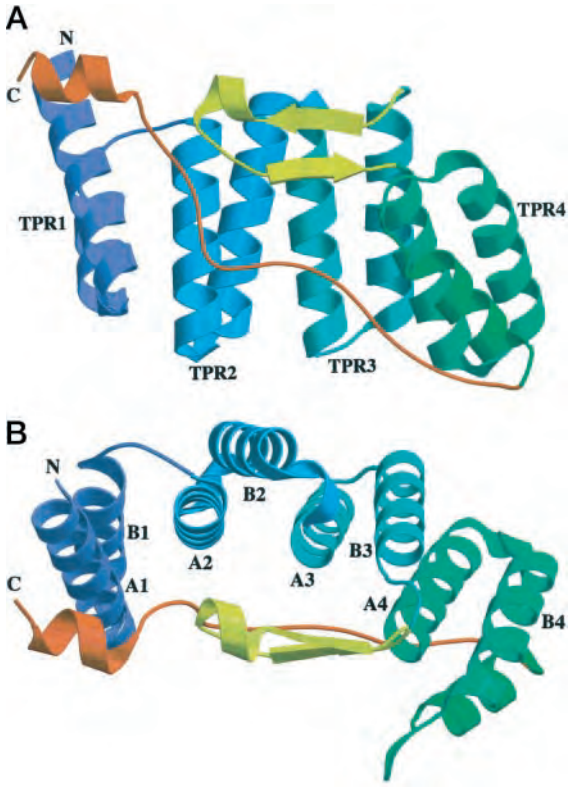

FIG. 2. **Overall structure.** A *ribbon* representation of the structure shows the four TPR motifs labeled in *a,* the A and B type helices are shown in *b*. The TPRs adopt an overall super-helix fold (*colored from blue to green*). The C terminus in *red* is in an extended conformation locked in the hydrophobic groove formed by the TPRs and ends with a short helix. The inserted β-strands between TPR 3 and 4 are shown in *yellow*. *a* and *b* are two perpendicular views of the molecule.

mainly composed of polar residues. Residues 170–185 interact extensively with residues belonging to the A helices of TPR motifs or to the inserted β-strands (Fig. 2*b*), probably stabilizing the overall structure. In particular, Arg-181 interacts with Gln-115. In the Rac-p67^{phox} complex, Arg-181 is replaced by Lys-181 and the same type of interaction is observed, consistent with the existence of a polymorphism (6). The sequence of p67^{phox} (1–213) is extremely rich in basic amino acids with 22 lysine and 6 arginine residues located mainly on the external surface of the super-helix. These residues are uniformly distributed at the surface without forming a highly basic patch. Residues downstream from Leu-193 are not visible in the electron density map.

The recent structure of Rac-p67^{phox}-(1–203) (12) showed that all the residues of p67^{phox} involved in the complex formation belong to the inserted β-strands (Arg-102, Asn-104, Leu-106, Asp-108) or to the loops connecting TPR1 to TPR2 (S37) and TPR2 to TPR3 (D67, H69). The structures of both the non-complexed and complexed forms of p67^{phox} can be remarkably well superimposed with a rmsd of 0.57 Å on main chain atoms, showing that the interaction of p67^{phox} (1–213) with Rac does not require structural rearrangements of this N-terminal region. In particular, the residues involved in the interaction with Rac are totally accessible in the non-complexed structure, their side chains pointing toward the solvent. Although the two constructs of p67^{phox} (1–203 in the complex and 1–213 in this study) differ only by ten amino acids in length, the first was reported to be inactive whereas the second fully activates NADPH oxidase *in vitro* (24). This drastic difference could be related to the presence of the C-terminal α-helix (residues 187–193) present in our model that is not seen in the Rac-p67^{phox} complex structure, although amino acids 1–203 of p67^{phox} are present in the crystal. The folding of this helix is probably facilitated by the presence of amino acids up to 213. From functional studies of various truncated forms of p67^{phox}, amino acids 199–210 of p67^{phox} were defined as an NADPH oxidase activation domain (24), and this region was reported to be involved in the regulation of electron transfer (27). The comparison of the structure of p67^{phox}-(1–213) to that of p67^{phox}-(1–203) in the Rac-p67^{phox} complex (12) suggests that the activation domain includes helix 187–193.

Mutations in p67^{phox} *That Cause Chronic Granulomatous Disease*—CGD is an inherited disorder of neutrophil function characterized by an increased susceptibility to infection because of a defect in the NADPH oxidase components. Mutations involving p67^{phox} are single cases and are located in the N-terminal region of the protein. An in-frame deletion of K58 was found to prevent Rac binding to p67^{phox} (28). Deletion of amino acids 19–21 renders the protein inefficient for oxidase activation (29). These amino acids are located between helices A and B of TPR1 and are exposed to solvent. Various point mutations encountered in p67^{phox} of CGD patients (R77Q, G78E, A128V, D160V/K161E) were studied and shown to be associated with the absence of the protein *in vivo* (6, 30). This observation accounts either for mRNA or protein instability or for an increased sensitivity to proteases. Amino acids Gly-78 and Ala-128 are located in similar positions in the α-helices of the TPR motifs (position 8 of helix A). Their mutations are likely to destabilize TPR packing. A sequence alignment of multiple TPRs shows that position 8 in helix A is restricted to glycine, alanine, or serine residues.

We produced G78E and A128V CGD mutants of p67^{phox}-(1–213). The G78E mutant was insoluble in bacteria. Because the A128V mutant showed lower solubility than the native protein, it was expressed at 15 °C instead of 37 °C. Surprisingly, this mutant was still able to bind Rac and to activate the NADPH oxidase in a cell-free system at 25 °C (Fig. 3), suggesting correct folding. Moreover, the CD spectra at 25 °C of the mutant and of the native proteins were identical and characteristic of α-helices, indicating no modification in the secondary structure (Fig. 4, *inset*). Altogether, these experiments do not explain the CGD phenotype of this mutant. To assess slight differences in the tertiary structure, the native protein and the A128V mutant were subjected to limited proteolysis by trypsin at 25 °C. As shown in Fig. 5, the native protein is poorly degraded up to 60 min, whereas the A128V mutant shows notable degradation starting at 15 min. Additionally, the CD spectrum as a function of the temperature shows that the native protein is still stable at 40 °C whereas the A128V mutant begins to loose its helical folding at 30 °C (Fig. 4) and precipitates at 40 °C.

The behavior of the two CGD mutants can be interpreted with respect to the structure of the native protein p67^{phox}-(1–213). The mutation G78E leads to a misfolding of the protein by steric hindrance within the TPR2 motif. In the less drastic

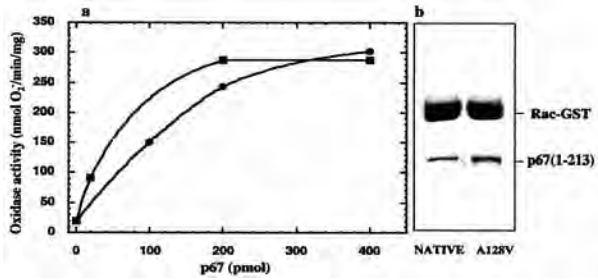

FIG. 3. **Functional assays of the A128V mutant.** *a* represents the amount of superoxide anion per min and per mg of membrane protein as a function of p67^{phox}. The activity of the native p67^{phox}-(1–213) and of the A128V mutant are shown with *squares* and *full circles*, respectively. The amounts of p47^{phox} and Rac were constant during each test. The SDS-polyacrylamide gel electrophoresis in *b* shows the binding of the native and the mutant proteins to Rac as described under "Experimental Procedures." No binding was observed when GST alone was present.

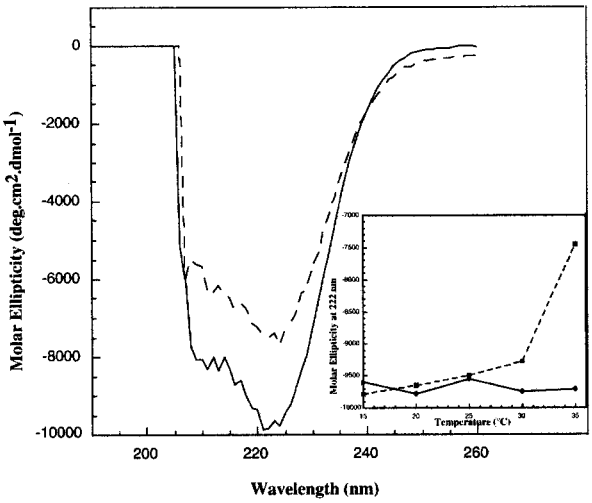

FIG. 4. **CD Spectra.** CD spectra at 15 °C (*solid line*) and 35 °C (*dashed line*) of the A128V mutant. The *inset* shows the molar ellipticity at 222 nm for the native protein (*circles, solid line*) and for the A128V mutant (*squares, dashed line*) as a function of the temperature.

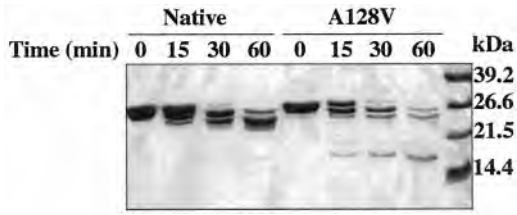

FIG. 5. **SDS-polyacrylamide gel after tryptic digestion of p67^{phox}-(1–213).** The *lanes* represent the native protein and the A128V mutant at 0, 15, 30, and 60 min digestion.

mutant A128V, Val-128 would be located at 2.2 Å of the carbonyl of Ala-140 or of the hydroxyl of Tyr-172 (Fig. 6). This hydroxyl in the native structure is stabilized by two hydrogen bonds. Although the environment should be able to accommodate this moderate steric change, the hydrogen-bond network is perturbed and the structure of the A128V mutant is weakened. Within the cellular environment at 37 °C, the decrease in stability because of this mutation probably leads to misfolded p67^{phox} protein. This mutation is akin to other point mutations introduced at position 8 of the A helix of a TPR motif in p62^{cdc23} (Ala→Thr or Gly→Asp), which also confer thermolability to the protein (31).

Thus, the structure of the active N-terminal domain of

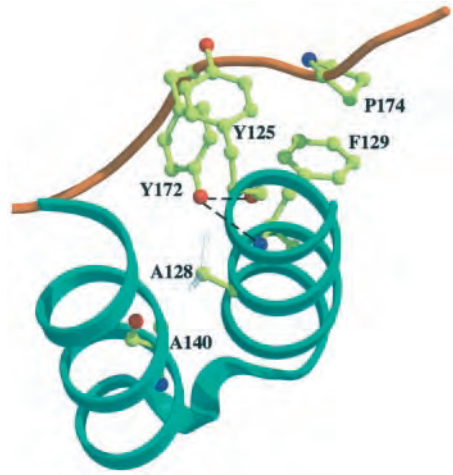

FIG. 6. **Environment of Ala-128.** The figure shows the interactions of the extended C terminus (*red*) with TPR4 (*green*). Ala-128 is tightly packed in this environment. Valine at position 128 (*light gray*) is superimposed on alanine.

p67^{phox}-(1–213) highlights a short α-helix that participates to the NADPH oxidase activation domain. Interestingly, most of the CGD mutants of p67^{phox} are located in the N-terminal region of p67^{phox}. The structural and functional studies reported here permit an elucidation of the instability of the G78E and A128V mutants and may be extended to mutations that affect TPR folding. The coordinates and the structure factors have been deposited in the Protein Data Bank with ID code 1hh8.

Acknowledgments—We thank A. Thompson, M. Roth, G. Leonard, D. Fleury, and S. Malbet for help with data collection at ESRF, M. Picard for technical assistance, J. P. Pichon for mass spectroscopy analysis, D. Madern for CD measurements, and P. V. Vignais for stimulating discussions and critical reading of the manuscript.

REFERENCES

1. Babior, B. M. (1999) *Blood* **93,** 1464–1476
2. Ponting, C. P. (1996) *Protein Sci.* **5,** 2353–2357
3. Fuchs, A., Dagher, M.-C., and Vignais, P. V. (1995) *J. Biol. Chem.* **270,** 5695–5697
4. DeLeo, F. R., and Quinn, M. T. (1996) *J. Leukoc. Biol.* **60,** 677–691
5. Diekmann, D., Abo, A., Johnston, C., Segal, A. W., and Hall, A. (1994) *Science* **265,** 531–532
6. Noack, D., Rae, J., Cross, A. R., Munoz, J., Salmen, S., Mendoza, J. A., Rossi, N., Curnutte, J. T., and Heyworth, P. G. (1999) *Hum. Genet.* **105,** 460–467
7. Goebl, M., and Yanagida, M. (1991) *Trends Biochem. Sci.* **16,** 173–177
8. Lamb, J. R., Tugendreich, S., and Hieter, P. (1995) *Trends Biochem. Sci.* **20,** 257–259
9. Das, A. K., Cohen, P. T. W., and Barford, D. (1998) *EMBO J.* **17,** 1192–1199
10. Ahmed, S., Prigmore, E., Govind, S., Veryard, C., Kozma, R., Wientjes, F. B., Segal, A. W., and Lim, L. (1998) *J. Biol. Chem.* **273,** 15963–15701
11. Koga, H., Terasawa, H., Nunoi, H., Takeshige, K., Inagaki, F., and Sumimoto, H. (1999) *J. Biol. Chem.* **274,** 25051–25060
12. Lapouge, K., Smith, S. J, Walker, P. A., Gamblin, S. J., Smerdon, S. J., and Rittinger, K. (2000) *Mol. Cell* **6,** 899–907
13. LeMaster, D. M., and Richards, F. M. (1985) *Biochemistry* **24,** 7263–7268
14. Fuchs, A., Dagher, M.-C., Jouan, A., and Vignais, P. V. (1994) *Eur. J. Biochem.* **226,** 587–595
15. Otwinowski, Z., and Minor, W. (1997) *Methods Enzymol.* **276,** 307–326
16. CCP N°4. (1994) *Acta Crystallogr. Sec. D* **50,** 905–921
17. Weeks, C. M., and Miller, R. (1999) *J. Appl. Crystallogr.* **32,** 120–124
18. Perrakis, A., Sixma, T. K., Wilson, K. S., and Lamzin, V. S. (1997) *Acta Crystallogr. Sec. D* **53,** 448–455
19. Jones, T. A., Zou, J.-Y., Cowan, S. W., and Kjeldgaard, M. (1991) *Acta Crystallogr. Sect. A* **47,** 110–119
20. Brünger, A. T., *et al.* (1998) *Acta Crystallogr. Sec. D* **54,** 905–921
21. Laskowski, R. A., MacArthur, M. W., Moss, D. S., and Thornton, J. M. (1993) *J. Appl. Crystallogr.* **26,** 283–291
22. Kraulis, P. J. (1991) *J. Appl. Crystallogr.* **24,** 946–950
23. Merrit, E. A., and Bacon, D. J. (1997) *Methods Enzymol.* **277,** 505–524
24. Han, C.-H., Freeman, J. L., Lee, T., Motalebi, S. A., and Lambeth, J. D. (1998) *J. Biol. Chem.* **273,** 16663–16668
25. de Mendez, I., Adams, A. G., Sokolic, R. A., Malech, H. L., and Leto, T. L;. (1996) *EMBO J.* **15,** 1211–1220
26. Scheufler, C., Brinker, A., Bourenkov, G., Pegoraro, S., Moroder, L., Bartunik,

H., Hartl, U., and Moarefi, I. (2000) *Cell* **101,** 199–210
27. Nisimoto, Y., Motalebi, S., Han, C.-H., and Lambeth, J. D. (1999) *J. Biol. Chem.* **274,** 22999–23005
28. Leusen, J. H., de Klein A., Hilarius P. M., Ahlin A., Palmblad J., Smith C. I., Diekmann D., Hall A., Verhoeven A. J., and Roos, D. (1996) *J. Exp. Med.* **184,** 1243–1249
29. Patino, P. J., Rae, J., Noack, D., Erickson, R., Ding, J., de Olarte, D. G., and Curnutte, J. T. (1999) *Blood* **94,** 2505–2514
30. de Boer, M., Hilarius-Stokman, P. M., Hossle, J.-P., Verhoeven, A. J., Graf, N., Kenney, R. T., Seger, R., and Roos, D. (1994) *Blood* **83,** 531–536
31. Sikorski, R. S., Michaud, W. A., and Hieter, P. (1993) *Mol. Cell. Biol.* **13,** 121–1221

Small-Angle X-Ray Scattering reveals an Extended Organization For The Auto-Inhibitory Resting State of the p47^{phox} Modular Protein.

Dominique Durand§, Dominique Cannella‡, Virginie Dubosclard‡, Eva Pebay-Peyroula‡, Patrice Vachette§ and Franck Fieschi‡**

§ IBBMC, CNRS UMR8619 Université Paris XI, Bât. 430, 91405 Orsay Cedex, France

‡ Institut de Biologie Structurale, UMR 5075 CEA/CNRS/Université Joseph Fourier, Laboratoire des Protéines membranaires, 41 rue Jules Horowitz 38027 Grenoble cedex 1, France

Running Title : An Extended Conformation for p47^{phox} in the resting state

*Corresponding authors :

F. Fieschi, Tel: +33 4 38789177; Fax: +33 4 38785494; E-mail: fieschi@ibs.fr

D. Durand, Tel: +33 1 69156421; Fax: +33 1 69853715; E-mail: dominique.durand@ibbmc.u-psud.fr

ABBREVIATIONS :

PX, Phox homology; SH3, src homology 3; CGD, chronic granulomatous disease; AIR, autoinhibitory region; NMR, Nuclear magnetic resonance; SAXS, small angle X-ray scattering; GST, glutathione S-transferase; IPTG, iso-propyl β−D-thiogalactopyranoside; DR, dummy residue; PDB, Protein Data Bank.

ABSTRACT : In response to microbial infection, neutrophiles promote the assembly of the NADPH oxidase complex in order to produce superoxide anions. This reaction is activated by the association of cytosolic factors, $p47^{phox}$, $p67^{phox}$, $p40^{phox}$ and a small G protein Rac with the membranous heterodimeric flavocytochrome b_{558}, composed of $gp91^{phox}$ and $p22^{phox}$. In the activation process, $p47^{phox}$ plays a central role as the target of phosphorylations and as a scaffolding protein conducting the translocation and assembly of cytosolic factors onto the membranous components. The PX and tandem SH3s of $p47^{phox}$ have been highlighted as being key determinants for the interaction with membrane lipids and the $p22^{phox}$ component respectively. In the resting state, the two corresponding interfaces are thought to be masked allowing its cytoplasmic localization. However, the resting state modular organisation of $p47^{phox}$ and its auto-inhibition mode are still not fully understood despite available structural information on separate modules. More precisely, it raises the question of the mutual arrangement of the PX domain and the tandem SH3 domains in the resting state. To address this question we have engaged a study of the entire $p47^{phox}$ molecule in solution using Small Angle X-ray Scattering. Despite internal auto-inhibitory interactions, $p47^{phox}$ adopts an extended conformation. First insights about the domain arrangement in whole $p47^{phox}$ can be derived. Our data allow to discard the usual representation of a globular and compact auto-inhibited resting state.

The NADPH oxidase of neutrophil is a multi-component enzyme essential in innate immunity as exemplified by a genetic disorder, chronic granulomatous disease (CGD), in which NADPH oxidase activity is impaired. This enzyme represents one of the best defence lines against microbial infection through its ability to catalyse oxygen reduction to superoxide as a first step toward a global reactive oxygen species production called the oxidative burst (*1*). This highly destructive power is at the origin of a number of diseases when inappropriately activated. Thus, a tight regulation of this membranous enzyme is required. NADPH oxidase is composed of a membrane-integrated flavocytochrome b_{558} ($gp91^{phox}$ and $p22^{phox}$), which constitutes the catalytic core of the enzyme, and of three cytosolic factors (the modular proteins $p47^{phox}$, $p67^{phox}$ and $p40^{phox}$) as well as a small G protein, Rac.

In the resting state, components involved in an active NADPH oxidase complex are physically separated. Indeed, they are partitioned in different subcellular location. Activation requires the translocation of the cytosolic factors and of the Rac protein to the membrane and their assembly with the flavocytochrome b_{558} to constitute a fully active NADPH oxidase complex. The cytosolic factors are modular proteins containing various domains allowing protein-protein or lipid-protein interactions (*2-4*). The molecular events occurring during translocation and assembly of the oxidase involve a complex set of interactions mediated by these protein modules. Upon exposure to specific stimuli, activation is initiated through multiple phosphorylation events on the cytosolic components. Among them, $p47^{phox}$ plays a central role in the assembly process. From the N- to the C-terminus, $p47^{phox}$ comprises a PX domain, a tandem of SH3 domains, a polybasic region involved in autoinhibition (Auto Inhibitory Region) and a polyProline motif towards the C-terminal end (Figure 1A). $p47^{phox}$ can be considered as the sensor of the activation signal through multiple phosphorylations (*5-9*). In CGD patients lacking $p47^{phox}$ no translocation of the $p67^{phox}$ and $p40^{phox}$ factors to the membrane takes place (*10, 11*). Thus, in addition to its “activation sensing” role, $p47^{phox}$ is a

scaffolding protein conducting translocation and assembly of the other cytosolic factors to the membrane component of the oxidase. Indeed, in its activated state, $p47^{phox}$ is able to interact with phosphatidyl inositol lipids of the plasma membrane through its PX domain (*12, 13*) and with the C-terminal polyProline motif of the $p22^{phox}$ subunit through its tandem of SH3 domains (Figure 1A) (*14-17*). In the fully assembled complex, additional interactions, still poorly characterized, have been reported between $p47^{phox}$ and $gp91^{phox}$ (*18, 19*). However, the PX and tandem SH3s mediated interactions have been pinpointed as being the key determinants initiating translocation to the membrane and docking the $p40^{phox}$-$p67^{phox}$-$p47^{phox}$ cytosolic complex onto the flavocytochrome b_{558} (*20, 21*). In the resting state, $p47^{phox}$ is unable to promote these two interactions. Numerous biochemical and, more recently, structural studies argue for the existence of an auto-inhibitory mechanism in the resting state in which binding sites on both the PX domain and the tandem SH3s are masked and thereby unavailable for interaction with their respective ligands, phosphatidyl inositol and $p22^{phox}$ polyProline motif (*13, 16, 20-22*). It has been shown that phosphorylation of C-terminal serines of $p47^{phox}$, and more precisely of Ser 303, 304 and 328, are necessary to activate the binding properties towards phosphatidyl inositol and $p22^{phox}$ polyProline motif, thereby allowing activation and assembly of the whole NADPH complex to proceed (*8, 13, 20*).

The auto-inhibitory state of $p47^{phox}$ and its mechanism of release have been the subject of detailed molecular studies. However, these various data have been interpreted in terms of conflicting models for the auto-inhibited $p47^{phox}$ state, so that to date no global model accounts for all $p47^{phox}$ properties. A first model for the regulation of the lipid binding properties of PX domain through the resting and the activated states was based on the presence of a consensus PxxP motif between α2 and α3 helices of this domain. This feature suggested a possible interaction with an SH3 domain masking the lipid binding site (Figure 1) (*13*). Such an interaction between PX and the second SH3 domain of $p47^{phox}$ ($SH3_B$) has been

observed and characterized by NMR using isolated domains (*23*). Moreover, W263R mutation in the polyproline binding site of $SH3_B$ has been shown to restore the phosphatidyl inositol phosphate binding capability of entire $p47^{phox}$ in a manner similar to the effect of C-terminal serine phosphorylation (*13*). These observations led to the proposal that lipid-binding inhibition results from an intramolecular interaction between PX and the $SH3_B$ domain.

A second model accounts for the auto-inhibition of the interaction of the $p47^{phox}$ SH3 domains with $p22^{phox}$. Fine and accurate biochemical studies have established the role of the polybasic region downstream from the $SH3_B$ domain (residues 296-340) through simultaneous interactions with both $SH3_A$ and $SH3_B$ (*14, 20, 24*). This model for inhibition has been strongly supported by the structure of the $p47^{phox}$ region encompassing residues 156 to 340, containing the two SH3 domains and the AIR/polybasic region (*16, 25*). This structure is based on the crystal structure of an intertwined dimer of $p47^{phox}$ (156-340) and shows that the AIR folds back, in an unusual manner, into a groove formed by the two SH3 domains interface. Therefore, the release of the AIR following phosphorylation can be easily explained by steric and electrostatic effects. Finally, combination of NMR and SAXS data confirmed this structural auto-inhibition of the SH3 tandem by the AIR in this $p47^{phox}$ (156-340) truncated form (*26*) in solution.

These two auto-inhibitory mechanisms relying on intramolecular interactions, have led to a widely accepted and extensively presented model of the $p47^{phox}$ autoinhibitory resting state organization as depicted in Figure 1B. However, both the PX domain inhibition and the $p22^{phox}$ interaction inhibition exhibit some mutual inconsistencies from a structural and a functional standpoint as already pointed out in a recent review (4). Both require the same interaction site with the $SH3_B$ domain as a key element in the locking system. This suggests that, in the context of the entire $p47^{phox}$ protein, the relations between the various domains are

more complicated than now depicted. More precisely, it raises the question of the actual auto-inhibitory interactions within the whole molecule, and in particular that of the mutual arrangement of the PX domain and the tandem SH3 domains. Further progress in our knowledge of the auto-inhibitory state of $p47^{phox}$ will not result from structural studies restricted to isolated domains. However, three-dimensional crystallographic structures of multi-domain proteins like $p47^{phox}$ are difficult to reach due to their modular and flexible character. We have therefore initiated a structural study of the entire $p47^{phox}$ in solution using Small Angle X-ray Scattering (SAXS). We present here the first insights about the domain architecture of the whole $p47^{phox}$ in its auto-inhibited state.

EXPERIMENTAL PROCEDURES

$p47^{phox}$ expression and purification.

The $p47^{phox}$ protein is expressed as a GST fusion protein using a pGex-6P derived vector containing the $p47^{phox}$ cDNA sequence. This vector has been kindly provided by M-C Dagher. The protein was expressed in *Escherichia coli* BL21(DE3) strain. Expression is induced with 0.5 mM IPTG, when cell culture reached an O.D. of 0.6 at 600 nm. After overnight induction at 20°C, cells were harvested and resuspended in chilled lysis buffer (50 mM Tris, pH 7, 0.3 M NaCl, 1 mM EDTA and 2 mM DTT). All following operations were carried out at 4°C. Cells were disrupted by sonication then centrifuged at 40 000 rpm for 40 min in a Beckman 45 Ti rotor. The supernatant was loaded onto a 4 mL Gluthation-Sepharose 4B column (Amersham) equilibrated in the previous buffer. Proteins were eluted at 1mL/min with 50 mL of elution buffer (50 mM Tris, pH 8, 0.1 M NaCl, 10 mM Glutathion). Fractions containing GST-$p47^{phox}$ were pooled and subjected to 4 h digestion at 4°C with 2.2 units Prescission protease per mg of protein (Amersham). Due to the genetic

construction, digested $p47^{phox}$ possesses 10 and 7 additional residues at its N- and C-terminus respectively. Digestion products were loaded at a flow rate of 0,5 mL/min onto a MonoS column (Amersham) equilibrated in 50 mM Hepes pH 8, 50 mM NaCl, 1 mM EDTA and 2 mM DTT. The proteins were eluted with a 40 mL linear gradient of NaCl (50 – 500 mM). The resulting protein fractions containing $p47^{phox}$ were concentrated, on a centrifugal concentration device with a 30 kDa cut off, to 300 μL and diluted in 4 mL of Hepes 50 mM, 100 mM NaCl, 1 mM EDTA, 2 mM DTT, 5% Glycerol. The proteins were finally re-concentrated and, at different concentrations, aliquots of $p47^{phox}$ were taken and stored for SAXS experiments.

SAXS measurements and data analysis.

Scattering data were recorded on the small angle X-ray scattering instrument D24 at LURE (Laboratoire pour l'Utilisation du Rayonnement Electromagnétique, Orsay, France) using the radiation emitted by a bending magnet of the storage ring DCI. The wavelength λ was selected by a bent Ge(111) monochromator and adjusted to 1.488 Å, calibrated by the nickel absorption edge. X-ray patterns were recorded using a linear position-sensitive detector with delay-line readout. The sample-to-detector distance was 1378 mm corresponding to the scattering vector range: $0.013\ Å^{-1} < Q < 0.34\ Å^{-1}$ (where $Q = 4\pi\sin\theta/\lambda$, 2θ is the scattering angle). The sample was placed in a quartz capillary, the temperature of which was kept constant (T = 4°C) via a water circulation. Air and window scattering was virtually eliminated by inserting the cell in an evacuated beam path (*27*). Several successive frames (usually eight) of 200 s each were recorded for both the sample and the corresponding buffer. Each frame was carefully inspected to check for any protein damage induced by X-rays (none was found) before calculating the average intensity and the associated experimental error. Each scattering spectrum was corrected for the detector response and scaled to the

transmitted intensity, using the scattering intensity from a reference carbon-black sample integrated over a given angular range. The scattering from the buffer was measured and subtracted from the corresponding protein sample pattern.

Scattering patterns were recorded at four different protein concentrations from 1 to 6.5 mg/ml. After scaling for concentration, the smallest angle data exhibited a slight increase with concentration indicative of moderate attractive interactions between molecules. Data were extrapolated to zero concentration following standard procedures using the second virial coefficient (*28*) (see inset to Figure 2A).. The scattering from a 5 mg/ml solution of lysozyme in 50 mM acetate buffer, pH 4.5, 100 mM NaCl was recorded and used as a calibration sample to derive the molecular mass from the intensity at the origin. The radius of gyration R_g was first evaluated using the Guinier approximation (*29*) using data points out to $Q_{max}R_g$ = 1.25. Restricting Q_{max} down to $Q_{max}R_g$ = 0.88 left the R_g value unchanged. The R_g value was also derived from the distance distribution function p(r) that represents the histogram of distances within the particle. Its value is equal to zero when r exceeds D_{max}, the maximum dimension of the protein. The p(r) function was computed using the indirect transform package GNOM (*30*). To make sure that no significant amount of oligomers nor even residual attractive concentration effects were affecting the data, a series of p(r) calculations was performed in which an increasing number of the smallest angle data points were eliminated reaching Q = 0.04 $Å^{-1}$, thereby excluding the entire Guinier region. No significant effect was detected in the resulting p(r) functions nor in the R_g value**.**

Modeling

The conformation in solution of $p47^{phox}$ was determined using three approaches. The program DAMMIN represents the protein as an assembly of closely packed small spheres (dummy atoms) of radius $r_0 << D_{max}$ inside a sphere of diameter D_{max} (*31*). The DAM structure

is defined by a configuration vector **X** with $N \approx (D_{max}/r_0)^3$ components; X(i) = 1 if the i^{th} dummy atom belongs to the protein and X(i) = 0 otherwise. Using simulated annealing, the program searches for a configuration that fits the experimental data while a looseness penalty ensures the compactness and connectivity of the solution. No particular condition of particle shape was imposed as constraint in these calculations.

The program GASBOR uses a protein representation as a chain of dummy residues (DR) centered at the Cα positions (*32*). Starting from a gas-like distribution of DRs inside the same search volume as DAMMIN, the program condenses this distribution so as to fit the experimental data under constraints that ensure the chain-like character of the DRs spatial distribution. Thus, each elementary step moves a DR to a new location 0.38 nm from another randomly chosen DR. Furthermore, the penalty function imposes a protein-like distribution of nearest neighbors, minimizes the number of discontinuities along the chain while maintaining the center of mass close to the center of the search volume. The program was run in default mode using standard values of the parameters. It was also used with a reduced weight of the penalty term ensuring that the nearest neighbor distribution would resemble that of a compact protein.

Like all Monte-Carlo approaches, neither DAMMIN nor GASBOR yield a unique solution. Therefore, several (typically ten) low-resolution models are constructed using each program before being superimposed using the program DAMAVER which calculates the normalized spatial discrepancy (NSD) between all pairs of models (*33*). This allows one, after elimination of outliers, to select the most typical model defined as the model with the smallest NSDs to all other models, *i.e*. that is most similar to other models.

Finally, the program BUNCH implements a combination of *ab initio* and rigid body modeling using the high-resolution structures of rigid domains of the protein when available (*34*). It finds the optimal positions and orientations of domains and probable conformations of

flexible linkers represented as DR chains that are attached to the appropriate end of domains. The scattering amplitudes of rigid domains are first calculated using the program CRYSOL (*35*). The scattering pattern is calculated using partial amplitudes of domains together with form factors of DRs describing the loops. To take into account the contribution to scattering of hydration water around DRs, the scattering amplitude of each DR was multiplied by a factor 1.2, a value derived from a rough estimate of the average amount of hydration water. The scattering pattern of the final model was calculated using CRYSOL and found to be practically undistinguishable from the BUNCH result, while differences were observed in the absence of correction (factor = 1.0), showing that this simple improvement was both necessary and effective.

RESULTS

The scattering pattern after correction for interparticle effects is shown in Figure 2A (dots) while the inset displays a close-up view of the affected part of the curve (see Materials and Methods for details). The corresponding distance distribution function p(r) is shown on Figure 2B (dots). The value of the maximal diameter of the molecule was found to be 125 Å ± 5 Å. The values of the radius of gyration derived from Guinier's law and the p(r) function are respectively 34.0 Å ± 0.5 Å and 34.7 Å ± 0.2 Å. Using lysozyme as a reference sample and taking into account the presence of 5% glycerol in the $p47^{phox}$ solution, the molecular mass for $p47^{phox}$ derived from the intensity at the origin was found close to 50 kDa, in agreement with the known molecular mass derived from the primary sequence (46365 Da), thereby ruling out any significant aggregation and showing that the protein is monomeric.

Both D_{max} and R_g values are considerably larger than those expected for a compact globular protein with the molecular mass of $p47^{phox}$ which are respectively of the order of

70–80 Å and 22 – 24 Å. This shows that the protein adopts an elongated conformation in solution. This is also strongly suggested by the p(r) function that exhibits a peak around 25 Å and a long falling edge extending to large r values, an asymmetric profile typical of an elongated particle.

Two *ab initio* modeling approaches implemented in DAMMIN and GASBOR programs were used to determine the shape of $p47^{phox}$ from scattering intensities out to Q_{max} = 0.25 and 0.34 $Å^{-1}$ respectively. Ten low-resolution models were constructed using each program before being superimposed using the program DAMAVER so as to determine the most typical model. The results from both approaches are very similar: all resulting models are elongated, most of them getting thinner at one end. All calculated scattering patterns are in excellent agreement with experimental data (χ ~ 0.9). A few Dummy Residue (DR) models obtained using GASBOR are presented in Figure 3A.

In a second modeling stage, protein domains whose structure had been determined by crystallography or NMR are positioned within the most typical low-resolution model. We have used the best representative conformer out of the 20 models of the PX domain determined by NMR (pdb file 1GD5 (*23*); r.m.s. deviation from average coordinates of about 1 Å over all non hydrogen atoms). Regarding the pair of SH3 domains, we assumed that their conformation within intact $p47^{phox}$ is close to that determined in the crystal for the truncated protein (157-332) comprising neither the PX domain nor the linker between this domain and the $SH3_A$ domain nor the C-terminal part, a conformation in which the SH3 tandem interacts with a polybasic region called the autoinhibitory region (AIR) (ref 20). Within the crystal, this truncated molecule is present as a dimer having swapped part of their $SH3_A$ domain (*16, 25*). Starting from the dimer structure (pdb file: 1ng2.pdb (*16*)) we have built a conformation of the monomer tandem-SH3s/AIR by restoring the exchanged fragment. These domains of

known structure were positioned within the most typical low-resolution model using the superimposition program SUPCOMB while imposing a distance restraint between the C-terminal end of the PX domain and the N-terminal end of the tandem-SH3s/AIR rigid domain (Figure 3B).

In a last step of the modeling process, the three missing parts are modeled as DR chains: the first 10 N-terminal residues, the 28 residue-long linker between PX and N-SH3 domains and the C-terminal part comprising 65 residues. This was performed using the program BUNCH. The PX domain and the tandem-SH3s/AIR domain were fixed at their initial position determined in the previous step. The resulting configurations compatible with this constraint exhibit a linker exposed to the solvent while remaining in the vicinity of the domains. The C-terminal stretch is always in an external position, away from the two domains. It appears to be poorly structured with no defined shape and its compactness, though variable, is lower than that of a structured domain. The corresponding calculated scattering patterns agree well with experimental data ($\chi \sim 0.85$ with randomly distributed residuals, see Figure 2). Two typical models are shown in Figure 3C. In this figure, each DR is represented by a sphere of radius 3.2 Å whose volume is equal to the average volume of an amino-acid residue, i.e. about 140 $Å^3$. Since the distance between two adjacent DRs is 3.8 Å (see Materials and Methods section), neighboring spheres are overlapping. Models were also calculated while releasing the constraint and leaving both domains free to move with respect to one another. In the resulting configurations, the two domains are not in contact any more but remain close with a closest distance of ca 5 Å and the intervening linker is rather compact but the orientation of the PX domain can vary widely as can be seen in the three models displayed in Figure 3D. The agreement between the calculated scattering pattern and the experimental data is equally good ($\chi \sim 0.83$). The values of R_g and D_{max} of all models

displayed in Figures 3C and 3D are the same as those derived from experimental data within experimental uncertainty.

DISCUSSION

Our results show that in the unphosphorylated, autoinhibited state, isolated $p47^{phox}$ adopts an elongated conformation in solution. The values of both the radius of gyration and the maximal diameter as well as *ab initio* models are unambiguous. The two structured domains (PX and the SH3 tandem/AIR domains) cannot form a globular assembly. We tried to simulate the experimental scattering curve starting from a conformation in which PX and the tandem SH3 form such a compact globule. All these attempts failed, yielding χ values $\geq$ 3. Therefore, the protection of PX phosphoinositol lipid binding sites necessary to the maintenance of the resting state does not involve a compact arrangement of domains. Many diagrams, admittedly with no claim to structural value, summarizing the various interactions within $p47^{phox}$ and the changes following phosphorylation show a transition from a "close", compact, conformation in the resting state to an "open" conformation in the activated state (see Fig. 1B and references therein). It follows from our results that "open" and "close" must be considered more in a functional than a structural sense. Besides, some of the proposed interactions appear to be mutually incompatible as mentioned earlier.

Both structured domains can easily be accommodated within the *ab initio* elongated envelope from Gasbor, thereby providing a starting point for modeling missing parts using BUNCH. This was done keeping the two structured domains fixed in their starting position or letting the program refine their position and orientation.

The various resulting conformations exhibit common features.

i) The C-terminal part, comprising 65 residues, does not adopt a well-defined structure, the chain being more or less compact, but it is always pointing away from the two structured domains. To quantify somewhat this description, we can compare the dimensions of the C-terminal part with those of a globular domain and with those of a chain with persistence length that is the adequate description for an unfolded polypeptide chain (*36*) . Assuming for such a chain a persistence length of the order of 9-10 Å, a value commonly found in the literature (*37*), the end-to-end distance is of the order of 60 Å for a 65 residue-long chain. The conformations found within our models exhibit shorter end-to-end distances, between 30 and 55 Å, which could be compatible with the presence of some structure in the C-terminal region. In contrast, the D_{max} value of the C-terminal part is comprised between 45 and 75 Å, larger than the value of around 30 Å expected for a 65-residue compact globular domain. The C-terminal extremity therefore appears to be mainly unstructured but not completely unfolded. We have examined the amino-acid sequence of the C-terminal 107 residues using several programs predicting unfolded segments (*38-45*). The results are very similar and summarized in Figure 4A: all programs predict the 65 C-terminal residues to be essentially disordered with, for three of them, the exception of the very last stretch. Programs predicting secondary structure elements (*46-49*) predict a unique helix formation for the very last residues. Interestingly enough, this helix has been experimentally observed when the C-terminal 30 residues from $p47^{phox}$ are complexed with the C-terminal SH3 domain from $p67^{phox}$ (*50*). The body of computational or experimental evidence presented above broadly agrees with a description of the C-terminal 65 residues in terms of a mostly unfolded chain with a few local structure elements. Finally, the fact that the C-terminal part is always pointing away from the two structured domains seems to rule out any role in the preservation of the resting state.

In contrast, predictions regarding the AIR region are more variable, the region appearing to be more or less structured in 5 out of 9 analyses (lines 1-5 in Fig.4A). This is in agreement with the fact that it appears to be ordered and in interaction with the SH3 tandem in both crystal and NMR studies (*16, 25*). Actually, the absence of a strong consensus towards a well-defined structure suggests that this segment is structured through its interaction with the two SH3 domains and that losing the interaction might cause the AIR region to lose its structure as well.

ii) The 28 residue-long linker connecting the PX domain to the tandem-SH3s/AIR region does not appear to adopt a random coil configuration nor a compact conformation in the BUNCH models. This parallels the results of sequence analysis programs that do not give a clear and consistent view of the region, neither structured nor totally unfolded, beyond a large solvent accessibility (Figure 4B). A contribution of this linker to constraining the mutual arrangement of the structured domains cannot be ruled out.

iii) The initial position of the PX domain and of the tandem SH3s/AIR domain directly derives from a combination of *ab initio* modeling (GASBOR model) and high-resolution crystal structures of the two domains. In this conformation, the two domains are weakly connected and a direct contact, highlighted in Figure 3C, can be observed which involves the PX domain and a loop from the AIR sequence, protruding from the tandem-SH3s/AIR complex. Furthermore, the accessibility of the arginine residues from PX to membrane lipids appears hindered by the tandem SH3s/AIR domain and the intervening linker in most configurations. However, the mutual orientation of the structured domains is not uniquely defined by the SAXS data. Allowing for position refinement by the program BUNCH results in configurations in which the two domains are not in contact anymore. They remain in close vicinity but the orientation of the PX domain appears to be hardly constrained as shown by the three models in Figure 3D in which the PX domain orientations, best

visualized by the short N-terminal tail, are very different from one another as well as from the original one seen in Figure 3C. Our data are thus compatible with two classes of models according to whether the structured domains are in direct interaction or not. SAXS data cannot by themselves discriminate between the two possibilities and should be complemented by other approaches such as NMR using residual dipolar couplings determination (*51, 52*) or mass spectrometry analysis of covalent cross-linking (*53*).

An intramolecular interaction of the PX domain seems necessary for the preservation of the resting state. Indeed, in the absence of stable contact with some part of the molecule, a well-defined position and orientation of the PX domain is difficult to conceive. It would most likely move fairly freely around the linker, thereby frequently exposing lipid binding arginine residues to the solvent, a situation difficult to reconcile with PX inhibition.

In a recent review, it has been proposed that the PX domain interacts with the whole tandem SH3s/AIR structured region rather than with the isolated $SH3_B$domain (*4*). Our models with interacting structured domains (Figure 3C) provide an example of such an interaction between the loop in the C-terminal part of the AIR and the PX domain that could ensure PX inhibition, with a possible contribution from part of the linker connecting the PX to the tandem SH3 domains. Other interactions are certainly possible which also make PX binding sites inaccessible to membrane lipids, but they all must exhibit a small buried interface imposed by the extended global conformation of $p47^{phox}$. Such an interaction between PX domain and following domains of $p47^{phox}$ is supported by microcalorimetric titration experiments (*16*). These data show that the presence of the PX domain increases by a factor of 3 the affinity of the tandem SH3s for a peptide corresponding to the AIR sequence (residue 296-330) with respect to the isolated tandem-SH3s region. It suggests some contribution from PX through either direct contact with the AIR sequence or indirect stabilizing effect *via* interaction with the tandem of SH3 domains.

Phosphorylation of Ser 303, 304 and 328 is generally believed to alter the AIR conformation so as to destabilize its interaction with tandem SH3 domains, thereby making them free to interact with the proline rich sequence of $p22^{phox}$. We simply propose that another, direct or indirect, consequence of AIR conformational change would be to set the PX domain essentially free to move around the linker to $SH3_A$, thereby making its lipid binding sites available for interaction with phosphatidyl inositol lipids from the plasma membrane. This hypothesis finds some support from data reported on a homologue of $p47^{phox}$, NoxO1 (or p41) a cytosolic factor of Nox1, a homologue of the flavocytochrome b_{558} which is constitutively activated (*54-56*). In NoxO1 the PX domain has been shown to interact constitutively with phosphatidyl inositol lipids (*57*). In addition the stimulus independent superoxide production by Nox1 can be converted into a stimulus dependent system when replacing NoxO1 by $p47^{phox}$ in a reconstituted whole cell system (*54*). Interestingly, in contrast to $p47^{phox}$, NoxO1 does not contain an AIR sequence, an absence which correlates with a constitutive association to the membrane.

In conclusion, we have shown that $p47^{phox}$ adopts an extended conformation in the resting state. The two structured domains must be in close vicinity but can only be weakly connected, when at all in contact, their interacting surface area being small, while the C-terminal part, essentially unstructured, extends away from the structured domains. Work is under way, using complementary approaches to SAXS, to characterize further the interactions ensuring PX inhibition.

ACKNOWLEDGMENTS

We are very grateful to Maxim Petoukhov for making the program Bunch available to us before its general distribution and for fruitful discussions regarding its use. We thank the technical staff from LURE-DCI. We thank M.C. Dagher for the kind gift of the $p47^{phox}$ containing expression vector.

REFERENCES

1. Vignais, P. V. (2002) The superoxide-generating NADPH oxidase: structural aspects and activation mechanism *Cell Mol Life Sci 59*, 1428-59.
2. Babior, B. M. (2004) NADPH oxidase *Curr Opin Immunol 16*, 42-7.
3. Perisic, O., Wilson, M. I., Karathanassis, D., Bravo, J., Pacold, M. E., Ellson, C. D., Hawkins, P. T., Stephens, L., and Williams, R. L. (2004) The role of phosphoinositides and phosphorylation in regulation of NADPH oxidase *Adv Enzyme Regul 44*, 279-98.
4. Groemping, Y., and Rittinger, K. (2005) Activation and assembly of the NADPH oxidase: a structural perspective *Biochem J 386*, 401-16.
5. El Benna, J., Faust, R. P., Johnson, J. L., and Babior, B. M. (1996) Phosphorylation of the respiratory burst oxidase subunit p47phox as determined by two-dimensional phosphopeptide mapping. Phosphorylation by protein kinase C, protein kinase A, and a mitogen-activated protein kinase *J Biol Chem 271*, 6374-8.
6. el Benna, J., Faust, L. P., and Babior, B. M. (1994) The phosphorylation of the respiratory burst oxidase component p47phox during neutrophil activation. Phosphorylation of sites recognized by protein kinase C and by proline-directed kinases *J Biol Chem 269*, 23431-6.
7. Johnson, J. L., Park, J. W., Benna, J. E., Faust, L. P., Inanami, O., and Babior, B. M. (1998) Activation of p47(PHOX), a cytosolic subunit of the leukocyte NADPH oxidase. Phosphorylation of ser-359 or ser-370 precedes phosphorylation at other sites and is required for activity *J Biol Chem 273*, 35147-52.
8. Inanami, O., Johnson, J. L., McAdara, J. K., Benna, J. E., Faust, L. R., Newburger, P. E., and Babior, B. M. (1998) Activation of the leukocyte NADPH oxidase by phorbol ester requires the phosphorylation of p47PHOX on serine 303 or 304 *J Biol Chem 273*, 9539-43.
9. Faust, L. R., el Benna, J., Babior, B. M., and Chanock, S. J. (1995) The phosphorylation targets of p47phox, a subunit of the respiratory burst oxidase. Functions of the individual target serines as evaluated by site-directed mutagenesis *J Clin Invest 96*, 1499-505.
10. Heyworth, P. G., Curnutte, J. T., Nauseef, W. M., Volpp, B. D., Pearson, D. W., Rosen, H., and Clark, R. A. (1991) Neutrophil nicotinamide adenine dinucleotide phosphate oxidase assembly. Translocation of p47-phox and p67-phox requires interaction between p47-phox and cytochrome b558 *J Clin Invest 87*, 352-6.
11. Dusi, S., Donini, M., and Rossi, F. (1996) Mechanisms of NADPH oxidase activation: translocation of p40phox, Rac1 and Rac2 from the cytosol to the membranes in human neutrophils lacking p47phox or p67phox *Biochem J 314*, 409-12.
12. Kanai, F., Liu, H., Field, S. J., Akbary, H., Matsuo, T., Brown, G. E., Cantley, L. C., and Yaffe, M. B. (2001) The PX domains of p47phox and p40phox bind to lipid products of PI(3)K *Nat Cell Biol 3*, 675-8.
13. Karathanassis, D., Stahelin, R. V., Bravo, J., Perisic, O., Pacold, C. M., Cho, W., and Williams, R. L. (2002) Binding of the PX domain of p47(phox) to

phosphatidylinositol 3,4-bisphosphate and phosphatidic acid is masked by an intramolecular interaction *EMBO J 21*, 5057-68.
14. Sumimoto, H., Kage, Y., Nunoi, H., Sasaki, H., Nose, T., Fukumaki, Y., Ohno, M., Minakami, S., and Takeshige, K. (1994) Role of Src homology 3 domains in assembly and activation of the phagocyte NADPH oxidase *Proc Natl Acad Sci U S A 91*, 5345-9.
15. Leto, T. L., Adams, A. G., and de Mendez, I. (1994) Assembly of the phagocyte NADPH oxidase: binding of Src homology 3 domains to proline-rich targets *Proc Natl Acad Sci U S A 91*, 10650-4.
16. Groemping, Y., Lapouge, K., Smerdon, S. J., and Rittinger, K. (2003) Molecular basis of phosphorylation-induced activation of the NADPH oxidase *Cell 113*, 343-55.
17. Ogura, K., Nobuhisa, I., Yuzawa, S., Takeya, R., Torikai, S., Saikawa, K., Sumimoto, H., and Inagaki, F. (2006) NMR Solution Structure of the Tandem Src Homology 3 Domains of p47phox Complexed with a p22phox-derived Proline-rich Peptide *Journal of Biological Chemistry 281*, 3660-3668.
18. DeLeo, F. R., Nausseef, W. M., Jesaitis, A. J., Burritt, J. B., Clark, R. A., and Quinn, M. T. (1995) A domain of p47phox that interacts with human neutrophil flavocytochrome b_{558} *J. Biol. Chem. 270*, 26246-51.
19. DeLeo, F. R., Yu, L., Burritt, J. B., Loetterle, L. R., Bond, C. W., Jesaitis, A. J., and Quinn, M. T. (1995) Mapping sites of interaction of p47-*phox* and flavocytochrome b with random-sequence peptide phage display libraries *Proc. Natl. Acad. Sci. U.S.A. 92*, 7110-4.
20. Ago, T., Nunoi, H., Ito, T., and Sumimoto, H. (1999) Mechanism for phosphorylation-induced activation of the phagocyte NADPH oxidase protein p47(phox). Triple replacement of serines 303, 304, and 328 with aspartates disrupts the SH3 domain-mediated intramolecular interaction in p47(phox), thereby activating the oxidase *J Biol Chem 274*, 33644-53.
21. Ago, T., Kuribayashi, F., Hiroaki, H., Takeya, R., Ito, T., Kohda, D., and Sumimoto, H. (2003) Phosphorylation of p47phox directs phox homology domain from SH3 domain toward phosphoinositides, leading to phagocyte NADPH oxidase activation *Proc Natl Acad Sci U S A 100*, 4474-9.
22. Shiose, A., and Sumimoto, H. (2000) Arachidonic acid and phosphorylation synergistically induce a conformational change of p47phox to activate the phagocyte NADPH oxidase *J Biol Chem 275*, 13793-801.
23. Hiroaki, H., Ago, T., Ito, T., Sumimoto, H., and Kohda, D. (2001) Solution structure of the PX domain, a target of the SH3 domain *Nat Struct Biol 8*, 526-30.
24. de Mendez, I., Homayounpour, N., and Leto, T. L. (1997) Specificity of p47phox SH3 domain interactions in NADPH oxidase assembly and activation *Mol Cell Biol 17*, 2177-85.
25. Yuzawa, S., Suzuki, N. N., Fujioka, Y., Ogura, K., Sumimoto, H., and Inagaki, F. (2004) A molecular mechanism for autoinhibition of the tandem SH3 domains of p47phox, the regulatory subunit of the phagocyte NADPH oxidase *Genes Cells 9*, 443-56.
26. Yuzawa, S., Ogura, K., Horiuchi, M., Suzuki, N. N., Fujioka, Y., Kataoka, M., Sumimoto, H., and Inagaki, F. (2004) Solution structure of the tandem Src homology 3 domains of p47phox in an autoinhibited form *J Biol Chem 279*, 29752-60.
27. Dubuisson, J. M., Decamps, T., and Vachette, P. (1997) Improved signal-to-background ratio in small-angle X-ray scattering experiments with synchrotron radiation using an evacuated cell for solutions *J. Appl. Cryst. 30*, 49 - 54.

28. Mangenot, S., Leforestier, A., Vachette, P., Durand, D., and Livolant, F. (2002) Salt-induced conformation and interaction changes of nucleosome core particles *Biophys J 82*, 345-56.
29. Guinier, A., and Fournet, G. (1955) *Small Angle Scattering of X-Rays*, Wiley, New York.
30. Svergun, D. I. (1992) Determination of the Regularization Parameter in Indirect-Transform Methods Using Perceptual Criteria *J. Appl. Cryst. 25*, 495 - 503.
31. Svergun, D. I. (1999) Restoring low resolution structure of biological macromolecules from solution scattering using simulated annealing *Biophys J 76*, 2879-86.
32. Svergun, D. I., Petoukhov, M. V., and Koch, M. H. (2001) Determination of domain structure of proteins from X-ray solution scattering *Biophys J 80*, 2946-53.
33. Kozin, M. B., and Svergun, D. I. (2001) Automated matching of high- and low-resolution structural models *J. Appl. Crystallogr. 34*, 33-41.
34. Petoukhov, M. V., and Svergun, D. I. (2005) Global rigid body modeling of macromolecular complexes against small-angle scattering data *Biophys J 89*, 1237-50. Epub 2005 May 27.
35. Svergun, D. I., Barberato, C., and Koch, M. H. (1995) CRYSOL - a program to evaluate X-ray solution scattering of biological macromolecules from atomic coordinates. *J. Appl. Crystallogr. 28*, 768-773.
36. Pérez, J., Vachette, P., Russo, D., Desmadril, M., and Durand, D. (2001) Heat-induced unfolding of neocarzinostatin, a small all-beta protein investigated by small-angle X-ray scattering *J Mol Biol 308*, 721-43.
37. Rowe, G., and Lopez Pineiro, A. (1990) Influence of the solvent on the conformational-dependent properties of random-coil polypeptides. I. The mean-square of the end-to-end distance and of the dipole moment *Biophys. Chem. 36*, 57-64.
38. Coeytaux, K., and Poupon, A. (2005) Prediction of unfolded segments in a protein sequence based on amino acid composition *Bioinformatics 18*, 18.
39. Linding, R., Jensen, L. J., Diella, F., Bork, P., Gibson, T. J., and Russell, R. B. (2003) Protein disorder prediction: implications for structural proteomics *Structure (Camb) 11*, 1453-9.
40. Linding, R., Russell, R. B., Neduva, V., and Gibson, T. J. (2003) GlobPlot: Exploring protein sequences for globularity and disorder *Nucleic Acids Res 31*, 3701-8.
41. Li, X., Romero, P., Rani, M., Dunker, A. K., and Obradovic, Z. (1999) Predicting protein disorder for N-, C-, and internal regions. *Genome Informatics 10*, 30-40.
42. Romero, P., Obradovic, Z., Li, X., Garner, E., Brown, C., and Dunker, A. K. (2001) Sequence complexity of disordered protein. *Proteins: Struct. Funct. Gen. 42*, 38-48.
43. Thomson, R., and Esnouf, R. (2004) Prediction of natively disordered regions in proteins using a bio-basis function neural network. *Lecture Notes in computer science 3177*, 108-116.
44. Uversky, V. N., Gillespie, J. R., and Fink, A. L. (2000) Why are "natively unfolded" proteins unstructured under physiologic conditions? *Proteins 41*, 415-27.
45. Ward, J. J., Sodhi, J. S., McGuffin, L. J., Buxton, B. F., and Jones, D. T. (2004) Prediction and functional analysis of native disorder in proteins from the three kingdoms of life *J Mol Biol 337*, 635-45.
46. Cuff, J. A., and Barton, G. J. (2000) Application of multiple sequence alignment profiles to improve protein secondary structure prediction *Proteins 40*, 502-11.
47. McGuffin, L. J., Bryson, K., and Jones, D. T. (2000) The PSIPRED protein structure prediction server *Bioinformatics 16*, 404-5.

48. Jones, D. T. (1999) Protein secondary structure prediction based on position-specific scoring matrices *J Mol Biol 292*, 195-202.
49. Rost, B., Yachdav, G., and Liu, J. (2004) The PredictProtein server *Nucleic Acids Res 32*, W321-6.
50. Kami, K., Takeya, R., Sumimoto, H., and Kohda, D. (2002) Diverse recognition of non-PxxP peptide ligands by the SH3 domains from p67(phox), Grb2 and Pex13p *EMBO J 21*, 4268-76.
51. Gabel, F., Simon, B., and Sattler, M. (2006) A target function for quaternary structural refinement from small angle scattering and NMR orientational restraints *Eur Biophys J*, 1-15.
52. Grishaev, A., Wu, J., Trewhella, J., and Bax, A. (2005) Refinement of multidomain protein structures by combination of solution small-angle X-ray scattering and NMR data *J Am Chem Soc 127*, 16621-8.
53. Back, J. W., de Jong, L., Muijsers, A. O., and de Koster, C. G. (2003) Chemical cross-linking and mass spectrometry for protein structural modeling *J Mol Biol 331*, 303-13.
54. Banfi, B., Clark, R. A., Steger, K., and Krause, K. H. (2003) Two novel proteins activate superoxide generation by the NADPH oxidase NOX1 *J Biol Chem 278*, 3510-3.
55. Geiszt, M., Lekstrom, K., Witta, J., and Leto, T. L. (2003) Proteins homologous to p47phox and p67phox support superoxide production by NAD(P)H oxidase 1 in colon epithelial cells *J Biol Chem 278*, 20006-12.
56. Suh, Y. A., Arnold, R. S., Lassegue, B., Shi, J., Xu, X., Sorescu, D., Chung, A. B., Griendling, K. K., and Lambeth, J. D. (1999) Cell transformation by the superoxide-generating oxidase Mox1 *Nature 401*, 79-82.
57. Cheng, G., and Lambeth, J. D. (2004) NOXO1, regulation of lipid binding, localization, and activation of Nox1 by the Phox homology (PX) domain *J Biol Chem 279*, 4737-42.
58. Grizot, S., Grandvaux, N., Fieschi, F., Faure, J., Massenet, C., Andrieu, J. P., Fuchs, A., Vignais, P. V., Timmins, P. A., Dagher, M. C., and Pebay-Peyroula, E. (2001) Small angle neutron scattering and gel filtration analyses of neutrophil NADPH oxidase cytosolic factors highlight the role of the C-terminal end of p47phox in the association with p40phox *Biochemistry 40*, 3127-33.
59. Ito, T., Nakamura, R., Sumimoto, H., Takeshige, K., and Sakaki, Y. (1996) An SH3 domain-mediated interaction between the phagocyte NADPH oxidase factors p40phox and p47phox *FEBS Lett 385*, 229-32.
60. Fuchs, A., Dagher, M. C., Faure, J., and Vignais, P. V. (1996) Topological organization of the cytosolic activating complex of the superoxide-generating NADPH-oxidase. Pinpointing the sites of interaction between p47phoz, p67phox and p40phox using the two-hybrid system *Biochim Biophys Acta 1312*, 39-47.
61. Fuchs, A., Dagher, M. C., and Vignais, P. V. (1995) Mapping the domains of interaction of p40phox with both p47phox and p67phox of the neutrophil oxidase complex using the two-hybrid system *J Biol Chem 270*, 5695-7.
62. Sumimoto, H., Hata, K., Mizuki, K., Ito, T., Kage, Y., Sakaki, Y., Fukumaki, Y., Nakamura, M., and Takeshige, K. (1996) Assembly and activation of the phagocyte NADPH oxidase. Specific interaction of the N-terminal Src homology 3 domain of p47phox with p22phox is required for activation of the NADPH oxidase *J Biol Chem 271*, 22152-8.
63. Ago, T., Takeya, R., Hiroaki, H., Kuribayashi, F., Ito, T., Kohda, D., and Sumimoto, H. (2001) The PX domain as a novel phosphoinositide- binding module *Biochem Biophys Res Commun 287*, 733-8.

64. Lapouge, K., Smith, S. J., Groemping, Y., and Rittinger, K. (2002) Architecture of the p40-p47-p67phox complex in the resting state of the NADPH oxidase. A central role for p67phox *J Biol Chem 277*, 10121-8.
65. Nauseef, W. M. (2004) Assembly of the phagocyte NADPH oxidase *Histochem. Cell. Biol. 122*, 277-91.

FIGURE CAPTIONS

Figure 1: Schematic representations of p47^{phox}, a cytosolic factor of the NADPH oxidase complex. (A) domain organization in p47^{phox}, arrows indicate all interactions that have been shown experimentally (*12, 14, 15, 24, 58-63*). (B) Proposed model for the domain organization in the autoinhibitory state of p47^{phox} (*4, 20, 21, 64, 65*).

Figure 2: (A) SAXS pattern of p47^{phox} after correction for interparticle effects. Dots: experimental points; solid line: fit to the data by the BUNCH model shown in Figure 3C Inset: experimental intensities in the smallest-angle region as a function of protein concentration (long-dashed line: 6.5 mg/ml; continuous line with x : 4 mg/ml; short-dashed line :2 mg/ml; thin continuous line : 1 mg/ml; thick continuous line : intensities extrapolated to infinite dilution). (B) distance distribution function p(r).

Figure 3: (A) Five models of p47^{phox} obtained using GASBOR (see text for details). (B) Crystal structures of PX and SH3 tandem fitted in the GASBOR model using SUPCOMB. The crystal structures are represented by their Cα trace (violet : PX; red : Tandem SH3s/AIR). The model is represented by its surface envelope in transparent light green. (C) Two examples of p47^{phox} conformations obtained using BUNCH with the two partial crystal structures (CPK representation) maintained at the fixed position derived from SUPCOMB (lavanda: SH3 tandem, cyan: PX). The *ab initio* models of the unknown linker and extremities are shown as orange spheres of radius 3.2 Å (see text for details).: T. (D) Three examples of p47^{phox} conformations obtained using BUNCH in which the mutual position of

the two partial crystal structures was refined by the program. The SH3 tandem is in the same position as in C. The *ab initio* models of the unknown linker and extremities are shown as magenta spheres of radius 3.2 Å . In Figure 4C and 4D, Arg45 and 92 are shown in black when at all visible. All figures have been made using the program WebLab ViewerLite 40 (molecular simulation ink).

Figure 4: Prediction of unfolded segments and secondary structure analysis of the C-terminal region (A) and of the 28 residue-long linker connecting the PX domain to the tandem-SH3s/AIRregion (B). Segments predicted to be unfolded are in bold. c: coil ; **h** : helix; **e** :extended . (1) Prelink (*38*); (2) DisEMBL, Loops/coils (*39*); (3) DisEMBL, Hot-loops; (4) DisEMBL, Remark-465; (5) Globplot (*40*); (6) PONDR (*41, 42*); (7) RONN (*43*); (8) Foldindex (http://bip.weizmann.ac.il/fldbin/findex); (9) DISOPRED (*45*); (10) JPRED (*46*); (11) PSIPRED (*47, 48*); (12) PHD (*49*).

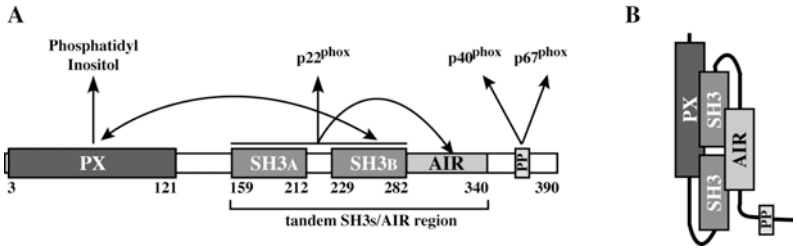

Figure 1

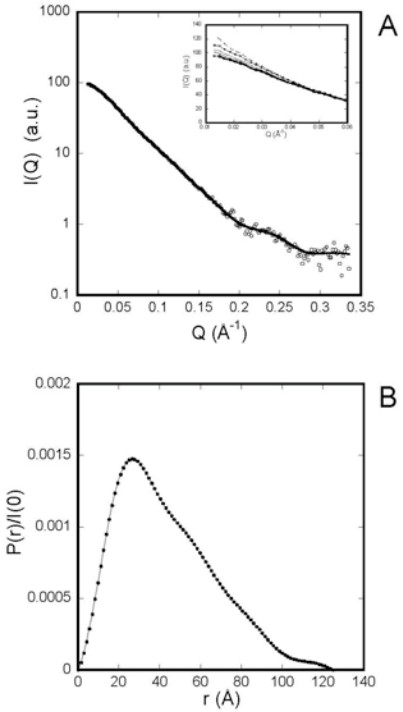

Figure 2

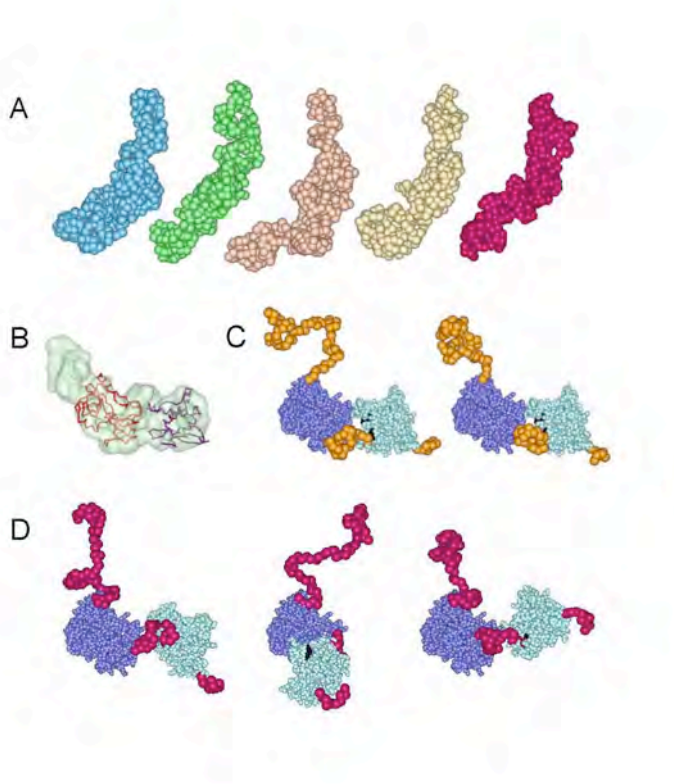

Figure 3

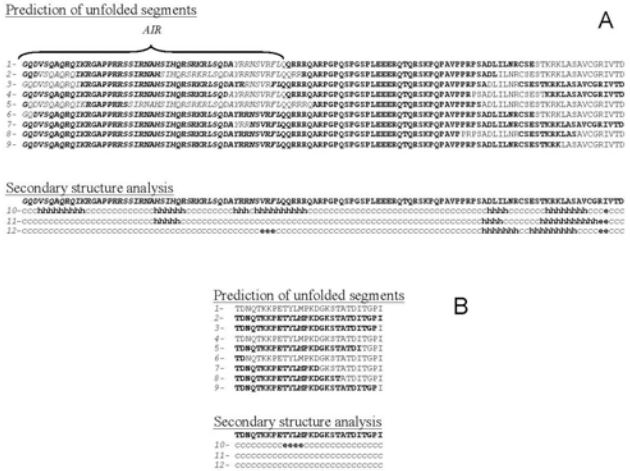

Figure 4

FOR TABLE OF CONTENTS USE ONLY

Small-Angle X-Ray Scattering reveals an Extended Organization For The Auto-Inhibitory Resting State of the p47^{phox} Modular Protein.

Dominique Durand§*, Dominique Cannella‡, Virginie Dubosclard‡, Eva Pebay-Peyroula‡, Patrice Vachette§ and Franck Fieschi‡*

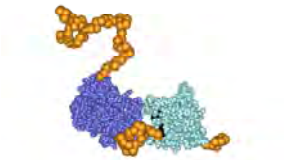

Abstracts

Article P11 : Royant *et al.* (2002) *J.Biol.Chem.*

Caractérisation du twinning des cristaux de p67^{phox} et de la bactériorohodpsin

Dans cet article de méthodologie en cristallographie, les propriétés de twinning des cristaux obtenus avec p67^{phox} et la bactériorhodopsine sont présentées et caractérisées. Des méthodes pour le détecter et en déterminer l'importance sont présentées et comparées afin de pouvoir corriger les intensités mesurés à partir de tels cristaux ou pour faciliter le tri de cristaux non-twinnés.

Article P10 : Grizot et al. (2001) *Biochemistry*

La structure du complexe Rac1/RhoGDI

Rac1 existe sous deux formes, active et inactive, suivant qu'elle lie du GTP ou du GDP, respectivement. La présence de l'une ou l'autre forme est régulée par des protéines. Rac1 est maintenue inactive par l'association à la protéine RhoGDI qui inhibe la dissociation du GDP et l'empêche de s'ancrer dans la membrane lipidique. Nous avons cristallisé le complexe et résolu sa structure à partir de données de diffraction à 2.7 Å. La structure révèle deux types d'interaction entre les deux protéines : l'une faisant intervenir des résidus de surface, l'autre faisant intervenir la chaîne isoprène qui est attachée à Rac1 de façon covalente et qui plonge dans une cavité hydrophobe à l'intérieur de RhoGDI. L'étude détaillée des acides aminés impliqués dans ces interactions permet de comprendre la spécificité de RhoGDI pour Rac1.

Article P8 :Grizot et al (2001) *Biochemistry*

Etudes en solution des propriétés d'interaction entre facteurs cytosoliques.

Nous avons étudié les interactions des facteurs cytosoliques en solution par des approches biochimiques (filtration sur gel) et biophysiques (diffusion des neutrons aux petits angles). L'interaction entre p47^{phox} et p40^{phox} est rationnalisée.

Acta Crystallographica Section D
Biological Crystallography
ISSN 0907-4449

Detection and characterization of merohedral twinning in two protein crystals: bacteriorhodopsin and p67^{phox}

Antoine Royant,[a,b]† Sylvestre Grizot,[a]†§ Richard Kahn,[a] Hassan Belrhali,[b]‡ Franck Fieschi,[a] Ehud M. Landau[c] and Eva Pebay-Peyroula[a]*

[a]Institut de Biologie Structurale, CEA–CNRS–Université Joseph Fourier UMR5075, 41 Rue Jules Horowitz, F-38027 Grenoble CEDEX 1, France, [b]European Synchrotron Radiation Facility, 6 Rue Jules Horowitz, BP 220, F-38043 Grenoble CEDEX, France, and [c]Membrane Protein Laboratory, Department of Physiology and Biophysics and Sealy Centers for Structural Biology and Molecular Science, The University of Texas Medical Branch, 301 University Boulevard, Galveston, TX 77555-0641, USA

† These authors contributed equally to this work.
‡ Current address: EMBL, 6 Rue Jules Horowitz, BP 181, F-38042 Grenoble CEDEX 9, France.
§ Current address: NIDDK/LMB, 50 South Drive, Bethesda, MD 20892-8030, USA.

Correspondence e-mail: pebay@ibs.fr

Received 25 October 2001
Accepted 28 February 2002

The estimation of the twinning ratio in crystals of two proteins, bacteriorhodopsin and a truncated form of p67^{phox}, is described. Various approaches are combined to detect and determine accurately the twinning ratio. For each protein, three data sets from crystals exhibiting twinning ratios ranging from 0 to almost 50% are analysed. Self-rotation functions and R_{sym} values considering space groups of higher symmetry are indicative of twinning. Precise values of the twinning ratios are derived from Yeates' statistical approaches and Britton plots. The twinning ratios are also obtained by analysing the second-, third- and fourth-order moments of the intensity distribution. The twinning ratios obtained from the various approaches are compared. Second-, third- and fourth-order moments of the intensity distribution are useful indicators for evaluating the twinning precisely in order to correct the intensities or to screen rapidly for non-twinned crystals.

1. Introduction

Twinning has recently been observed in numerous protein crystal systems (Luecke *et al.*, 1998; Valegard *et al.*, 1998; Royant *et al.*, 2000; Frazão *et al.*, 1999; Ban *et al.*, 1999; Taylor *et al.*, 2000). Twinning is a crystal-growth defect that arises when two or more domains within a crystal have different orientations and may even vary among crystals grown in the same batch. If the lattices of the various domains overlay perfectly in three dimensions, the twinning is merohedral. As a consequence, the reciprocal lattices of these domains coincide, summing the intensities of the Bragg spots corresponding to different Miller indices. Hemihedral twinning is a special case of merohedral twinning that occurs when two crystal domains exist. In the case of a 50% hemihedral twinning, the crystal is composed of two domains of equal volume and it is impossible to retrieve the diffracting intensities for each of the individual domains. For twinning ratios smaller than 50% diffraction intensities can be corrected. It is known from small-molecule studies that some space groups favour twinning. This is particularly the case for hexagonal, trigonal or tetragonal space groups (for reviews, see Yeates, 1997; Chandra *et al.*, 1999). Because small-molecule crystals usually diffract to very high resolution, the ratio between the number of refined parameters and the number of experimental observations is large enough to allow a global refinement of both crystal domains at the same time.

The mixing of diffraction spots with different Miller indices affects the global intensity distribution and adds additional symmetry relationships, relative to crystallographic symme-

Articles

Crystal Structure of the Rac1−RhoGDI Complex Involved in NADPH Oxidase Activation[†,‡]

S. Grizot,[§] J. Fauré,[||,⊥] F. Fieschi,[§] P. V. Vignais,[||] M.-C. Dagher,*[,||] and E. Pebay-Peyroula*[,§]

Institut de Biologie Structurale, CEA-CNRS-UJF, UMR 5075, 41 Rue Jules Horowitz, 38027 Grenoble Cedex 1, France, and Laboratoire BBSI/CEA-CNRS-UJF, UMR 5092/Département de Biologie Moléculaire et Structurale/CEA Grenoble, 17 Rue des Martyrs, 38054 Grenoble Cedex 9, France

Received February 9, 2001; Revised Manuscript Received May 15, 2001

ABSTRACT: A heterodimer of prenylated Rac1 and Rho GDP dissociation inhibitor was purified and found to be competent in NADPH oxidase activation. Small angle neutron scattering experiments confirmed a 1:1 stoichiometry. The crystal structure of the Rac1−RhoGDI complex was determined at 2.7 Å resolution. In this complex in which Rac1 is bound to GDP, the switch I region of Rac1 is in the GDP conformation whereas the switch II region resembles that of a GTP-bound GTPase. Two types of interaction between RhoGTPases and RhoGDI were investigated. The lipid−protein interaction between the geranylgeranyl moiety of Rac1 and RhoGDI resulted in numerous structural changes in the core of RhoGDI. The interactions between Rac1 and RhoGDI occur through hydrogen bonds which involve a number of residues of Rac1, namely, $Tyr64_{Rac}$, $Arg66_{Rac}$, $His103_{Rac}$, and $His104_{Rac}$, conserved within the Rho family and localized in the switch II region or in its close neighborhood. Moreover, in the switch II region of Rac1, hydrophobic interactions involving $Leu67_{Rac}$ and $Leu70_{Rac}$ contribute to the stability of the Rac1−RhoGDI complex. Inhibition of the GDP−GTP exchange in Rac1 upon binding to RhoGDI partly results from interaction of $Thr35_{Rac}$ with $Asp45_{GDI}$. In the Rac1−RhoGDI complex, the accessibility of the effector loops of Rac1 probably accounts for the ability of the Rac1−RhoGDI complex to activate the NADPH oxidase.

The small G protein, Rac, a member of the Rho family, plays essential roles in a large variety of cellular processes, such as cell growth, the regulation of the actin cytoskeleton (*1*), and the inflammatory response, via the activation of the stress-activated protein kinases p38 and c-Jun kinase (*2*). Rac has also a key role in the assembly and activation of phagocyte NADPH oxidase (*3*). Rac cycles between an inactive GDP-bound state and an active GTP-bound state. This cycle is tightly regulated by guanine−nucleotide exchange factors (GEFs)[1] that catalyze the GDP−GTP exchange reaction and by GTPase-activating proteins (GAPs) that enhance the intrinsic GTPase activity of the small G proteins (*4*). Rac undergoes a posttranslational modification that allows its localization to the plasma membrane. It consists of the covalent binding of a geranylgeranyl group to the cysteine residue of the C-terminal CAAX motif via a thioether linkage, a reaction that is catalyzed by a geranylgeranyl transferase. The last three amino acids are then released, and the C-terminal cysteine residue is carboxymethylated. Three isoforms of Rac have been reported in humans, namely, Rac1, which is ubiquitously expressed, Rac2, which is predominantly present in the cells of the myeloid lineage (*5*), and Rac3, which was recently cloned from a breast cancer cell line (*6*).

In resting cells, most of the Rho-related proteins are located in the cytosol, associated with a GDP dissociation inhibitor protein, RhoGDI (*7*), which is ubiquitously expressed. Another isoform, called LyGDI (also termed D4-GDI or RhoGDI2), is only present in the hematopoietic tissues (*8*, *9*). A third isoform, RhoGDIγ, with an N-terminal extension of 20 amino acids, was shown to be preferentially expressed in brain and pancreas (*10*). RhoGDI was first isolated as an inhibitor protein for the GDP−GTP exchange reaction on RhoB (*11*). RhoGDI inhibits the release of GDP from the active site of the RhoGTPases. It can also associate with the GTP-bound form of Rho proteins, and then it inhibits the intrinsic and GAP-catalyzed GTPase activity of

[†] This work was supported by the PCV-CNRS program, the Emergence/Region-Rhone-Alpes program, the Direction Générale des Forces et de la Prospective, the Fondation pour la Recherche Médicale, and the Association pour la Recherche sur le Cancer.

[‡] The coordinates and the structure factors have been deposited in the Protein Data Bank with ID code 1hh4.

* Corresponding authors.

[§] Institut de Biologie Structurale, CEA-CNRS-UJF, UMR 5075.

[||] Laboratoire BBSI/CEA-CNRS-UJF, UMR 5092/Département de Biologie Moléculaire et Structurale/CEA Grenoble.

[⊥] Present address: Laboratoire de Biochimie, Université Sciences II, 30 quai E. Ansermet, 1211 Geneva-4, Switzerland.

[1] Abbreviations: GEF, guanine−nucleotide exchange factor; GAP, GTPase-activating protein; GDI, guanine−nucleotide dissociation inhibitor; ERM, ezrin, radixin, and moesin; rmsd, root mean square deviation; CRIB, Cdc42/Rac interaction binding.

10.1021/bi010288k CCC: $20.00
Published on Web 08/03/2001

Small Angle Neutron Scattering and Gel Filtration Analyses of Neutrophil NADPH Oxidase Cytosolic Factors Highlight the Role of the C-Terminal End of p47^{phox} in the Association with p40^{phox} †

S. Grizot,[‡,§] N. Grandvaux,[§,||,⊥] F. Fieschi,[‡] J. Fauré,[||,@] C. Massenet,[‡] J.-P. Andrieu,[‡] A. Fuchs,[||] P. V. Vignais,[||] P. A. Timmins,[#] M.-C. Dagher,*[,||] and E. Pebay-Peyroula*[,‡]

Institut de Biologie Structurale, CEA-CNRS-UJF, UMR 5075, 41 rue Jules Horowitz, 38027 Grenoble Cedex 1, France, Laboratoire BBSI, CEA-CNRS-UJF, UMR 5092/Département de Biologie Moléculaire et Structurale/CEA Grenoble, 17 Rue des Martyrs, 38054 Grenoble Cedex 9, France, and Institut Laue-Langevin, 6 Rue Jules Horowitz, BP156, 38042 Grenoble Cedex 9, France

Received November 13, 2000; Revised Manuscript Received January 22, 2001

ABSTRACT: The NADPH oxidase of phagocytic cells is regulated by the cytosolic factors p47^{phox}, p67^{phox}, and p40^{phox} as well as by the Rac1−Rho-GDI heterodimer. The regulation is a consequence of protein−protein interactions involving a variety of protein domains that are well characterized in signal transduction. We have studied the behavior of the NADPH oxidase cytosolic factors in solution using small angle neutron scattering and gel filtration. p47^{phox}, two truncated forms of p47^{phox}, namely, p47^{phox} without its C-terminal end (residues 1−358) and p47^{phox} without its N-terminal end (residues 147−390), and p40^{phox} were found to be monomeric in solution. The dimeric form of p67^{phox} previously observed by gel filtration experiments was confirmed. Our small angle neutron scattering experiments show that p40^{phox} binds to the full-length p47^{phox} in solution in the absence of phosphorylation. We demonstrated that the C-terminal end of p47^{phox} is essential in this interaction. From the comparison of the presence or absence of interaction with various truncated forms of the proteins, we confirmed that the SH3 domain of p40^{phox} interacts with the C-terminal proline rich region of p47^{phox}. The radii of gyration observed for p47^{phox} and the truncated forms of p47^{phox} (without the C-terminal end or without the N-terminal end) show that all these molecules are elongated and that the N-terminal end of p47^{phox} is globular. These results suggest that the role of amphiphiles such as SDS or arachidonic acid or of p47^{phox} phosphorylation in the elicitation of NADPH oxidase activation could be to disrupt the p40^{phox}−p47^{phox} complex rather than to break an intramolecular interaction in p47^{phox}.

Neutrophils play an important role in host defense against invading microorganisms. They possess a multicomponent system, the NADPH oxidase, capable of producing superoxide anions O_2^- and other microbicidal derivatives upon activation. The superoxide-generating NADPH oxidase complex of phagocytic cells consists of a heterodimeric flavocytochrome *b*, cytosolic factors p40^{phox} (phox[1] for phagocyte oxidase), p47^{phox}, and p67^{phox}, and a small G-protein Rac1/Rac2 combined with its GDP dissociation inhibitor Rho-GDI (for reviews see refs *1* and *2*). The minimal complex which leads to the production of O_2^- ions requires the translocation of p47^{phox}, p67^{phox}, and Rac to the membrane and the association of these cytosolic factors with the flavocytochrome *b*. The translocation of the cytosolic factors is concomitant with the transient appearance of heterodimeric or heterotrimeric complexes, mediated by protein−protein interactions. The primary event for these interactions is most probably the phosphorylation of p47^{phox} which has seven phosphorylatable serine residues (*3*). Phosphorylation induces conformational changes modifying the topology of the protein and exposing domains that become accessible to specific partners (*4*). Phosphorylation also occurs on p40^{phox} and p67^{phox}, although its role is less well documented (*5*−*7*). Sequence analysis of the cytosolic factors reveals that these proteins are composed of various domains: SH3 (Src homology 3), PX (phox domain), TPR (tetratricopeptide repeat), PC (phox/Cdc42 motif), and polyPro (proline rich target) (Figure 1 and refs *8* and *9*). SH3 domains are involved in signal transduction through specific interactions with polyPro motifs. Although the presence of SH3 domains in p47^{phox}, p40^{phox}, and p67^{phox} and polyPro motifs in p47^{phox} and p67^{phox} favors such interactions, they are not the only

† The work was supported by the PCV-CNRS program, the Emergence/Region-Rhone-Alpes program, the Institut Universitaire de France, and the Direction Générale de l'Armement.

* To whom correspondence should be addressed. E-mail: pebay@ibs.fr. Telephone: 33(0)4 76 88 95 83. Fax: 33(0)4 76 88 54 94.

‡ Institut de Biologie Structurale, CEA-CNRS-UJF.

§ These authors contributed equally to this work.

|| Laboratoire BBSI, CEA-CNRS-UJF.

⊥ Present address: Molecular Oncology Group, Lady Davis Institute for Medical Research, Jewish General Hospital, 3755 chemin de la cote Sainte Catherine, H3T1E2 Montreal, Quebec, Canada.

@ Present address: Laboratoire de Biochimie, Université Sciences II, 30 quai E. Ansermet, 1211 Geneva-4, Switzerland.

Institut Laue-Langevin.

[1] Abbreviations: phox, phagocyte oxidase; SH3, Src homology 3; PX, PhoX domain (present in the N-terminal region of p47^{phox} and p40^{phox}); TPR, tetratricopeptide repeat; PC, phox/Cdc24p motif (present in p40^{phox} and Cdc24p); polyPro, proline rich target; Trx, thioredoxin; SANS, small angle neutron scattering; MBP, maltose binding protein.

10.1021/bi0028439 CCC: $20.00
Published on Web 02/15/2001

Chapitre II.

Récepteurs viraux :

CCR5 et CXCR4 co-récepteurs du VIH

DC-SIGN : récepteur de multiples pathogènes

I. Contamination HIV : de l'exposition à l'infection.

Les cellules dendritiques (CD) sont des professionnelles de la présentation d'antigènes. Elles sont présentes dans tous les tissus périphériques, épiderme et muqueuse, qui sont les zones de premiers contacts avec les agents pathogènes. Suite à la capture d'un pathogène, les CD initient leur maturation et entament leur migration vers les organes lymphoïdes où elles présentent l'antigène processé aux lymphoïdes T naïfs résidents. C'est ainsi que se déclenche la réponse immunitaire spécifique primaire. Les cellules dendritiques sont les seules capables d'initier une telle réponse immunitaire primaire (c'est à dire consécutive à une première exposition à un antigène). Les lymphocytes T sont responsables, une fois activés, de détruire les cellules infectées présentant à leur surface un antigène spécifique. Ils sont donc des acteurs clés dans la lutte contre les infections, notamment virales.

Dans le cas de l'infection VIH, ce sont précisément ces deux types cellulaires, essentiels dans la mise en place d'une réponse immunitaire spécifique, qui sont détournés et utilisés pour le bénéfice du virus. Ainsi, celui-ci est effectivement capturé par les cellules dendritiques des muqueuses génitales mais échappe aux étapes de "processing" et reste parfaitement intègre et infectieux. Il utilise ces cellules pour être convoyé vers sa cible privilégiée dans les organes lymphoïdes, les lymphocytes T. Lors de la présentation de l'antigène par les CD aux lymphocytes T, c'est en fait un virus infectieux qui est présenté et l'efficacité de l'infection est potentialisée lors de cette étape. Une série d'interactions entre le virus et le lymphocyte T se met en place et conduit à la fusion des membranes virale et cellulaire. Le lymphocyte T est infecté et participera *in fine* à la réplication de nouveaux virus (voir figure ci-dessous).

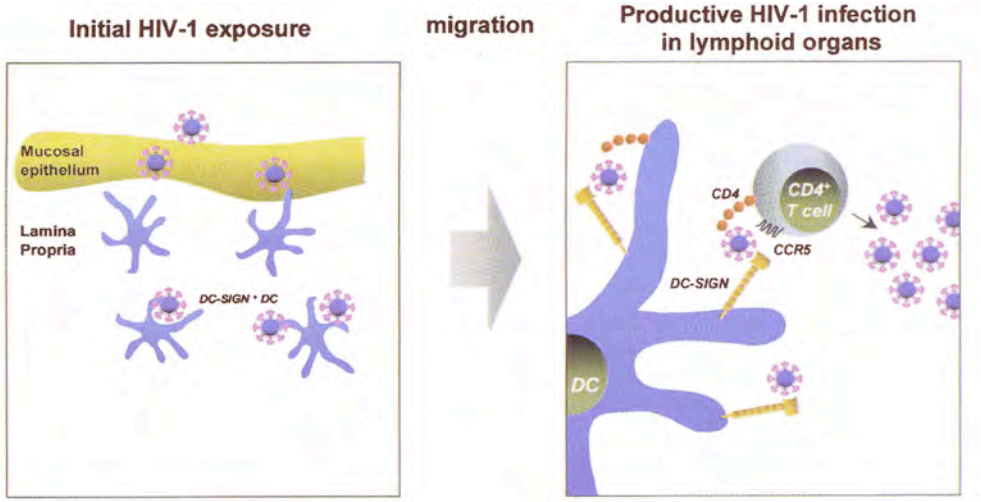

Ce processus requiert des interactions entre le virus et les cellules cibles et donc l'existence de récepteurs spécifiques à la surface de chacune de ces cellules. En 2000, la protéine DC-SIGN, un récepteur lectinique membranaire, a été découverte et impliquée dans la reconnaissance et le transport du VIH par les cellules dendritiques. Au niveau des lymphocytes T, outre CD4, un co-récepteur membranaire joue un rôlé clé dans le processus de fusion virale et d'infection. Cette protéine, CCR5 ou CXCR4, est un récepteur de chimiokine à 7 hélices transmembranaires.

Ces deux types de récepteurs, DC-SIGN et les co-récepteurs CCR5 et CXCR4, reconnaissent la protéine d'enveloppe du VIH, gp120. Dans le premier cas, ce sont les sucres présents à la surface de gp120 (60% de sa masse) qui sont reconnus, dans le deuxième cas l'interaction gp120/co-récepteurs est de type protéine/protéine. Ces deux types de récepteurs et

de complexe font l'objet des deux projets que je développe au laboratoire et qui sont présentés dans ce chapitre.

Il va sans dire que ces deux projets se situent dans un contexte international très compétitif. DC-SIGN ne possède q'un ancrage membranaire et il est donc possible, en le supprimant, d'obtenir une forme soluble facilement manipulable. Ce n'est pas le cas des co-récepteurs. De ce point de vue, ce projet présente de nombreuses difficultés et écueils additionnels qui vont être détaillés ci-dessous.

II. Les co-récepteurs CCR5 et CXCR4 du virus HIV et l'infection des lymphocytes T.

La compréhension fine des mécanismes de l'entrée du virus dans les cellules cibles, essentiellement les lymphocytes T, est un champ intense de recherche. En effet, ce processus est une des étapes du cycle viral qui peut être ciblée dans l'espoir d'un traitement thérapeutique ou préventif de cette maladie (Dimitrov 1997). Ainsi, il est bon de rappeler brièvement l'état des connaissances sur l'entrée du HIV au niveau de la membrane plasmique des cellules cibles (pour revue voir Doms et Trono, 2000).

II.A Etat des connaissances

MODE D'ENTREE DU VIH DANS LA CELLULE:

Le processus de l'entrée du virus peut être conceptualisé en trois étapes distinctes même si le phénomène est une dynamique continue *in vivo*. On parlera ainsi d'une première phase d'attachement du virus à la surface cellulaire, d'un évènement "d'ajustage conformationnel" des protéines de surface du virus, et pour finir la fusion entre les membranes plasmique et virale conduisant à l'entrée de la particule virale dans le cytoplasme. L'ensemble du processus est schématisé dans la figure ci-dessous.

La protéine d'enveloppe Env est la clef indispensable dont dispose le HIV pour pénétrer dans la cellule. Elle est produite sous la forme d'un polypeptide trimérique qui est ensuite clivé par une protéase cellulaire (lors du cycle viral précédent). Cette maturation par protéolyse conduit à un complexe de deux sous-unités associées non covalemment, gp120 et gp41. Ces deux sous-unités portent respectivement les fonctions d'attachement cellulaire et de fusion membranaire.

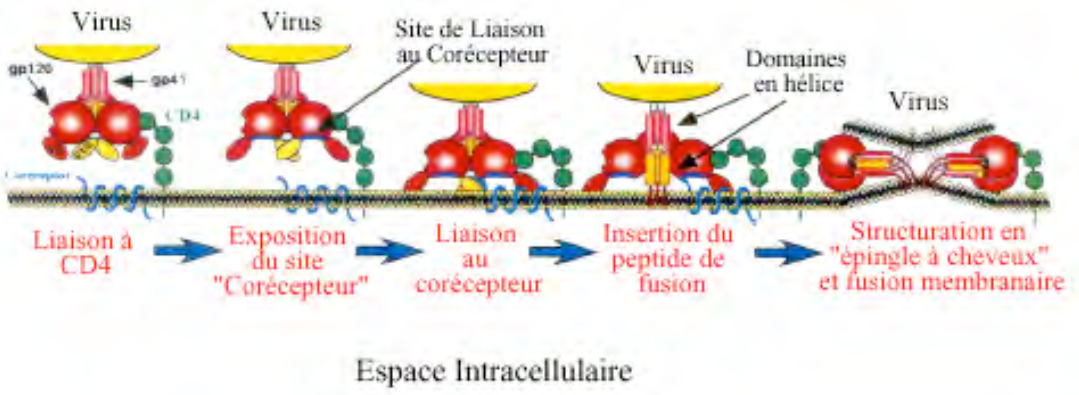

Modèle d'entrée du VIH dans la cellule (d'après Doms et Trono, 2000)

L'attachement : L'accrochage initial du virus à la surface est réalisé par l'interaction de gp120 avec la protéine CD4 (largement présente à la surface des lymphocytes T et des macrophages). Cet événement moléculaire ne suffit pas à induire l'ajustage conformationnel

permettant la fusion entre la membrane virale et cellulaire. Ce premier accrochage CD4-gp120 pilote l'exposition de nouveaux sites de gp120 capable d'interagir avec un nouveau partenaire protéique de la membrane cellulaire, le co-récepteur.

L'ajustage conformationnel : il existe deux co-récepteurs majeurs, CCR5 et CXCR4, définissant respectivement les virus T et M tropiques (Berger *et al.* 1999). Ces récepteurs à chimiokines sont des protéines membranaires intégrales à 7 hélices transmembranaires qui appartiennent à la large famille des récepteurs couplés à des protéines G (GPCR pour G Protein Coupled Receptor). Cette liaison de gp120 au co-récepteur entraîne des changements conformationnels dans les deux protéines d'enveloppe (gp120 et gp41), aboutissant à l'exposition des peptides hydrophobes de fusion du trimère de gp41.

Fusion membranaire : les peptides N-terminaux de gp41 s'insèrent dans la membrane cible sous forme d'un trimère de domaine hélical. Les trimères en hélices N-terminal et C-terminal de gp41 se replient l'un sur l'autre pour former une structure en épingle à cheveux. Ceci a pour effet de rapprocher les deux membranes, virales et plasmique, et de conduire à leur fusion.

II.B Les co-récepteurs, une cible pour une thérapie anti-infectieuse.

L'élaboration, par modélisation puis synthèse chimique, de molécules actives empêchant l'interaction gp120-corécepteurs nécessite l'obtention d'informations structurales relatives à ces GPCRs. Peu d'informations structurales sont aujourd'hui disponibles sur les GPCRs car, d'une part, leurs niveaux d'expression naturelle sont très bas et d'autre part, la conformation native de ces protéines dépend fortement de leur environnement membranaire. Aucun système d'expression permettant l'obtention de GPCR en quantité et qualité satisfaisante compatible avec des études structurales n'est actuellement disponible.

Ce projet vise dans un premier temps à mettre au point les outils de production nécessaire pour des objectifs plus long terme ambitionnant de déterminer les structures des 2 co-récepteurs. Le franchissement de cette première barrière méthodologique visant la surexpression de telles protéines membranaires intégrales est en soi est un défi d'envergure. Il va sans dire que la mise à disposition d'un outil de production à grande échelle de ces corécepteurs aurait des retombés allant bien au delà de l'étude structurale et ce notamment au niveau des applications en pharmacologie.

II.C Un projet méthodologique : production des co-récepteurs pour des études structurales.

Ce projet s'est bâti et a démarré en 2000 sur la base d'un réseau de compétences, constitué et financé par l'ANRS, et impliquant des groupes grenoblois, strasbourgeois et de l'Institut Pasteur de Paris. Les autres participants étaient : Hugues Lortat Jacob (IBS), Fernando Arenzana-Seisdedos (Institut Pasteur), Françoise Baleux (I.Pasteur), Franc Pattus (Strasbourg)

Différentes approches pour l'expression ont été confiées aux différents membres du réseau.

- cellules de mammifères avec le virus de la forêt de Semliki : Institut Pasteur
- cellules d'insectes : Institut de Biologie Structurale (Hugues Lortat Jacob) + Franc Pattus, Strasbourg
- levures *Hansenula polymorpha* : Franc Pattus, Strasbourg
- *Escherichia coli* (corps d'inclusion) : Institut de Biologie Structurale (F.Fieschi) + (Bernard Mouillac et Jean Louis Banères), Montpellier.

ETAT D'AVANCEMENT DU PROJET AU LABORATOIRE.

E.coli ne permet pas (en règle général) la surproduction sous forme fonctionnelle de protéine membranaire d'origine eucaryote. Par contre, dans certains cas, des quantités très importantes de protéines eucaryotes, dont des GPCRs, ont pu être obtenues sous forme de corps d'inclusions (Kiefer et al, 1996 and 2000). Nous nous sommes donc engagés dans l'expression de CXCR4 et CCR5 dans *E.coli* sous forme de corps d'inclusions (CI) avec pour optique de produire de grandes quantités de protéines sous forme dénaturée et de procéder ensuite à leur repliement en présence de détergents.

Dans sa définition, un tel projet est à fort caractère méthodologique et présente également des risques importants d'échec, avec peu de possibilité de valorisation intermédiaire. C'est un travail sur lequel il est difficile de mettre un étudiant ou un stagiaire post-doctoral. Dans ce contexte, l'ANRS a financé un Contrat CDD d'ingénieur pour le soutien en personnel à ce projet. C'est dans ce cadre que Corinne Vivès est arrivée au laboratoire.

Sur cette approche, les progrès n'ont pas été rapides et de nombreuses difficultés ont été rencontrées ; nous ne sommes pas encore à un stade ou une valorisation de ce travail par voie de publication est possible. Pour cette raison, je vais présenter un peu plus en détail les stratégies et résultats obtenus sur cette thématique (tout en restant le plus bref possible). Ce travail a été soutenu dans le cadre de deux phases de financement du réseau présenté ci-dessus. Je garderai ce découpage chronologique pour présenter ce travail. De plus, je ne présenterai pas le travail réalisé par les autres groupes du réseau (ce n'est pas le lieu ici) juste un bilan global des acquis à la fin de cette section.

PHASE I (2000-2002) : EVALUATION DU POTENTIEL D'EXPRESSION DU SYSTEME *E.COLI*.

Nous avons tenté d'optimiser l'expression à tous les niveaux pouvant être critiques.

Niveau transcriptionnel :
Les gènes sauvages et optimisés des co-récepteurs ont été clonés dans un vecteur pET sous contrôle d'un promoteur fort. Un tag polyhistidine a été ajouté en C-terminal de la région codante afin de faciliter la purification des protéines.

Niveau traductionnel :
Une importante partie de notre travail a consisté en la production synthétique de gènes optimisés, c'est-à-dire favorables à une synthèse par la bactérie, sans présence de codon rare. La stratégie de synthèse de tels gènes se trouve résumée dans la figure ci-dessous.

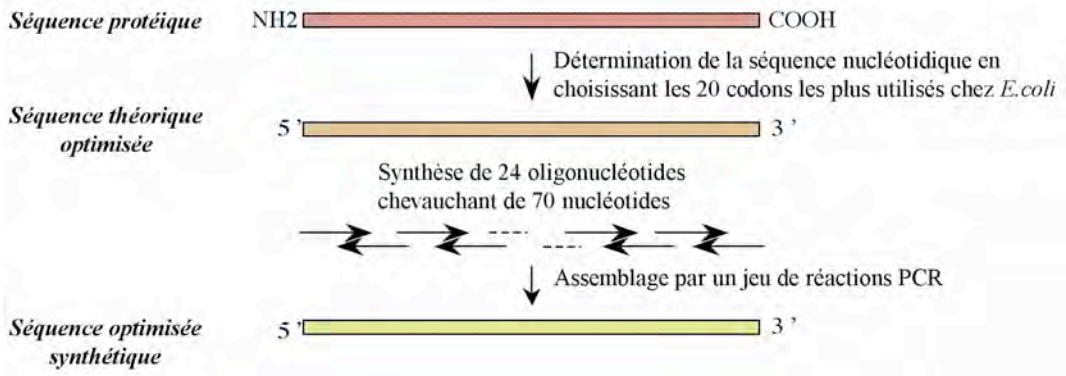

Stratégie de synthèse des gènes synthétiques

La construction des gènes optimisés s'est révélée complexe, de nombreuses mutations ayant été incorporées lors des multiples étapes de PCR de la synthèse du gène. Leur correction par mutagenèse dirigée a dû être effectué mutation par mutation.

Criblage de souches d'expression (importance du contexte génétique) :
Des tests d'expression des gènes sauvages et optimisés ont été réalisés dans un panel de souches (DE3) lysogènes d'*E.coli* . L'expression des gènes peut-être observée par Western blotting mais n'est pas suffisante pour être visible en bleu de Coomassie et aucun effet lié à l'optimisation des gènes ou au contexte génétique de souches n'a pu être identifié dans un premier temps (cf. un exemple dans la figure suivante).

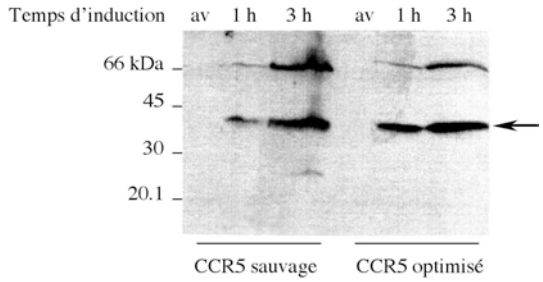

Expression des gènes sauvages et optimisés de CCR5 dans BL21(DE3).
Echantillons de culture prélevés à différents temps d'induction et analysés par Western blot avec un anticorps anti-TagHis. La bande au dessus de 30 kDa (indiquée par la flèche) correspond à la protéine recombinante. La bande de taille supérieure est probablement due à des protéines aggrégées (dimères).

Dans le cas de ces deux GPCR, il semble que l'adressage à des corps d'inclusion cytoplasmique (CI) ne soit pas spontané et entraine un effet de toxicité, par agrégation avec les membranes. Ceci conduit à une limitation importante de l'expression. Un effort d'ingénierie a dû être mis en place pour diriger les protéines vers les CI et lever cette toxicité.

Adressage aux corps d'inclusions (ou *comment empêcher l'interaction avec les membranes ?*)

Cet objectif a été abordé selon les deux stratégies illustrées dans la figure ci-dessous.

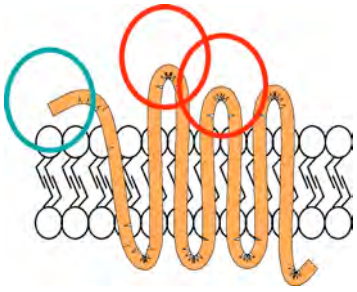

Régions sensibles pour l'insertion membranaire.
1) L'insertion de charge positives dans les boucles extracellulaires (en rouge) est à même de perturber l'insertion, l'interaction avec la membrane.
2) L'accroissement de l'extrémité N-terminale (en vert) est une gêne à l'initiation de l'insertion membranaire.

Stratégie 1 :Le principe de la « positive inside rule » décrite par Von Heijne (1986) prédit que les charges positives sur les boucles externes gênent à l'insertion des protéines membranaires dans la membrane. Des ajouts de résidus basiques par mutations ont permis d'augmenter de manière considérable l'expression recombinante d'autres GPCRs (Kieffer et al, 2000), en limitant l'interaction avec la membrane et augmentant la formation de corps d'inclusion. Nous avons introduit et testé différentes mutations dans les boucles de CCR5 et CXCR4. Dans le cas de nos récepteurs, cela n'a pas eu de conséquence importante sur l'adressage aux CI.

Stratégie 2 :Nous avons tenté de favoriser la formation de corps d'inclusion en rajoutant en N-terminal une autre protéine en fusion, la GST. L'expression des co-récepteurs en fusion protéique conjointement à l'optimisation du gène a donné pour la première fois un accroissement très significtif de l'expression. Cependant malgré cette amélioration, les quantités ne sont pas encore au niveau de celles nécessaire pour aborder des études structurales. Les protéines produites étaient effectivement isolées dans une fraction insoluble de type CI. Leur

solubilisation en détergent et leur purification, sous forme dénaturée, sur colonne de Ni^{2+} s'est avérée possible. Il fallait pouvoir donc encore augmenter les taux d'expression.

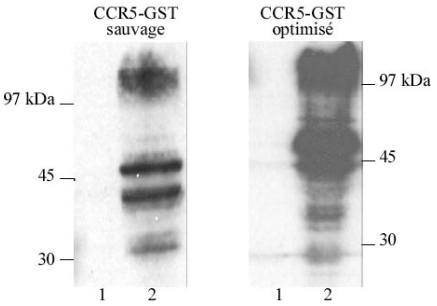

Expression des gènes fusionnés avec la GST dans BL21(DE3).
Echantillons prélevés avant (1) induction ou (2) 3h après induction
Analysés par SDS-PAGE et Western blot avec un anticorps anti-GST. Taille attendue pour le monomère : 60 kDa.

A l'issue de la première phase du projet émergeait une stratégie d'expression des corécepteurs en fusion avec un partenaire protéique d'adressage. La recherche de partenaire de fusion plus efficace que la GST était l'étape suivante pour atteindre l'objectif "surproduction".

PHASE II (2003-2005) : MISE AU POINT DE LA SUREXPRESSION ET DE LA PURIFICATION.

Parallèlement à ce travail, Jean-Louis Banères et Bernard Mouillac de Montpellier (où existe une longue tradition de biochimie des GPCRs) venaient de définir une série de partenaires de fusion permettant des taux de surexpression de l'ordre de plusieurs mg/L de culture pour leurs GPCR d'intérêt[8]. Nous les avons contactés pour une collaboration et ils ont intégré le réseau pour cette deuxième phase de travail. À partir de nos gènes optimisés, différents partenaires de fusion, parmi ceux identifiés, ont été testés. Finalement, la fusion avec l'integrine α5 permet la surexpression de CCR5, et pour CXCR4 il a fallu recourir à une double fusion (intégrine α5-V2 vasopressine recepteur-CXCR4) pour atteindre cet objectif. De plus, il a été observé que les conditions de cultures sont particulièrement critique pour ces deux co-récepteurs (composition des milieux, température, etc…). Enfin, la solubilisation des CI suivie d'une purification sur colonne de Ni^{2+}-NTA en conditions dénaturantes, permet la purification des protéines fusion avec un rendement final de 4-5 mg/L de culture de protéines dénaturées.

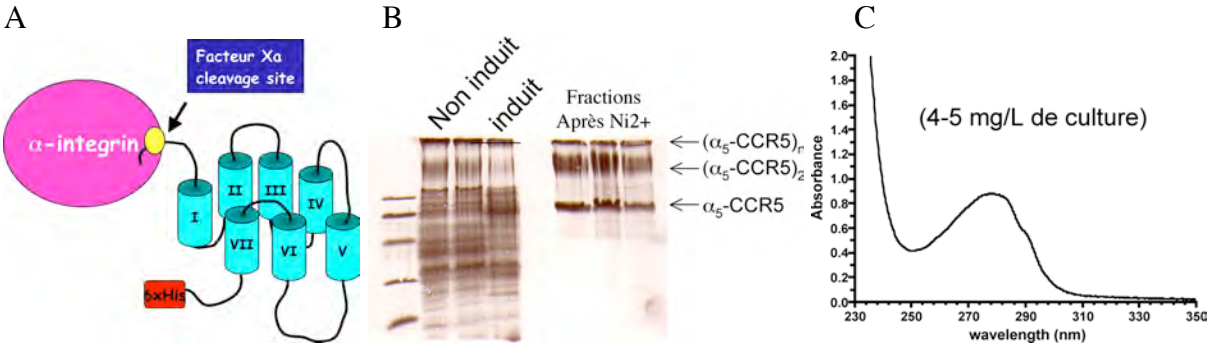

D

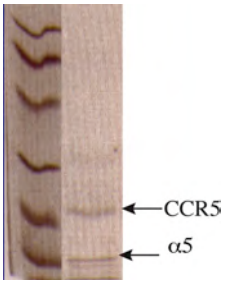

Surexpression et purification de la fusion α5-CCR5 :

A) Construction α5-CCR5
B) Gel SDS-Page coloré au bleu de coomassie :
Suivi d'expression à droite et fractions d'élution d'une colonne de Ni-NTA en conditions dénaturantes.
C) Spectre UV-Visible du pool des fractions d'élutions de α5-CCR5.
D) Suivi de la coupure protéolytique de α5-CCR5

[8] Leurs partenaires de fusion et les développements associés font l'objet d'un brevet Inserm.

Le protocole de coupure des protéines de fusion a également été mis au point. La méthodologie a été réimplanté sur Grenoble, non sans difficulté, et les taux de production sont maintenant reproductibles sur les deux sites[9]. Nous en sommes donc maintenant au stade où le problème de la surexpression de ces protéines dans des quantités compatibles avec des études structurales est résolu. De même la purification et l'élimination du partenaire de fusion sont également des étapes contrôlées. Cependant, nous sommes encore loin du but. En effet au stade où nous en sommes la protéine est encore sous forme dénaturée. Les prochains efforts à engager seront donc dans la recherche de conditions de renaturation de ces protéines et de leur stabilisation en solution.

En parallèle à ce travail avec le système *E.coli*, des outils ont été mis en place par les autres membres du réseau. Parmi ceux -ci : la synthèse peptidiques des chimiokines ligands de CCR5 et CXCR4, indispensable pour tester l'activité de nos futures protéines repliées, des tests d'interaction fonctionnelle en Biacore et un système d'expression de récepteurs sous forme native (en cellules de mammifères) qui est source de protéines fonctionnelles de références (bien sûr à des quantités bien moindres en l'état actuel des choses). L'ensemble de ces outils sera de premières importances dans la poursuite de nos objectifs.

Perspectives : Les perspectives directes sont bien évidemment la mise en place de procédure de renaturation de ces protéines en présence de détergent. Cette partie du travail se fera conjointement à Montpellier (collaboration Jean-Louis Banères) et à l'IBS, compte tenu de l'ampleur du travail et des conditions de criblage possibles sur deux corécepteurs différents. De plus, une stratégie de renaturation alternative, avec des molécules non détergentes, utilisant des amphipols ou des détergents hémifluorés va être mis en place avec le groupe de Jean-Luc Popot (un projet est déposé dans le cadre d'une ANR).

III. DC-SIGN : un récepteur de multiples pathogènes

III.A) Rôle de DC-SIGN et des cellules dendritiques dans les premiers stades de la dissémination virale.

Dans les muqueuses, la fonction physiologique des cellules dendritiques est de piéger l'antigène à son lieu de pénétration, de l'apprêter et de le présenter sur les molécules de complexes majeurs d'histocompatibilité sous formes de peptides. Puis, après migration vers les organes lymphoïdes, les antigènes sont présentés aux cellules T. La réponse immunitaire est initié. Dans le cas de l'infection par le VIH, de nombreux travaux ont suggéré puis souligné le détournement des fonctions naturelles des cellules dendritiques par le VIH à 2 niveaux :

a) la capture des virus par ces cellules au niveau des muqueuses génitales (au stade initial de l'infection) (Blauvelt *et al*. 1997).

[9] Lors des premiers essais au labo avec les nouvelles constructions venant de Montpellier, nous avions, de manière non rationnelle, des cultures qui surexprimaient ou qui se lysaient spontanément avant ou après induction. Ces problèmes de stabilité d'expression ne s'observait dans le labo que sur les cultures de co-récepteurs et on a longtemps pensé à une toxicité de l'expression chez nous lié à une différence subtile, par rapport à Montpellier, dans les milieux ou la mise en œuvre. Après de nombreux essais où l'on a succesivement changé tous les composants du milieu (et même avec un séjour à Montpellier pour voir comment ils procédaient). On s'est finalement rendu compte que nos cultures, ici, étaient en fait contaminé par un bactériophage qui était resté cantonné à ces cultures particulières sans s'étendre à l'ensemble de l'activité du labo pendant tout ce temps. Il a fallu procéder à une contamination globale de tout le laboratoire et de nos appareillages (ce qui a immobilisé toute activité au labo pendant plusieurs semaines). L'ensemble de cette aventure nous a fait perdre plus de 6 mois sur ce projet.

b) la transmission des virus à leur cible, les lymphocytes T CD4+ (Cameron *et al.* 1992; Weissman *et al.* 1995; Granelli-Piperno *et al.* 1999).

Il a en effet été montré que les cellules dendritiques possèdent la capacité de capturer le virus et de générer une intense réplication virale lorsqu'elles sont co-cultivées avec des lymphocytes T (Blauvelt *et al.* 1997) avec un mécanisme de reconnaissance virale distinct des récepteurs connus pour l'infection des lymphocyte T (CD4, CXCR4 ou CCR5) (Blauvelt *et al.* 1997).

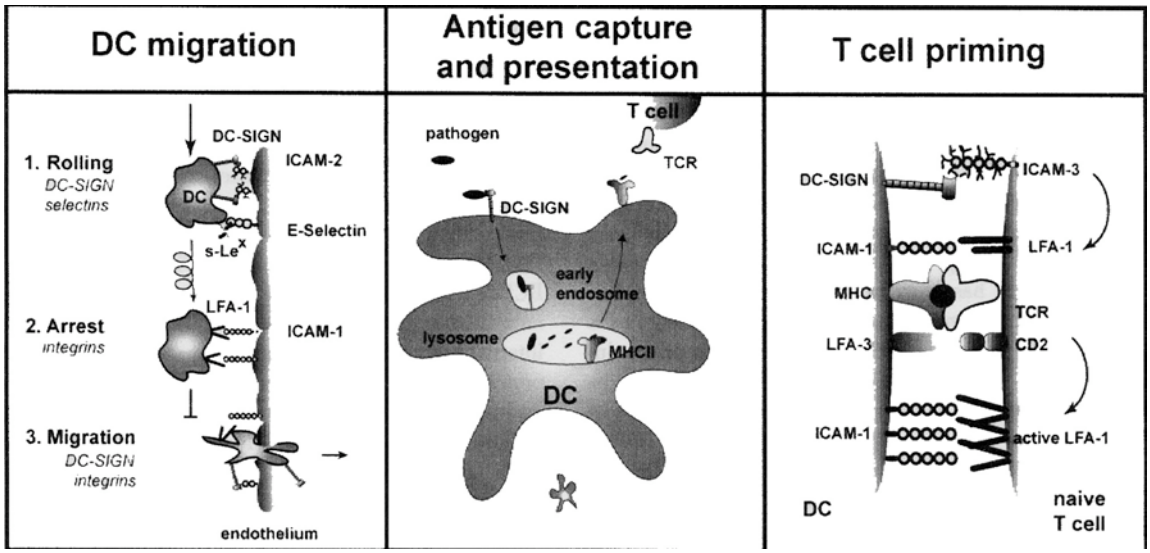

Les différents niveaux d'action de DC-SIGN dans la biologie des cellules dendritiques et l'activation de la réponse immunitaire (Geijtenbeek et al. 2002)

Ce n'est que récemment que le mécanisme qui permet la capture du VIH par les cellules dendritiques à été partiellement élucidé (Geijtenbeek *et al.* 2000b). Une lectine présente à la surface des cellules dendritiques reconnaît spécifiquement la gp120 de VIH et permet une infection très efficace des cellules T dans les co-cultures. Parallèlement à son rôle de récepteur pour le VIH, cette lectine, de type C, spécifique des cellules dendritiques, a été caractérisée pour sa très forte affinité pour ICAM-3 présent à la surface des cellules T (Geijtenbeek *et al.* 2000c)(DC-SIGN pour "dendritic cell-specific ICAM-3 grabbing nonintegrin").

Ces découvertes ont déclenché un investissement considérable sur cette lectine au cours des quatres années écoulées. De ce foisonnement de résultats, il ressort que DC-SIGN occupe une place centrale dans la biologie des cellules dendritiques et l'activation de la réponse immunitaire. Ainsi, DC-SIGN participe à chacune des phases essentielles entre le contact avec un antigène et l'activation immunitaire (figure ci dessus):

- la capture et l'internalisation des antigènes (pour leur présentation par le complexe majeur d'histocompatibilité) (Engering *et al.* 2002)
- la migration des cellules dendritiques jusqu'aux organes lymphoïdes par le biais d'une interaction avec la protéine ICAM2 (Geijtenbeek *et al.* 2000a)
- la mise en place de la « synapse immunologique » entre les cellules dendritiques et les lymphocytes T, permettant ainsi leur activation (Geijtenbeek *et al.* 2000b).

La capture du VIH par DC-SIGN serait efficace et stable grâce à une organisation en aggrégat localisé au sein de microdomaines dans les radeaux lipidiques de la membrane plasmique (Cambi *et al*. 2004).

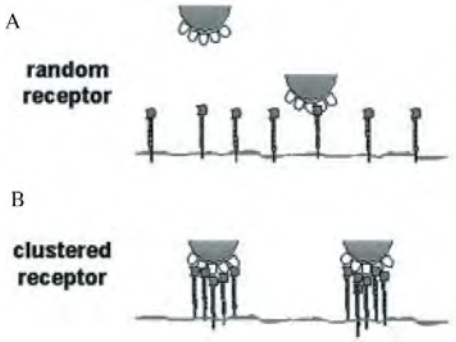

Une organisation en assemblages multiprotéiques de DC-SIGN (B), par opposition à une distribution aléatoire (A), permet une capture et une liaison forte et stable des virus à la membrane (Cambi et al. 2004).

Dans le cas particulier du VIH, il semble que, suite à sa capture par DC-SIGN et son internalisation dans un compartiment endosomal précoce, le virus arrive à échapper au processus de digestion en vue de la présentation par le complexe majeur d'histocompatibilité (Kwon *et al*. 2002). Le VIH reviendrait au final à la surface cellulaire pour être « offert » aux lymphocyte T. Un mécanisme, propre au VIH, a été suggéré. Il permet d'amplifié ce phénomène de présentation (si la cellule dendritique est elle–même infectée) par le biais d'une signalisation intracellulaire impliquant la protéine virale Nef. Celle-ci favorise la redistribution de DC-SIGN à la membrane en bloquant son internalisation. Cela conduit à accroître les capacités d'adhérence cellulaire avec les lymphocytes T et la quantité de virus présentés (Sol-Foulon *et al*. 2002).

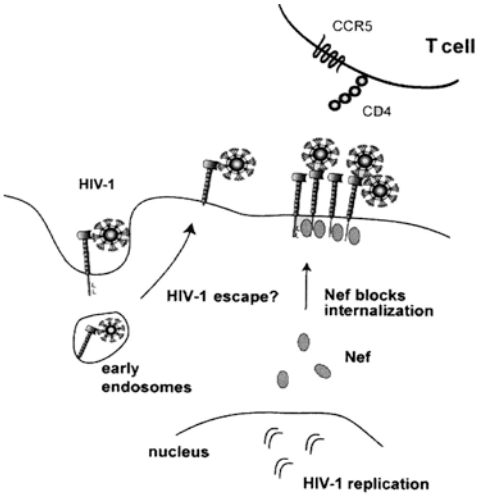

Détournement des fonctions biologiques de DC-SIGN par le VIH (Geijtenbeek et al. 2002).

L'ensemble des données accumulées jusqu'à présent démontre que la lectine DC-SIGN exprimée par les cellules dendritiques localisées dans les muqueuses génitales est un récepteur clé dans un nouveau mécanisme proposé pour l'établissement de l'infection. Cette protéine permet au virus de détourner les cellules dendritiques mucosales de leur fonction immunologique, et de les utiliser comme transporteurs pour atteindre les cellules T où ils pourront se répliquer (voir revue (Geijtenbeek *et al*. 2002)).

III.B) Implication d'autres lectines des cellules dendritiques

DC-SIGN est seulement exprimée par les cellules dendritiques interstitielles. D'autres lectines, spécifiques du mannose, sont présentes à la surface des cellules dendritiques et leur rôle possible dans l'infection par VIH commence juste à être étudié. Ainsi, il a été démontré qu'un récepteur lectine de type C n'était pas le seul responsable de la fixation de l'enveloppe virale dans toutes les sous-populations de cellules dendritiques (DC) (Turville et al. 2002). Selon les sous-familles de cellules dendritiques, cette propriété peut échoir à DC-SIGN, le récepteur Mannose ou encore la Langerine. La Langerine est une lectine de type-C présente uniquement sur les cellules de Langerhans, des cellules dendritiques immatures localisées dans l'épiderme et les tissus muqueux (Valladeau et al. 2000). Cette lectine semble jouer un rôle particulier dans la capture des antigènes, car elle permet leur séquestration dans des organites particuliers, nommés granules de Birbeck (Valladeau et al. 2000; Mc Dermott et al. 2002). Les cellules de Langerhans des muqueuses exposées au VIH sont supposées participer à la première étape de la propagation virale (Hu et al. 2000) et sont connues pour transmettre efficacement le VIH à des lymphocytes T.

III.C) Connaissances structurales sur DC-SIGN et les lectines de type C

La DC-SIGN et la Langerine sont des protéines membranaires de type II. Leurs séquences peptidiques (404 et 328 aa) montrent un court segment N-terminal cytoplasmique, un segment transmembranaire hydrophobe, une tige (région Neck) d'une centaine d'acides aminés contenant des séquences répétées et, enfin, un domaine de reconnaissance des carbohydrates (CRD) d'environ 150 acides aminés. La comparaison avec les architectures connues de lectines de type C indique que la DC-SIGN et la Langerine appartiennent à un groupe de lectines endocytiques dont le prototype est le récepteur hépatique de l'asialoglycoprotéine, une lectine qui sert de point d'entrée dans le foie pour certain virus (Becker *et al*. 1995; Treichel *et al*. 1997). Les études biochimiques ont montré que DC-SIGN s'associe en tétramère et la Langerine en trimère (Mitchell *et al*. 2001, Feinberg *et al*. 2005, Stambach et al 2003).

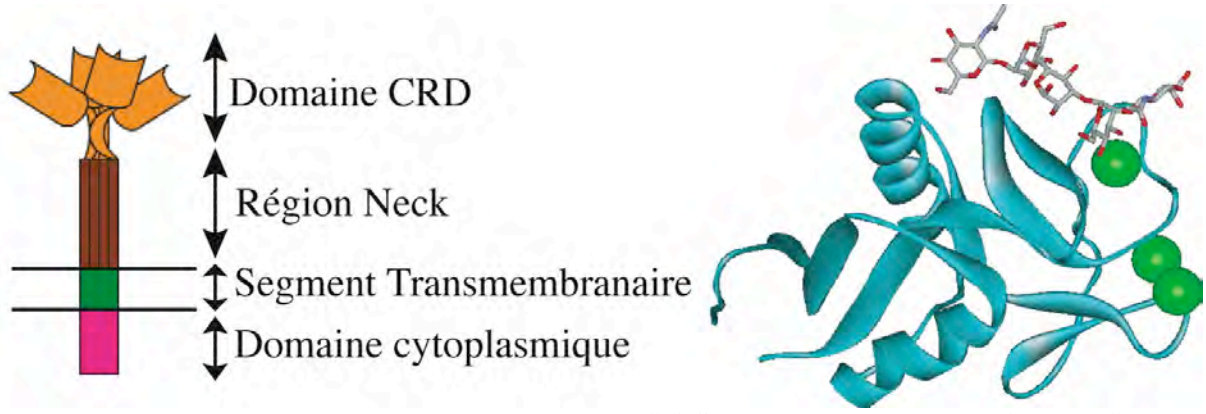

Organisation multimérique des lectines endocytiques (ici DC-SIGN) et structure cristallographique du CRD de DC-SIGN (ruban bleu : protéine , bâtons : oligosaccharide, sphères vertes : ions calcium).

La structure cristallographique du CRD de la DC-SIGN a été résolue très tôt sous la forme de complexe avec un pentasaccharide contenant un mannose (Feinberg *et al*. 2001). Comme dans les autres lectines de type C, le monosaccharide est reconnu via un ion calcium. Récemment, deux structures différentes d'une même forme tronquée de DC-SIGN ont pu être obtenues. Cette protéine possède le domaine CRD et deux des huit motifs répétés qui constituent la tige. Elle présente un mode d'association dimérique différent de la protéine sauvage, et donc *à priori* artefactuel, mais donne accès à la structure d'un des motifs répétés. Sur la base de ces structures et d'études hydrodynamiques sur la forme tétramèrique de DC-

SIGN (DC-SIGN ECD pour Extra Cellular Domain), des modèles d'organisation possible des tétramères et donc du positionnement des CRD ont été proposés (*Feinberg et al*. 2005). Dans chacun des modèles, les têtes CRD possèdent une orientation relative différente. Actuellement, rien ne se dégage encore clairement sur le type d'organisation relative des têtes CRD ou même sur la plasticité éventuelle de celle-ci.

III.D) Implication de DC-SIGN dans la reconnaissance d'autres pathogènes.

Simultanément aux efforts fournis dans la compréhension des mécanismes et des relations entre DC-SIGN et l'infection VIH décrite ci dessus, plusieurs travaux semblent faire de DC-SIGN un acteur privilégié dans d'autres pathologies. Ainsi, DC-SIGN est décrit comme un récepteur pour le virus Ebola (Alvarez *et al*. 2002), le parasite *Leshmania pifanoi* (Colmenares *et al*. 2002) et *Mycobacterium tuberculosis* (Tailleux et al. 2003). De plus, nous avons nous-mêmes, dans le cadre d'un travail collaboratif, participé à la mise en évidence du rôle de récepteur de DC-SIGN dans l'infection au Cytomégalovirus (CMV), le virus de l'hépathite C et celui la Dengue (Hallary et al. 2002, Lozach et al. 2003, Navarro-Sanchez et al 2003). Ces derniers éléments ne font qu'amplifier l'intérêt croissant qui se cristallise sur cette lectine et l'enjeu qu'il y a à avancer vers sa caractérisation structurale. En effet, de telles informations peuvent être un point de départ vers la recherche de molécules actives.

III.E) Etat d'avancement du projet, définition des objectifs et réalisations.

HISTORIQUE DU PROJET AU LABORATOIRE :

Lorsque j'ai décidé de démarrer un travail centré sur DC-SIGN au laboratoire, cela faisait un an que cette protéine et son rôle dans l'infection HIV étaient connus. Aucune information structurale n'était disponible et son implication au niveau d'autres pathologies n'était pas mis en évidence.

Ce projet a pu démarrer en 2001 grâce à l'obtention d'une subvention Sidaction et du financement d'un stagiaire postdoctoral, Corinne Houlès par l'ANRS (ce travail se plaçait dans le contexte d'une collaboration avec Anne Imberty du CERMAV). Nous avons construit différentes formes tronquées de la région extracellulaire de DC-SIGN. Ainsi, nous avons obtenu : (1) une forme oligomérique comprenant l'ensemble de la région extracellulaire, c'est à dire avec les 8 séquences de répétition (DCSIGN-ECD), (2) une forme qui n'en comporte qu'une (DCSIGN-1R) et (3) une construction se limitant au CRD (DCSIGN-CRD). La surexpression de ces constructions a été possible dans *E. coli* sous forme de corps d'inclusions. Nous avons donc dû mettre au point au laboratoire un protocole de renaturation des formes agrégées ainsi obtenues. Puis nous avons établi un protocole de purification nous permettant de purifier la protéine, mais également de trier celles correctement repliées et fonctionnelles à l'issue de la renaturation. Nous sommes en mesure de produire de manière reproductible ces protéines avec une qualité compatible avec une étude cristallographique du point de vue de la pureté et de l'homogénéité. De manière similaire, nous avons mis au point la surexpression du CRD et du ECD de la Langerine, autre récepteurs lectinique de cellules dendritiques (je ne reviendrai pas sur les développements associés à la langerine dans ce document pour simplifier la présentation).

Toujours dans cette phase préliminaire de démarrage de projet (2001-2003), nous avons mis en place des tests d'interactions fonctionnelles basé sur l'utilisation de la technologie Biacore (et le soutien de Hugues Lortat-Jacob). L'acquisition de la maîtrise de cet outil, la

résonance plasmonique de surface, a été un effort indispensable dans le cadre de ce projet DC-SIGN afin de pouvoir tester la fonctionnalité de nos préparations et entamer des caractérisations fonctionnelles des interactions hôtes-pathogènes. Je tiens donc ici à remercier Hugues Lortat-Jacob pour son soutien et sa disponibilité lors de ma phase d'initiation. J'ai également profité de mon année de délégation au CNRS (2004-2005) pour suivre trois formations Biacore et acquérir ainsi l'autonomie nécessaire dans l'utilisation de cette méthodologie.

Sur la base de ces outils, formes tronquées solubles de DC-SIGN et tests d'interactions biacore, j'ai pu définir trois axes de travail au labo et au travers de collaborations.

DEFINITION DES OBJECTIFS

Caractérisation des interactions DC-SIGN-Pathogènes (spectre de reconnaissance).

Nous avons pu participer, par la production de nos formes recombinantes de DC-SIGN, par leur utilisation dans le cadre d'expériences d'interaction (Biacore) ou d'inhibition d'infections, à différentes études en collaboration (notamment avec le groupe de Fernando Arenzana de l'Institut Pasteur) visant à caractériser l'implication de DC-SIGN visà vis d'autres virus que le HIV. À cette occasion, nous avons pu mettre en évidence le rôle de DC-SIGN dans la reconnaissance de la glycoprotéine B du Cytomégalovirus et ainsi, son rôle dans l'infection en *cis* et en *trans* par ce virus (Hallary *et al*. 2002). Outre le CMV, nous avons participé, dans le même contexte de collaboration, à la caractérisation d'un rôle analogue de DC-SIGN dans la reconnaissance des virus de l'hépatite C et de la Dengue (Lozach et *al*. 2003, Navarro-Sanchez et *al*. 2003). Notre contribution modeste, mais significative, dans ces différentes études d'envergure, nous a permis de valoriser assez rapidement les outils moléculaires que nous venions de mettre en place.

Perspective : Cette approche va être approfondie dans le cadre du réseau de travail sur le virus de la dengue auquel nous participons. Dans ce contexte, il est prévu de caractériser plus finement les interactions DC-SIGN/protein E de dengue, selon l'isotype vitale et avec notamment des protéines virales mutées sur les sites de glycosilations, ou en jouant sur la densité des surfaces DC-SIGN (réalisation de surfaces mimétiques des microdomaines cellulaires de DC-SIGN).

Publications issues de cet axe de travail : P14, P13, P12 (voir page 8 et premières pages ci-après).

Caractérisation structurale de DC-SIGN oligomérique.

Pour certaines lectines telles que la MBP, il a été démontré que l'oligomérisation permet de présenter les CRDs de manière optimale pour interagir de manière coopérative avec les glycoconjugués sur une surface cellulaire (Weis et al. 1994). Ainsi, la détermination de l'organisation spatiale des quatre têtes CRD de DC-SIGN dans le tétramère est un objectif important dans le but de pouvoir concevoir de futurs inhibiteurs sur des bases les plus rationnelles possibles.

Alors que nous en étions à nos premiers tests de surexpression, la structure du CRD de DC-SIGN était déjà publiés (Feinberg et *al*. 2001) Soit un an après la découverte de cette protéine. Nous avions donc dés le départ un retard difficile à combler, en effet ce travail a été complété depuis avec la structure d'un dimère. Mais actuellement il n'y a toujours aucune

information structurale sur la forme tétramérique physiologique. Bien sûr, nous avons démarré des essais de cristallogenèse sur la construction la plus longue ECD (tétramèrique). Cet objectif sera poursuivi mais n'a jusqu'à présent pas débouché sur la mise en évidence de cristaux exploitable. Une approche basse résolution par diffusion de rayons X aux petits angles (SAXS) a donc été engagée en parallèle. En collaboration avec Dominique Durand (Paris XI) de premières mesures ont été effectuées et permettent l'obtention d'une première enveloppe basse résolution mais surtout d'établir de meilleures conditions pour les prochaines expériences de collectes de données.

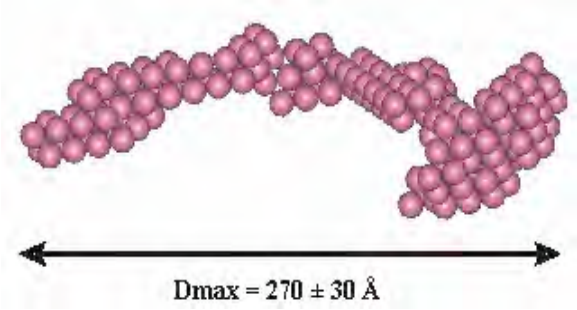

Modèle SAXS préliminaire pour l'enveloppe moléculairede DC-SIGN ECD

Perspectives :

Nous allons investir des efforts sur l'approche "SAXS" (peut être moins concurrentielle). Cette approche est également motivé par la difficulté à cristalliser le domaine ECD (entre nos mains mais également chez nos concurrents). Dans l'objectif de placer des élements structuraux à haute résolution dans une telle enveloppe SAXS, nous allons produire la région Neck de DC-SIGN (la structure haute résolution du CRD étant déjà connue). Cette région Neck cristallisera peut être plus facilement que la région ECD.

De plus, dans le cadre d'un réseau sur le virus de la dengue, la cristallogenèse d'un complexe entre la protéine d'enveloppe de la Dengue et le CRD de DC-SIGN sera abordée dans le cadre d'une collaboration avec Félix Rey.

Stratégies pour la production d'inhibiteurs de l'interaction DC-SIGN/Virus.

L'affinité des CRD pour les sucres est de l'ordre du millimolaire. Cette faible affinité naturelle est compensée par la présentation multivalente d'unités glycosidiques, la nature oligomèrique de DC-SIGN, et l'organisation de DC-SIGN en aggrégats au sein de microdomaine dans les "rafts" de la membrane plasmique (Cambi et al, 2004). Cet état de fait encourage l'élaboration de structures osidiques multivalentes pour pouvoir interférer avec l'interaction biologique. Parmi les systèmes multivalents, les glycodendrimères sont un des systèmes les plus répandus (Bezouska 2002) et ont été utilisés précédemment pour différent processus et notamment le blocage de récepteurs viraux (Landers *et al*. 2002, Reuter *et al*. 1999). Lors de travaux précédents, le groupe de Javier Rojo de Séville (avec qui nous collaborons sur ce projet) ont montré de nombreux avantages associés à des structures glycodendritiques, basées sur le polymère branché BoltornH30. Ainsi, ces molécules présentent une faible cytotoxicité, une forte solubilité dans les milieux physiologiques et un coût relativement bas (Arce et *al*. 2003).

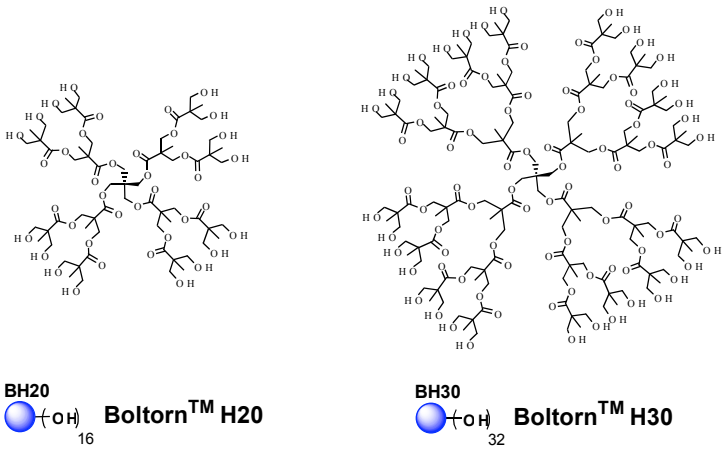

Polymères dendritiques de type Boltorn de seconde et troisième génération.

Ainsi, des glycodendrimères présentant, greffés sur les hydroxyles, des unités osidiques choisis sur la base de la spécificité de DC-SIGN d'une part et des contraintes de synthèse chimique d'autres part seront préparés. Puis leurs capacités de liaison vis-à-vis de DC-SIGN seront évaluées ainsi que leur pouvoir inhibiteur de l'interaction DC-SIGN/gp120 *in vitro*. La caractérisation des propriétés interactantes des glycodendrimères avec la lectine a été abordée par résonnance plasmonique de surface avec une première série de composés où l'unité osidique est un simple mannose (voir figure ci-dessous).

A) 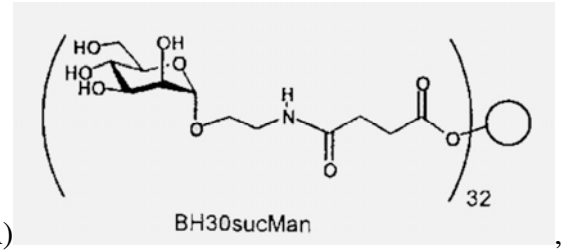

, B) 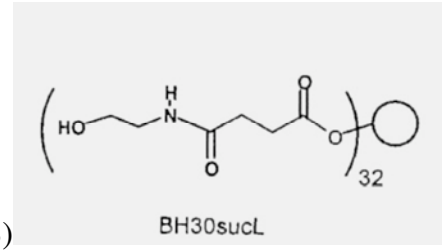

A) Structure de l'unité mannose et son linker : molécule BH30suc Man B) Molécules controles sans le mannose : BH30sucL.

Cette première étude a permis de mettre en évidence les propriétés particulières d'interactions de ces molécules en fonction de la nature du mode de fonctionnalisation de la surface et également la mise en évidence des propriétés inhibitrices de l'interaction gp120/DC-SIGN par la molécule BH30sucMan (Tabarani et *al.* 2005, P17).

Perspective : Les aller-retours entre la validation Biacore et la synthèse vont nous permettre de faire évoluer les molécules vers une efficacité et une spécificité croissantes. Parmi les possibilités d'évolution des molécules, il est envisagé de faire varier le degré de réticulation, la taille du linker liant l'unité osidique au dendrimère, et bien sûr la nature des unités osidiques associées au dendrimère. De plus, des fonctionnalisations additionnelles sont envisagées sur ces molécules. Les molécules les plus intéressantes pourront être testées en inhibition d'infection virale dans le cadre de collaboration. Avec Javier, nous tentons actuellement de fédérer un certain nombre de groupes de chimistes et biologistes sur la base de ce projet (élargi) avec l'idée de monter à terme un réseau européen.

Publication issue de cet axe de travail : P17 (publication soumise à *Angewandte Chemie*, voir page 8 et ci-après)

Références Bibliographiques

Alvarez, C.P., Lasala, F., Carrillo, J., Muniz, O., Corbi, A.L., and Delgado, R. (2002) C-type lectins DC-SIGN and L-SIGN mediate cellular entry by Ebola virus in cis and in trans. *J. Virology* **76**: 6841-6844.

Arce, A, Nieto, P.M, Diaz, V, Garcia castro, R, Bernad, A, and Rojo, J. (2003) Glycodendritic structures based on Boltorn hyperbranched polymers and their interactions with *Lens culinaris* Lectin. Bioconj. Chem. **14**: 817-823

Becker, S., Spiess, M., and Klenk, H.D. (1995) The asialoglycoprotein receptor is a potential liver-specific receptor for Marburg virus. *J. Gen. Virol.* **76**: 393-399.

Berger EA, Murphy PM, Farber JM. (1999) Chemokine receptors as HIV-1 coreceptors: roles in viral entry, tropism, and disease. Annu Rev Immunol.;**17**: 657-700.

Bezouska, K (2002). Design, functionnal evaluation and biochemical applications of carbohydrate dendrimers (glycodendrimers). J. Biotechnol. 90 : 269-290.

Blauvelt, A., Asada, H., Saville, M.W., Klaus-Kovtun, V., Altman, D.J., Yarchoan, R., and Katz, S.I. (1997) Productive infection of dendritic cells by HIV-1 and their ability to capture virus are mediated through separate pathways. *J. Clin. Invest.* **100**: 2043-2053.

Cambi A, de Lange F, van Maarseveen NM, Nijhuis M, Joosten B, van Dijk EM, de Bakker BI, Fransen JA, Bovee-Geurts PH, van Leeuwen FN, Van Hulst NF, Figdor CG. (2004) Microdomains of the C-type lectin DC-SIGN are portals for virus entry into dendritic cells. *J Cell Biol.* **164**:145-55.

Cameron, P.U., Freudenthal, P.S., Barker, J.M., Gezelter, S., Inaba, K., and Steinman, R.M. (1992) Dendritic cells exposed to human immunodeficiency virus type-1 transmit a vigorous cytopathic infection to CD4+ T cells. *Science* **257**: 383-387.

Colmenares, M., Puig-Kroger, A., Pello, O.M., Corbi, A.L., and Rivas, L. (2002) Dendritic cell (DC)-specific intercellular adhesion molecule 3 (ICAM-3)-grabbing nonintegrin (DC-SIGN, CD209), a C-type surface lectin in human DCs, is a receptor for *Leishmania amastigotes*. *J Biol Chem* **277**: 36766-36769.

Dimitrov DS. (1997) How do viruses enter cells? The HIV coreceptors teach us a lesson of complexity. Cell **91** : 721-30

Doms RW, Trono D. (2000) The plasma membrane as a combat zone in the HIV battlefield. *Genes Dev*. 14 : 2677-88

Engering, A., T.B. Geijtenbeek, S.J. van Vliet, M. Wijers, E. van Liempt, N. Demaurex, A. Lanzavecchia, J. Fransen, C.G. Figdor, V. Piguet and Y. van Kooyk (2002). The dendritic cell-specific adhesion receptor DC-SIGN internalizes antigen for presentation to T cells. *J. Immunol.* **168**: 2118-2126.

Feinberg, H., Mitchell, D.A., Drickamer, K., and Weis, W.I. (2001) Structural basis for selective recognition of oligosaccharides by DC- SIGN and DC-SIGNR. *Science* **294**: 2163-2166.

Feinberg H, Guo, Y, Mitchell, D, Drickammer, K, and Weiss, W. (2005) Extended Neck regions stabilize tetramers of the receptors DC-SIGn and DC-SIGNR. *J.Biol.Chem* **280** : 1327-1335.

Geijtenbeek, T.B., Kwon, D.S., Torensma, R., van Vliet, S.J., van Duijnhoven, G.C., Middel, J., Cornelissen, I.L., Nottet, H.S., KewalRamani, V.N., Littman, D.R., Figdor, C.G., and van Kooyk, Y. (2000a) DC-SIGN, a dendritic cell-specific HIV-1-binding protein that enhances trans-infection of T cells. *Cell* **100**: 587-597.

Geijtenbeek, T.B., Torensma, R., van Vliet, S.J., van Duijnhoven, G.C., Adema, G.J., van Kooyk, Y., and Figdor, C.G. (2000b) Identification of DC-SIGN, a novel dendritic cell-specific ICAM-3 receptor that supports primary immune responses. *Cell* **100**: 575-585.

Geijtenbeek, T.B., R. Torensma, S.J. van Vliet, G.C. van Duijnhoven, G.J. Adema, Y. van Kooyk and C.G. Figdor (2000c). Identification of DC-SIGN, a novel dendritic cell-specific ICAM-3 receptor that supports primary immune responses. *Cell* **100**: 575-585.

Geijtenbeek, T.B., Engering, A., and Van Kooyk, Y. (2002) DC-SIGN, a C-type lectin on dendritic cells that unveils many aspects of dendritic cell biology. *J. Leukoc .Biol.* **71**: 921-931.

Granelli-Piperno, A., Finkel, V., Delgado, E., and Steinman, R.M. (1999) Virus replication begins in dendritic cells during the transmission of HIV-1 from mature dendritic cells to T cells. *Current Biol.* **9**: 21-29.

Halary, F., Amara, A., Lortat-Jacob, H., Messerle, M., Delaunay, T., Houles, C., Fieschi, F., Arenzana-Seisdedos, F., Moreau, J.F., and Dechanet-Merville, J. (2002) Human cytomegalovirus binding to DC-SIGN is required for dendritic cell infection and target cell trans-infection. *Immunity* **17**: 653-664.

Hu, J., Gardner, M.B., and Miller, C.J. (2000) Simian immunodeficiency virus rapidly penetrates the cervicovaginal mucosa after intravaginal inoculation and infects intraepithelial dendritic cells. *J. Virol.* **75**: 6087-6095.

Kiefer H, Vogel R, Maier K. (2000) Bacterial expression of G-protein-coupled receptors: prediction of expression levels from sequence.*Receptors Channels.* **7**:109-19.

Kiefer H, Krieger J, Olszewski JD, Von Heijne G, Prestwich GD, Breer H. (1996) Expression of an olfactory receptor in Escherichia coli: purification, reconstitution, and ligand binding. *Biochemistry*. 35 :16077-84.

Kwon, D.S., Gregorio, G., Bitton, N., Hendrickson, W.A., and Littman, D.R. (2002) DC-SIGN-mediated internalization of HIV is required for trans- enhancement of T cell infection. *Immunity* **16**: 135-144.

Landers, J.J.Z. Cao, I. Lee, L.T. Piehler, P.P.,Myc, A., Myc, T., Hamouda, A.T, Galecki, and Baker JR Jr (2002). Preventionof influenza pneumonitis by sialic acid-conjugated dendritic polymers .J. Infect. Dis. 186: 1222-1230.

Lozach, P.Y., Lortat-Jacob, H., de Lacroix de Lavalette, A., Staropoli, I., Foung, S., Amara, A., Houles, C., Fieschi, F., Schwartz, O., Virelizier, J.L., Arenzana-Seisdedos, F., and Altmeyer, R. (2003) DC-SIGN and L-SIGN are high affinity binding receptors for hepatitis C virus glycoprotein E2. *J Biol Chem* **278**: 20358-20366.

Mc Dermott, R., Ziylan, U., Spehner, D., Bausinger, H., Lipsker, D., Mommaas, M., Cazenave, J.P., Raposo, G., Goud, B., de la Salle, H., Salamero, J., and Hanau, D. (2002) Birbeck granules are subdomains of endosomal recycling compartment in human epidermal Langerhans cells, which form where Langerin accumulates. *Mol Biol Cell* **13**: 317-335.

Mitchell, D.A., Fadden, A.J., and Drickamer, K. (2001) A novel mechanism of carbohydrate recognition by the C-type lectins DC- SIGN and DC-SIGNR. Subunit organization and binding to multivalent ligands. *J. Biol. Chem.* **276**: 28939-28945.

Navarro-Sanchez, E., Altmeyer, R., Amara, A., Schwartz, O., Fieschi, F., Virelizier, J.L., Arenzana-Seisdedos, F., and Despres, P. (2003) Dendritic-cell-specific ICAM3-grabbing non-integrin is essential for the productive infection of human dendritic cells by mosquito-cell-derived dengue viruses. *EMBO Rep* **4**: 723-728.

Sol-Foulon, N., A. Moris, C. Nobile, C. Boccaccio, A. Engering, J.P. Abastado, J.M. Heard, Y. van Kooyk and O. Schwartz (2002). HIV-1 Nef-induced upregulation of DC-SIGN in dendritic cells promotes lymphocyte clustering and viral spread. *Immunity* **16**: 145-155.

Stambach, N.S., and Taylor, M.E. (2003) Characterization of carbohydrate recognition by langerin, a C-type lectin of Langerhans cells. *Glycobiology* **13**: 401-410.

Tailleux, L., Schwartz, O., Herrmann, J.L., Pivert, E., Jackson, M., Amara, A., Legres, L., Dreher, D., Nicod, L.P., Gluckman, J.C., Lagrange, P.H., Gicquel, B., and Neyrolles, O. (2003) DC-SIGN is the major Mycobacterium tuberculosis receptor on human dendritic cells. *J Exp Med* **197**: 121-127.

Treichel, U., K.H. Meyer zum Buschenfelde, H.P. Dienes and G. Gerken (1997). Receptor-mediated entry of hepatitis B virus particles into liver cells. *Arch. Virol.* **142**: 493-8.

Turville, S.G., Cameron, P.U., Handley, A., Lin, G., Pohlmann, S., Doms, R.W., and Cunningham, A.L. (2002) Diversity of receptors binding HIV on dendritic cell subsets. *Nat Immunol* **3**: 975-983.

Valladeau, J., Ravel, O., Dezutter-Dambuyant, C., Moore, K., Kleijmeer, M., Liu, Y., Duvert-Frances, V., Vincent, C., Schmitt, D., Davoust, J., Caux, C., Lebecque, S., and Saeland, S. (2000) Langerin, a novel C-type lectin specific to Langerhans cells, is an endocytic receptor that induces the formation of Birbeck granules. *Immunity* **12**: 71-81.

Von Heijne G (1986).Mitochondrial targeting sequences may form amphiphilic helices. *EMBO J.* 5:1335-42

Weis, W.I. and K. Drickamer (1994). Trimeric structure of a C-type mannose-binding protein. *Structure* **2**: 1227-40.

Weissman, D., Y. Li, J. Ananworanich, L.J. Zhou, J. Adelsberger, T.F. Tedder, M. Baseler and A.S. Fauci (1995). Three populations of cells with dendritic morphology exist in peripheral blood, only one of which is infectable with human immunodeficiency virus type 1. *Proc. Nat. Acad. Sci. USA* **92**: 826-830.

Article présenté en intégralité

Article P17 : Tabarani et al (2005) submitted to *Angewandte Chemie*

L'affinité de BH30sucMan, un glycodendrimère présentant 32 mannoses, pour DC-SIGN a été étudié et les modalités de son interaction caractérisée. Ainsi, une spécificité pour des surfaces denses en DC-SIGN a été mise en évidence avec des affinités inférieures au μM. De plus cette molécule est capable d'inhiber l'interaction DC-SIGN/gp120 avec un EC_{50} de l'ordre de 50 μM et peut donc être considéré comme un antiviral potentiel.

Mannose Hyperbranched Dendritic Polymers Interact with Clustered Organization of DC-SIGN and Inhibit gp120 Binding

Georges Tabarani[1], José J. Reina[2], Christine Ebel[1], Corinne Vivès[1], Hugues Lortat-Jacob[1], Javier Rojo[2]* and Franck Fieschi[1]*

[1] Institut de Biologie Structurale, UMR 5075 CEA/CNRS/Université Joseph Fourier, 41, rue Jules Horowitz, 38027 Grenoble Cedex 1, France
[2] Grupo de Carbohidratos, Instituto de Investigaciones Químicas, CSIC, Américo Vespucio 49, 41092 Sevilla, SPAIN

*Corresponding authors:
Javier Rojo, Fax : + 34 954 46 05 65; E-mail: javier.rojo@iiq.csic.es
Franck Fieschi, Fax: + 33 (0)4 38 78 54 94 ; E-mail: franck.fieschi@ibs.fr

Abstract

DC-SIGN is a C-type lectin receptor of dendritic cells and is involved in the initial steps of numerous infectious diseases. Surface Plasmon Resonance has been used to study the affinity of a glycodendritic polymer with 32 mannoses, to DC-SIGN. This glycodendrimer binds to DC-SIGN surfaces in the submicromolar range. This binding depends on a clustered organization of DC-SIGN mimicking its natural organization as microdomain in the dendritic cells plasma membrane. Moreover, this compound inhibits DC-SIGN binding to the HIV glycoprotein gp120 with an IC_{50} in the μM range and therefore can be considered as a potential antiviral drug.

Keywords

Carbohydrates; DC-SIGN; gp120; Multivalency; Surface Plasmon Resonance, antiviral compound

1. Introduction

DC-SIGN (Dendritic Cell-Specific ICAM-3 Grabbing Non-Integrin) is a C-type lectin able to recognize high glycosylated proteins, especially those presenting high mannose structures such as the viral envelop glycoproteins gp120 (HIV) [1], GP1 (Ebola) [2] or glycoprotein E (Dengue) [3]. A Few years ago, *in vitro* studies carried out by van Kooyk et al. suggested a role for DC-SIGN in HIV infection [1]. New evidences have demonstrated that this lectin is able to interact with a large number of pathogens such as virus, bacteria, fungi and parasites as well [4]. The broad pathogen spectrum that could use DC-SIGN during their infection process places this lectin as new target in infectious diseases.

DC-SIGN, expressed at the surface of dendritic cells, has a C-terminus carbohydrate recognition domain (CRD). Ultracentrifugation [5] and hydrodynamic [6] studies have demonstrated that this protein oligomerize into homotetramers thus presenting four CRDs. Moreover, at the plasma membrane level, DC-SIGN is organized in microdomains, within lipids rafts, proposed to act as docking site for pathogens [7]. The interaction of this C-type lectin with high mannose structures displayed by the pathogen glycoproteins is multivalent and calcium dependent [5,8]. Inhibition of this interaction could be considered as new strategy to design compounds with antiviral activity. In this aim, a multivalent presentation of mannosyl oligosaccharides on an adequate scaffold mimicking the natural organization of high mannose structures should be required. Taking this into account, we have recently described the synthesis of mannosyl glycodendritic structures based on second and third generations of Boltorn hyperbranched dendritic polymers (BH20 and BH30) that have been functionalized with mannose (figure 1) [9].

These compounds showed a high solubility in physiological conditions and no cytotoxicity against several cell lines [9]. We have also demonstrated that at least the third generation with 32 mannoses at the surface (BH30sucMan) inhibited the infection process of pseudotyped viral particles presenting the Ebola viral glycoprotein GP1 at the surface [10,11]. This inhibition presumably occurs through the blockage, by the glycodendritic polymer BH30sucMan, of the

receptor DC-SIGN expressed by the target cell surface. To further investigate this binding at the molecular level, we adopted a method in which DC-SIGN is coupled to a solid phase, at different density, and BH30sucMan binding is analysed by surface plasmon resonance (SPR). Biosensors have already been successfully applied to study carbohydrate-protein interactions [12] including DC-SIGN [13] and to determine the kinetic and thermodynamic parameters. Surfaces functionalized with increasing DC-SIGN density may mimic, to some extend, the presentation of DC-SIGN as microdomain at the cell surface, but also enable us to analyse possible “avidity” for mannose carrying molecule if binding occurs at more than one site and the role of multivalency from the point of view of the receptor. This information could be very useful to improve the design of better inhibitors for this protein.

2. Materials and Methods

2.1 Multivalent compounds

Synthesis of dendritic compounds BH20sucL, BH30sucL, BH20sucMan and BH30sucMan have been previously described [9].

2.2 Expression of CRD and ECD of DC-SIGN in E. Coli

Plasmids pET30b (Novagen) containing cDNA encoding CRD (corresponding to aminoacids 254-404) or ECD (corresponding to aminoacids 66-404) of DC-SIGN were used for overproduction as described previously[14]. Proteins produced in inclusion bodies have been refolded as already described [5]. Purification of functional DC-SIGN proteins were achieved by an affinity chromatography on Mannan-agarose column (Sigma) equilibrated in 25 mM Tris-Hcl pH 7.8, 150 mM NaCl, 4 mM $CaCl_2$ (Buffer A) and eluted in same buffer lacking $CaCl_2$ but supplemented with 10 mM EDTA. This step was followed by a superose 6 size exclusion chromatography equilibrated in buffer A.

2.3 Biosensor experiments

All experiments were performed on a BIAcore 3000 using functionalized CM4 chips and the corresponding reagents from BIAcore. Four flow cells were activated as described [14]. Flow cell one was then blocked with 50 µl of 1 M ethanolamine and served as a control surface. For binding assays, the three other ones were treated with the ECD (60 or 6 µg/mL) or CRD (57 µg/mL) of DC-SIGN in 10 mM acetate buffer, pH 4. Different amounts of immobilized protein were obtained by varying the injected volume. Flow cell 2 was functionalized with DC-SIGN CRD at "high density" (CRD-HD, 600 RU immobilized), flow cell 3 and 4 were functionalized with DC-SIGN ECD at high and low density respectively (4920 and 750 RU immobilized for ECD-HD and ECD-LD respectively). Remaining activated groups were blocked with 50 µL of 1 M ethanolamine. For controling surface activity, gp120 protein was injected at 25 µg/mL for 2 min over for the association phase, after which running, buffer alone was injected for the dissociation phase. For binding studies, glycodendritic polymers were solubilized in running buffer (buffer A supplemented with 0.005% P20 surfactant) and injected at 10 µL/min. The curve fitting has been done using BIAeval program.

For gp120 binding inhibition assays, EDC/NHS activated flow cells were treated with gp120 HXB2 (5 to 50 µg/mL) in 10 mM acetate buffer, pH 4. The ECD of DC-SIGN was co-injected with increasing amount of glycodendritic polymers at 20 µL/min, in running buffer, on gp120 flow cells of increasing density.

2.4 Analytical ultracentrifugation experiments.

Sedimentation velocity experiments were performed in a Beckman XL-I analytical ultracentrifuge using an AN-60 TI rotor (Beckman instruments), at 20 °C. Samples were handled in the size exclusion chromatography elution buffer (buffer A). The molar mass and partial specific volume of DC-SIGN ECD tetramer were estimated from the amino-acid composition to be M_P = 154 858 g/mol and $\bar{v}_P$ = 0.731 ml/g, respectively, using the Sednterp software (available at www.bbri.org/RASMB/rasmb.html). The partial specific volume for the protein-BH30sucMan complex, $\bar{v}_{complex}$, was approximated to the one of the protein alone considering the ten times ratio

in molecular mass in favor of the protein.

Sedimentation velocity experiments were carried out at 42,000 rpm, using 100 μl or 400 μl protein samples, loaded respectively in the two-channel 0.3 cm or 1.2 cm path length centerpieces equipped with sapphire windows, and followed at 5 min interval using absorbance and interference optics. Absorbance scans were recorded overnight at 252 or 280 nm (depending on the protein concentration) with a radial step size of 0.003 cm. Sedimentation velocity profiles were analyzed using the size distribution analysis from the program Sedfit (version 9.2 developed by P. Schuck and available at www.analyticalultracentrifugation.com) providing a continuous distribution of apparent sedimentation coefficients, c(s) [15]. Typically 20 regularly-spaced experimental profiles obtained for a total of 6 h sedimentation were globally modeled. The continuous distribution of apparent sedimentation coefficients (c(s)) analysis was performed considering 200 particles on a grid of 300 radial points, calculated with a frictional ratio f/f° of 2.3 (fitted in Sedfit and corresponding to a very elongated shape as previously demonstrated [6]). For the regularization procedure a confidence level of 0.7 was used.

3. Results

3.1 BH30sucMan interacts with DC-SIGN functionalised surfaces in a multivalent and surface density dependance.

We have produced two different forms of DC-SIGN: the monomeric Carbohydrate Recognition Domain (CRD) and the tetrameric ExtraCellular domain (ECD). These two forms enabled us to analyze the binding mode since the CRD possess only one binding site while the tetrameric ECD contains four sites for carbohydrates ligands and can promote multivalent binding. These proteins (CRD and ECD) were overexpressed as inclusion bodies in *E. Coli*, refolded, purified and used to functionalize biosensor surfaces (see Materials and Methods). We have prepared three different types of surfaces, with these two proteins, using a carboxydextran CM4 chip from BIAcore (see Material and Methods for details). The first two flow cells where functionalized with two different level of DC-SIGN ECD and are referred as high density ECD and

low density ECD surfaces. The third one was functionalized with DC-SIGN CRD at a molecular density corresponding to the high density tetrameric ECD surface. Thus, this surface is then designed as high density monomeric CRD surface. Despite a same density in protein molecules for the two high density surfaces, the DC-SIGN ECD surface, as a consequence of its tetrameric organisation, displays 4 times more CRD units than the monomeric CRD surface (figure 2A). These three surfaces are active, as shown by their ability to bind gp120 envelope protein from HIV (figure 2A and 2B), demonstrating that the immobilisation process is compatible with the protein activity. These surfaces have then been used to test the binding properties of different dendrimeric compounds. Dendritic structures without carbohydrates (BH20sucL and BH30sucL) did not significantly bind to any of the three surfaces (not shown). The second generation with 16 mannoses at the surface (BH20sucMan) showed almost the same behaviour than the controls (not shown). Dendritic compounds with 32 mannoses (BH30sucMan) clearly interact with the high density tetrameric ECD surface. However, despite a similar density of protein, the monomeric CRD surface was not significantly recognized by BH30sucMan, suggesting a multivalent mode of interaction for BH30sucMan. These data show that a high density and proximity of CRD domain are essential to promote this multivalent binding. This is supported by the fact that when increasing further the density of DC-SIGN CRD on a sensor chip, it is possible to obtain BH30sucMan binding as observed (in Fig 2D) with the high density DC-SIGN ECD surface (data not shown). Adding EDTA to the flow buffer allowed calcium removal from the active site and the destruction of the interaction between the glycodendritic structure and DC-SIGN.

To analyze the interaction of BH30sucMan with DC-SIGN, a range of dendrimer concentrations was injected over the high density tetrameric ECD surface. Visual inspection of the sensorgrams (figure 3) showed that BH30sucMan bound to the immobilized DC-SIGN and formed stable complexes (low dissociation). The binding curves have been analysed using several kinetic model and allow to evaluate an apparent K_d in the submicroMolar range for this type of surface with clustered DC-SIGN ECD (with an average values between the different model used around 100

nM) (see Table S.I and figure S.1 of supplementary material). Fitting of the binding curves to any of the standard model was not obvious since the binding mechanism between multivalent BH30sucMan and different randomly presented CRD on the tetrameric high density ECD surface (thus generating several types of binding sites) is most probably a complex combination of the different binding models used.

3.2 Confirmation of bridging interaction of BH30sucMan between DC-SIGN ECD complexes in solution using sedimentation velocity.

Analytical Ultracentrifugation experiments were performed to investigate the formation of complex between the protein and BH30sucMan. Continuous distribution of sedimentation coefficients were used to describe the sample homogeneity and evolution. Firstly, measurements were done on DC-SIGN ECD alone at four concentrations ranging from 1.2 to 21 µM. The protein was homogenous at all concentrations with $s_{20,w}$ value at low concentration of 5.4 S. Analysis in terms of sedimentation and diffusion coefficients provided a molar mass of 148 kDa, very close to the 155 kDa theoretical value of a tetramer. Combining the values of $s_{20,w}$ with the theoretical tetramer mass for the tetramer provided a Stokes radius of 6.8 nm and a frictional ratio f/f° of 1.9. The corresponding value for a globular compact protein is 1.2-1.3. The large f/f° is in agreement with the very elongated shape of DC-SIGN previously described [6]. At high concentration of 21 µM, the $s_{20,w}$ value decreased slightly to 5.1 S, which was expected from excluded volume effect. There was no indication of any auto-association: the c(s) profile showed only one peak (Figure 4, panel C and D). The glycodendrimer by itself sedimented slower, with a mean $s_{20,w}$ -value of 2.8S, which was evidenced using interference optics, since it does not display significant absorbance properties (data not shown).

The c(s) distribution for two mixtures, with a conserved concentration of dendrimer of 50 µM is compared to that of DC-SIGN ECD on Figure 4. Panel A shows for one of the mixtures a selection of the sedimentation profiles and their modeling, panel B the residuals (superimposition of

the differences between the experimental and fitted curves). Panel C and D give the superimposition of the c(s) for the three samples using absorbance and interference optics, respectively. Although the details of the distribution differ slightly, the same main features are observed whatever the detection used. The complexation is obvious, with average $s_{20,w}$ values of 5.1S for DC-SIGN ECD alone, going to 5.4 and 6.3 S in the presence of 50µM dendrimer with increasing DC-SIGN ECD concentrations of 12 and 35 µM, respectively. Peaks are broader for the complexes, this can have different origins and will not be analyzed further. The c(s) analysis from interference suggests that increasing the concentration of DC-SIGN ECD at constant concentration of BH30sucMan, the proportion of a species at 6.3 S increases at the expense of others at around 5.4S. The c(s) analysis also shows a limited proportion of aggregates with $s_{20,w}$ -values above 8S.

To interpret the c(s) analysis, we compared the experimental s- scale with calculated values for different complexes. We approximated the f/f° and partial specific volume to the values of DC-SIGN ECD, which represents the main part of the complexes (its molar mass being more than ten times that of the glycodendrimer). Then we have calculated for different DC-SIGN ECD:BH30sucMan stoechiometries of 1:1, 2:1 and 1:4, theoretical s-values of 5.4S, 8.3S, and 6.5S, respectively. The first value is close to that of the 5.3S peaks on Panels D suggesting that the peak correlates with a 1:1 complex. The second is much larger and the third one close to that of the 6.3S experimental peak. The discrepancy between the second theoretical value and the experimental one could be related to an underestimated f/f° value (a complex comprising 2 DC-SIGN ECD moieties could be more anisotropic than 1 DC-SIGN ECD). Alternatively, the saturation of the equilibrium might have not been reached, and/or association dissociation phenomena in the ultracentrifuge could have provided peaks in the c(s) profiles below the characteristic s-values for the 2:1 complex. The 6.3 S can only be considered as a minimal value characterizing the complexed species. The third calculation corresponds to a complex comprising an excess of 4 BH30sucMan, since DC-SIGN ECD has 4 sugar binding site and BH30sucMan concentration corresponds to a large excess of sugar moieties in the solutions (32 mannose per compounds x 50 µM = 1,6 mM of mannose

ends), and leads to a calculated s value closer to the experimental one. From our set of experimental data, the analysis of the s-values by itself does not allow to discriminate between complexes comprising an excess of DC-SIGN ECD versus an excess of BH30sucMan.

More insight on the complex composition can be obtained from the analysis of the intensity obtained by absorbance (A) and interference (J). We have globally analyzed the main species of s between 4 and 7 S. Sedimentation velocity data for the protein at 21 µM and the mixture DC-SIGN ECD:BH30sucMan 35µM:50µM were obtained at a common wavelength of 252 nm. J/A_{252nm} changed only slightly: for the protein J/A=3.9 and for the mixture: J/A=4.0. From A252nm and interference signals of DC-SIGN and BH30sucMan alone, theoretical J/A ratios have been calculated for different complex stoichiometries. Going from DC-SIGN ECD:BH30sucMan complexes with an excess of glycodendrimer (1:2) to complexes with increasing proportion of protein (1:1, 2:1, and 3:1 stoichiometry), theoretical J/A ratio are 4.28, 4.11, 4.02, 3.99, respectively. The comparison with the experimental value of 4.0 suggests that the mixture has globally an excess of DC-SIGN ECD over BH30sucMan, and not the contrary.

In summary, the experiments show complexes in solution of moderate sizes, even if a small proportion of large assemblies are detected. Combining the analysis in terms of s-values and J/A ratio indicates complexes of DC-SIGN bridged by BH30sucMan.

3.3 Inhibition of DC-SIGN:gp120 interaction by BH30sucMan

After analyzing the binding of our dendritic compounds to the receptor DC-SIGN, we have studied the interaction of DC-SIGN with the HIV viral glycoprotein gp120 in competition with the synthetic glycodendritic compounds. To perform the competition experiments, we have functionalized the biosensor chip with gp120 and co-injected increasing amounts of the multivalent compounds together with a fixed concentration of DC-SIGN ECD. When we use the dendritic control BH30sucL without carbohydrates, the sensorgrams demonstrated that this compound is not able to inhibit the binding of ECD with gp120 and for all concentrations of the control tested the

curves remain unchanged (figure 5B and 5C). In the presence of BH30sucMan, the binding response decrease with the increasing amounts of this compound, indicating an ECD binding inhibition with the gp120 surface (figure 5A and 5C). From the analysis of the curves it is possible to estimate an IC_{50} for BH30sucMan of 50 µM (figure 5C). Moreover, using surface functionalized with increasing density of gp120 lead to an increase of the BH30sucMan IC_{50} (see figure S.2 supplementary materials).

4. Discussion

We have been able to prove the binding of our glycodendritic structures (the analyte) to a surface functionalized with DC-SIGN and showed that at least 32 mannoses and a high density of DC-SIGN are required for the binding. These results clearly confirm that this binding is calcium and carbohydrate dependent and therefore is likely to take place through the carbohydrate recognition domain of the protein. Also, it demonstrates that BH30sucMan binding is multivalent and can be achieved only if the number of displayed CRD units is high enough. However, it does not interact with the four CRD units present within one molecule of tetrameric ECD since no binding was observed on the low density tetrameric ECD surface (figure 2D). Multivalency on the high density tetrameric ECD surface was thus probably achieved in a bridging manner using CRD units belonging to different tetrameric ECD molecules on the surface (figure 2C). Therefore, the density of tetrameric ECD is crucial to promote BH30sucMan binding as shown by comparison between the low and high density surfaces.

This binding analysis confirms the idea that the binding is multivalent and require a close proximity of independent CRD in space (CRD belonging to the same tetramer are not close enough or are not adequate oriented with respect to the three others to allow a binding to our glycodendritic polymer as deduced by the absence of binding with a low density ECD surface). In fact, this type of surface (high density of ECD) presumably better mimics the natural organization of DC-SIGN in microdomains at the cell surface clustered into specific regions denoted as lipid rafts[7].

Using this binding assay we also set up a competition assay in which different glycodendritic structures were analysed for their ability to inhibit the gp120/DC-SIGN interaction. Previous studies have demonstrated the application of SPR to analyze the binding of different envelop viral glycoproteins of cytomegalovirus (CMV), hepatitis C (HCV) with DC-SIGN [3,14,16]. The glycoprotein gp120 at the surface of HIV is a highly glycosylated viral protein with several high mannose N-glycan structures. This viral protein displays an affinity constant in the nM range for DC-SIGN and this binding is a critical step used by HIV in T-cell trans-infection using dendritic cells as intermediates [1]. Competitions experiments enabled us to determine whether the glycodendritic structures can inhibit the recognition process between gp120 and DC-SIGN and could be used as an antiviral compounds inhibiting the infection process at one of the earliest stages. The IC_{50} value found in the competition experiments (50 μM) is higher than expected considering the apparent K_d, in the sub-microMolar range, evaluated from kinetic analysis (see supplementary material). In this set up, DC-SIGN ECD are not pre-organized on a surface but are free in solution. In that situation multivalency of binding with respect to DC-SIGN ECD can not be easily achieved, leading to a less efficient binding of the glycodendrimers. In similar experimental conditions, with respect to the relative concentrations of DC-SIGN ECD and BH30sucMan, sedimentation velocity experiments allowed us to confirm in solution the capacity of BH30sucMan to promote the bridging of DC-SIGN ECD in assembly of moderate size but also of small amount of bigger complexes. This DC-SIGN ECD sequestering can account for the inhibitory effect of BH30sucMan in our competition assay. Because of the context of a solution, this BH30sucMan bridging effect is achieved at higher concentration than with a functionalised surface. However, despite an under estimation of the real inhibiting capacity, this test proves its ability to compare relative efficiency between series of dendrimeric compounds (figure 5C). Using surface functionalized with increasing density of gp120 lead to an increase of the BH30sucMan IC_{50} suggesting that with the increase of gp120 density appears an increase of the multivalent binding for the free tetrameric DC-SIGN ECD and appearance of an avidity binding mechanism. So, the lower

the gp120 density is, the better the inhibitory power of BH30sucMan will be. Electron tomography studies of HIV-1 virion revealed an average of 8 to 10 trimers of gp120 at the virus surface [17]. This natural low density of the envelope glycoprotein at the virion surface strengthens our inhibitory approach using glycodendrimeric compounds.

Using SPR we have demonstrated that the third generation of the Boltorn hyperbranched dendritic polymer functionalized with 32 mannoses binds to DC-SIGN with an apparent affinity in the sub microMolar range and is capable to inhibit the interaction of DC-SIGN to gp120. The level of apparent affinity reaches with the third generation of the Boltorn polymer confirms us in the choice of this scaffold for a multivalent presenting system. After this proof of concept where submicromolar apparent affinity have been reach presenting the simplest carbohydrate ligand of DC-SIGN (a monosaccharide), compounds with very high affinity and specificity can be expected by using more complex and DC-SIGN specific carbohydrate moiety. Additional improvement might be obtained by modifying the linker and the multivalent scaffold. Moreover, we have set up DC-SIGN surfaces that represented good mimics of the DC-SIGN microdomains of the plasma membrane. Such surfaces will be important tools in the objective to study interaction properties of such microdomains and for the evaluation of new compounds specific for this type of DC-SIGN organization. These preliminary results encourage us to pursuit the development of better inhibitors that should be able to block the HIV binding to dendritic cells and can be used as microbicides. With the help of biosensors, the analysis of new candidates will help us to select the best one to go to further *in vitro* and *in vivo* inhibitory studies.

Acknowledgements

We would like to thank CSIC -2004FR0027- (JR); FIS -PI030093- (JR) and Ensemble contre le SIDA-Sidaction (FF) for funding support. We acknowledge Dr Francisco Véas and Alain Méchulam for the kind gift of gp120 HXB2.

Legends of figures

Figure 1. Chemical structures of dendritic compounds. A) structure of the hyperbranched polymer BoltornH20 and BoltornH30. B) Schematic representation of BH20sucL, BH30sucL, BH20sucMan and BH30sucMan

Figure 2. SPR analysis of the interaction properties of DC-SIGN surfaces as a function of the oligomerization form, ECD and CRD, and the density of functionalization. A) Schematic representation of the three functionalized surfaces interacting with gp120. B) Sensorgram for DC-SIGN/gp120 interaction with the three surfaces. The gp120 protein was injected at 25 µg/mL. C) Schematic representation of the three functionalized surfaces interacting with BH30sucMan. D) Sensorgram for binding process of BH30sucMan (injected at a concentration of 130 µM for 20 min) with the three surfaces.

Figure 3. Surface plasmon resonnance analysis of BH30sucMan/DC-SIGN Interactions. The BH30sucMan used at concentrations of 10, 7.5, 5, 2.5, 1, and 0.5 µM were injected for 20 min over a DC-SIGN ECD high density activated surface (7260 RU immobilized).

Figure 4. Sedimentation velocity of DC-SIGN ECD in the presence or absence of BH30sucMan. A) Superimposition of experimental sedimentation profiles and the fitted curves from the c(s) analysis (using Sedfit) of DC-SIGN ECD at 35 µM in the presence of 50 µM of BH30sucMan. B) Superimposition of the differences between the experimental and fitted curves from A); C) and D) c(s) analysis using absorbance or interference optics respectively. c(s) presented are DC-SIGN ECD alone (21 µM) or in the presence of 50 µM of BH30sucMan at 12 and 35 µM (continuous, dashed and dotted lines, respectively). The distributions are normalised to the main peak values.

Figure 5. Inhibition of the DC-SIGN/gp120 interactions. DC-SIGN ECD at 45 µM is incubated 1h with A) BH30sucMan or B) BH30sucL at concentrations 0, 3.5, 14, 28, 57, 85, 128 µM and co-injected on a gp120 functionalized surface (176 RU immobilized). C) Comparison of the inhibitory power of the different dendritic and glycodendritic polymers towards the DC-SIGN/gp120 interaction. ○) BH30sucL, △)BH20sucL, ▲) BH20sucMan, ●) BH30sucMan.

References

[1] Geijtenbeek, T.B. et al. (2000) DC-SIGN, a dendritic cell-specific HIV-1-binding protein that enhances trans-infection of T cells *Cell* 100, 587-97.

[2] Alvarez, C.P., Lasala, F., Carrillo, J., Muniz, O., Corbi, A.L. and Delgado, R. (2002) C-type lectins DC-SIGN and L-SIGN mediate cellular entry by Ebola virus in cis and in trans *J Virol* 76, 6841-4.

[3] Navarro-Sanchez, E., Altmeyer, R., Amara, A., Schwartz, O., Fieschi, F., Virelizier, J.L., Arenzana-Seisdedos, F. and Despres, P. (2003) Dendritic-cell-specific ICAM3-grabbing non-integrin is essential for the productive infection of human dendritic cells by mosquito-cell-derived dengue viruses *EMBO Rep* 4, 723-8.

[4] van Kooyk, Y. and Geijtenbeek, T.B. (2003) DC-SIGN: escape mechanism for pathogens *Nat Rev Immunol* 3, 697-709.

[5] Mitchell, D.A., Fadden, A.J. and Drickamer, K. (2001) A novel mechanism of carbohydrate recognition by the C-type lectins DC-SIGN and DC-SIGNR. Subunit organization and binding to multivalent ligands *J Biol Chem* 276, 28939-45.

[6] Feinberg, H., Guo, Y., Mitchell, D.A., Drickamer, K. and Weis, W.I. (2005) Extended neck regions stabilize tetramers of the receptors DC-SIGN and DC-SIGNR *J Biol Chem* 280, 1327-35.

[7] Cambi, A. et al. (2004) Microdomains of the C-type lectin DC-SIGN are portals for virus entry into dendritic cells *J Cell Biol* 164, 145-55.

[8] Feinberg, H., Mitchell, D.A., Drickamer, K. and Weis, W.I. (2001) Structural basis for selective recognition of oligosaccharides by DC-SIGN and DC-SIGNR *Science* 294, 2163-6.
[9] Arce, E., Nieto, P.M., Diaz, V., Castro, R.G., Bernad, A. and Rojo, J. (2003) Glycodendritic structures based on Boltorn hyperbranched polymers and their interactions with Lens culinaris lectin *Bioconjug Chem* 14, 817-23.
[10] Lasala, F., Arce, E., Otero, J.R., Rojo, J. and Delgado, R. (2003) Mannosyl glycodendritic structure inhibits DC-SIGN-mediated Ebola virus infection in cis and in trans *Antimicrob Agents Chemother* 47, 3970-2.
[11] Rojo, J. and Delgado, R. (2004) Glycodendritic structures: promising new antiviral drugs *J Antimicrob Chemother* 54, 579-81.
[12] Duverger, E., Frison, N., Roche, A.C. and Monsigny, M. (2003) Carbohydrate-lectin interactions assessed by surface plasmon resonance *Biochimie* 85, 167-79.
[13] Frison, N., Taylor, M.E., Soilleux, E., Bousser, M.T., Mayer, R., Monsigny, M., Drickamer, K. and Roche, A.C. (2003) Oligolysine-based oligosaccharide clusters: selective recognition and endocytosis by the mannose receptor and dendritic cell-specific intercellular adhesion molecule 3 (ICAM-3)-grabbing nonintegrin *J Biol Chem* 278, 23922-9.
[14] Halary, F. et al. (2002) Human cytomegalovirus binding to DC-SIGN is required for dendritic cell infection and target cell trans-infection *Immunity* 17, 653-64.
[15] Schuck, P. (2000) Size-distribution analysis of macromolecules by sedimentation velocity ultracentrifugation and lamm equation modeling *Biophys J* 78, 1606-19.
[16] Lozach, P.Y. et al. (2003) DC-SIGN and L-SIGN are high affinity binding receptors for hepatitis C virus glycoprotein E2 *J Biol Chem* 278, 20358-66.
[17] Zhu, P., Chertova, E., Bess, J., Jr., Lifson, J.D., Arthur, L.O., Liu, J., Taylor, K.A. and Roux, K.H. (2003) Electron tomography analysis of envelope glycoprotein trimers on HIV and simian immunodeficiency virus virions *Proc Natl Acad Sci U S A* 100, 15812-7.

Figure 1

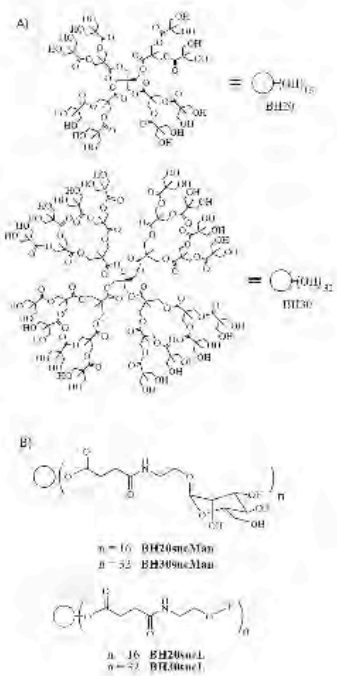

Figure 2

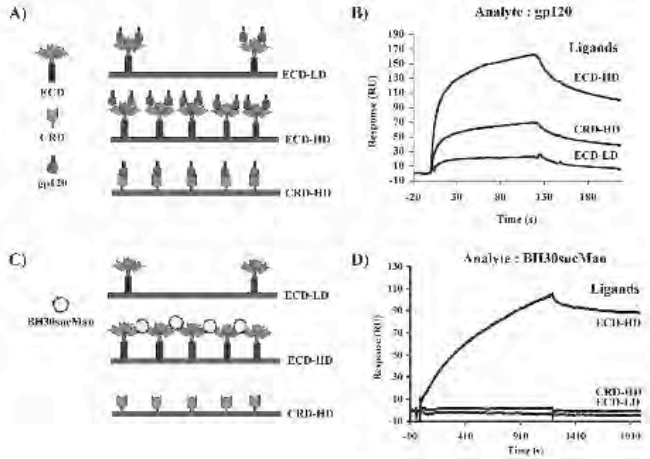

Figure 3

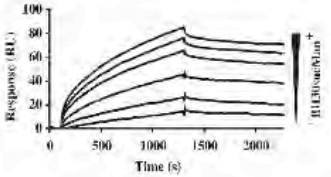

Figure 4

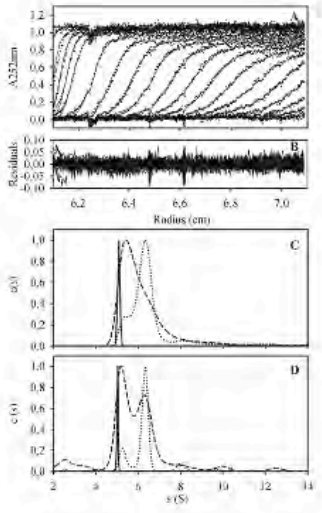

Figure 4

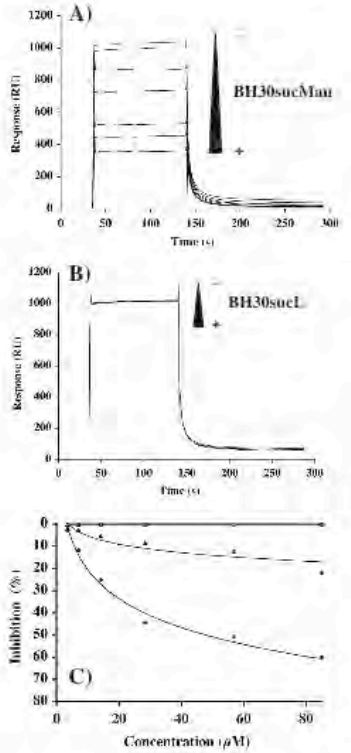

Abstracts

Article P12 : Halary et al (2005) *Immunity*
Cet article met en évidence le rôle de DC-SIGN dans l'infection en cis et en trans pour le Cytomégalovirus. L'interaction de DC-SIGN avec la protéine d'enveloppe virale, gB, est caractérisé par Biacore. L'affinité de cette interaction est comparable à celle de DC-SIGN avec la protéine gp120 du VIH.

Article P13 : Lozach et al (2005) *J.Biol.Chem.*
L'interaction entre la protéine d'enveloppe E2, du virus de l'hépatite C, est caractérisé comme étant de haute affinité. De plus, l'analyse Biacore de cette interaction met l'accent sur l'importance de l'oligomérisation de DC-SIGN dans le processus de reconnaissance.

Article P14 : Navarro-Sanchez et al (2005) *Embo reports*
La nécessité de DC-SIGN pour permettre l'infection de cellules dendritiques par des virus de la dengue, provenant de moustiques est ici démontré. L'utilisation de DC-SIGN ECD soluble dans le milieu, lors d'expériences d'infections, permet de titrer le virus et d'inhiber l'infection.

Immunity, Vol. 17, 653–664, November, 2002, Copyright ©2002 by Cell Press

Human Cytomegalovirus Binding to DC-SIGN Is Required for Dendritic Cell Infection and Target Cell *trans*-Infection

Franck Halary,[1] Ali Amara,[2] Hugues Lortat-Jacob,[3] Martin Messerle,[4] Thierry Delaunay,[5] Corinne Houlès,[3] Franck Fieschi,[3] Fernando Arenzana-Seisdedos,[2] Jean-François Moreau,[1] and Julie Déchanet-Merville[1,6]

[1]Laboratoire d'immunologie
CNRS UMR 5540
Université Bordeaux 2
33000 Bordeaux
[2]Unité d'Immunologie Virale
Département de Médecine Moléculaire
Institut Pasteur
75015 Paris
[3]Institut de Biologie Structurale
CEA-CNRS-Université Joseph Fourier
UMR 5075
38027 Grenoble
France
[4]Virus Cell Interaction Group
Medical Faculty
University of Halle-Wittenberg
06120 Halle
Germany
[5]Département de Pathologie Végétale
INRA
33883 Villenave d'Ornon
France

Summary

Cytomegalovirus (CMV) infection is characterized by host immunosuppression and multiorganic involvement. CMV-infected dendritic cells (DC) were recently shown to display reduced immune functions, but their role in virus dissemination is not clear. In this report, we demonstrated that CMV could be captured by DC through binding on DC-SIGN and subsequently transmitted to permissive cells. Moreover, blocking DC-SIGN by specific antibodies inhibited DC infection by primary CMV isolates and expression of DC-SIGN or its homolog DC-SIGNR rendered susceptible cells permissive to CMV infection. We demonstrated that CMV envelope glycoprotein B is a viral ligand for DC-SIGN and DC-SIGNR. These results provide new insights into the molecular interactions contributing to cell infection by CMV and extend DC-SIGN implication in virus propagation.

Introduction

Human Cytomegalovirus (CMV) is a double-strand DNA virus belonging to the herpesviridae family and is a ubiquitous pathogen in humans. CMV interaction with its host is characterized by a primary infection followed by lifelong persistence in the host organism and viral reactivation episodes. CMV infection is asymptomatic in most immunocompetent individuals because of an efficient antiviral immune response. In contrast, CMV remains a major cause of morbidity and mortality in newborn and immunocompromised patients, namely in organ-transplanted recipients or AIDS patients. In any cases, CMV disease is characterized by a wide viral spread toward multiple organs (i.e., salivary glands, lung, kidney, gastrointestinal tract, liver, retina, CNS).

In vitro, a number of cell types are susceptible to CMV infection when considering virus entry and viral immediate early gene expression. However, full replication of virus DNA and subsequent progeny of infectious virions is limited to permissive cells (i.e., fibroblasts, endothelial cells, the U373 MG astrocytoma cell line, etc.; for review see Plachter et al., 1996). In fibroblasts (the prototypic cell type for in vitro studies of CMV infection), CMV entry occurs in sequential steps involving several viral envelope (Env) glycoproteins. Initial attachment of virus to host cells is mediated through interaction between Env glycoproteins gB (CMV gB) and/or CMV gM with cell surface heparan sulfate proteoglycans (Compton et al., 1993; Kari and Gehrz, 1992). Thereafter, binding of CMV gB with non-heparin cellular receptors probably allows more stable attachment of virus to cell surface (Boyle and Compton, 1998). Subsequent pH-independent fusion events between viral envelope and cell membrane are necessary for viral entry (Compton et al., 1992; Milne et al., 1998). Cell proteins involved in CMV attachment and/or fusion have not been identified precisely, although two candidates have been proposed. The first one is annexin II, which interacts with CMV gB (Pietropaolo and Compton, 1997). The second one is a 92.5 kDa protein binding to CMV gH (Baldwin et al., 2000). Fusion events are followed by penetration of the capsid which is transported to the nucleus. In some permissive cells, such as retinal pigment epithelial cells, CMV can also penetrate into cells by a mechanism of endocytosis (Bodaghi et al., 1999).

Recently, DC, which are refractory to infection by laboratory-adapted CMV strains, were shown to be permissive to CMV infection and replication when infected with primary, clinical viral isolates (Riegler et al., 2000). The mechanism of CMV entry into DC has not been investigated yet. It was recently shown that DC express a lectin called DC-SIGN (DC-Specific ICAM-Grabbing Nonintegrin). DC-SIGN, also called CD209, is a ligand for IntraCellular Adhesion Molecule-2 (ICAM-2) and ICAM-3 (Geijtenbeek et al., 2000a, 2000c) and is involved in the attachment of Human Immunodeficiency Virus-1 (HIV-1) (Geijtenbeek et al., 2000b) and Ebola (Alvarez et al., 2002) to DC. DC-SIGN was originally cloned from a placental cDNA library on the basis of its capacity to bind to the surface subunit HIV-1 Env glycoprotein 120 (HIV-1 gp120) (Curtis et al., 1992). DC-SIGN mediates HIV binding and internalization into DC, conferring to these cells the ability to transmit HIV to permissive $CD4^+$ T cells independently from HIV-1 replication (Geijtenbeek et al., 2000b). These findings suggest that DC-SIGN efficiently captures HIV-1 at mucosal sites of inoculation and facilitates its transport to sites of infection by using the migra-

[6]Correspondence: julie.dechanet@umr5540.u-bordeaux2.fr

THE JOURNAL OF BIOLOGICAL CHEMISTRY
Vol. 278, No. 22, Issue of May 30, pp. 20358–20366, 2003

Printed in U.S.A.

DC-SIGN and L-SIGN Are High Affinity Binding Receptors for Hepatitis C Virus Glycoprotein E2*

Received for publication, February 5, 2003, and in revised form, February 27, 2003
Published, JBC Papers in Press, February 27, 2003, DOI 10.1074/jbc.M301284200

Pierre-Yves Lozach‡, Hugues Lortat-Jacob§, Agnès de Lacroix de Lavalette‡, Isabelle Staropoli‡, Steven Foung¶, Ali Amara‡‖, Corinne Houlès§, Frank Fieschi§, Olivier Schwartz, Jean-Louis Virelizier‡, Fernando Arenzana-Seisdedos‡, and Ralf Altmeyer‡ ‡‡**

*From ‡Unité d'Immunologie Virale and **Groupe Virus et Immunité, Institut Pasteur, 28, rue du Dr. Roux, 75015 Paris, France, the §Institut de Biologie Structurale, CEA-CNRS-UJF, Unite Mixté de Recherche 5075, 41 Avenue des Martyrs, 38027 Grenoble, Cedex 01, France, and the ¶Department of Pathology, Stanford University Medical Center, Stanford, California 94305*

The hepatitis C virus (HCV) genome codes for highly mannosylated envelope proteins, which are naturally retained in the endoplasmic reticulum. We found that the HCV envelope glycoprotein E2 binds the dendritic cell-specific intercellular adhesion molecule 3-grabbing nonintegrin (DC-SIGN) and the related liver endothelial cell lectin L-SIGN through high-mannose *N*-glycans. Competing ligands such as mannan and an antibody directed against the carbohydrate recognition domains (CRD) abrogated binding. While no E2 interaction with distant monomeric CRDs on biosensor chips could be detected, binding is observed if CRDs are closely seeded (K_d = 48 nM) and if the CRD is part of the oligomeric-soluble extracellular domain of DC-SIGN (K_d = 30 nM). The highest affinity is seen for plasma membrane-expressed DC-SIGN and L-SIGN (K_d = 3 and 6 nM, respectively). These results indicate that several high-mannose *N*-glycans in a structurally defined cluster on E2 bind to several subunits of the oligomeric lectin CRD. High affinity interaction of viral glycoproteins with oligomeric lectins might represent a strategy by which HCV targets to and concentrates in the liver and infects dendritic cells.

Hepatitis C virus (HCV)[1] is the major causative agent of non-A, non-B hepatitis throughout the world with more than 170 million people infected (1). Contamination with infected blood by injecting drug users is the primary risk factor for acquiring HCV infection. The majority of infected patients are unable to clear the virus, and many develop chronic liver disease, cirrhosis, and hepatocellular carcinoma (2). Replication of the HCV genome could be demonstrated *in vivo* and *in vitro* in liver hepatocytes (3, 4) and hematopoietic cells including dendritic cells and B cells (5, 6). However, the molecular mechanism by which the virus targets to these sites of replication, notably in the liver, is not known.

HCV is a small, enveloped, plus-strand RNA virus belonging to the family flaviviridae and genus *hepacivirus*. The HCV RNA genome is 9600 nucleotides in length and encodes a single polyprotein that is post-translationally cleaved into up to 10 polypeptides including three structural proteins (core, E1, and E2), located at the N terminus, and five nonstructural proteins (1, 7, 8). Shortly after translocation into the endoplasmic reticulum (ER), oligosaccharide transferase catalyzes addition of Glc3Man9GlcNAc2 complexes at up to 6 (E1) and 11 (E2) *N*-glycosylation sites (for review see Ref. 9). Glucose residues are removed by glucosidases I and II, and correctly folded proteins are released from ER chaperones calnexin and calreticulin (10–13). The transmembrane domains of E1 and E2 are responsible for both heterodimerization (14) and retention of the glycoproteins in a high-mannose EndoH-sensitive glycoform in the ER (15–17). By analogy to other flaviviruses it is assumed that HCV capsids bud from the cytoplasm into the ER and that enveloped particles follow the secretion pathway through the Golgi. However, attempts to produce secreted HCV particles *in vitro* have not been successful so far (18–20), and it is not known if E1 and E2 on mature infectious virions possess a high-mannose, complex, or mixed glycosylation.

Several receptors have been proposed that could play a role in HCV entry into hepatocytes. The low density lipoprotein (LDL) receptor has been shown to mediate HCV internalization via binding to virus-associated LDL particles (21, 22). A second putative HCV receptor, the tetraspanin CD81, has been identified as a high affinity binding receptor (1.8 nM) for soluble recombinant E2 from HCV genotype 1a (23, 24). CD81 and LDL receptor are expressed in most cell types and thus likely do not account for the hepatic tropism of the virus. Furthermore E2 binds to the hepatoblastoma cell line HepG2, which does not express CD81 (25). More recently two novel E2 binding receptors have been identified on HepG2 cells, the scavenger receptor type B class I (SR-BI) (25) and the galactose binding C-type lectin asialoglycoprotein receptor (26). The lack of an efficient cell culture model has precluded functional confirmation of these receptor candidates at the level of virus entry.

It has recently been shown that C-type mannose binding

* This work was supported by a Ministére de l'Education Nationale de la Recherche et de la Technologie doctoral thesis grant (to P. Y. L.) and partially supported by Public Health Service Grants AI47355, CA34233, and DA06596 (to S. F.). Financial support was also received from the French Hepatitis Network and the National Agency for AIDS Research (ANRS). The costs of publication of this article were defrayed in part by the payment of page charges. This article must therefore be hereby marked "*advertisement*" in accordance with 18 U.S.C. Section 1734 solely to indicate this fact.

‖ Present address: Skirball Institute of Biomolecular Medicine, New York University Medical Center, New York, NY 10016.

‡‡ To whom correspondence should be addressed. Tel.: 33-1-40-61-36-49; Fax: 33-1-45-68-89-41; E-mail: altmeyer@pasteur.fr.

[1] The abbreviations used are: HCV, hepatitis C virus; ER, endoplasmic reticulum; LDL, low density lipoprotein; CRD, carbohydrate recognition domains; SFV, Semliki Forest virus; BHK, baby hamster kidney; sE2, soluble E2; TM, transmembrane; aa, amino acids; ECD, extracellular domain; EDC, *N*-ethyl-*N*′-(3-dimethyl-aminopropyl)-carbodiimide hydrochloride; EndoH, endoglycosidase H; RU, resonance units; DC, dendritic cells; PNGase F; peptide:*N*-glycosidase F; mAb, monoclonal antibody; DMEM, Dulbecco's modified Eagle's medium; FCS, fetal calf serum; DMJ, 1-deoxymannojirimycin hydrochloride; FACS, fluorescence-activated cell sorter; NHS, *N*-hydroxysuccinimide; HIV, human immunodeficiency virus.

EMBO reports

scientific report

Dendritic-cell-specific ICAM3-grabbing non-integrin is essential for the productive infection of human dendritic cells by mosquito-cell-derived dengue viruses

Erika Navarro-Sanchez[1], Ralf Altmeyer[2], Ali Amara[2†], Olivier Schwartz[3], Franck Fieschi[4], Jean-Louis Virelizier[2], Fernando Arenzana-Seisdedos[2+] & Philippe Desprès[1++]

[1]Interactions Moléculaires Flavivirus-Hôtes, [2]Immunologie Virale, and [3]Virus et Immunité, Institut Pasteur, Paris, France, and [4]Institut de Biologie Structurale, CEA-CNRS-UJF, Grenoble, France

Dengue virus (DV) is a mosquito-borne flavivirus that causes haemorrhagic fever in humans. DV primarily targets immature dendritic cells (DCs) after a bite by an infected mosquito vector. Here, we analysed the interactions between DV and human-monocyte-derived DCs at the level of virus entry. We show that the DC-specific ICAM3-grabbing non-integrin (DC-SIGN) molecule, a cell-surface, mannose-specific, C-type lectin, binds mosquito-cell-derived DVs and allows viral replication. Conclusive evidence for the involvement of DC-SIGN in DV infection was obtained by the inhibition of viral infection by anti-DC-SIGN antibodies and by the soluble tetrameric ectodomain of DC-SIGN. Our data show that DC-SIGN functions as a DV-binding lectin by interacting with the DV envelope glycoprotein. Mosquito-cell-derived DVs may have differential infectivity for DC-SIGN-expressing cells. We suggest that the differential use of DC-SIGN by viral envelope glycoproteins may account for the immunopathogenesis of DVs.

EMBO reports **4**, 723–728 (2003)
doi:10.1038/sj.embor.embor866

INTRODUCTION

Dengue virus (DV) is an arthropod-borne flavivirus that belongs to the *Flaviviridae* family (Rice, 1996). Four antigenically distinct serotypes, DV types 1–4, are transmitted to humans through the mosquito vector, *Aedes aegypti* (Guzman & Kouri, 2002). DVs are lipid-enveloped viruses with a single-stranded, positive-sense RNA genome that encodes the structural proteins C (capsid), M (membrane) and E (envelope), and eight non-structural proteins, NS1 to NS5 (Rice, 1996). The E-glycoprotein, which is exposed on the surface of the viral membrane (Kuhn *et al*., 2002), mediates viral attachment to cells (Hung *et al*., 1999). The DV E-glycoprotein has two potential sites for *N*-linked glycosylation at positions Asn 67 and Asn 153, which are differentially used by the four DV serotypes (Johnson *et al*., 1994).

DV infection can cause self-limiting fever or severe haemorrhagic fever and shock-syndrome (Halstead, 1989; Rothman & Ennis, 1999; Lei *et al*., 2001). The pathogenesis of DV is still poorly understood. Immature dendritic cells (DCs), in contrast with macrophages and monocytes, are permissive for DV infection (Palucka, 2000; Wu *et al*., 2000; Ho *et al*., 2001; Marovich *et al*., 2001). The skin-epidermal Langerhans cells, which are considered to be immature DCs, have been proposed to be the primary target cells after the initial bite by an infected *Aedes* mosquito (Wu *et al*., 2000). Early interactions between mosquito-cell-derived DV and DCs may be crucial for transporting viral antigens to secondary lymphoid organs and for developing antiviral immunity (Kelsa *et al*., 2002). Consistent with this, DV infection of immature DCs is considered to be a crucial step in the establishment of viral infection. However, DV interactions with DCs are poorly understood at the molecular level (Wu *et al*., 2000). The attachment sites for viral entry into leukocytes might contribute to the severity of the disease (Morens *et al*., 1991). Here, we show the importance of the lectin, DC-specific ICAM3-grabbing non-integrin (DC-SIGN; also known as CD209), for the productive infection of monocyte-derived DCs (MDDCs) by mosquito-cell-derived DVs.

RESULTS AND DISCUSSION

The ability of immature human MDDCs that lack the monocytic CD14 marker and express DC-SIGN (Fig. 1A) to support DV type-1 (DV-1) virus infection was investigated. MDDCs were infected with the virulent DV-1 virus, FGA/NA d1d, which was grown in *Aedes* AP61 cells (Desprès *et al*., 1998; Duarte dos Santos *et al.,* 2000). Inoculation with five AP61 focus-forming units (FFU) per cell was needed to infect 50%

[1]Interactions Moléculaires Flavivirus-Hôtes, [2]Immunologie Virale, and [3]Virus et Immunité, Institut Pasteur, 25 Rue du Dr Roux, 75724 Paris, France
[4]Institut de Biologie Structurale, CEA-CNRS-UJF, UMR 5075, 41 Avenue des Martyrs, 38027 Grenoble, France
[†]Present address: Skirball Institute of Biomolecular Medicine, New York University Medical Center, 540 1st Avenue, New York, New York 10016, USA
[+]Corresponding author. Tel: +33 1 45688263; Fax: +33 1 45688941; E-mail: farenzan@pasteur.fr
[++]Corresponding author. Tel: +33 1 40613563; Fax: +33 1 40613774; E-mail: pdespres@pasteur.fr

Received 6 February 2003; revised 7 April 2003; accepted 24 April 2003
Published online 2 June 2003

Chapitre III.

Post-Doctorat,
Doctorat,
et pré-Doctorat

Autour de la Ribonucléotide réductase.

1. Stage postdoctoral effectué en Suède de Janv. à Nov. 97 inclus (11 mois).

Department of molecular biology, Arrhenius laboratory, University of Stockholm, 10691 Stockholm, Sweden. Superviseur : Pr. Britt-Marie Sjöberg.

La ribonucléotide réductase de *Corynebacterium ammoniagenes*.

Thème du stage postdoctoral : Isolation, clonage, purification et caractérisation de la ribonucléotide réductase (RNR) de *Corynebacterium ammoniagenes*. Démonstration de son appartenant à la famille des RNR à fer de la classe Ib.

Contexte, but et résultats du travail :

Les ribonucléotides réductases (RNR) sont des enzymes absolument essentielles à toutes cellules vivantes. Elles catalysent la réduction des ribonucléotides fournissant ainsi les 2'déoxyribonucléotides nécessaires à la synthèse de l'ADN. Trois classes de RNR bien caractérisées ont été décrites à ce jour. Elles ont toutes en commun l'utilisation d'un radical organique pour initier la catalyse par un mécanisme radicalaire. En revanche, elles diffèrent par leur structure quaternaire, la nature du radical initiant la réaction et leur cofacteur métallique (1). Les enzymes de classe I ($\alpha_2\beta_2$) contiennent un radical tyrosinyle stable et un centre dinucléaire de fer. Les enzymes de classe II (α ou α_2)utilisent l'adénosylcobalamine comme cofacteur et peuvent générer un radical 5'deoxyadénosyle (2). Les enzymes anaérobies de la classe III ($\alpha_2\beta_2$) possèdent un radical glycinyle stable et un centre fer-soufre (3). De plus, différents réducteurs physiologiques et modes de régulations allostériques définissent les sous-classes Ia et Ib au sein des enzymes de classe I.

Dans les années 80 Auling, et ses collaborateurs ont rapporté la purification et la caractérisation d'une activité RNR chez *Corynebacterium ammoniagenes* unique par sa dépendance vis à vis du Manganese (Mn) (4,5,6). La présence de deux sous unités constituant cette RNR de *C. ammoniagenes* a pu être suggéré a l'issue de sa purification (5): une composante appelée alors B1 (rebaptisé par nous R1E) et une composante contenant un cofacteur métallique appelée B2 (rebaptisé par nous R2F). La présence de Mn avait été suggérée sur la base d'une incorporation spécifique de Mn^{54} dans la sous-unité R2F. De plus, un nouveau type de radical organique stable avait été rapporté pour cette RNR (7). Cependant, d'autres propriétés, telle que la sensibilité à l'hydroxyurée et la taille des sous unités de cette RNR de *C. ammoniagenes,* suggèraient une similitude avec les enzymes de la classe I.

La question de la nature de cette RNR de *C. ammoniagenes*, un prototype d'une nouvelle classe d'enzymes ou bien simplement un nouveau sous-type d'une classe déjà existante, était toujours en suspens. Obtenir une réponse à cette question était l'objectif de mon stage postdoctoral.

La protéine a été purifiée à partir d'extrait de *Corynebacterium ammoniagenes* en 4 étapes. A partir des 2 sous unités purifiées, le séquençage N-terminal des protéines a permis l'identification des gènes et l'appartenance de cette RNR à la classe Ib. La protéine recombinante a pu être exprimée dans *E. coli* avec un très fort rendement (plus de 50 % des protéines totales), l'étude des propriétés catalytiques et allostériques ainsi que la caractérisation du centre métallique par RPE (et diverses autres méthodes spectroscopiques) ont pu être mené à leur terme. Des études de reconstitution du centre métallique à partir de préparation d'apoprotéine R2F recombinante a permis de montrer que le Fer comme le Mn pouvant être incorporé dans la protéine. Par contre, seule l'incorporation de Fer conduit à la génération d'un radical tyrosynile stable et à une protéine active. L'ensemble de ce travail a permis de clore un débat sur cette enzyme. Nous avons clairement démontré dans ce travail (8,9) que la RNR dite "Mn-dépendante" de *C. ammoniagenes* ne représente pas une nouvelle classe d'enzymes comme cela a été annoncé précédemment durant une vingtaine d'année par

le groupe de Auling. Elle possède en fait un centre dinucléaire de fer à pont μ-oxo, dans son état actif, classique de ce type de protéine.

(1) Reichard, P. (1997) Trends Biochem Sci. 22, 81-85
(2) Booker, S., Licht, S., Broderick, J., and Stubbe, J. (1994) Biochemistry 33, 12676-12685
(3) Sun, X. Y., Ollagnier, S., Schmidt, P. P., Atta, M., Mulliez, E., Lepape, L., Eliasson, R., Gräslund, A., Fontecave, M., Reichard, P., and Sjöberg, B.-M. (1996) J. Biol. Chem. 271, 6827-6831
(4) Schimpff-Weiland, G., Follmann, H., and Auling, G. (1981) Biochem Biophys Res Commun 102, 1276-1282
(5) Willing, A., Follmann, H., and Auling, G. (1988) Eur. J. of Biochem. 170, 603-611
(6) Plönzig, J., and Auling, G. (1987) Arch Microbiol 146, 396-401
(7) Griepenburg, U., Lassmann, G., and Auling. (1996) Free Radical Res 24, 473-481
(8) Fieschi, F. Torrents, E., Toulokhonova, L., Jordan, A., Hellman, U., Gibert, I., Barbe, J., Karlsson, M., and Sjöberg, B.M. (1998)) *Journal of Biological Chemistry*, 273, 4329-4337.
(9) Huque, Y, Fieschi, F, Torrents, E, Gibert, I, Eliasson, R, Reichard, P, Sahlin, M and Sjöberg B-M (2000) soumis à *Journal of Biological Chemistry*.

Publications issus de ce travail post-doctoral : Articles P5 et P7 (voir page 8 et pages suivantes).

2. DEA + Thèse de l'université Joseph Fourier de Oct. 92 à Oct. 96.
Laboratoire du Pr. Marc Fontecave au L.E.D.S.S. V, Université Joseph Fourier (présentée le 16 octobre 96).

Titre de la thèse : Etude structure fonction de la NADPH:Flavine réductase de *E. coli*.

La NAD(P)H:Flavine oxydoréductase (Fre) d'*Escherichia coli* a été initialement identifiée comme composante du système d'activation de la ribonucléotide réductase d'*E. coli*. Fre est une protéine monomérique de 26 kDa dépourvue de groupement prosthétique qui catalyse la réduction de flavines libres en utilisant le NAD(P)H comme donneur d'électrons. Ainsi, elle est le prototype d'une nouvelle famille d'enzymes qui utilisent les flavines comme substrat et non comme cofacteur. Au cours de ce travail nous nous sommes consacré à l'étude structure-fonction de Fre et à l'identification des modifications structurales nécessaires, entre les flavines réductases et les flavoprotéines, afin d'utiliser alternativement les flavines comme substrat ou cofacteur respectivement.

Afin de caractériser le site de fixation des flavines nous avons réalisé des études cinétiques de Fre à l'aide de flavines modifiées. Nous avons ainsi montré que Fre possède un mécanisme séquentiel ordonné et que seul le noyau isoalloxazine de la flavine, et non pas sa chaîne carbonée, est impliqué dans la reconnaissance des flavines par Fre. Par contre, les groupements OH en 2' et 3' de la chaîne de la riboflavine ont un effet positif sur la constante catalytique de la réaction. De plus, un inhibiteur de Fre s'est révélé être, par voie de conséquence, un inhibiteur de la réactivation de la RNR in vivo.

Des comparaisons de séquences ont révèlé qu'une série de régions, dont un motif de 4 résidus ($R_{46}XFS_{49}$) de Fre, sont conservés entre Fre et les flavoprotéines de la famille des ferrédoxine-$NADP^+$ réductase (FNR). Par mutagénèse dirigée nous avons montré que le mutant S49A ne possède plus que 5 % de l'activité de la protéine sauvage et donc que la Ser 49 est un résidu essentiel pour l'activité. De plus, l'utilisation de la 5-déazariboflavine à permis de montrer qu'il existe une interaction spécifique entre le OH de la Ser 49 de Fre et le N-5 du cycle isoalloxazine de la flavine et ceci comme dans le cas de la FNR. Pour finir, par l'utilisation de la RMN et de substrats marqués isotopiquement nous avons montré que le transfert d'hydrure catalysé par Fre est *pro-R* stéréospécifique vis-à-vis du NAD(P)H et ceci comme les protéines de la famille FNR.

Tous ces résultats étayaient fortement l'hypothèse d'un lien structural et/ou évolutif entre ces deux familles, les flavines réductases de type Fre et les flavoprotéines de la famille FNR. Ultérieurement, la résolution de la structure tridimensionnelle de Fre a permis d'interpréter et de confirmerl'ensemble des résultats biochimiques obtenus durant la thèse. La plus faible affinité envers les flavines s'expliquait par l'absence, chez Fre, d'une boucle impliquée, dans les flavoprotéines, dans un réseau d'interaction avec la chaîne ribitol des flavines.

Publications issues de ce travail de thèse : Articles P2, P3, P4, P6, PO2 et PO3 (voir page 8 et 9 et pages suivantes).

3. Stages pré-doctoral, Université Paris XI-Orsay, 6 mois (année 90-91)

A mon arrivée, le Dr. Michel Lepoivre venait de montrer que l'activité NO Synthase des macrophages inhibait la synthèse d'ADN des cellules cibles par l'inactivation de la ribonucléotide réductase. Or, la NO synthase catalyse la synthèse de citrulline et d'oxyde nitrique (NO·) à partir de la L-Arginine. Pour montrer que le NO· produit était l'inhibiteur direct de la ribonucléotide réductase (RNR) nous avons testé une série de composés, donneurs de NO·, pour leur capacité à inhiber la RNR. Ceci a nécessité la réalisation d'essai ribonucléotide réductase, la purification des désoxyribonucléotides produits par HPLC, et la quantification des produits par comptage de radioactivité. L'ensemble de ce travail à permis de conclure à une implication directe du NO·, et non pas de ses dérivés nitrate et nitrite, dans l'inactivation de la ribonucléotide réductase.

Publications issues de ce travail de thèse : Articles P1, et P1 (voir page 8 et 9 et pages suivantes).

Articles présentés en intégralité

Article P5 : Fieschi et al (1998) ***J.Biol.Chem***
Stage Post Doctoral

Article P2 : Fieschi et al (1995) ***J.Biol.Chem***
Doctorat

Abstracts

Article P7 : Huque et al (2000) ***J.Biol.Chem***
Stage Post Doctoral

Article P6 : Nivière et al (1999) ***J.Biol.Chem***
Doctorat

Article P4 : Nivière et al (1996) ***J.Biol.Chem***
Doctorat

Article P3 : Fieschi et al (1996) ***Eur.J.Biochem***
Doctorat

Article P1 : Lepoivre et al (1991) ***Biochem.Biophys.Res.Comm.***
Stage Pre Doctoral

THE JOURNAL OF BIOLOGICAL CHEMISTRY
Vol. 273, No. 8, Issue of February 20, pp. 4329–4337, 1998

Printed in U.S.A.

The Manganese-containing Ribonucleotide Reductase of *Corynebacterium ammoniagenes* Is a Class Ib Enzyme*

(Received for publication, October 10, 1997)

Franck Fieschi‡§¶, Eduard Torrents§‖, Larisa Toulokhonova‡§‡‡, Albert Jordan‖, Ulf Hellman§§, Jordi Barbe‖, Isidre Gibert‖, Margareta Karlsson‡, Britt-Marie Sjöberg‡¶¶**

From the ‡Department of Molecular Biology, Stockholm University, S-106 91 Stockholm, Sweden, the ‖Department of Genetics & Microbiology, Faculty of Sciences, Autonomous University of Barcelona, Bellaterra, 08193 Barcelona, Spain, and the §§Ludwig Institute for Cancer Research, Biomedical Center, Box 595, S-751 24 Uppsala, Sweden

Ribonucleotide reductases (RNRs) are key enzymes in living cells that provide the precursors of DNA synthesis. The three characterized classes of RNRs differ by their metal cofactor and their stable organic radical. We have purified to near homogeneity the enzymatically active Mn-containing RNR of *Corynebacterium ammoniagenes*, previously claimed to represent a fourth RNR class. N-terminal and internal peptide sequence analyses clearly indicate that the *C. ammoniagenes* RNR is a class Ib enzyme. In parallel, we have cloned a 10-kilobase pair fragment from *C. ammoniagenes* genomic DNA, using primers specific for the known class Ib RNR. The cloned class Ib locus contains the *nrdHIEF* genes typical for class Ib RNR operon. The deduced amino acid sequences of the *nrdE* and *nrdF* genes matched the peptides from the active enzyme, demonstrating that *C. ammoniagenes* RNR is composed of R1E and R2F components typical of class Ib. We also show that the Mn-containing RNR has a specificity for the NrdH-redoxin and a response to allosteric effectors that are typical of class Ib RNRs. Electron paramagnetic resonance and atomic absorption analyses confirm the presence of Mn as a cofactor and show, for the first time, insignificant amounts of iron and cobalt found in the other classes of RNR. Our discovery that *C. ammoniagenes* RNR is a class Ib enzyme and possesses all the highly conserved amino acid side chains that are known to ligate two ferric ions in other class I RNRs evokes new, challenging questions about the control of the metal site specificity in RNR. The cloning of the entire *NrdHIEF* locus of *C. ammoniagenes* will facilitate further studies along these lines.

Ribonucleotide reductases (RNRs)[1] catalyze the reduction of ribonucleotides providing 2′-deoxyribonucleotides for DNA replication and repair. Three well-characterized classes of RNRs, with limited sequence similarities, have been described. They differ in their overall protein structure and cofactor requirement but have in common an allosteric regulation and the use of an organic radical to initiate catalysis through free radical chemistry (1, 2) .

Apart from the similarity in mechanism, the radical chain initiator and the accompanying metal cofactor differ between the three classes. Class I enzymes ($\alpha_2\beta_2$) contain a stable tyrosyl radical and a dinuclear iron center. Class II enzymes (α or α_2) use adenosylcobalamin as cofactor and cleave it to produce a 5′-deoxyadenosyl radical (3, 4). The anaerobic class III enzymes ($\alpha_2\beta_2$) possess a stable glycyl radical and an iron-sulfur cluster (5). Moreover, the different RNRs require their specific physiological reductants thioredoxin, glutaredoxin, and formate, respectively (6–8). At the beginning of the 1990s, only these three classes of RNR were known, and they were found to cover all major branches of the tree of life. However, additional types of RNRs may remain to be discovered, and questions about non-exhaustively characterized atypical RNRs have to be answered.

During the last few years, an additional operon, in practice silent under normal laboratory growth conditions, coding for a new type of RNR, was found in *Salmonella typhimurium* and *Escherichia coli* (9–11). These enzymes share with class I enzymes the subunit composition and distinct sequence similarity, including all highly conserved residues, such as the iron ligands, the tyrosyl radical, and active site cysteines. Thus, the discovery of these enzymes led to the division of the class I RNR in two subclasses, classes Ia and Ib (12). The class Ia reductase is encoded by the *nrdA* and *nrdB* genes, coding for the homodimeric proteins R1 and R2, respectively, and the class Ib reductase is encoded by the *nrdE* and *nrdF* genes, coding for the homodimeric proteins R1E and R2F, respectively. In *E. coli* and *S. typhimurium*, the low expression of the *nrdE* and *nrdF* genes of class Ib cannot support aerobic growth, and these bacteria are totally dependent on class Ia (11). Moreover, the physiological role of these "silent" enzymes is still unknown. However, the *Lactococcus lactis* RNR was found to be a func-

* This work was supported by grants from the Swedish Cancer Society, the Swedish Research Council for Engineering Sciences and the Swedish National Board for Technical Development (to B.-M. S.); from the Spanish DGICYT (PB94-0687) and the CUR de la Generalitat de Catalunya (GRQ93-2049) (to I. G. and J. B.); and from Stiftelsen Lars Hiertas Minne, Magn. Bergvalls stiftelse, and Jeanssonska stiftelserna (to M. K.).

The nucleotide sequence(s) reported in this paper has been submitted to the GenBank™/EBI Data Bank with accession number(s) Y09572.

§ These three authors, listed in alphabetical order, contributed equally to the study.

¶ Supported by the European Molecular Biology Organisation and the Human Frontier Science Project Organisation. Present address: Institut de Biologie Structurale/CEA-CNRS/Université Joseph Fourier, 41 Ave. des Martyrs, F-38027 Grenoble Cedex 1, France.

** Supported by a predoctoral fellowship from Direcci-General d'Universitats de la Generalitat de Catalunya.

‡‡ Supported by the Swedish Institute and the Stockholm University Science Faculty program for East European collaborations. Present address: Dept. of Biochemistry & Biophysics, University of Pennsylvania, 3700 Hamilton Walk, Philadelphia, PA 19104-6089. The costs of publication of this article were defrayed in part by the payment of page charges. This article must therefore be hereby marked "*advertisement*" in accordance with 18 U.S.C. Section 1734 solely to indicate this fact.

¶¶ To whom correspondence should be addressed. Tel.: 46-8-164150; Fax: 46-8-152350; E-mail: Britt-Marie.Sjoberg@molbio.su.se.

[1] The abbreviations used are: RNR, ribonucleotide reductase; DTT, dithiothreitol; EPR, electron paramagnetic resonance; PAGE, polyacrylamide gel electrophoresis; PCR, polymerase chain reaction; bp, base pair(s); kb, kilobase pair(s).

tionally active reductase of the class Ib type (12), and the purified enzyme from *Mycobacterium tuberculosis* also turned out to belong to this class (13, 48). Class Ib genes have also been described in *Bacillus subtilis, Mycoplasma genitalium,* and *M. pneumoniae* (14–16).

The isolation and characterization of a unique manganese-dependent RNR activity in *Corynebacterium* (formerly *Brevibacterium*) *ammoniagenes* was reported in the 1980s (17, 18). The specific Mn requirement of *C. ammoniagenes* was first observed in the 1960s during studies of factors controlling nucleotide overproduction (19, 20). Mn-starved cells showed so-called "unbalanced growth death" because they were arrested in DNA synthesis (17) due to inhibition of DNA precursor synthesis (21). Upon addition of manganese ions to the medium, DNA synthesis and growth were rapidly restored to the level of a nonstarved culture. The main target of Mn starvation was suggested to be RNR activity, which was very low in a Mn-depleted culture but was increased when manganese ions were supplied *in vivo* (17). Similar correlations between RNR activity and Mn-starvation conditions have been demonstrated in other coryneform bacteria, such as *Arthrobacter citreus*, *A. globiformis*, and *A. oxydans*, and in *Micrococcus luteus*, (17, 21, 22).

The partially purified *C. ammoniagenes* RNR was suggested to consist of two subunits (18, 23), a nucleotide-binding component called B1 (in this report renamed R1E) and a metal-containing component called B2 (in this report renamed R2F). The presence of Mn was suggested on the basis of specific ^{54}Mn incorporation into the R2F subunit, as well as appearance of a characteristic Mn six-line EPR spectrum after denaturation of a protein preparation containing R2F. Recently, a novel type of stable organic free radical signal was reported for partially purified *C. ammoniagenes* RNR (24). However, the radical has not been characterized in detail. Generally, a new metal center and a novel organic radical would be enough to define a new class of RNR. However, other properties, such as the sensitivity to hydroxyurea and the polypeptide sizes of this *C. ammoniagenes* RNR, suggest a similarity with the well known class I. An intriguing question is therefore whether the *C. ammoniagenes* RNR is a prototype of a new class of RNR or a subtype of one of the existing classes.

In this study, we report that the Mn-containing RNR of *C. ammoniagenes* is of the class Ib type. We have followed two parallel approaches: identification of class Ib genes in the *C. ammoniagenes* genome by PCR and purification to homogeneity of the active RNR from *C. ammoniagenes*, followed by N-terminal and internal peptide amino acid sequence analysis of the α- and β-polypeptide chains. The amino acid sequences obtained from the enzyme proper matched the cloned and sequenced class Ib genes *nrdE* and *nrdF*. In addition, the sequence of the neighboring genes *nrdH* and *nrdI* is reported.

EXPERIMENTAL PROCEDURES

Materials, Strains, and Plasmids—Wild type *C. ammoniagenes* (ATCC 6872), obtained from the collection of A. N. Bach (Institute of Biochemistry, Russian Academy of Sciences, Moscow, Russia) and *E. coli* DH5αF′ (CLONTECH) strains were used. Plasmid vectors used were pBluescript SK(+) (pBSK, Stratagene) for subcloning and sequencing and pGEM-T (Promega Corp.) for cloning of PCR-generated fragments.

Oligonucleotide primers were from MWG-Biotech (Germany). Restriction endonucleases and other enzymes were from Boehringer Mannheim. [5-^{3}H]CDP was obtained from Amersham Corp. *E. coli* thioredoxin was purified from SK3981 (25). *C. ammoniagenes* NrdH-redoxin was obtained from an overproducing strain carrying a recombinant vector with the *nrdH* gene.[2]

Growth Conditions and General Recombinant DNA Techniques—C. ammoniagenes ATCC 6872 and *E. coli* strains were grown aerobically in LB medium at 30 and 37 °C, respectively. Ampicillin was added at 50 μg/ml when selecting for plasmid-containing clones. Genomic DNA from *C. ammoniagenes* was extracted as described (26) and purified by ultracentrifugation on a cesium chloride gradient. ExoIII deletions were constructed by using the double-stranded nested deletions kit (Pharmacia Biotech Inc.) following the supplier's instructions. DNA sequencing was carried out using the dideoxynucleotide sequencing method with fluorescent universal primers (M13 direct and reverse) and the Automated Laser Fluorescent DNA sequencer (Pharmacia). Other general DNA manipulations and Southern hybridizations were done by standard procedures (27). Sequence analyses were made with the University of Wisconsin Genetics Computer Group package (version 9.0 for UNIX).

PCR Amplification of Partial nrdF Gene—For PCR amplification of the *nrdF* gene of *C. ammoniagenes*, two primers were designed from conserved R2F peptide sequences (GYKYQ and NHDFFS, respectively; indicated in Fig. 3): CoryFup, 5′-GGCTACAAGTACCAG-3′, and CoryFlow, 5′-AACCACGACTTCTTCTC-3′ (antisense). Genomic DNA (0.2 μg) was used as template in a 50-μl PCR amplification reaction with 50 pmol of each primer, all dNTPs (0.2 mM each), 5 μl of 10× PCR buffer (Boehringer Mannheim), and 1.5 units of *Taq* polymerase. The reaction was run with the following program: (*a*) 3 min at 94 °C; (*b*) 30 cycles of 1 min at 94 °C, 1 min at 50 °C, and 1 min at 72 °C; and (*c*) 7 min at 72 °C. The amplification product was purified from an ethidium bromide, 3% Nusieve-agarose gel by melting the band in 6 M NaI at 50 °C and using the Wizard DNA Clean-up system (Promega Corp.), and cloned in pGEM-T according to the manufacturer's protocol. This fragment was labeled with the DIG DNA labeling and detection kit (Boehringer Mannheim).

Construction and Screening of a Chromosomal C. ammoniagenes λ *Phage Library*—The library of *C. ammoniagenes* ATCC 6872 genomic DNA consisted of a mixture of partially digested DNA. Freshly prepared genomic DNA (15 μg) was partially digested with *Sau*3A. Fragments of 6–11 kb were pooled, and restriction-generated ends were filled in with A and G nucleotides by incubation at 37 °C for 30 min with 10 units of Klenow DNA polymerase (Boehringer Mannheim). Lambda GEM-12 vector (Promega) was prepared by filling in *Xho*I-generated ends with T and C nucleotides. After ligation of insert DNA to vector, the library was packaged using Packgene extracts (Promega).

Statistical calculations (28) indicate that about 3900 recombinant phages would cover the entire *C. ammoniagenes* genome with a probability of 99.99% when an insert length of 11 kb and a genome size of 3 Mb (29) are assumed. A library with a titer of 1.8×10^4 plaque-forming units/ml was obtained and screened by phage-DNA hybridization after blotting to Hybond-N nylon membranes (Amersham Corp.) by using the DIG DNA labeling and detection kit from Boehringer Mannheim and following the supplier's recommendations. Phage λ DNA was isolated as described by Sambrook *et al.* (27).

Fermentation and Purification of RNR—C. ammoniagenes ATCC 6872 was inoculated from a slant (1% yeast extract, 1% glucose, 1% $CaCO_3$, 2% agar; Difco) grown at 30 °C for 24 h in 100 ml of inoculate medium (2% glucose, 1% peptone, 1% yeast extract, 0.3% NaCl, 0.05 mg/ml biotin) and cultivated at 30 °C overnight. The overnight culture was used to inoculate several 1-liter batches of minimal fermentation medium (21), and cultivation was continued in 5-liter flasks at 30 °C and 220 rpm. After 10 h of growth, 10 μM $MnCl_2$ was added to the medium, and 1 h after Mn repletion, cells were harvested by centrifugation. The cell paste was washed with Buffer A (85 mM potassium phosphate buffer, pH 7.0, 2 mM DTT), frozen on dry ice, and stored at −80 °C.

Unless otherwise indicated, all purification procedures were carried out at 4 °C. In a typical experiment, 24 g of wet weight frozen cells were disrupted through a X-press (BIOX). The disintegrated cells were homogenized and extracted with 3 volumes (per wet weight cells) of Buffer A by stirring for 45 min and then centrifuged for 30 min to remove cell debris. Nucleic acids were precipitated by dropwise addition of streptomycin sulfate to a final concentration of 1.5%. After stirring for 30 min, the precipitate was removed by centrifugation. The supernatant was dialyzed in SpectraPor membrane tubing (cutoff, molecular weight of 3500; Spectrum Medical Industries, Inc.) against 10 mM potassium phosphate buffer, pH 7.0, 2 mM DTT for 1 h. Precipitated proteins were removed by centrifugation, and the supernatant was further dialyzed against the same buffer overnight. Precipitated proteins (called low salt fraction) were collected by centrifugation, dissolved in a minimal volume (15–25 ml) of Buffer A, and stored at −80 °C for further purification.

Aliquots of the low-salt protein fraction (≤100 mg of protein) were

[2] E. Torrents, unpublished data.

applied on a MemSep column HP1500 (DEAE-cellulose) equilibrated with Buffer A. The separation was performed by ConSep system at a flow rate of 20 ml/min. After a washing step with 200 ml of Buffer A, the elution was continued with 400 ml of 0.15 M NaCl in Buffer A followed by a 0.15–0.4 M NaCl linear gradient in Buffer A in a total volume of 800 ml. Fractions of 10 ml were collected, and RNR activity was eluted between 0.15–0.25 M NaCl. RNR-containing fractions were pooled and concentrated by ultradialysis (Sartorius; cutoff, molecular weight of 12,000) in Buffer A and stored at −80 °C for further purification.

The concentrated enzyme solution was loaded onto a Superdex 200 column (30 × 1.3 cm) previously equilibrated in Buffer A containing 10% glycerol at room temperature. Proteins were eluted with the same buffer at a flow rate of 0.5 ml/min. Active fractions were pooled and concentrated at 4 °C in Centricon 30 (Amicon) and stored at −80 °C.

The concentrated protein was then adsorbed to a 1-ml MonoQ-anion exchange column run at room temperature. After a first washing of the column by 5 ml of Buffer A containing 10% glycerol and 0.28 M NaCl, the proteins were eluted with a linear NaCl gradient at a flow rate of 1 ml/min (25 ml of 0.28–0.7 M NaCl in Buffer A containing 10% glycerol). Fractions (0.5 ml) were collected in tubes immersed in an ice bath, pooled according to the UV absorption profile, concentrated at 4 °C in Centricon 30, and analyzed for protein concentration and reductase activity. The procedure separated two protein components that together are required for enzyme activity. The purified components were stored at −80 °C.

Enzyme Activity Assay—RNR activity was assayed in 50-μl mixtures containing 120 mM potassium phosphate buffer, pH 7.0, 1 mM dATP as a positive effector, 1 mM magnesium acetate, 10 mM DTT, 13 μM *E. coli* thioredoxin, 5–20 μl of the concentrated protein solution. The reaction was started by addition of [^{3}H]CDP (specific activity, 60,000–80,000 cpm/nmol) to a final concentration of 0.5 mM. Assay mixtures were incubated for 20 min at 30 °C and stopped by addition of 0.5 ml of ice-cold 1 M perchloric acid. One unit of enzyme activity corresponds to 1 nmol of dCDP formed per min of incubation (30).

SDS-PAGE and Protein Blotting—To obtain partial peptide amino acid sequences, SDS-PAGE was used. Protein samples (50 μg of total protein) were first denatured in a mixture of 125 mM Tris-HCl, pH 6.8, 2.5% SDS, 10 mM DTT, 15% glycerol, and 0.01% bromphenol blue. After boiling for 2–3 min and cooling to room temperature, the incubation was continued with 20 mM iodoacetamide for another 20 min in darkness at room temperature. Reduced and alkylated protein samples were separated on 7.5% SDS-polyacrylamide gel, stained with 0.1% Coomassie Brilliant Blue R-250 in 50% methanol, and destained in 50% methanol, 10% acetic acid. Protein bands corresponding to the α- and β-polypeptide chains of RNR were excised from the gel and used for subsequent proteolytic digestions.

For N-terminal sequence analysis, protein samples were treated as described above, but the alkylation step was omitted. After separation by SDS-PAGE as above, nonstained protein bands were blotted from the gel onto prewet (100% methanol) polyvinylidene difluoride membranes (Fluorotrans; pore size, 0.22 μM; Pall Filtron) in a blotting buffer containing 23 mM Tris base, 192 mM glycine, 20% methanol. After overnight blotting at 200 mA in a cold room, the proteins were visualized by staining with Coomassie Brilliant Blue R-250 (0.1% in 50% methanol) for 2 min and destaining in several changes of 50% methanol, 10% acetic acid, followed by rinsing with MilliQ water. Membrane pieces were subjected to automated Edman degradation in a Perkin-Elmer-Applied Biosystems Model 494A sequencer, operated according to the manufacturer's instructions.

Proteolytic Digestion and Amino Acid Sequence Analysis—The two excised gel bands containing the alkylated α- and β-polypeptides, respectively, were treated for in-gel digestion to prepare internal peptides for amino acid sequence analysis. Briefly, the gel pieces were washed with Tris-HCl/acetonitrile to remove SDS and the Coomassie dye and to put the gel pieces in the appropriate digestion environment. After complete drying of the gel pieces, a solution containing 0.5 μg of *Achromobacter lyticus* protease Lys-C (Wako Chemicals GmbH, Neuss, Germany) was allowed to absorb into the gel pieces. Rehydration with digestion buffer was continued until the gels were soaked, and incubation was carried out overnight at 30 °C. After acidifying the incubation mixtures, generated peptides were extracted from the gels and isolated by narrow-bore reversed phase liquid chromatography on a μRPC C2/C18 SC 2.1/10 column operated in the SMART System (Pharmacia). A full description is found elsewhere (31). Of the collected peptides, some were selected for automated Edman degradation in a Perkin-Elmer-Applied Biosystems Model 494A sequencer, operated according to the manufacturer's instructions.

Spectroscopic Methods—EPR spectra at 9.36 GHz measured at 77 K were recorded on a Bruker ESP 300 spectrometer using a cold finger Dewar flask for liquid nitrogen. Subtractions were performed using the ESP 300 software. Denaturation was done by adjusting the sample to pH 1 by addition of 1 M nitric acid. Buffer from the flow-through of the centricon concentration step prior to the EPR analysis was used as background control for the native sample. For the denatured sample, the same amount of nitric acid as added to the protein sample was added to the background control sample. Background spectra were recorded under conditions identical to those for the native and denatured protein and thereafter subtracted from the total spectrum to give the spectra presented in Fig. 7.

Atomic absorption measurements were made on a Perkin-Elmer Z3030 graphite furnace. Calibrations for each metal were made by the use of several solutions of known metal concentration in the same buffer as used for the sample.

Other Methods—Protein concentration was determined either by the modified Lowry method (32) or the Bradford method (33) using bovine serum albumin as standard. Analytical protein gel electrophoresis was done by the Phast gel system (Pharmacia) in 7.5% or 10–15% denaturing polyacrylamide gels with Coomassie or silver staining.

RESULTS

PCR Isolation of an Internal Fragment of the C. ammoniagenes nrdF Gene—The deduced amino acid sequences of all known RNR class Ib *nrdF* genes contain some highly conserved regions that allow the design of NrdF-specific oligonucleotides for PCR amplification. Primers CoryFup and CoryFlow (see "Experimental Procedures") were designed from the R2F conserved regions GYKYQ and NHDFFS, respectively, according to the *Corynebacterium* codon usage (34) and used for PCR amplification of selected parts of genomic DNA extracted from *C. ammoniagenes*. A single 297-bp product, which was of the expected size range, was amplified, cloned in pGEM-T plasmid DNA, and sequenced in both directions. The sequence of the amplified and cloned product corresponded to a *nrdF* gene fragment according to its high homology to the *S. typhimurium nrdF* gene (60.7% identity at the nucleotide sequence level). The cloned fragment was used as a probe for screening a genomic *C. ammoniagenes* library.

Cloning of the C. ammoniagenes nrdEF Genes—Our cloning strategy assumed that the *nrdE* and *nrdF* genes would be located in close proximity to each other in the *C. ammoniagenes* genome as in all bacterial *nrdEF* operons studied thus far (9, 11, 12, 14–16). The amplified *nrdF* fragment was used as a hybridization probe for screening a λ phage genomic *C. ammoniagenes* library enriched for 6–11 kb fragments (see "Experimental Procedures"). Several positive phage plaques were purified, and their DNA was extracted and checked by restriction endonuclease analysis and Southern hybridization and found to contain the *nrdF* gene. Several fragments derived from the endonuclease digestion of these λ phage DNA clones were cloned into pBSK(+) and sequenced from both extremes to localize the *nrdE* and *nrdF* genes. A 10 kb *Sac*I fragment from one of these positive plaques was assumed to contain both genes and was subcloned into *Sac*I-digested pBSK(+), resulting in plasmid pUA728.

Southern hybridization was performed to confirm that the cloned *Sac*I fragment originated from *C. ammoniagenes* genomic DNA and was not hybridizing with some other bacterial chromosomes (data not shown). Plasmid pUA728 was then used for DNA sequencing. To obtain the full-length sequence, a combination of fragment subcloning and generation of progressive unidirectional nested deletions for both strands were applied. A sequence of 6054 bp, covering the *nrdHIEF* genes of *C. ammoniagenes* (Fig. 1), has been deposited into the GenBank data base.

Analysis of the nrdHIEF Gene Sequence—Five different open reading frames are present in the nucleotide sequence obtained from plasmid pUA728 (Fig. 1). Four of them correspond to the previously reported genes *nrdH* (228 bp), *nrdI* (435 bp), *nrdE* (2

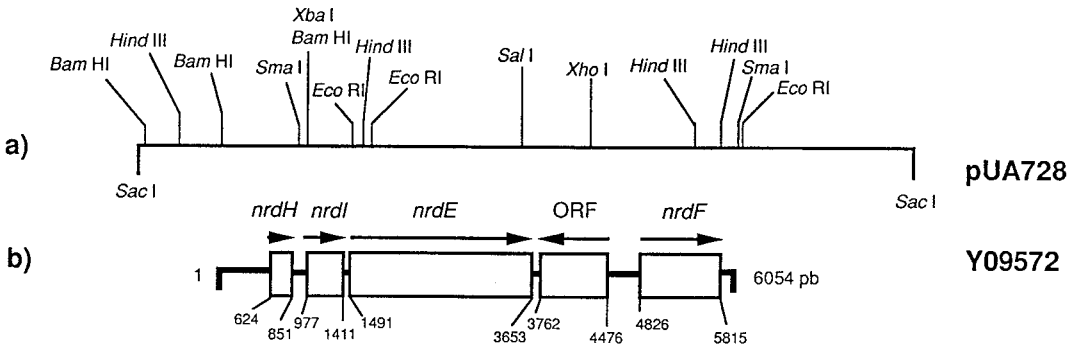

FIG. 1. *a*, restriction map of the *C. ammoniagenes* 10-kb *Sac*I fragment obtained from the λ phage library and used for DNA sequencing. *pAU728* denotes the resulting pBSK(+) derivative. *b*, gene organization of all open reading frames found in the 6054 bp deposited in the GenBank data base under the accession number Y09572.

163 bp), and *nrdF* (990 bp). The fifth putative open reading frame (714 bp), located between *nrdE* and *nrdF*, would be transcribed in the opposite direction to the *nrd* genes. The function of this open reading frame still remains unknown, although comparison with the current data bases shows the highest homologies to several bacterial transcription regulatory proteins of similar size.

The G+C contents of the *nrd* genes (*nrdH*, 53.5%; *nrdI*, 50%; *nrdE*, 51.5%; and *nrdF*, 48.5%), as well as their codon usage, are in accordance with those described for genes of corynebacterial origin (34). The putative translational start codon of genes *nrdE, nrdF*, and *nrdI* is GTG; that of *nrdH* is ATG. Putative RBS sequences complementary to the 3′ end of the 16S rRNA of *B. subtilis* (35) are located 14 nucleotides upstream of *nrdE* (GAAAGG), 13 nucleotides upstream of *nrdF* (AGCAGGG), 14 nucleotides upstream of *nrdH* (AAAGG), and 10 nucleotides upstream of *nrdI* (AAAGGAGG).

When we searched for a hypothetical promoter region, we found a putative TATA box (TATAGT) 111 bp upstream of the *nrdH* gene. Sixteen base pairs upstream of the TATA box, a −35 promoter sequence (TTGCAG) was identified by its resemblance to the consensus promoter sequence from *C. glutamicum* (36). No promoter sequences were identified upstream of the *nrdF* gene. Nevertheless, because there exists a large intergenic region between *nrdE* and *nrdF* (1.2 kb), more evidence is needed to confirm that the *nrdHIEF* genes form an operon with a unique polycistronic mRNA, as occurs in the previously characterized *nrdHIEF* operons of Enterobacteriaceae (11) and *nrdIEF* from *B. subtilis* (14). In addition, no putative transcriptional terminator could be clearly identified, although two weak stem loops with ΔG (25 °C) of −10.2 and −12.5 kcal/mol can be found downstream from the *nrdE* and *nrdF* genes.

The hypothetical product encoded by the *nrdH* gene (75 residues, 8.3 kDa) corresponds to the previously described NrdH-redoxin from *E. coli* (37). The NrdH product has been found to be a specific electron donor for the class Ib enzyme of *S. typhimurium* and *L. lactis* (12, 37). The deduced NrdI product comprises 144 amino acid residues and has a predicted molecular mass of 15.8 kDa. The *nrdI* gene is conserved in all known *nrdEF* operons (Fig. 2), but its function remains to be clarified. A preliminary study has shown its stimulatory effect on the activity of the *S. typhimurium* NrdEF system (37) .

The deduced amino acid sequences of *C. ammoniagenes nrdE* and *nrdF* strongly resemble previously sequenced class Ib proteins. The percentages of identical amino acids are 70% for the *C. ammoniagenes* and *E. coli* R1E proteins and 66% for the R2F proteins (compare Figs. 2 and 3). Nevertheless, when comparing all known R1E and R2F sequences, the *C. ammoniagenes* proteins are more closely related to the *M. tuberculosis* proteins (13, 48) than to any other known class Ib proteins (Fig. 2). Also, the predicted molecular masses of both proteins, 81.2 kDa for R1E (720 residues) and 37.9 kDa for R2F (329 residues), are in agreement with other known class Ib proteins. As expected for class Ib proteins, only limited similarities exist between the *C. ammoniagenes* RNR proteins and the class Ia enzymes; the percentages of similarity to the *E. coli* R1 and R2 proteins are 35 and 37%, respectively. The corresponding similarities for class Ia and Ib proteins within one species are on the same order (38). Interestingly, all residues that are functionally important in the class I proteins are also present in the deduced *C. ammoniagenes* RNR proteins. Among others, in the R1E protein, there are five cysteine residues known to be involved in catalysis and enzyme turnover in *E. coli* R1, and in the R2F protein, there is the potential radical harboring residue Tyr-115, as well as residues forming a hydrophobic pocket around the tyrosyl radical in *E. coli* R2 (Fig. 3). In addition, all residues postulated to participate in radical transfer between R1 and R2 during catalysis are preserved in the deduced *C. ammoniagenes* R1E and R2F proteins. Most striking is that all six residues that act as ligands for the μ-oxo-bridged diiron site in the *E. coli* R2 protein also occur in equivalent positions in the deduced *C. ammoniagenes* R2F sequence (Fig. 3).

Purification of Active RNR from C. ammoniagenes—To correlate our genetic results with previously published biochemical observations, we essentially followed the published strategy (18) for cell growth and the first steps of enzyme purification. Cells grown in Mn-deficient medium lost their colony-forming ability after about 10 h of fermentation, but addition of 10 μM $MnCl_2$ at that time fully preserved the viability of the cells. The cells were harvested 1 h after manganese repletion and used as a starting material for purification of enzymatically active RNR.

Purification of the holoenzyme (described in detail under "Experimental Procedures") involved three major steps: precipitation by dialysis of cell-free extract against low salt buffer, chromatography on a weak anion exchanger, and size fractionation by Superdex 200 gel filtration. At this stage, the specific enzyme activity was 6.5 units/mg, and the overall yield was 35% (Table I). Separation of the R1E and R2F components was achieved by fast protein liquid chromatography anionic chromatography (Fig. 4), resulting in preparations of 70 and >90% purity, respectively (Fig. 5). Mixing of the two components resulted in a specific activity of 34 units/mg. In general, the specific activities obtained by us in the different purification steps are approximately an order of magnitude higher than those reported earlier (18) .

The RNR activity eluted from the gel filtration column at a volume corresponding to an apparent molecular mass of 160 kDa, according to a calibration of the column with gel filtration standard protein. Considering the theoretical molecular mass

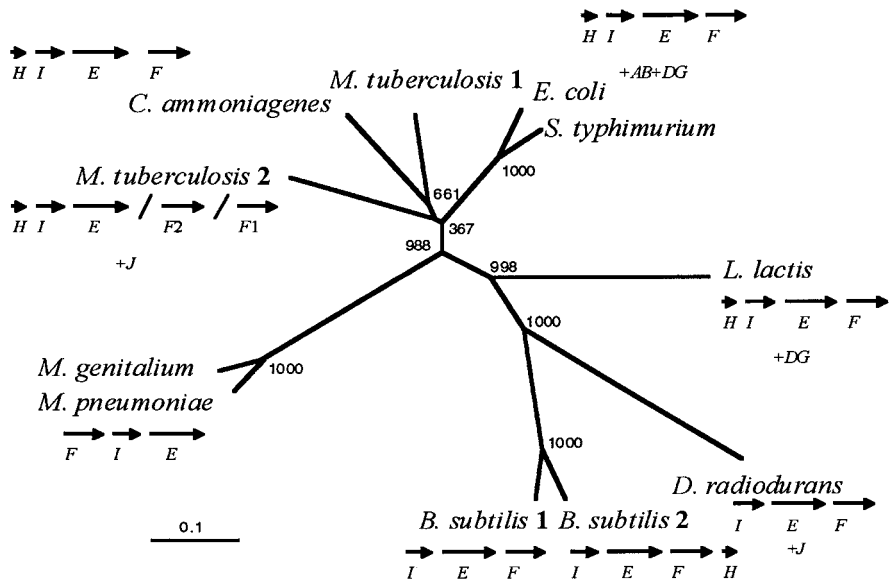

FIG. 2. **Phylogenetic tree of all available NrdF proteins.** The following protein sequences from the Swiss-Prot data base were used: RIR4_ECOLI (*E. coli*), RIR4_SALTY (*S. typhimurium),* RIR2_BACSU (*B. subtilis*), RIR2_MYCGE (*M. genitalium*), RIR2_MYCPN (*M. pneumoniae*), and RIR2_MYCTU (*M. tuberculosis 1*). NrdF2 sequence from *B. subtilis* was from Ref. 49 and NrdF sequences from *L. lactis*, *M. tuberculosis* 2, and *D. radiodurans* were from G. Buist (personal communication), H. Rubin (48), and The Institute for Genomic Research (personal communication), respectively. The CLUSTAL W (version 1.7) program (46) was used for sequence alignment. The tree was generated with 1000 bootstrap trials; the bootstrap values are indicated at the nodes. For each species, a schematic representation of the gene organization in the *nrdEF* locus, including the *nrdH* and *nrdI* genes, is shown, and when known, the presence of *nrdAB*, *nrdJ*, or *nrdDG*, encoding class Ia, class II, or class III RNRs, respectively, is shown.

```
                                                                        60
NrdF E.c. ------------------MKLSRISAINWNKISDDKDLEVWNRLTSNFWLPEKVPLSNDIP
NrdF S.t. ------------------MKLSRISAINWNKIQDDKDLEVWNRLTSNFWLPEKVPLSNDIP
NrdF C.a. --------SNEYDEYIANHTDPVKAINWNVIPDEKDLEVWDRLTGNFWLPEKIPVSNDIQ
NrdB E.c. AYTTFSQTKNDQLKEPMFFGQPVNVARYDQQKYDIFEKLIEKQLSFFWRPEEVDVSRDRI
                                . :.. .::    :   :: ::  . ** **:: :*.*
                                                                       120
NrdF E.c. AWQTLTVVEQQLTMRVFTGLTLLDTLQNVIGAPSLMPDALTPHEEAVLSNISFMDAVHAR
NrdF S.t. AWQTLSAAEQQLTIRVFTGLTLLDTIQNIAGAPSLMADAITPHEEAVLSNISFMDAVHAR
NrdF C.a. SWNKMTPQEQLATMRVFTGLTLLDTIQGTVGAISLLPDAETMHEEAVYTNIAFMESVHAK
NrdB E.c. DYQALPEHEKHIFISNLKYQTLLDSIQGRSPNVALLPLISIPELETWVETWAFSETIHSR
           :: :.  *:   :  :.  ****::*.     :*:.     . *:   . :* *::*::
                                                                       180
NrdF E.c. SYSSIFSTLCQTKDVDAAYAWSEENAPLQRKAQIIQQHYR------------GD------
NrdF S.t. SYSSIFSTLCQTKEVDAAYAWSEENPPLQRKAQIILAHYV------------SD------
NrdF C.a. SYSNIFMTLASTPQINEAFRWSEENENLQRKAKIIMSYYN------------GD------
NrdB E.c. SYTHIIRNIVNDPSV--VFDDIVTNEQIQKRAEGISSYYDELIEMTSYWHLLGEGTHTVN
          **: *: .: .  .:  .:     *  :*::*: *  :*             .:
                                                                       240
NrdF E.c. --------DPLKKKI-----ASVFLESFLFYSGFWLPMYFSSRGKLTNTADLIRLIIRDE
NrdF S.t. --------EPLKKKI-----ASVFLESFLFYSGFWLPMYFSSRGKLTNTADLIRLIIRDE
NrdF C.a. --------DPLKKKV-----ASTLLESFLFYSGFYLPMYLSSRAKLTNTADIIRLIIRDE
NrdB E.c. GKTVTVSLRELKKKLYLCLMSVNALEAIRFYVSFACSFAFAERELMEGNAKIIRLIARDE
                  ****:     :   **:: ** .*  .: ::.*  : ..*.:**** ***
                                                                       300
NrdF E.c. AVHGYYIGYKY---QKNMEKISLGQ-REELKSFAFDLLLELYDNELQYTDELYAE---TP
NrdF S.t. AVHGYYIGYKY---QIALQKLSAIE-REELKLFALDLLMELYDNEIRYTEALYAE---TG
NrdF C.a. SVHGYYIGYKY---QQGVKKLSEAE-QEEYKAYTFDLMYDLYENEIEYTEDIYDD---LG
NrdB E.c. ALSLTGTQHMLNLLRSGADDPEMAEIAEECKQECYDLFVQAAQQEKDWADYLFRDGSMIG
          ::*     :     :   .. .  :  ** *    **: :  ::*  ::: :: :
                                                                       358
NrdF E.c. WADDVK-AFLCYNANKALMNLGYEPLFPAEMAEVNPAILAALSPNADENHDFFSGSGSSY
NrdF S.t. WVNDVK-AFLCYNANKALMNLGYEALFPPEMADVNPAILAALSPNADENHDFFSGSGSSY
NrdF C.a. WTEDVK-RFLRYNANKALNNLGYEGLFPTDETKVSPAILSSLSPNADENHDFFSGSGSSY
NrdB E.c. LNKDILCQYVEYITNIRMQAVGLDLPFQTRSNPIPWINTWLVSDNVQVAPQEVEVS--SY
            .*:   :: * :*  :  :* :  * .    :       :* *.:   : .. *  **
                                 377
NrdF E c. VMGKAVETEDED--WNF--
NrdF S.t. VMGKTVETEDED--WNF--
NrdF C.a. VIGKAEDTTDDD--WDF--
NrdB E.c. LVGQIDSEVDTDDLSNFQL
          ::*:  .  * *   :*
```

FIG. 3. **Sequence alignment of the R2F from *C. ammoniagenes* with some other class Ib R2F (NrdF) proteins and class Ia R2 (NrdB) from *E. coli*.** Comparison of the predicted amino acid sequence of the *C. ammoniagenes* (*C.a*) NrdF product with the NrdF sequences from *E. coli* (*E.c.*; Swiss-Prot: RIR4_ECOLI), and *S. typhimurium* (*S.t.*; Swiss-Prot: RIR4_SALTY) and NrdB from *E. coli*. (*E. c.*; Swiss-Prot: RIR2_ECOLI). The numbering refers to the *E. coli* NrdB sequence. *Asterisks* (*) mark identical amino acid residues in all four proteins; *colons* (:) mark high similarity residues; and *periods* (.) mark low similarity residues. The alignment was made using multiple sequence alignment program CLUSTAL W (version 1.7) (46). *Underlined* residues correspond to the peptides identified in the peptide sequence analyses (Table II). Peptides used for the design of NrdF-specific PCR primers (see "Experimental Procedures") and present in all three NrdF sequences are *boxed*. Conserved residues corresponding to the iron ligands and tyrosyl radical in *E. coli* R2 protein (47) are shown with *black* background.

of NrdE and NrdF polypeptides as deduced from nucleotide sequence analyses, this would fit with an $\alpha\beta_2$ subunit composition for the *C. ammoniagenes* RNR. A previous study also reported an $\alpha\beta_2$ composition according to gel filtration and sucrose gradient centrifugation experiments (18). Such a quaternary structure is, however, in contrast to the $\alpha_2\beta_2$ composition of other class Ib RNRs (39) and is not very likely to be the true *in vivo* composition. A lower than expected molecular mass may be explained by a high dissociation constant, low protein concentration, and/or the absence of positive allosteric effector nucleotides. Further characterization of this particular point has to await the overexpression of cloned material.

Identification of the Active RNR as a Class Ib Enzyme by Amino Acid Sequence Analyses—The enzyme preparation after DEAE-cellulose chromatography contained several protein bands when analyzed by SDS-PAGE, but after Superdex 200 chromatography, the two most prominent bands were of the expected sizes for RNR α- and β-polypeptides (Fig. 5). Material from the 80- and 40-kDa bands was subjected to partial amino acid sequence analyses using the techniques described under "Experimental Procedures." N-terminal sequences, as well as partial internal peptide sequences, were obtained for both subunits (Table II). The peptides were analyzed by comparison to the deduced NrdE (deposited in GenBank) and NrdF (Fig. 3) sequences of *C. ammoniagenes* and found to match perfectly in all positions of the internal peptides. The N-terminal peptides obtained from the blotted α- and β-polypeptide bands were also in accordance with the gene sequences. The N-terminal se-

TABLE I
Purification of RNR from C. ammoniagenes ATCC 6872

The table summarizes the averaged purification result from three different purifications using the procedure described under "Experimental Procedures," starting with 8 liters of culture (approximately 30 g of wet cells).

Fraction	Protein	Total activity	Specific activity	Recovery	Purification factor
	mg	*units*[a]	*units · mg*$^{-1}$	*%*	
Cell-free extract	983	24	0.024	100	1
Low-salt precipitate	132	35	0.26	146[b]	11
DEAE-cellulose	5.1	16	3	67	125
Superdex 200	1.3	8.5	6.5	35	271
MonoQ[c]	0.045	1.5	34[d]	6	1417

[a] 1 unit is defined as 1 nmol of CDP reduced per min.
[b] Increase was probably due to the removal of inhibitory compounds from the cell extract.
[c] Data reported on this line concern only the R2F purified fraction, not a holoenzyme complex.
[d] Activity was measured by complementation with the R1E fraction, but the specific activity was calculated considering only R2F protein concentration.

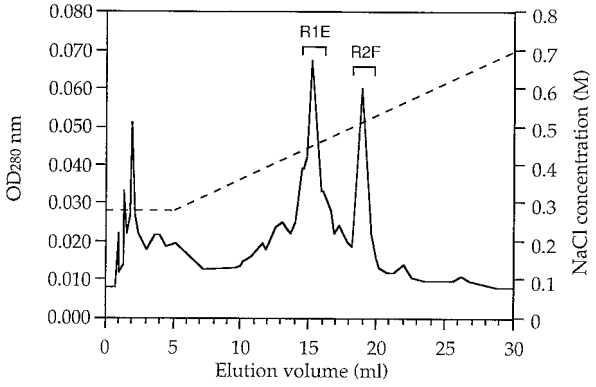

FIG. 4. **Separation of the R1E and R2F by weak anion exchange chromatography.** The RNR protein fraction after Superdex 200 gel filtration step was chromatographed on a MonoQ column (see "Experimental Procedures"). *Solid line*, absorbance at 280 nm; *dashed line*, NaCl gradient. No enzyme activity was found in isolated fractions, but it was obtained by combining the two pools containing R1E and R2F (Table II), as demonstrated by SDS-PAGE analysis (Fig. 5).

quencing results indicate that the initiator methionines have been processed during protein maturation, confirming that both genes, as suggested from the nucleotide sequence results, start with a GTG initiator codon that is read as methionine instead of valine.

Preliminary Characterization of C. ammoniagenes RNR—The nucleoside triphosphates ATP, dTTP, and dATP were found to be positive allosteric effectors for CDP reduction. At low concentrations of effector, dATP was more effective than ATP (Fig. 6*a*). Optimal activity with dATP was obtained at nucleotide concentrations as low as 0.02 mM, and no significant inhibition was seen even with 1 mM dATP. When ATP was used, a concentration of at least 0.12 mM was needed for optimal activity (Fig. 6*a*). This type of allosteric regulation is typical of class Ib enzymes and differs from that of class Ia enzymes (10, 12) .

During the entire purification procedure of *C. ammoniagenes* RNR, high levels of both DTT and *E. coli* thioredoxin were included as potential reductants, because we were not able to detect any species-specific "redoxin"-like activity in the supernatant fraction after the low-salt precipitation. With the *C. ammoniagenes* RNR obtained after the gel filtration step, we

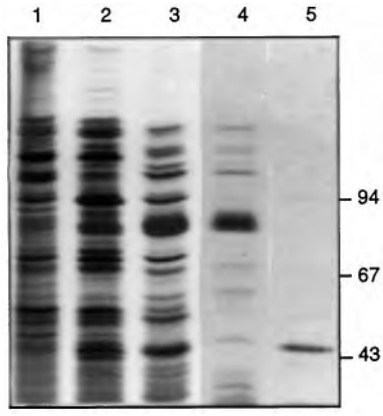

FIG. 5. **SDS-PAGE after each step of purification of *C. ammoniagenes* ribonucleotide reductase (see "Experimental Procedures").** *Lane 1*, low salt precipitate: *lane 2*, after DEAE-cellulose chromatography; *lane 3*, after Superdex 200 gel filtration; *lane 4*, R1E pool after MonoQ chromatography; *lane 5*, R2F pool after MonoQ chromatography. The electrophoretic mobilities of low molecular weight markers (Pharmacia) have been indicated.

then characterized the reductant requirement (Fig. 6*b*). Homogeneous *C. ammoniagenes* NrdH-redoxin obtained from an overproducing strain[2] was an effective reductant even at a low DTT concentration, whereas *E. coli* thioredoxin did not have any significant effect. The distinct requirement of NrdH-redoxin further supports the idea that RNR from *C. ammoniagenes* behaves as a typical class Ib enzyme.

The enzyme activity was sensitive to hydroxyurea in a concentration-dependent manner (Fig. 6*c*). This behavior is typical of class I RNRs, in which the stable tyrosyl radical essential for activity is sensitive to radical scavenging. The degree of sensitivity observed for *C. ammoniagenes* RNR is comparable to that observed earlier for *E. coli* class Ia RNR (40) .

The Purified C. ammoniagenes R2F Protein Contains Bound Manganese Ions—EPR analysis of the active R2F component obtained after the MonoQ purification step showed no signal corresponding to an organic free radical or a metal center (Fig. 7*a* and data not shown). However, upon denaturation of R2F by nitric acid, a 6-line EPR spectrum typical of Mn^{2+} in solution ($S = 5/2$) was observed. This shows that the native R2F protein contained EPR-silent Mn bound to the polypeptide chain. Preliminary atomic absorption spectroscopic analysis of the nitric acid-denatured R2F protein showed that it contained approximately 0.5 mol of manganese ions/mol of R2F polypeptide (Table III). In contrast, the content of iron in the R2F preparation was close to that of the buffer control, and essentially no cobalt was found, confirming that we have purified the previously described Mn-containing RNR of *C. ammoniagenes*.

DISCUSSION

To date, three different classes of RNR have been described in detail. Suggestions had been put forward as to the existence of a fourth, manganese-dependent class, based on the presence of metal ion and the radical signal in *C. ammoniagenes* RNR (18, 24). This enzyme was, however, shown to have certain features (*e.g.* hydroxyurea sensitivity and polypeptide sizes) in common with the well characterized class I RNR of eukaryotes and bacteria (18, 23). Our purpose was to establish whether the manganese-dependent RNR really is a new class that could be fitted into the evolutionary pattern described by the other three classes. We therefore purified the active RNR of *C. ammoniagenes* to obtain partial amino acid sequence results of its components and to clone the genes for this enzyme. We also wanted to establish whether *C. ammoniagenes* has the widespread (in bacteria) class Ib RNR.

TABLE II
Peptide sequences of C. ammoniagenes R1E and R2F

Source	Origin	Sequence[a,b]
R1E	N terminus	^{1}*X*(T)Qg(Q)LGKTVAEPVKN^{14}
R1E	Internal peptide 1	^{35}KIQFDK^{40}
R1E	Internal peptide 2	^{226}KHIENQSSGI^{235}
R2F	N terminus	^{1}*X*(S)NEYDEYIANHTDPVKAIN*X*(W)NVIPDEKDL^{29}
R2F	Internal peptide 2	^{44}KIPVSNDIQSWNK^{56}
R2F	Internal peptide 3	^{56}KMTPQEQLATMRV^{68}
R2F	Internal peptide 4	^{112}KSYSNIF^{118}

[a] *X* denotes unidentified residue with corresponding residue deduced from nucleotide sequencing in parenthesis; lowercase indicates differences from nucleotide sequencing results with corresponding residue deduced from nucleotide sequencing in parenthesis; superscript numbers refer to numbering of protein products as deduced from nucleotide sequencing of the corresponding genes (see GenBank accession no. Y09572 for R1E sequences and Fig. 3 for R2F sequences).

[b] The Lys in front of all internal peptides was not obtained from the sequencing results but was introduced based on the known specificity of Lys-C protease. The correctness of this assumption is evident from a comparison with the corresponding gene sequence.

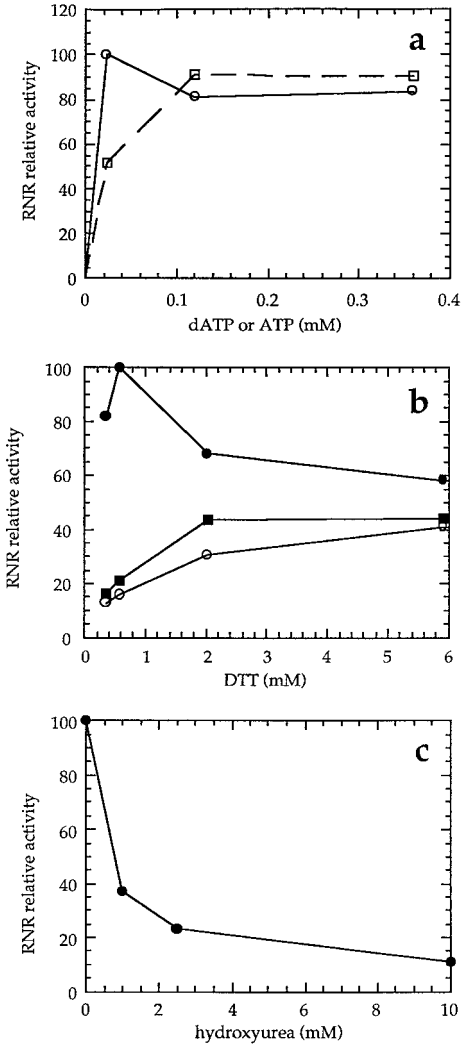

FIG. 6. *a*, effect of ATP and dATP on CDP reduction. Incubations were as described under "Experimental Procedures," except that 1 mM dATP was replaced with the indicated concentrations of either ATP (□) or dATP (○). *b*, effect of DTT and redoxin on CDP reduction. Incubations were as described under "Experimental Procedures" except for the concentration of DTT, which is shown on the *abscissa*; ○, without redoxin; ■, with 13 μM Trx; ●, with 13 μM NrdH-redoxin. *c*, hydroxyurea-dependent inhibition of CDP reduction. Aliquots of *C. ammoniagenes* RNR were incubated for 30 min at 4 °C with the indicated concentration of hydroxyurea, diluted into the assay mixture, and incubated as described under "Experimental Procedures." 100% activity corresponds to 4 (*a*), 110 (*b*), or 27 (*c*) milliunits.

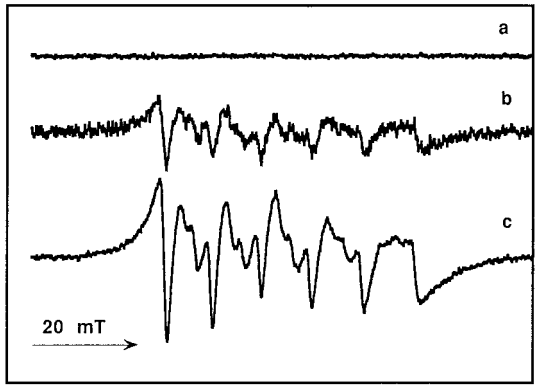

FIG. 7. **X-band EPR spectra at 77K of native (1 scan) (*a*) and denatured (16 scans) (*b*) R2F from *C. ammoniagenes*, compared with a standard of 30 μM $MnCl_2$ (6 scans) (*c*).** The R2F protein sample and the $MnCl_2$ standard were in 85 mM potassium phosphate buffer containing 10% glycerol. Spectra *a* and *b* were obtained after subtraction of background (see "Experimental Procedures"). Recording conditions were as follows: microwave frequency, 9.36 GHz; modulation amplitude, 0.5 millitesla; sweep width, 100 millitesla; time constant, 82 ms; sweep time, 167 s; microwave power, 1 mW.

TABLE III
Atomic absorption metal ion analysis of nitric acid-denatured R2F purified from C. ammoniagenes

Metal ion	Metal:R2F stoichiometry[a]
	mol/mol
Manganese	0.45
Iron	0.08
Cobalt	0

[a] Calculated with a known R2F concentration of 12 μM in the sample and the corresponding metal molecular weight. Numbers given are expressed as number of metal ions per R2F polypeptide chain.

In this report, we show that the active Mn-containing RNR of *C. ammoniagenes* is of the class Ib type and that the *nrd* genomic region contains the same open reading frames as previously seen for the class Ib operon in enterobacteria and *L. lactis* (11, 12). These are the two genes for R1E and R2F, as well as the gene for a thioredoxin-like protein called NrdH-redoxin and a fourth open reading frame of unknown function called *nrdI*. The *nrdH* gene is not present in all *nrdEF* clusters; it is absent in *B. subtilis* and in *Mycoplasma* species (14–16). As in other class Ib systems, we found that the species-specific NrdH-redoxin was the preferred reductant for the *C. ammoniagenes* RNR. The *nrdI* gene is present in all known *nrdEF* loci, and preliminary studies with the *S. typhimurium* system have shown that the NrdI protein stimulates the NrdEF-dependent CDP reduction in the presence of NrdH-redoxin (37). As shown in Fig. 2, the gene organization of the *nrd* locus of *C. ammoniagenes* is homologous to the ones present in enterobacteria, *L. lactis, B. subtilis*, and *Deinococcus radiodurans* and to *M. tuberculosis* (in which the two *nrdF* genes are less closely linked to the rest of the operon). A different organization is found in

Mycoplasma species, in which the *nrdF* gene is located upstream from the *nrdI* and *nrdE* genes.

The deduced NrdEF proteins from *C. ammoniagenes* are currently most closely related to the R1E and the active R2F protein of *M. tuberculosis.* Both species belong to the phylogenetic group of Gram-positive eubacteria with a high G+C content. It was recently reported that *M. tuberculosis* contains a second *nrdF* gene, which is inactive (48). We have not been able to find a second *C. ammoniagenes nrdF* gene by PCR amplification or Southern blotting. The identification of the active RNR from *C. ammoniagenes* as belonging to class Ib helps to replace the initial idea, based on the enterobacterial loci, that *nrdEF* genes are generally silent. As exemplified in the phylogenetic tree of R2F proteins (Fig. 2), class Ib enzymes are widely spread among eubacteria, and the completely sequenced genomes of *B. subtilis*, *Mycoplasma genitalium*, and *M. pneumoniae* code only for class Ib RNRs (15, 16, 49).

The specific activity of the Mn-containing RNR of *C. ammoniagenes* obtained by us, even if improved at least an order of magnitude compared with previous studies (18, 23), is only 12 and 18% of the specific activities described for class Ib RNR from *S. typhimurium* and *L. lactis*, respectively (10, 12). There are some obvious reasons for the low enzyme activity obtained by us. First, our preliminary studies indicate that inclusion of species-specific NrdH-redoxin will increase the *C. ammoniagenes* RNR activity at least 2-fold. Second, the substoichiometric amount of metal ion per R2F polypeptide observed after the four-step purification procedure may lead to substoichiometric levels of organic free radical.

Atomic absorption analysis of the isolated *C. ammoniagenes* R2F protein showed about 0.5 mol/mol Mn/R2F polypeptide chain. Because of the homology with the well known diiron-RNRs, 2 metal ions per R2F was expected. The EPR analysis suggests that the manganese ions may be magnetically coupled, but the substoichiometric amount of metal ion does not allow a definitive conclusion about the structure of the metal center at this point. However, our EPR and atomic absorption analyses clearly confirm earlier published observations (18) that the active *C. ammoniagenes* RNR contains manganese, and as we show here, in essence, it lacks iron. The strong amino acid sequence homology between active Mn-containing RNR from *C. ammoniagenes* and class Ib RNRs is thus in many respects remarkable: (*a*) all previously described class I enzymes are diiron proteins, including the class Ib enzyme from *S. typhimurium* (10); (*b*) all iron binding residues in the Fe-RNRs (class Ia and Ib) are conserved in the *C. ammoniagenes* RNR (Fig. 3); and (*c*) even though both *E. coli* class Ia R2 and mouse R2 can bind manganese at their metal centers, Mn substitutions have invariably led to nonactive enzymes (41, 42).

Our results bring a series of new fascinating questions to the field of RNR research, in particular concerning metal specificity and diversity despite high sequence similarities. The metal ion content of the class Ib enzymes has currently only been investigated for the recombinant *S. typhimurium* (10) and native *C. ammoniagenes* enzymes. Even though the *S. typhimurium* R2F has a diiron center, it is not known whether it can also work with manganese. Likewise, it is not yet known whether the *C. ammoniagenes* enzyme will work with iron. A clear definition of the metal ion dependence of the *C. ammoniagenes* RNR will have to await the design of an overproducing system. In addition, manganese activation experiments should be performed with other class Ib enzymes. Interestingly, the R2F sequences in the two *Mycoplasma* species both lack 3 of the metal ligating residues conserved in the rest of the class I enzymes. However, because it is not known which metal ions are present in other class Ib reductases, neither the deduced *C. ammoniagenes* NrdF amino acid sequence nor the phylogenetic tree can yet be used for predictions about metal ion specificity. Specific three-dimensional features in the vicinity of the metal site may have to be identified to explain a Mn dependence.

Some other enzymatic systems are known to use, alternatively, iron or manganese and have similar or identical metal binding residues (43). In the superoxide dismutase family, the enzyme from *Propionibacterium shermanii* is functional with either Fe or Mn, *i.e.* cambialistic, whereas other superoxide dismutases are strictly manganese- or iron-dependent. Comparisons of their three-dimensional structures revealed that the metal ligands are the same in all three types and that differences are localized to the second coordination sphere of the metal center (44). A similar phenomenon seems to occur among extradiol-cleaving catechol dioxygenases. All members of this family are iron enzymes except the 3,4-dihydroxyphenylacetate 2,3-dioxygenase from *Arthrobacter globiformis*, which contains manganese instead of iron (45). Comparison using the structure of one iron enzyme, sequence alignment, and site-directed mutagenesis of the 3,4-dihydroxyphenylacetate 2,3-dioxygenase suggests that differences can be seen only in the second coordination sphere and that all direct ligands of the two metal ions are the same. These observations suggest a major role for the residues of the second coordination sphere in determining the metal specificity. The hypothesis may also apply to the metal specificity in RNR, because the well known diiron-binding site of *E. coli* class Ia R2 is intrinsically capable of binding manganese, albeit without activating the protein (41). Perturbations of the second coordination sphere might modify the redox properties of such a Mn center and lead to an active enzyme. One striking difference between prokaryotic class Ia and Ib R2 proteins is the substitution of Gln-43 and Ser-114, which form hydrogen bonds to the iron ligand His-241 in *E. coli* R2, for hydrophobic counterparts in the class Ib NrdF sequences. However, a preliminary modeled structure of the *C. ammoniagenes* R2F protein, based on the *E. coli* R2 structure, highlights only differences between class Ia and class Ib but none that are specific to the *C. ammoniagenes* RNR and absent from the other NrdF sequences.[3]

The characterization of the *C. ammoniagenes* RNR as a class Ib enzyme evokes new, challenging questions. The cloning of the *NrdHIEF* locus will facilitate future studies on this RNR, whereby new insights in the design and fine-tuning of metal-active sites may be gained.

Note Added in Proof—Preliminary experiments indicate that binding of manganese ions to *S. typhimurium* apo R2F protein results in enzymatically inactive protein (P. Reichard, personal communication) and that cloned and overproduced *C. ammoniagenes* R2F can bind either manganese or ferrous ions and generate a characteristic tyrosine radical EPR signal.

Acknowledgments—We are grateful to Margareta Sahlin for help with the EPR analyses and evaluations and for constructive discussions and to Agneta Slaby for help with purification of *E. coli* thioredoxin. We thank the Institute for Genomic Research for availability of sequence data prior to publication.

REFERENCES

1. Sjöberg, B.-M. (1997) *Struct. Bond.* **88,** 139–173
2. Reichard, P. (1997) *Trends Biochem. Sci.* **22,** 81–85
3. Booker, S., and Stubbe, J. (1993) *Proc. Natl. Acad. Sci. U. S. A.* **90,** 8352–8356
4. Booker, S., Licht, S., Broderick, J., and Stubbe, J. (1994) *Biochemistry* **33,** 12676–12685
5. Sun, X. Y., Ollagnier, S., Schmidt, P. P., Atta, M., Mulliez, E., Lepape, L., Eliasson, R., Gräslund, A., Fontecave, M., Reichard, P., and Sjöberg, B.-M. (1996) *J. Biol. Chem.* **271,** 6827–6831
6. Holmgren, A., and Björnstedt, M. (1995) in *Biothiols, Part B* (Packer, L., ed) Vol. 252, pp. 199–208, Academic Press Inc., San Diego, CA
7. Holmgren, A., and Åslund, F. (1995) in *Biothiols, Part B* (Packer, L., ed) Vol.

[3] J. Nilsson, personal communication.

252, pp. 283–292, Academic Press Inc., San Diego, CA
8. Mulliez, E., Ollagnier, S., Fontecave, M., Eliasson, R., and Reichard, P. (1995) *Proc. Natl. Acad. Sci. U. S. A.* **92,** 8759–8762
9. Jordan, A., Gibert, I., and Barbé, J. (1994) *J. Bacteriol.* **176,** 3420–3427
10. Jordan, A., Pontis, E., Atta, M., Krook, M., Gibert, I., Barbé, J., and Reichard, P. (1994) *Proc. Natl. Acad. Sci. U. S. A.* **91,** 12892–12896
11. Jordan, A., Aragall, E., Gibert, I., and Barbé, J. (1996) *Mol. Microbiol.* **19,** 777–790
12. Jordan, A., Pontis, E., Åslund, F., Hellman, U., Gibert, I., and Reichard, P. (1996) *J. Biol. Chem.* **271,** 8779–8785
13. Yang, F. D., Lu, G. Z., and Rubin, H. (1994) *J. Bacteriol.* **176,** 6738–6743
14. Scotti, C., Valbuzzi, A., Perego, M., Galizzi, A., and Albertini, A. M. (1996) *Microbiology* **142,** 2995–3004
15. Fraser, C. M., Gocayne, J. D., White, O., Adams, M. D., Clayton, R. A., Fleischmann, R. D., Bult, C. J., Kerlavage, A. R., Sutton, G., Kelley, J. M., Fritchman, J. L., Weidman, J. F., Small, K. V., Sandusky, M., Fuhrmann, J., Nguyen, D., Utterback, T. R., Saudek, D. M., Phillips, C. A., Merrick, J. M., Tomb, J. F., Dougherty, B. A., Bott, K. F., Hu, P. C., Lucier, T. S., Peterson, S. N., Smith, H. O., Hutchison, C. A., and Venter, J. C. (1995) *Science* **270,** 397–403
16. Himmelreich, R., Hilbert, H., Plagens, H., Pirkl, E., Li, B. C., and Herrmann, R. (1996) *Nucl. Acids Res.* **24,** 4420–4449
17. Schimpff-Weiland, G., Follmann, H., and Auling, G. (1981) *Biochem. Biophys. Res. Commun.* **102,** 1276–1282
18. Willing, A., Follmann, H., and Auling, G. (1988) *Eur. J. Biochem.* **170,** 603–611
19. Oka, T., Udagawa, K., and Kinoshita, S. (1968) *J. Bacteriol.* **96,** 1760–1767
20. Furuya, A. (1976) in *Microbial Production of Nucleic Acid Related Substances* (Ogata, K., Kinoshita, S., Tsunoda, T., and Aida, K., eds) pp. 125–156, Kodansha, Tokyo
21. Plönzig, J., and Auling, G. (1987) *Arch. Microbiol.* **146,** 396–401
22. Webley, D. M., Duff, R. B., and Anderson, G. (1962) *J. Gen. Microbiol.* **29,** 179–187
23. Willing, A., Follmann, H., and Auling, G. (1988) *Eur. J. Biochem.* **175,** 167–173
24. Griepenburg, U., Lassmann, G., and Auling, G. (1996) *Free Radical Res.* **24,** 473–481
25. Lunn, C. A., Kathju, S., Wallace, B. J., Kushner, S. R., and Pigiet, V. (1984) *J. Biol. Chem.* **259,** 10469–10474
26. Hoch, J. A. (1991) *Methods Enzymol.* **204,** 305–320
27. Sambrook, J., Fritsch, E. F., and Maniatis, T. (1989) *Molecular Cloning: A Laboratory Manual* 2nd Ed., Cold Spring Harbor Laboratory, Cold Spring Harbor, NY
28. Clarke, L., and Carbon, J. (1976) *Cell* **9,** 91–99
29. Bathe, B., Kalinowski, J., and Puhler, A. (1996) *Mol. Gen. Genet.* **252,** 255–265
30. Thelander, L., Sjöberg, B.-M., and Eriksson, S. (1978) *Methods Enzymol.* **51,** 227–237
31. Hellman, U. (1997) in *Protein Structure Analysis. Preparation, Characterization, and Microsequencing.* (Kamp, R. M., Choli-Papadopoulou, T., and Wittmann-Liebold, B., eds) pp. 97–104, Springer-Verlag, Heidelberg
32. Peterson, G. L. (1977) *Anal. Biochem.* **83,** 346–356
33. Bradford, M. M. (1976) *Anal. Biochem.* **72,** 248–254
34. Malumbres, M., Gil, J. A., and Martin, J. F. (1993) *Gene* **134,** 15–24
35. Moriya, S., Ogasawara, N., and Yoshikawa, H. (1985) *Nucl. Acids Res.* **13,** 2251–2265
36. Patek, M., Eikmanns, B. J., Patek, J., and Sahm, H. (1996) *Microbiology* **142,** 1297–1309
37. Jordan, A., Åslund, F., Pontis, E., Reichard, P., and Holmgren, A. (1997) *J. Biol. Chem.* **272,** 18044–18050
38. Jordan, A., Gibert, I., and Barbé, J. (1995) *Gene* **167,** 75–79
39. Eliasson, R., Pontis, E., Jordan, A., and Reichard, P. (1996) *J. Biol. Chem.* **271,** 26582–26587
40. Karlsson, M., Sahlin, M., and Sjöberg, B. M. (1992) *J. Biol. Chem.* **267,** 12622–12626
41. Atta, M., Nordlund, P., Åberg, A., Eklund, H., and Fontecave, M. (1992) *J. Biol. Chem.* **267,** 20682–20688
42. Rova, U., Goodtzova, K., Ingemarson, R., Behravan, G., Gräslund, A., and Thelander, L. (1995) *Biochemistry* **34,** 4267–4275
43. da Silva, F. J. J. R., and Williams, R. J. P. (1991) *The Biological Chemistry of the Elements. The Inorganic Chemistry of Life.* Clarendon Press, Oxford
44. Schmidt, M., Meier, B., and Parak, F. (1996) *J. Biol. Inorg. Chem.* **1,** 532–541
45. Boldt, Y. R., Whiting, A. K., Wagner, M. L., Sadowsky, M. J., Que, L., and Wackett, L. P. (1997) *Biochemistry* **36,** 2147–2153
46. Thompson, J. D., Higgins, D. G., and Gibson, T. J. (1994) *Nucleic Acids Res.* **22,** 4673–4680
47. Nordlund, P., and Eklund, H. (1993) *J. Mol. Biol.* **232,** 123–164
48. Yang, F. D., Curran, S. C., Li, L. S., Avarbock, D., Graf, J. D., Chua, M. M., Lui, G. Z., Salem, J., and Rubin, H. (1997), *J. Bacteriol.* **179,** 6408–6415
49. Kunst, F., *et al.* (1997) *Nature* **390,** 249–256

THE JOURNAL OF BIOLOGICAL CHEMISTRY
Vol. 270, No. 51, Issue of December 22, pp. 30392–30400, 1995

Printed in U.S.A.

The Mechanism and Substrate Specificity of the NADPH:Flavin Oxidoreductase from *Escherichia coli**

(Received for publication, July 26, 1995, and in revised form, October 6, 1995)

Franck Fieschi, Vincent Nivière, Christelle Frier, Jean-Luc Décout, and Marc Fontecave‡

From the Laboratoire d'Etudes Dynamiques et Structurales de la Sélectivité, URA 332, CNRS, Université Joseph Fourier, BP 53 X, 38041 Grenoble Cedex 9, France

The NAD(P)H:flavin oxidoreductase from *Escherichia coli*, Fre, is a monomer of 26.2 kDa that catalyzes the reduction of free flavins by NADPH or NADH. Overexpression in *E. coli* now allows the preparation of large amounts of pure protein. Structural requirements for recognition of flavins as substrates and not as cofactors were studied by steady-state kinetics with a variety of flavin analogs. The entire isoalloxazine ring was found to be the essential part of the flavin molecule for interaction with the polypeptide chain. Methyl groups at C-7 and C-8 of the isoalloxazine ring and the N-3 of riboflavin also play an important role in that interaction, whereas the ribityl chain of the riboflavin is not required for binding to the protein. On the other hand, the presence of the 2′-OH of the ribityl chain stimulates the NADPH-dependent reaction significantly. Moreover, a study of competitive inhibitors for both substrates demonstrated that Fre follows a sequential ordered mechanism in which NADPH binds first followed by riboflavin. Lumichrome, a very good inhibitor of Fre, may be used to inhibit flavin reductase in *E. coli* growing cells. As a consequence, it can enhance the antiproliferative effect of hydroxyurea, a cell-specific ribonucleotide reductase inactivator.

Flavins are well known as key prosthetic groups of a large number of redox enzymes named flavoproteins. More recently, protein-free flavins, riboflavin, FMN, or FAD, were also suggested to play, as electron transfer mediators, important biological functions, for example during ferric iron reduction (1–3), activation of ribonucleotide reductase (4, 5), bioluminescence (6, 7), and oxygen activation (8) (Scheme 1).

The reduction of free flavins by reduced pyridine nucleotides NADPH or NADH is not an efficient reaction. The kinetics is slow unless very high nonphysiological concentrations of both reactants are present in the reaction mixture (8). As a consequence, living organisms have evolved enzymes that catalyze the reduction of riboflavin, FMN, and FAD by NADPH and NADH and are called NAD(P)H:flavin oxidoreductases or flavin reductases. It is now well established that such enzymes are present in all microorganisms, including the luminous marine bacteria, and also in mammals (1). A recent study has shown that flavin reductase activities are present in erythrocytes and in various human tissues (liver, heart, kidney, and lung) (9).

In most cases, a single living organism contains multiple flavin reductases different in enzymatic nature and molecular mass. The luminous bacteria, *Vibrio harveyi*, contains at least three types of FMN reductases (10–14). In *Escherichia coli* at least two flavin reductases have been isolated. One, named Fre, is a 26.2-kDa enzyme using both NADH and NADPH as electron donors (4), whereas the other is the sulfite reductase, a 780-kDa enzyme using NADPH exclusively (15).

Still very little is known on the structure and the mechanisms of flavin reductases. No three-dimensional structure of such an enzyme is available yet, and only recently were the corresponding genes cloned, sequenced and overexpressed (9–12, 16–19). Only in the cases of *E. coli* and *V. harveyi* were the enzymes obtained in a pure form and characterized (4, 13, 15). In spite of such a limited information, it is nevertheless possible to propose a classification of flavin reductases in two groups.

In the first group, enzymes are flavoproteins, using a flavin prosthetic group for electron transfer from NAD(P)H to the flavin substrate. The prototype of this group is the NADPH-specific flavin reductase from *V. harveyi* (flavin reductase P) (13). It is a monomer of 26 kDa with a tightly bound FMN cofactor and has been recently crystallized. Preliminary x-ray diffraction analysis of the protein has been reported (20). The sulfite reductase of *E. coli* carries both FAD and FMN as cofactors and thus belongs to this group. This class of enzymes is characterized by ping-pong bisubstrate biproduct reaction mechanisms (14, 21).

In the second group, enzymes do not contain any prosthetic group. The visible spectrum of the protein gives no evidence for a chromophore and excludes the presence of flavins. When added, FMN or FAD does not bind tightly, and the enzyme thus should not be classified as a flavoprotein. The prototype of this group is Fre, the NAD(P)H:flavin oxidoreductase from *E. coli* (4). It consists of a single polypeptide chain of 233 amino acids, with a molecular mass of 26,212 Da. The NADH-specific FMN reductase enzyme from *V. harveyi* (flavin reductase D) belongs to this group and actually has significant amino acid sequence homology with Fre (48% identity) as well as a similar molecular weight (10). A number of ferric reductases, for example from *Rhodopseudomonas sphaeroïdes*, *Pseudomonas aeruginosa*, or *Neisseria gonorrhoeae*, which absolutely require free flavins for activity, probably also belong to this group (22, 23).

Such flavin reductases are interesting systems to study in that they utilize flavin only as a substrate and not as a coenzyme. It is thus important to understand how the polypeptide chain accomodates both reduced pyridine nucleotide and flavin to allow the electron transfer to proceed efficiently. It is also important to appreciate the structural basis for the difference in flavin recognition between flavoproteins and flavin reductases in order to delineate the different possible ways of interaction between the flavin and the polypeptide chain in relation with the function.

* The costs of publication of this article were defrayed in part by the payment of page charges. This article must therefore be hereby marked "*advertisement*" in accordance with 18 U.S.C. Section 1734 solely to indicate this fact.

‡ To whom correspondence should be addressed. Tel.: 33-76-51-44-67; Fax: 33-76-51-43-82.

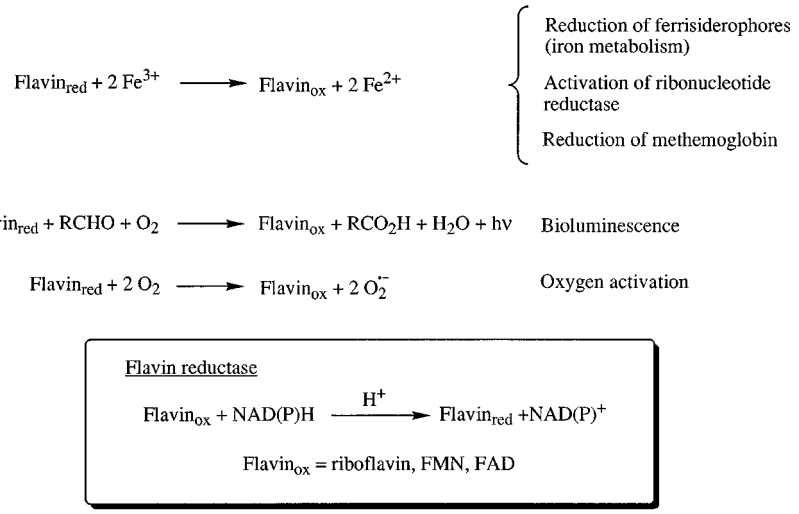

SCHEME 1. **Biological functions of free flavins.**

In this paper we have used a variety of flavin analogs (substrates and inhibitors) to probe the structural requirements of the flavin binding site of Fre, the NAD(P)H:flavin oxidoreductase from *E. coli*. Detailed kinetic studies of flavin reduction, in the presence of NADPH, show that the reductase follows a sequential mechanism, in agreement with the absence of a protein-bound mediator. Orders of substrate binding and product release have been determined. It is clearly established that the binding of the flavin occurs mainly through the isoalloxazine ring. In addition, lumichrome was found to be a very good inhibitor of the flavin reductase and to potentiate hydroxyurea as an inhibitor of ribonucleotide reductase and *E. coli* cell growth.

MATERIALS AND METHODS

Biochemical and Chemical Reagents—Restriction enzymes and DNA modifying enzymes were obtained from Eurogentec. Yeast extract and tryptone were from Biokar Diagnostics. Riboflavin **1**, lumiflavin **2**, alloxazine **9**, lumichrome **10**, AMP, NADH, NADPH, NADP$^+$, FMN, and FAD were obtained from Sigma. 3-Bromo-1,2-propanediol, 6-chlorouracil, 3,4-dimethylaniline, and *N*-methylaniline were purchased from Lancaster, and 2-bromoethanol and 3-bromopropanol were from Janssen. Other reagent grade chemicals were obtained either from Sigma, Aldrich, Interchim, Pharmacia Biotech Inc., or Bio-Rad.

Synthesis—Melting points were determined with a Buchi 530 apparatus and are reported uncorrected. The NMR spectra were recorded on Brucker spectrometers WP 80, AC 200, AC 250, or AM 300. Chemical shifts are reported in ppm relative to the residual signal of the solvent (^{1}H NMR: $CDCl_3$ 7.24 ppm, Me_2SO-d_6 2.49 ppm; ^{13}C NMR: $CDCl_3$ 77.0 ppm, Me_2SO-d_6 39.5 ppm). In D_2O, ^{1}H chemical shifts are measured relative to sodium 3-trimethylsilyl-propionate-2,2,3,3-d_4. Chemical shifts in ^{31}P-NMR are relative to the signal of orthophosphoric acid as external reference. The multiplicities are reported using the following abbreviations; br, broad; s, singlet; d, doublet; dd, doublet of doublet; t, triplet; m, multiplet. Mass spectra were recorded on a quadripolar Nermag R 1010 C spectrometer. Elemental analyses were obtained from Service Central de Microanalyses du CNRS (Lyon, France). Isoalloxazines **3–5** and **8** and riboflavin 5-oxide **13d** were synthesized according to the method of preparation of 10-alkylisoalloxazines and riboflavin described by Yoneda *et al.* (24). Due to the presence of hydroxyl function(s) in the side chain, the conditions of preparation of the 6-(*N*-substituted aniline)uracil intermediates were modified. The *N*-oxides were reduced with a different reagent, dithiothreitol.

*Synthesis of Isoalloxazines **3**, **4**, and **5***—The intermediates **11**, **12**, and **13** have been prepared with different side chains referred to as **a** for 2-hydroxyethyl (starting compound, 2-bromoethanol), **b** for 3-hydroxypropyl (starting compound, 3-bromopropanol), and **c** for 2,3-dihydroxypropyl (starting compound, 3-bromo-1, 2-propanediol).

For 3,4-dimethylaniline derivatives **11a**, **b**, and **c**, a mixture of 3,4-dimethylaniline (9.1 g; 75 mmol), triethylamine (15 cm^3), and bromoalcohol (25 mmol) was stirred at 110 °C for 5 h. After cooling and addition of dichloromethane (2 × 100 cm^3), the solution was washed with an aqueous Na_2CO_3 solution (10%; 40 cm^3). The aqueous layer was extracted with dichloromethane (200 cm^3). The combined organic extracts were dried over $MgSO_4$ and evaporated under reduced pressure. Compound **11a** was purified by chromatography on silica gel eluting with a dichloromethane/methanol mixture (98:2) (yield, 70% oil). ^{1}H NMR (80 MHz, $CDCl_3$) δ 7.02 (1H, d, J = 8 Hz, Ar*H*); 6.53 (1H, s, Ar*H*); 6.42 (1H, d, J = 8 Hz, Ar*H*); 3.75 (2H, t, CH_2-OH or CH_2-NH); 3.55 (2H, br s, N*H* and O*H*); 3.27 (2H, t, CH_2-NH or CH_2-OH); 2.25 (6H, s, 2 CH_3). ^{13}C NMR (20 MHz, $CDCl_3$) δ 146.5; 137.0; 130.1 (Ar*C*H); 125.5; 115.3 (Ar*C*H); 110.8 (Ar*C*H); 60.6 (*C*H_2-OH or *C*H_2-NH); 46.3 (*C*H_2-NH or *C*H_2-OH); 19.7 (*C*H_3); 18.4 (*C*H_3). MS (EI) *m/e* 165 (88, M$^+$); 164 (100, (M-1)$^+$); 105 (50, (M-NHCH_2CH_2OH)$^+$). Compound **11b** was obtained in a pure form after chromatography on silica gel eluting with a dichloromethane/methanol mixture (98:2) or after distillation under reduced pressure (yield, 80% oil). b.p. 107–110 °C (p = 0.1 mm Hg). ^{1}H NMR (300 MHz, $CDCl_3$) δ 6.98 (1H, d, J = 8 Hz, Ar*H*); 6.70 (1H, s, Ar*H*); 6.67 (1H, d, J = 8 Hz, Ar*H*); 3.82 (2H, m, CH_2-OH or CH_2-NH); 3.60 (1H, m, N*H* or O*H*); 3.40 (1H, br s, O*H* or N*H*); 3.32 (2H, m, CH_2-NH or CH_2-OH); 2.19 (3H, s, CH_3); 2.16 (3H, s, CH_3); 1.90 (2H, m, CH_2). ^{13}C NMR (75 MHz, $CDCl_3$) δ 146.3; 136.9; 130.0 (Ar*C*H); 125.4; 115.0 (Ar*C*H); 110.6 (Ar*C*H); 61.0 (*C*H_2-OH or *C*H_2-NH); 42.1 (*C*H_2-NH or *C*H_2-OH); 31.8 (*C*H_2); 19.8 (*C*H_3); 18.4 (*C*H_3). Compound **11c** was purified by washing of the crude residue with dichloromethane (yield, 64%). m.p. 100–102 °C. ^{1}H NMR (200 MHz, Me_2SO-d_6) δ 6.79 (1H, d, J = 8 Hz, Ar*H*); 6.38 (1H, d, J < 2 Hz, Ar*H*); 6.30 (1H, dd, J = 8 Hz, J < 2 Hz, Ar*H*); 4.90 (1H, t, O*H* or N*H*); 4.68 (1H, d, J = 4.7 Hz, CHO*H*); 4.52 (1H, t, J = 5.6 Hz, N*H* or O*H*); 3.60 (1H, br s, C*H*OH); 3.33 (2H, m, CH_2-OH or CH_2-NH); 2.90 (2H, m, CH_2-NH or CH_2-OH); 2.08 (3H, s, CH_3); 2.04 (3H, s, CH_3). ^{13}C NMR (50 MHz, Me_2SO-d_6) δ 147.1; 136.1; 130.0 (Ar*C*H); 123.0; 114.0 (Ar*C*H); 109.7 (Ar*C*H); 70.1 (*C*H-OH); 64.1 (*C*H_2-OH or *C*H_2-NH); 46.8 (*C*H_2-NH or *C*H_2-OH); 19.8 (*C*H_3); 18.4 (*C*H_3). MS (FAB [+], glycerol) *m/e* 196 (100, (M+1)$^+$); 121 (14, (M+1-CH_2CHOHCH_2OH)$^+$).

For 6-(*N*-substituted anilino)uracil derivatives **12a**, **b**, and **c**, compound **11** (21 mmol) was dissolved in water (**11c**, 30 cm^3) or in a 1:1 water/dioxane mixture (**11a**, 35 cm^3; **11b**, 40 cm^3). The solution was heated at reflux under argon and stirred during addition of 6-chlorouracil (1.03 g; 7 mmol). After 15 h of reflux and cooling, the pH was increased to 11 by addition of aqueous NaOH (10%). For **12a** and **b**, the resulting solution was extracted with dichloromethane (3 × 100 cm^3) to remove unreacted starting compound **11**. Aqueous HCl was added to the aqueous layer to reach pH 3. The resulting precipitate was collected by filtration, washed with water, and then crystallized from water. A second fraction of **12a** or **12b** was obtained after evaporation of the filtrates. The residue was stirred with methanol and filtered. Methanol was evaporated, and the residual solid was crystallized from water (yields: **12a**, 50%; **12b**, 87%). **12a**: m.p. 250–251 °C. ^{1}H NMR (200 MHz, Me_2SO-d_6) δ 10.35 (1H, br s, N*H*); 10.0 (1H, br s, N*H*); 7.20 (1H, d, J = 8 Hz, Ar*H*); 7.07 (1H, d, Ar*H*); 7.00 (1H, dd, J = 8 Hz, Ar*H*); 5.40 (1H, br s, O*H*); 4.03 (1H, s, 5-C*H*); 3.70 (2H, m, 3′-CH_2 or 1′-CH_2); 3.50 (2H, m, 1′-CH_2 or 3′-CH_2); 2.22 (6H, s, 2 CH_3). ^{13}C NMR (50 MHz, Me_2SO-d_6) δ 163.6 (C=O); 155.0 (C=O); 151.0 (C_6); 140.3; 137.9; 135.7; 130.6 (Ar*C*H); 128.5 (Ar*C*H); 124.9 (Ar*C*H); 77.4 (5-*C*H); 58.7 (3′-CH_2 or 1′-CH_2); 53.8 (1′-CH_2 or 3′-CH_2); 19.3 (*C*H_3); 18.9 (*C*H_3). MS (EI) *m/e* 275 (63, M$^+$); 274 (83, (M−1)$^+$). **12b**: m.p. 238–240 °C. ^{1}H NMR (300 MHz, Me_2SO-d_6) δ 10.30 (1H, br s, N*H*); 10.00 (1H, br s, N*H*); 7.21 (1H,

d, J = 8 Hz, Ar*H*); 7.04 (1H, d, J < 2 Hz, Ar*H*); 7.00 (1H, dd, J = 8 Hz, J < 2 Hz, Ar*H*); 4.80 (1H, br s, O*H*); 4.13 (1H, s, 5-C*H*); 3.65 (2H, t, 3′-CH_2 or 1′-CH_2); 3.44 (2H, t, 1′-CH_2 or 3′-CH_2); 2.49 (3H, s, CH_3); 2.22 (3H, s, CH_3); 1.60 (2H, m, 2′-CH_2). ^{13}C NMR (50 MHz, Me_2SO-d_6) δ 163.8 (C=O); 154.8 (C=O); 151.2 (C_6); 139.7; 138.1; 135.8; 130.7 (Ar*C*H); 128.5 (Ar*C*H); 124.8 (Ar*C*H); 77.2 (5-*C*H); 57.3 (3′-*C*H_2 or 1′-*C*H_2); 48.1 (1′-*C*H_2 or 3′-*C*H_2); 29.9 (2′-*C*H_2); 19.4 (*C*H_3); 19.0 (*C*H_3). MS (FAB [+], glycerol) *m/e* 290 (16, $(M+1)^+$); 232 (2, $(M+1\text{-}C_3H_6OH)^+$). **12c**: After the addition of aqueous NaOH (10%), the unreacted starting compound **11c** was removed by filtration and washed with water. Aqueous HCl was added to the filtrate to reach pH 3. Compound **12c** was collected by filtration and purified by crystallization from water (yield, 65%). m.p. 237–238 °C. ^{1}H NMR (200 MHz, Me_2SO-d_6) δ 10.35 (1H, br s, N*H*); 10.20 (1H, br s, N*H*); 7.20 (1H, d, J = 8 Hz, Ar*H*); 7.06 (1H, d, J < 2 Hz, Ar*H*); 7.04 (1H, dd, J = 8 Hz, J < 2 Hz, Ar*H*); 5.80 (1H, br s, 2′-CHO*H*); 4.87 (1H, t, 3′-CH_2O*H*); 3.95 (1H, s, 5-C*H*); 3.65 (3H, m, 1′-CH_2 and 2′-C*H*); 3.31 (2H, m, 3′-CH_2); 2.50 (3H, s, CH_3); 2.22 (3H, s, CH_3). ^{13}C NMR (50 MHz, Me_2SO-d_6) δ 163.7 (C=O); 155.7 (C=O); 151.0 (C_6); 140.8; 138.1; 135.8; 130.7 (Ar*C*H); 128.5 (Ar*C*H); 124.9 (Ar*C*H); 77.6 (5-*C*H); 69.7 (2′-*C*H$_2$ or 1′-*C*H$_2$); 62.9 (3′-*C*H$_2$ or 1′-*C*H$_2$); 55.1 (1′-*C*H$_2$ or 3′-*C*H$_2$); 19.4 (*C*H_3); 19.0 (*C*H_3). MS (FAB [+], glycerol) *m/e* 306 (100, $(M+1)^+$); 231 (2, $(M+1\text{-}CH_2CHOHCH_2OH)^+$).

For isoalloxazine 5-oxides **13a**, **b**, and **c**, sodium nitrite (1.7 g; 25 mmol) was added to a solution of compound **12** (5 mmol) in acetic acid in the dark. The mixture was stirred at room temperature for 3 h, and then water (6 cm^3) was added. The suspension was stirred again for 3 h, and the solvents were evaporated under reduced pressure. **13a:** The residue was washed with water and then with methanol to yield the compound (yield, 76%). m.p. 280–282 °C. ^{1}H NMR (200 MHz, Me_2SO-d_6) δ 11.00 (1H, s, N*H*); 8.07 (H, s, Ar*H*); 7.87 (H, s, Ar*H*); 4.87 (1H, m, CH_2O*H*); 4.63 (2H, t, 2′-CH_2 or 1′-CH_2); 3.76 (2H, m, 1′-CH_2 or 2′-CH_2); 2.38 (3H, s, CH_3); 2.34 (3H, s, CH_3). MS (DCI, NH_3 + isobutane) *m/e* 303 (30, M^+); 287 (100, $(M\text{-}16)^+$). **13b**: The residue was washed with water and then crystallized from ethanol (2 liters) (yield, 75%). m.p. 260 °C (dec.). ^{1}H NMR (300 MHz, Me_2SO-d_6) δ 11.00 (1H, br s, N*H*); 8.08 (1H, s, Ar*H*); 7.79 (1H, s, Ar*H*); 4.70 (1H, br s, CH_2O*H*); 3.58 (2H, t, 3′-CH_2 or 1′-CH_2); 3.55 (2H, m, 1′-CH_2 or 3′-CH_2); 2.45 (3H, s, CH_3); 2.38 (3H, s, CH_3); 1.89 (2H, m, 2′-CH_2). MS (FAB[+], NBA) *m/e* 317 (90, $(M+1)^+$); 301 (41, $(M+1\text{–}16)^+$). UV (H_2O, 50 mM Tris-HCl, pH 7.5), λ_{max} (ε): 460 nm (5280). **13c**: The residue was chromatographed on C18 reversed phase eluting with water. A crystallization from ethyl acetate yielded pure compound (yield, 82%). m.p. 239 °C (dec.). MS (FAB [+], NBA)[1] *m/e* 333 (100, $(M+1)^+$), 259 (48, $(M\text{-}CH_2CHOHCH_2OH)^+$).

For *isoalloxazines **3**, **4**, and **5**, an aqueous solution of dithiothreitol (1.4 g; 20 cm^3) was added to a suspension of *N*-oxide **13** (2 mmol) in ethanol (**13a** and **13b**, 500 cm^3; **13c**, 600 cm^3). The mixture was heated at reflux with stirring for 20 min under argon. The solvent was evaporated under reduced pressure, and the residue was crystallized from a water/ethanol mixture (50:50) for **3** and **4** (respective yields: 70% and 92%) and from ethyl acetate for **5** (yield, 76%). **3**: m.p. 275–277 °C. ^{1}H NMR (200 MHz, Me_2SO-d_6) δ 11.30 (1H, br s, N*H*); 7.67 (2H, s, 2 Ar*H*); 4.92 (1H, t, CH_2O*H*); 4.66 (2H, t, 2′-CH_2 or 1′-CH_2); 3.80 (2H, m, 1′-CH_2 or 2′-CH_2); 2.39 (6H, s, 2 CH_3). ^{13}C NMR (75 MHz, Me_2SO-d_6) δ 160.8; 158.7; 156.9; 149.5; 147.2; 137.1; 134.0; 132.3; 131.0 (Ar*C*H); 117.5 (Ar*C*H); 57.3 (2′-*C*H$_2$ or 1′-*C*H$_2$); 46.5 (1′-*C*H$_2$ or 2′-*C*H$_2$); 21.6 (*C*H_3); 20.5 (*C*H_3). MS (DCI, NH_3 + isobutane) *m/e* 287 (100, M^+); 243 (45, $(M\text{-}CH_2CH_2OH)^+$). **4**: m.p. 295 °C (dec.). ^{1}H NMR (200 MHz, Me_2SO-d_6) δ 11.30 (1H, br s, N*H*); 7.90 (1H, s, Ar*H*); 7.78 (1H, s, Ar*H*); 4.75 (1H, m, CH_2O*H*); 4.61 (2H, t, 3′-CH_2 or 1′-CH_2); 3.55 (2H, m, 1′-CH_2 or 3′-CH_2); 2.39 (6H, s, 2 CH_3); 1.89 (2H, m, 2′-CH_2). ^{13}C NMR (75 MHz, Me_2SO-d_6) δ 159.8; 155.5; 150.1; 146.4; 139.9; 135.7; 133.8; 131.0 (Ar*C*H); 130.7; 115.9 (Ar*C*H); 57.3 (3′-*C*H$_2$ or 1′-*C*H$_2$); 46.5 (1′-*C*H$_2$ or 3′-*C*H$_2$); 29.7 (2′-*C*H$_2$); 20.6 (*C*H_3); 18.7 (*C*H_3). MS (FAB [+], NBA) *m/e* 301 (84, $(M+1)^+$); 243 (35, $(M\text{-}(CH_2)_3OH)^+$). UV (H_2O, 50 mM Tris-HCl, pH 7.5), λ_{max} (ε): 444 nm (12200).

$C_{15}H_{16}N_4O_3$ (300.33)
Calculated: C 59.99 H 5.37 N 18.76
Found: C 59.57 H 5.38 N 18.76

5: m.p. 300 °C (dec.). ^{1}H NMR (200 MHz, Me_2SO-d_6) δ 11.29 (1H, s, N*H*); 8.02 (1H, s, Ar*H*); 7.87 (1H, s, Ar*H*); 4.94 (2H, m, 2 O*H*); 4.72 (2H, t, 3′-CH_2 or 1′-CH_2); 3.55 (2H, br s, 1′-CH_2 or 3′-CH_2); 2.41 (6H, s, 2 CH_3); 2.30 (1H, br s, 2′-C*H*).^{13}C NMR (50 MHz, Me_2SO-d_6) δ 161.0; 157.0; 151.1; 148.1; 137.5; 136.7; 134.9; 132.7 (Ar*C*H); 131.5; 117.9 (Ar*C*H); 69.2 (*C*H_2); 64.1 (*C*H_2); 48.8 (*C*H_2); 21.6 (*C*H_3); 19.5 (*C*H_3). MS (FAB [+], NBA) *m/e* 317 (65, $(M+1)^+$).

$C_{15}H_{16}N_4O_4$, $1H_2O$ (334.33)
Calculated: C 53.89 H, 5.43 N 16.76
Found: C 53.79 H, 5.24 N 16.48

*Compound **6** (H-Phosphonate)*—A suspension of compound **4** (50 mg; 0.16 mmol) was heated at 110 °C in pyridine (10 cm^3) under argon in the dark until dissolution. The solution was then allowed to cool at 30 °C. After the addition of phosphorous acid (54 mg; 0.66 mmol) and 2,4,6-triisopropylbenzenesulfonylchloride (48 mg; 0.16 mmol), the mixture was stirred for 15 h. Compound **6** was collected by filtration and washed with diethylether. It was chromatographed on C18 reversed phase eluting with water (yield, 76%). m.p. 200 °C (dec.). ^{31}P NMR (81 MHz, Me_2SO-d_6) δ 7.21 ($J_{P\text{-}H}$ = 657 Hz). ^{1}H NMR (200 MHz, Me_2SO-d_6) δ 11.27 (1H, s, N*H*); 8.58 (d, Py$^+$); 7.88 (1H, s, Ar*H*); 7.79 (1H, s, Ar*H*); 7.77 (m, Py$^+$); 7.39 (m, Py$^+$); 6.76 (1H, d, $J_{H\text{-}P}$ = 657 Hz, P*H*); 4.65 (2H, t, 3′-CH_2 or 1′-CH_2); 4.05 (2H, m, 1′-CH_2 or 3′-CH_2); 2.49 (3H, s, CH_3); 2.39 (3H, s, CH_3); 2.07 (2H, m, 2′-CH_2). MS (FAB [+], NBA) *m/e* 365 (54, $(M+1)^+$).

*N^3-Methylriboflavin **7***—Riboflavin (0.68 g; 1.81 mmol) was heated under argon atmosphere at 100 °C in *N*,*N*-dimethylformamide (250 cm^3) with stirring until dissolution. The resulting solution was allowed to cool at 40 °C before addition of K_2CO_3 (5 g; 36 mmol) and then at room temperature, before the addition of methyl iodide (20 cm^3). The mixture was stirred for 4.5 h and filtered to remove the mineral salts. The filtrate was evaporated to dryness under reduced pressure, and the residue was washed with diethylether and then dissolved in methanol. The insoluble material was removed by filtration, and the methanol was evaporated under reduced pressure. The residue was washed with water and then crystallized from methanol to afford **7** (yield, 65%). For biological experiments, a fraction of **7** was chromatographed on C18 reversed phase eluting with water/methanol mixtures. m.p. 272 °C (dec.), litt. (25) 275 °C (dec). ^{1}H NMR (300 MHz, Me_2SO-d_6) δ 7.94 (2H, s, 2 Ar*H*); 5.10 (1H, br s, O*H*); 4.98 (1H, m, C*H*); 4.90 (1H, br s, O*H*); 4.80 (1H, br d, O*H*); 4.63 (1H, m, C*H*); 4.50 (1H, br s, O*H*); 4.25 (1H, m, C*H*); 3.63 (2H, m, CH_2); 3.45 (2H, m, CH_2); 3.26 (3H, s, N-CH_3); 2.38 (3H, s, CH_3). ^{1}H NMR (200 MHz, D_2O) δ 8.0 (1H, s, Ar*H*); 7.94 (1H, s, Ar*H*); 3.45 (3H, s, N-CH_3); 2.59 (3H, s, CH_3); 2.48 (3H, s, CH_3). MS (FAB[+], NBA) *m/e* 391 (100, $(M+1)^+$).

*10-Methylisoalloxazine **8***—For 6-(*N*-methylanilino)uracil **14**, 6-chlorouracil (4.7 g; 32 mmol) was added with stirring to a solution of *N*-methylaniline (10.3 g; 96 mmol) in an ethanol/water mixture (2:1; 150 cm^3) heated at reflux under argon. The mixture was refluxed for 24 h and then cooled. A first fraction of **14**, which crystallized from the solution, was obtained by filtration. The filtrate was evaporated under reduced pressure, and the unreacted *N*-methylaniline was removed by coevaporation with water. The residue was washed with diethylether and then crystallized from an ethanol/water mixture (75:25) (yield, 63%). m.p. 287–289 °C. ^{1}H NMR (300 MHz, $CDCl_3$) δ 7.60 (1H, br s, N*H*); 7.50 (3H, m, 3 Ar*H*); 7.23 (2H, m, 2 Ar*H*); 7.00 (1H, br s, N*H*); 4.89 (1H, s, 5-H); 3.26 (3H, s, CH_3). For 10-methylisoalloxazine 5-oxide **15**, sodium nitrite was added (0.7 g; 10.1 mmol) to a solution of **14** (0.47 g; 2.34 mmol) in acetic acid (20 cm^3) in the dark. The resulting solution was stirred for 2 h at room temperature, and then water (40 cm^3) was added. The mixture was kept at 4 °C overnight. Compound **15** was collected by filtration and washed with water and then diethylether (yield, 87%). m.p. >300 °C, litt. (24) >360 °C. For 10-methylisoalloxazine **8**, a mixture of compound **15** (0.15 g; 0.64 mmol) and *N*,*N*-dimethylformamide (50 cm^3) was refluxed for 1 h under argon. The solvent was removed under reduced pressure, and the residue was washed with diethylether and then ethanol. It was crystallized from acetic acid. A second crystallization from acetic acid afforded pure compound **8** (yield, 66%). ^{1}H NMR (200 MHz, Me_2SO-d_6) δ 11.40 (1H, br s, N*H*); 8.12 (1H, d, Ar*H*); 7.94 (2H, m, 2 Ar*H*); 7.64 (1H, m, Ar*H*); 3.97 (3H, s, CH_3). MS (DCI, NH_3+isobutane) *m/e* 229 (100, $(M+1)^+$).

$C_{11}H_8N_4O_2$, 1/4 CH_3CO_2H (243.22)
Calculated: C 56.79 H 3.73 N 23.04
Found: C 56.60 H 3.66 N 23.10

*Riboflavin 5-Oxide **13d***—This compound was prepared according to the method described by Yoneda *et al.* (24). m.p. 225 °C (dec.), litt. (24) 225 °C (dec). ^{1}H NMR (200 MHz, Me_2SO-d_6) δ 11.00 (1H, br s, N*H*); 8.07 (1H, d, Ar*H*); 7.92 (1H, s, Ar*H*); 5.05 (1H, br s, CHO*H*); 4.83 (2H, m, 2 O*H*); 4.70 (2H, dd, 5′-CH_2 or 1′-CH_2); 4.45 (1H, br s, O*H*); 4.20 (1H, br s, O*H*); 3.60 (2H, br s, 2 C*H*OH); 4.54 (2H, d, 1′-CH_2 or 5′-CH_2); 2.38 (3H, s, CH_3); 2.26 (3H, s, CH_3). MS (FAB [−], glycerol) *m/e* 392 (34, $(M\text{-}1)^+$).

[1] The abbreviations used are: NBA, 3-nitrobenzylalcohol; IPTG, isopropyl β-D-thiogalactopyranoside.

UV (H_2O, 50 mM Tris-HCl, pH 7.5): λ_{max} (ϵ): 463 nm (5280).

Enzyme Assay—Flavin reductase activity was determined at room temperature from the decrease of the absorbance at 340 nm (ϵ_{340} = 6.22 mM^{-1} cm^{-1}) due to the oxidation of NADPH, using a Kontron Uvikon 930 spectrophotometer. Under standard conditions, the spectroscopic cuvette contained, in a final volume of 500 μl, 50 mM Tris-HCl, pH 7.5, and variable concentrations of NADPH or NADH and flavins. The reaction was initiated by adding 0.3 μg of enzyme except in the case of Fig. 3 where 0.5 μg was used. One unit of activity is defined as the amount catalyzing the oxidation of 1 nmol NADPH/min. The hydrophobic compounds lumichrome, alloxazine, and lumiflavin were dissolved in Me_2SO. For lumichrome and lumiflavin, stock solutions were prepared by a further 1:3 dilution with water (final Me_2SO concentration, 3.5 M), and in the enzymatic assays the final Me_2SO concentration was 87 mM. For alloxazine, the Me_2SO concentration in the assay was 350 mM. Me_2SO concentration up to 350 mM had no measurable effect on K_m and V_m values.

Construction of Plasmid pFN3 That Overexpresses Fre—Plasmid pEE1011 (16) contains the coding part of the flavin reductase gene, a 0.8-kilobase *Cla*I–*Bgl*II fragment cloned into the *Eco*RI and *Bam*HI sites of pUC18. In order to have an unique *Sal*I site located into the *fre* gene, the *Sal*I site of the polycloning site was removed as follows. Plasmid pEE1011 was cleaved with *Xba*I and *Pst*I and then incubated with the Klenow enzyme in the presence of dNTP. After ethanol precipitation, the generated blunt ends were religated and transformed into DH5α. The recombinant plasmids were analyzed with restriction enzymes. Plasmid pEE1014, which contains only one *Sal*I site located into the *fre* gene, was chosen for further studies. Plasmid pEE1014 was cleaved with *Eco*RI and *Hin*dIII and the 0.8-kilobase fragment containing the *fre* gene was ligated with pJF119EH (26), which was cleaved with *Eco*RI and *Hin*dIII. The resulting vector was named pFN3. This construction allowed the expression of the *fre* gene under the control of the IPTG-inducible *tac* promotor.

Overexpression and Purification of Fre—*E. coli* K12 carrying a pFN3 plasmid was grown at 37 °C in Luria-Bertani medium (9 × 500 ml of Luria-Bertani medium in a 1-liter Erlenmeyer flask) in the presence of 100 μg/ml ampicillin. Growth was monitored by following the absorbance at 600 nm. Induction of Fre recombinant protein was done by adding IPTG to a final concentration of 0.4 mM when the optical density of the solution was about 0.3. The cells were collected by centrifugation at the late exponential phase. Extraction of bacteria was performed by lysozyme digestion of the cell membrane and freeze-thawing cycles as described in (4). All of the following operations were carried out at 4 °C. After ultracentrifugation at 45,000 rpm during 90 min in a Beckman 60 Ti rotor, the supernatant was used as soluble extract for further purification. Soluble extract (~30 ml, ~1 g of protein) was treated with 30% (w/v) ammonium sulfate for 30 min and then centrifuged for 20 min at 14,000 × *g*. The supernatant was loaded onto a phenyl-Sepharose column (20 ml) previously equilibrated with 25 mM Tris-HCl, pH 7.5, 10% (v/v) glycerol, 30% (w/v) ammonium sulfate (buffer A). Proteins were eluted at a flow rate of 1 ml·min^{-1} with buffer A until the baseline was recovered. Then ammonium sulfate concentration in buffer A was changed to 5% (w/v), and a flow rate of 1 ml·min^{-1} was maintained. When the absorption at 280 nm reached again the baseline, flavin reductase activity was eluted with 25 mM Tris-HCl pH 7.5, 10% (v/v) glycerol (buffer B). Fractions containing flavin reductase activity were pooled and concentrated to 2 ml using a Diaflo cell equipped with a YM10 membrane. The concentrated enzyme solution was loaded onto a Superdex 75 column (120 ml) from Pharmacia previously equilibrated with buffer B. Proteins were eluted with buffer B at a flow rate of 0.8 ml·min^{-1}. Flavin reductase was eluted as a single well defined peak. Active fractions were pooled and stored at −80 °C.

E. coli Growth Inhibition by Hydroxyurea and Lumichrome—*E. coli* K12 was used as wild type strain. *E. coli* LS1312 (*fre::kan*) was derived by ΦP1 transduction of K12 as already described (15). 100 ml of M9 medium, supplemented with 0.4% glucose and 140 μM lumichrome when necessary, was inoculated at 1% with a preculture collected in the early exponential phase (OD_{650} = 0.1). Growth was monitored by following the absorbance at 650 nm. Hydroxyurea (crystalline, freshly dissolved in culture media) was added at the beginning of the exponential phase at an absorbance of about 0.05.

RESULTS

Overexpression and Purification of Recombinant Fre—Plasmid pJF119EH, a pKK223–3 derivative, is a broad host range plasmid that contains a polylinker sequence flanked on one side by the inducible *tac* promotor and on the other side by two strong transcriptional terminators (26). The gene for the *lac* repressor, *lacI*^{q}, was also present in this plasmid, and as a consequence, the plasmid can be utilized in strains lacking the repressor.

E. coli K12 was transformed by plasmid pFN3, which contains the *fre* gene inserted at the polylinker site of pJF119EH, and overexpression was tested in Luria-Bertani medium in the presence of IPTG. Overexpression was maximal when the cells were in the late log phase. The flavin reductase specific activity of *E. coli* K12 soluble extracts was around 50 units/mg of protein. Typically, extracts from *E. coli* K12 carrying pFN3 gave values of 5,000–7,500 units/mg after IPTG induction, thus showing a 100–150-fold overexpression of the enzyme. On the basis of a specific activity of 130,000 units/mg for the pure flavin reductase, it can be estimated that the overexpressed Fre enzyme represents 5% of the total soluble proteins. Extracts from *E. coli* K12 (pFN3) obtained in the absence of IPTG gave activity values of 300 units/mg, confirming the good control of pJF119EH derivative plasmids by the inducer. In addition, during growth, no significant loss of pFN3 in the presence or absence of IPTG has been noticed.

A two-step purification protocol, with a phenyl-Sepharose chromatography followed by gel filtration on Superdex 75, has been developed. From 4.5-liter cultures of *E. coli* K12 (pFN3) and 1-g protein extracts, 15–20 mg of about 90–95% pure flavin reductase, as judged by SDS-polyacrylamide gel electrophoresis, was obtained. The yield of the purification was 45%. The specific activity of the purified flavin reductase was 120,000 units/mg.

Mechanistic Studies of the Flavin Reductase—The experiments described here have been done under aerobic conditions when reduced flavins were rapidly reoxidized by oxygen. The reaction was monitored by following the disappearance of the absorbance of NAD(P)H at 340 nm. With this assay, we measured the dependence of the reaction on various flavins and on reduced pyridine nucleotides. For such a bisubstrate-biproduct reaction, mechanisms with respect to orders of substrate binding can be delineated by kinetic analysis. Double reciprocal plots of initial velocities *versus* substrate concentrations show intersecting patterns for the sequential mechanism and parallel patterns for the ping-pong mechanism (27). In Fig. 1, flavin reductase activity was determined as a function of NADPH concentration at several levels of riboflavin (Fig. 1*A*) and as a function of riboflavin concentration at several levels of NADPH (Fig. 1*B*). Initial velocities followed typical Michaelis-Menten kinetics because double reciprocal plots of the results show a series of lines. Moreover, a ping-pong mechanism can be excluded because the lines are intersecting each other at the same point to the left of the vertical axis. A sequential mechanism for flavin reductase is thus indicated. The equations representing the ordered sequential Bi Bi mechanism and the rapid equilibrium random sequential Bi Bi mechanism have identical functional dependence on both substrates. However the ordered mechanism may be experimentally distinguished from the random mechanism through inhibition studies (28).

When the enzyme activity was determined as a function of NADPH concentration in the absence or in the presence of three concentrations of AMP, a dead-end inhibitor, double reciprocal plots of values obtained reflected typical competitive inhibition kinetics (Fig. 2*A*). A rather large K_i value (0.5 mM) for AMP can be determined from these lines. On the other hand, patterns of noncompetitive inhibition was observed with respect to riboflavin (Fig. 2*B*).

Furthermore, lumichrome is both a strong competitive inhibitor of riboflavin with a K_i value of 0.5 μM (Fig. 3*A*) and an uncompetitive inhibitor of NADPH (Fig. 3*B*). All these data

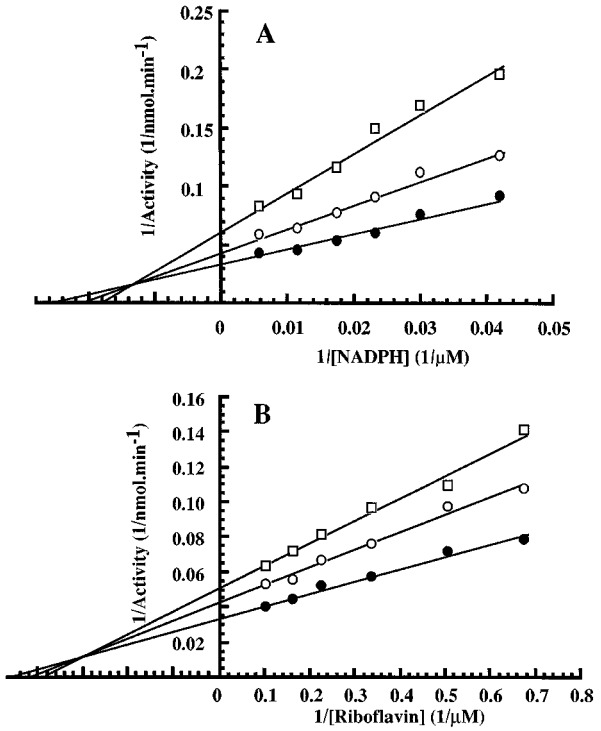

FIG. 1. *A*, flavin reductase activity as a function of NADPH concentration in the presence of 1 (□), 2 (○), or 4 μM (●) riboflavin. *B*, flavin reductase activity as a function of riboflavin concentration in the presence of 24 (□), 36 (○), or 60 μM (●) NADPH. The results are presented as double reciprocal plots with straight lines determined by a linear regression program.

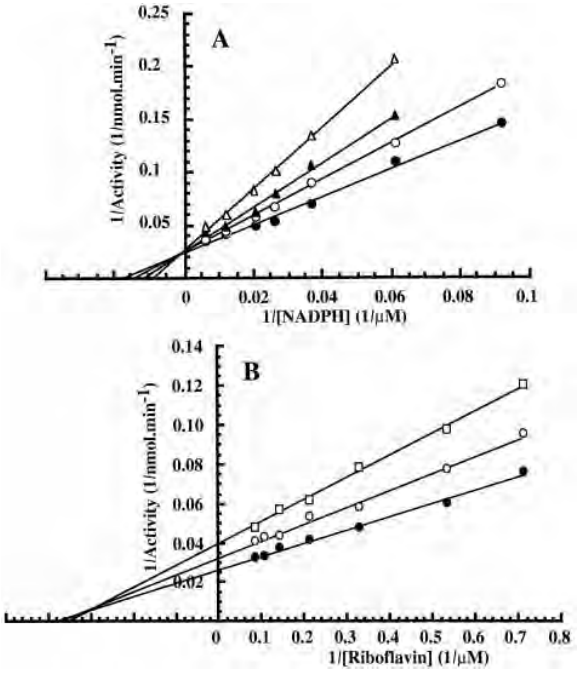

FIG. 2. *A*, AMP as a competitive inhibitor for NADPH. The enzyme activity was assayed as a function of NADPH concentrations using 15 μM riboflavin in the absence (●) or in the presence of 200 (○), 400 (▲), or 600 μM (△) AMP. *B*, AMP as a noncompetitive inhibitor for riboflavin. The enzyme activity was assayed as a function of riboflavin concentrations using 180 μM NADPH in the absence (●) or in the presence of 600 μM (○) or 2 mM (□) AMP.

support the conclusion that the flavin reductase has an ordered mechanism with NADPH binding first (28).

The kinetic mechanism of product release has been deter-

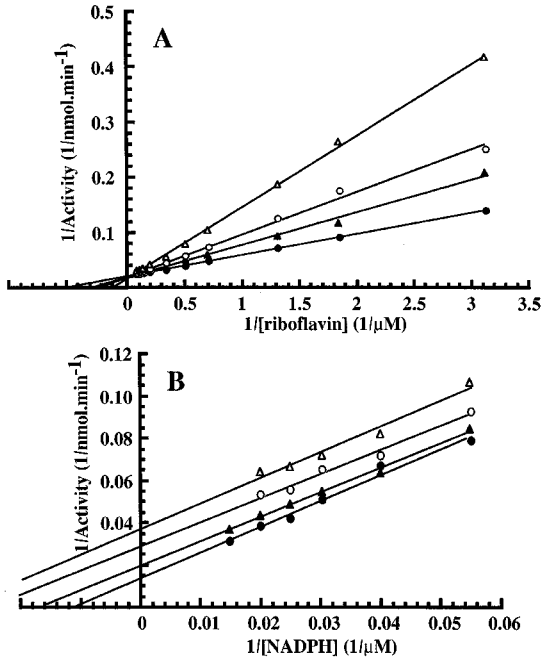

FIG. 3. *A*, lumichrome as a competitive inhibitor for riboflavin. The enzyme activity was assayed as a function of riboflavin concentrations using 180 μM NADPH in the absence (●) or in the presence of 0.5 (▲), 1 (○), or 2 μM (△) lumichrome. *B*, lumichrome as an uncompetitive inhibitor for NADPH. The enzyme activity was assayed as a function of NADPH concentrations using 15 μM riboflavin in the absence (●) or in the presence of 1 (▲), 3 (○), or 5 μM (△) lumichrome.

mined by studying inhibition by products (29). When NADPH concentration was varied with a fixed concentration of riboflavin, inhibition by $NADP^+$ was found to be competitive with respect to NADPH with a K_i value of 5 mM. When riboflavin was varied at a fixed NADPH concentration, $NADP^+$ appeared to inhibit noncompetitively (data not shown). This now suggests that the first product to be released is the reduced flavin, followed by $NADP^+$.

Flavin Substrate Specificity of the Flavin Reductase—Scheme 2 shows the structures of the various flavin analogs studied. Table I shows the kinetic data obtained with the flavin reductase. The apparent K_m values were determined in experiments where flavin reductase activity was measured as a function of a substrate concentration under saturating concentrations of the other substrate. The k_{cat} values were obtained from the experimental maximum velocity. In the presence of riboflavin, the K_m values for NADPH and NADH are 30 and 9 μM, respectively. A more detailed mathematical treatment of the steady-state initial rate measurements, developed by Dalziel (30) in the case of dehydrogenases with an ordered mechanism, was also applied to Fre. It clearly showed that K_m values for neither NADPH nor flavin have any simple physical significance as dissociation constants. However, some useful information can be obtained from this analysis. First, from the data of Fig. 1, treatment by the method of Dalziel yields K_m values for NADPH (30 μM) and riboflavin (1.9 μM) similar to those reported in Table I, which had been determined by varying the concentration of the flavin at a fixed high concentration of NAD(P)H. Thus the K_m values shown in Table I are approximately the same as those of the true kinetic constants. Second, the dissociation constant K_d value for NADPH can be obtained from the data of Fig. 1. We found that the K_d of NADPH is 61 μM, a value slightly different from the K_m of NADPH of 30 μM. That the K_m value of NADPH does not reflect the K_d value of NADPH is obvious from the linear dependence of K_m of NADPH with respect to k_{cat} as described in (30). We verified

that for the various flavins studied here (riboflavin and lumiflavin) k_{cat}/K_m of NADPH was a constant equal to the rate of binding of NADPH to the enzyme (1×10^8 M^{-1}·min^{-1}).

On the other hand, the theory shows that it is impossible to determine the K_d values for the flavin precisely. One has to rely on K_m values to analyze how changes in flavin structure affects the flavin-protein interaction. In a first approximation, we may consider that large variations in K_m values roughly reflect variations in flavin recognition by the enzyme when the substrates give k_{cat} values of the same order of magnitude.

As previously reported (4), the K_m values for riboflavin and FMN were in the 1–3 μM range with either NADPH or NADH. Riboflavin in both cases gave the highest k_{cat} value, but the differences between flavins were much greater with NADPH.

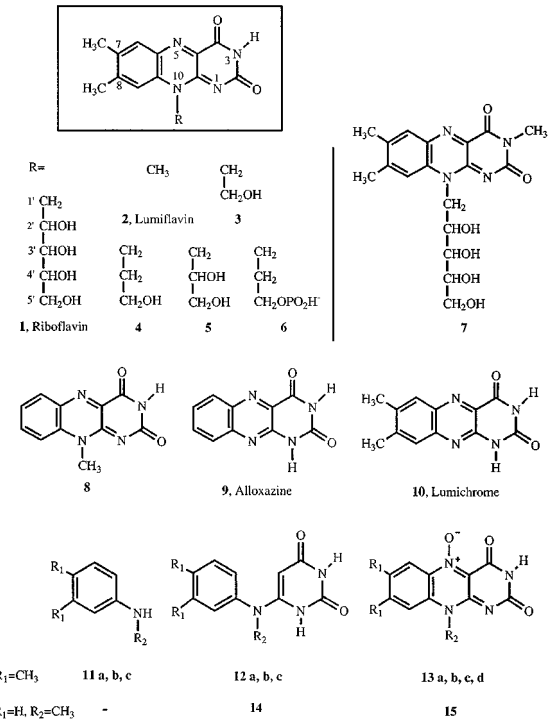

SCHEME 2. **Structure of the riboflavin derivatives and synthesis intermediates.** Compounds **11**, **12**, and **13** were prepared with different R_2 chains referred to as *a* for R_2 = CH_2-CH_2OH, *b* for R_2 = $(CH_2)_2$-CH_2OH, and *c* for R_2 = CH_2-CHOH-CH_2OH. Compound **13d** was with R_2 = 1′-deoxyribityl.

The presence of a terminal phosphate group on the ribityl chain, as in FMN, greatly altered the catalytic efficiency of the reaction. FAD gave no reaction with NADPH. Also the introduction of a H-phosphonate group led to a large decrease of the k_{cat} value (compare compounds **4** and **6**).

Lumiflavin, with a methyl group at N-10, was also a substrate with K_m values similar to those of natural substrates and k_{cat} larger than that of FMN. This now shows that the ribityl chain is not essential for recognition by the enzyme. Accordingly, ribitol has no inhibitory effect on the NADPH-riboflavin reductase activity even at 100 mM concentration. Moreover, as shown above, lumichrome, which lacks the ribityl chain, is a very efficient competitive inhibitor with respect to riboflavin.

On the other hand, k_{cat} but not K_m can be modulated significantly by chemical modification of the sugar chain. Charge, discussed above, is not the only parameter, because a large difference in k_{cat} is also observed between riboflavin and lumiflavin. In order to get deeper insight into such a modulation, we also tested a series of flavin derivatives in which the sugar moiety has been modified. Table I shows that the 2′-OH may play a role in the NADPH-dependent reaction because similar catalytic efficiency (k_{cat}/K_m) is found for riboflavin and compounds **3** and **5**, whereas the reaction was 2- and 5-fold less catalytically efficient with compound **4** and lumiflavin, respectively.

Because binding of the flavin molecule seems to occur mainly through the isoalloxazine ring, it is important to determine which sites of that ring are participating to the recognition of the molecule by the polypeptide chain.

First, methyl groups at C-7 and C-8 seem to play an important role in the binding because compound **8**, the lumiflavin derivative that lacks these methyls, is also a substrate but with a K_m value 10-fold larger than that for lumiflavin. Furthermore, alloxazine, the lumichrome analog lacking the methyl groups, is also an inhibitor but with a K_i value about 200-fold larger than that for lumichrome. The only compound in this study containing a modification at N-5 was riboflavin *N*-oxide (**13d**). The catalytic activity of the enzyme was not affected by the presence of the oxo group (data not shown).

Methylation at the N-3 of riboflavin (compound **7**) greatly decreased the catalytic efficiency of the reaction, due to both a large increase of the K_m value and a large decrease of the k_{cat} value. Because N-3 plays only a limited role in flavin redox chemistry, with redox potentials insensitive to N-3 alkylation,

TABLE I

Apparent kinetic constants for flavin derivatives with NADPH or with NADH (numbers in parentheses) as electron donor

The concentration of NADPH and NADH for the determination of the apparent K_m and k_{cat} values was 180 and 50 μM, respectively.

flavin derivative	Properties	K_m	k_{cat}[a]	k_{cat}/K_m[b]	K_i
		μM			μM
Riboflavin	Substrate	2.5 (1.3)	3144 (1834)	1257 (1410)	
FMN	substrate	2.2 (1.5)	161 (681)	73 (454)	
Lumichrome	inhibitor competitive/riboflavin				0.5
Alloxazine	inhibitor competitive/riboflavin				96
Ribitol	no inhibition up to 100 mM				
7	substrate	60	757	12	
8	substrate	25	777	31	
Lumiflavin	substrate	2.5 (1)	631 (1032)	252 (1032)	
4	substrate	2	1378	689	
3	substrate	1.6	2421	1513	
5	substrate	2.7	3300	1222	
6	substrate	4.7	300	64	

[a] k_{cat} is expressed in min^{-1}.
[b] k_{cat}/K_m is expressed in 10^6 min^{-1}·M^{-1}.

it appears that this site may be involved in flavin binding (31).

Finally, compounds **12**, which contain both the dimethylphenyl and pyrimidine moieties, were totally devoid of inhibitory properties (data not reported), showing that the binding site of the enzyme has a specific requirement for the whole isoalloxazine ring.

Inhibition of the Reactivation of Ribonucleotide Reductase by Lumichrome in Vivo—The small subunit of ribonucleotide reductase, named protein R2, contains a tyrosyl radical in its active form. Inactivation of the enzyme and thus inhibition of DNA synthesis can be achieved by hydroxyurea, which scavenges the radical and generates the inactive form, named metR2. Such a reaction is the basis of the utilization of hydroxyurea as an antiproliferative agent in clinics (5). We have previously shown that the flavin reductase in *E. coli* is involved in the repair of the ribonucleotide reductase activity by regenerating the radical and thus transforming metR2 to R2. The flavin reductase thus protects *E. coli* from radical scavengers such as hydroxyurea (15). The present discovery that lumichrome was a good inhibitor of the *E. coli* flavin reductase led us to investigate the potential of a combination hydroxyurea/lumichrome for inhibition of bacterial growth. The data are shown in Fig. 4.

When *E. coli* K12 cells were grown aerobically in M9 medium, the addition of 40 mM hydroxyurea at an OD_{650} of about 0.05 resulted, as expected, in a significant decrease of the growth rate. Lumichrome, instead, had no effect. When now a combination of 40 mM hydroxyurea and 140 μM lumichrome was added to the culture medium, bacteria stopped growing totally, indicating a strong and remarkable synergic effect of the combination.

Similar behavior was observed when the flavin reductase was inactivated genetically. Growth of an *E. coli* mutant strain, LS1312, lacking an active *fre* gene was fully inhibited by addition of 40 mM hydroxyurea alone, confirming the function of the flavin reductase during repair of hydroxyurea-treated *E. coli* cells. As far as growth inhibition by hydroxyurea is concerned, addition of lumichrome or inactivation of the *fre* gene gave similar phenotypes.

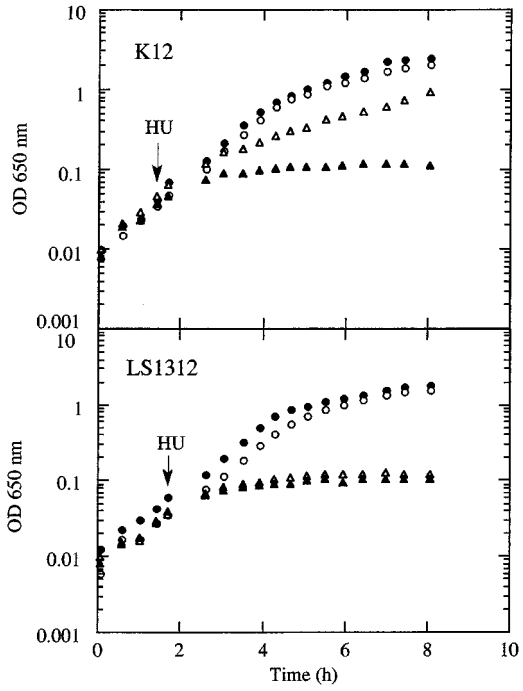

FIG. 4. **Inhibition of cell growth by lumichrome and hydroxyurea.** Growth of *E. coli* K12 or LS1312 under standard conditions (●) or in the presence of 140 μM lumichrome (○), 40 mM hydroxyurea (△), or 40 mM hydroxyurea and 140 μM lumichrome (▲).

DISCUSSION

In order to study the structure and the mechanism of the NAD(P)H:flavin oxidoreductase from *E. coli*, an overproducing strain of *E. coli* was obtained. The transformation of *E. coli* K12 by plasmid pFN3, which contains the *fre* gene under the control of the *tac* promotor, led, after IPTG induction, to a 100–150-fold overexpression of the enzyme. Such an overexpression allowed purification of the soluble enzyme by two chromatographic steps, phenyl-Sepharose and Superdex 75. Crystallization of such preparations is presently under investigation.

The NAD(P)H:flavin oxidoreductase from *E. coli* is the prototype of the class of flavin reductases, which do not contain any light-absorbing (flavins, metals) prosthetic group for mediating the electron transfer from reduced pyridine nucleotide to free oxidized flavin. The kinetic analysis of the enzymatic reaction demonstrated that the flavin reductase has an ordered mechanism (Scheme 3). The catalysis by the 26-kDa polypeptide chain is thus achieved by providing a site where both substrates bind and interact. NADPH binds first to the active site, followed by the flavin. After electron transfer, the first product to be released is the reduced flavin, followed by

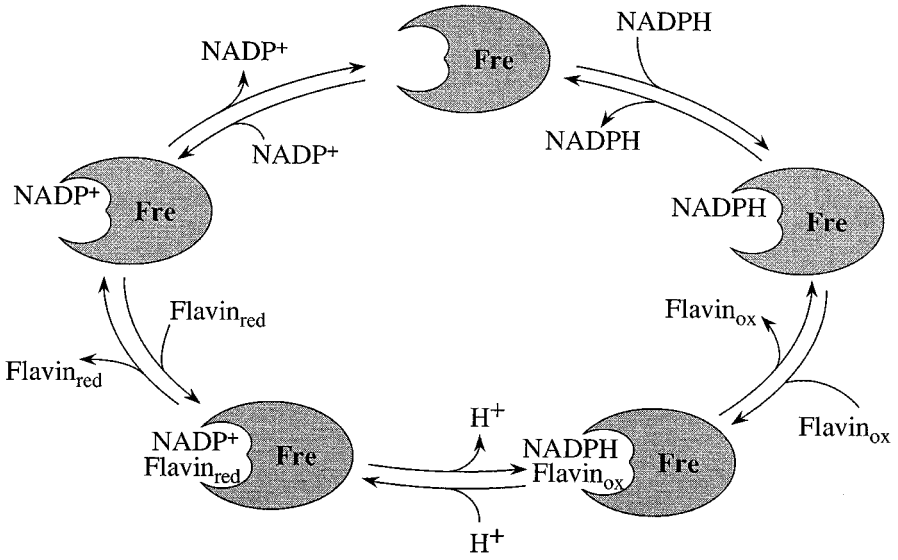

SCHEME 3. **Proposed reaction mechanism of the flavin reductase Fre.**

$NADP^+$. This is in full agreement with AMP and $NADP^+$ being competitive inhibitors with respect to NADPH and noncompetitive with respect to flavin and lumichrome being a competitive inhibitor with respect to flavin and noncompetitive with respect to NADPH. Similar results were obtained in the case of flavin reductase D, the NADH-dependent flavin reductase from *V. harveyi* (32).

The remarkable efficiency of lumichrome as an inhibitor of the flavin reductase *in vitro* (K_i = 500 nM) led us to test whether it may also affect the activity under *in vivo* conditions. As a matter of fact, lumichrome greatly potentiated the inhibitory effect of hydroxyurea, a specific inhibitor of ribonucleotide reductase, on the growth of *E. coli* K12 cells (33). This is a very interesting observation because (i) it is in good agreement with the observation that in bacteria, flavin reductase plays a crucial role in the activation of hydroxyurea-inactivated ribonucleotide reductase and (ii) it shows for the first time that the combination of an inhibitor of ribonucleotide reductase such as hydroxyurea and an inhibitor of flavin reductase might have potential applications for inhibition of DNA synthesis and for general antiproliferative activity. Whether such a strategy could be applied not only to microorganisms but also to human beings, for example for cancer treatment, is of course just speculative. It is important also to note that very recently hydroxyurea has received renewed attention in the context of AIDS research because it was found to greatly potentiate the anti-HIV effects of nucleoside analogs such as 2′,3′-dideoxyinosine (34).

The riboflavin substrate is composed of two distinct regions, a highly hydrophobic isoalloxazine ring and a ribityl side chain linked at N-10. The results reported in this study show that the binding to the polypeptide chain occurs mainly through the isoalloxazine ring as a whole. This is clear from the following observations: (i) lumichrome, an analog of isoalloxazine with no sugar chain, is a very good inhibitor with a low K_i (0.5 μM), indicating a strong binding to the enzyme, while ribitol has no inhibitory properties; (ii) the rigidity of the ring seems to be an important parameter, because compounds **12** have no inhibitory effects; (iii) similar K_m values were found for riboflavin, lumiflavin, and for flavin analogs with various side chains. The same K_m values were found for FMN, FAD, and compound **6** in spite of the presence of a negatively charged group and of the important size of the side chain. In addition, the methyl groups at position 7 and 8 (compare the K_i for lumichrome and alloxazine and the K_m values for lumiflavin and compound **8**) and nitrogen at position 3 (compare the K_m values for riboflavin and compound **7**) play an important role in the binding of the flavin ring.

In the absence of a three-dimensional structure for the enzyme and for a substrate-enzyme complex, it is just possible to use our data as a basis for predicting some structural characteristics of the flavin reductase involved in flavin recognition. The following analysis was based on the refined structures of flavoproteins. In flavodoxin (35) and ferredoxin-$NADP^+$ reductase (36), possessing FMN and FAD, respectively, as an integral component of the protein, aromatic residues (tryptophan or tyrosine) are involved in the recognition of the isoalloxazine ring through π-orbital overlaps. This seems to be a general strategy that may operate in the case of flavin reductase as well. On the other hand, in flavoproteins, extensive interactions also exist between the protein and the ribityl phosphate or ribityl phosphate-AMP and contribute to the overall affinity of the apoprotein for the cofactor significantly. These interactions seem to be very weak in the case of the flavin reductase, in agreement with the low specificity of the enzyme as well as its weak affinity for flavin substrates.

On the other hand, as shown in Table I, some of the hydroxyl groups of the ribityl chain seem to slightly contribute to decreasing the activation barrier for catalysis. Actually, in the presence of NADPH, the k_{cat} value for lumiflavin is about 5-fold lower than that for riboflavin. The magnitude of the effect of the ribityl group is most conveniently expressed as a decrease in the free energy of activation, calculated from the corresponding k_{cat} values according to $\Delta G = -RT\ln[k_{cat}(\text{ribo})/k_{cat}(\text{lumi})]$, where k_{cat}(ribo) and k_{cat}(lumi) refer to riboflavin and to lumiflavin. The decrease in the free energy of catalysis is about 0.9 kcal/mol, indicating a limited but nevertheless significant role of the sugar chain in enzyme catalysis. From the substrates tested here, it is possible to identify the important hydroxyl groups for this effect. The 4′- and 5′-OH do not contribute at all because compound **5** had the same k_{cat} value as riboflavin. On the other hand, 2′-OH and to a lesser extent 3′-OH may be involved in decreasing the activation barrier of the reaction (compounds **3** and **4**).

Catalysis seems to be also controlled by the charge of the side chain. Actually with NADPH, which contains a pyrophosphate and a phosphate group, as a reducing agent, the k_{cat} value for FMN, which contains one phosphate group, is 20-fold smaller than that for the neutral riboflavin, and moreover the enzyme is unable to catalyze the reduction of FAD, which contains a pyrophosphate group. Furthermore, weaker discrimination is obtained with NADH (riboflavin:FMN:FAD = 1:0.37:0.37), which has one phosphate group less than NADPH. The negative effect of a charge on the flavin substrate is also seen from the low activity of compound **6**.

In addition, it is interesting to note that, as an FMN reductase, Fre is more specific for NADH. This further supports the similarity to flavin reductase D, one of the flavin reductases from *V. harveyi*, which has been described, with FMN as the electron acceptor, to be specific for NADH (13).

Acknowledgments—We are grateful to Dr. Elisabeth Haggard-Ljungquist for the gift of plasmids pEE1001 and pEE1011. We acknowledge Dr. Jacques Covès for good advice in protein purification. We thank Dr. Alain Dolla for providing plasmid pJF119EH.

REFERENCES

1. Fontecave, M., Covès, J., and Pierre, J. L. (1994) *Biometals* **7,** 3–8
2. Hallé, F., and Meyer, J. M. (1992) *Eur. J. Biochem.* **209,** 621–627
3. Covès, J., and Fontecave, M. (1993) *Eur. J. Biochem.* **211,** 635–641
4. Fontecave, M., Eliasson, R., and Reichard, P. (1987) *J. Biol. Chem.* **262,** 12325–12331
5. Reichard, P. (1988) *Annu. Rev. Biochem.* **57,** 349–374
6. Yubisui, T., Matsuki, T., Tanishima, K., Takeshita, M., and Yoneyama, Y. (1977) *Biochem. Biophys. Res. Commun.* **76,** 174–182
7. Meighen, E. A. (1991) *Microbiol. Rev.* **55,** 123–142
8. Gaudu, P., Touati, D., Nivière, V., and Fontecave, M. (1994) *J. Biol. Chem.* **269,** 8182–8188
9. Quandt, K. S., and Hultquist, D. E. (1994) *Proc. Natl. Acad. Sci. U. S. A.* **91,** 9322–9326
10. Izumoto, Y., Mori, T., and Yamamoto, K. (1994) *Biochim. Biophys. Acta* **1185,** 243–246
11. Lei, B., Liu, M., Huang, S., and Tu, S. C. (1994) *J. Bacteriol.* **176,** 3552–3558
12. Zenno, S., and Saigo, K. (1994) *J. Bacteriol.* **176,** 3544–3551
13. Jablonski, E., and DeLuca, M. (1977) *Biochemistry* **16,** 2932–2936
14. Watanabe, H., and Hastings, J. W. (1982) *Mol. Cell. Biochem.* **44,** 181–187
15. Covès, J., Nivière, V., Eschenbrenner, M., and Fontecave, M. (1993) *J. Biol. Chem.* **268,** 18604–18609
16. Spyrou, G., Haggard Ljungquist, E., Krook, M., Jornvall, H., Nilsson, E., and Reichard, P. (1991) *J. Bacteriol.* **173,** 3673–3679
17. Zenno, S., Saigo, K., Kanoh, H., and Inouye, S. (1994) *J. Bacteriol.* **176,** 3536–3543
18. Inouye, S. (1994) *FEBS Lett.* **347,** 163–168
19. Chikuba, K., Yubisui, T., Shirabe, K., and Takeshita, M. (1994) *Biochem. Biophys. Res. Commun.* **198,** 1170–1176
20. Tanner, J., Lei, B., Liu, M., Tu, S. C., and Krause, K. L. (1994) *J. Mol. Biol.* **241,** 283–287
21. Eschenbrenner, M., Covès, J., and Fontecave, M. (1995) *J. Biol. Chem.* **270,** 20550–20555
22. Moody, M. D., and Dailey, H. A. (1985) *J. Bacteriol.* **163,** 1120–1125
23. Le Faou, A. E., and Morse, S. A. (1991) *Biometals* **4,** 126–131
24. Yoneda, F., Sakuma, Y., Ichiba, M., and Shinomura, K. (1976) *J. Am. Chem. Soc.* **98,** 830–835
25. Yoneda, F., Sakuma, Y., and Shinomura, K. (1978) *J. Chem. Soc. Perkin Trans. I* **1,** 348–351

26. Furste, J. P., Pansegrau, W., Frank, R., Blöcker, H., Scholz, P., Bagdasarian, M., and Lanka, E. (1986) *Gene (Amst.)* **48,** 119–131
27. Fromm, H. J. (1979) *Methods Enzymol.* **63,** 42–53
28. Fromm, H. J. (1979) *Methods Enzymol.* **63,** 467–486
29. Rudolph, F. B. (1983) in *Contemporary Enzyme Kinetics and Mechanism* (Purich, D. L, ed) pp. 207–232, Academic Press, New York
30. Dalziel, K. (1973) in *The Enzymes* (Boyer, P. D., ed), 3rd Ed., Vol. XI, pp. 2–59, Academic Press, New York
31. Hall, L. H., Bowers, M. L., and Durfor, C. N. (1987) *Biochemistry* **26,** 7401–7409
32. Nefsky, B., and DeLuca, M. (1982) *Arch. Biochem. Biophys.* **216,** 10–16
33. Sinha, N. K., and Snustad, D. P. (1972) *J. Bacteriol.* **112,** 1321–1334
34. Lori, F., Malykh, A., Cara, A., Sun, D., Weinstein, J. N., Lisziewicz, J., and Gallo, R. C. (1994) *Science* **266,** 801–805
35. Mayhew, S. G., and Tollin, G. (1992) in *Chemistry and Biochemistry of Flavoenzymes* (Muller, F., ed) Vol. III, pp. 389–426, CRC Press, Inc., Boca Raton, FL
36. Karplus, P. A., Daniels, M. J., and Herriott, J. R. (1991) *Science* **251,** 60–66

THE JOURNAL OF BIOLOGICAL CHEMISTRY
Vol. 275, No. 33, Issue of August 18, pp. 25365–25371, 2000

Printed in U.S.A.

The Active Form of the R2F Protein of Class Ib Ribonucleotide Reductase from *Corynebacterium ammoniagenes* Is a Diferric Protein*

Received for publication, March 31, 2000
Published, JBC Papers in Press, May 4, 2000, DOI 10.1074/jbc.M002751200

Yasmin Huque‡, Franck Fieschi§¶, Eduard Torrents‖, Isidre Gibert‖, Rolf Eliasson‡‡, Peter Reichard‡‡, Margareta Sahlin‡, and Britt-Marie Sjöberg‡ §§**

From the ‡Department of Molecular Biology, Arrhenius Laboratories F3, Stockholm University, S-10691 Sweden, the §Institut de Biologie Structurale, Laboratoire de Cristallographie Macromoléculaire, 41 rue Jules Horowitz, F-38027 Grenoble Cedex 1, France, the ‖Departament de Genètica i Microbiologia and Institut de Biologia Fonamental, Bacterial Molecular Genetics Group, Autonomous University of Barcelona, 08193 Bellaterra, Spain, and ‡‡Biokemi I, the Department of Medical Biochemistry and Biophysics, Karolinska Institutet, S-17177 Stockholm, Sweden

Corynebacterium ammoniagenes **contains a ribonucleotide reductase (RNR) of the class Ib type. The small subunit (R2F) of the enzyme has been proposed to contain a manganese center instead of the dinuclear iron center, which in other class I RNRs is adjacent to the essential tyrosyl radical. The *nrdF* gene of *C. ammoniagenes*, coding for the R2F component, was cloned in an inducible *Escherichia coli* expression vector and overproduced under three different conditions: in manganese-supplemented medium, in iron-supplemented medium, and in medium without addition of metal ions. A prominent typical tyrosyl radical EPR signal was observed in cells grown in rich medium. Iron-supplemented medium enhanced the amount of tyrosyl radical, whereas cells grown in manganese-supplemented medium had no such radical. In highly purified R2F protein, enzyme activity was found to correlate with tyrosyl radical content, which in turn correlated with iron content. Similar results were obtained for the R2F protein of *Salmonella typhimurium* class Ib RNR. The UV-visible spectrum of the *C. ammoniagenes* R2F radical has a sharp 408-nm band. Its EPR signal at g = 2.005 is identical to the signal of *S. typhimurium* R2F and has a doublet with a splitting of 0.9 millitesla (mT), with additional hyperfine splittings of 0.7 mT. According to X-band EPR at 77–95 K, the inactive manganese form of the *C. ammoniagenes* R2F has a coupled dinuclear Mn(II) center. Different attempts to chemically oxidize Mn-R2F showed no relation between oxidized manganese and tyrosyl radical formation. Collectively, these results demonstrate that enzymatically active *C. ammoniagenes* RNR is a generic class Ib enzyme, with a tyrosyl radical and a diferric metal cofactor.**

Deoxyribonucleotides are synthesized in all organisms from ribonucleotides, in a reaction catalyzed by the enzyme ribonucleotide reductase (RNR).[1] Common to all RNRs is that they proceed via a radical mechanism (1). However, based on amino acid sequence similarities and polypeptide compositions (2), as well as metal and radical cofactors, three well-characterized RNR classes (I–III) can be distinguished. Class I RNRs consist of two homodimeric components, the larger R1 protein and the smaller R2 protein. Protein R1 contains the active site, and protein R2 contains a stable tyrosyl radical in close proximity to a diferric center. Class II RNRs are monomeric or homodimeric proteins that bind and utilize a vitamin B_{12} cofactor (deoxyadenosine cobalamin). Class III RNRs consist of two proteins. The larger protein contains in its active form a stable glycyl radical close to the active site. The smaller protein generates this radical with the aid of a 4Fe-4S cluster and *S*-adenosylmethionine. The class I RNRs are further subdivided into class Ia and class Ib based on amino acid sequence similarities (3, 4), allosteric properties, and dependence on different physiological reductants (5). Among prokaryotes several different classes and subclasses of RNR may be encoded in the same genome. In class Ia RNRs, the R1 protein is encoded by the *nrdA* gene and the R2 protein by the *nrdB* gene (1). In class Ib RNRs, the *nrdE* gene codes for the R1E protein and the *nrdF* gene codes for the R2F protein (3–6).

The three-dimensional structures of proteins R1 and R2 of class Ia RNR from *Escherichia coli* are known (7, 8). Four carboxylate residues and two histidines ligate the di-iron site in protein R2. In the native, enzymatically competent form, the two ferric ions are bridged by a μ-oxo bridge and one of the carboxylates (7). The iron ligands and the stable tyrosyl radical residue are conserved among all class I sequences (1). Recently, the three-dimensional structure of the class Ib R2F protein from *Salmonella typhimurium* was solved (9). The ligand sphere is slightly different in *S. typhimurium* R2F as compared with *E. coli* R2.

In this study we characterize the radical and metal cofactor of enzymatically competent R2F protein of a class Ib RNR from *Corynebacterium ammoniagenes.* It has been suggested that R2F from *C. ammoniagenes* binds and is activated by manganese instead of iron, because manganese is needed for growth of the orga-

* This work was supported in part by the Swedish Cancer Foundation and the European Commission, Training and Mobility of Researchers, Iron-Oxygen Protein Network (ERBFMRXCT 980207) (to B.-M. S.), a grant from the Karolinska Institute (to P. R.), the Spanish Dirección General de Enseñanza Superior e Investigación Científica (PB97-0196), and partially by Fundació Maria Francesca de Roviralta, Spain. The costs of publication of this article were defrayed in part by the payment of page charges. This article must therefore be hereby marked "*advertisement*" in accordance with 18 U.S.C. Section 1734 solely to indicate this fact.

¶ Supported by the Human Frontier Science Project Organization.

** A recipient of a predoctoral fellowship from the Direcció General d'Universitats de la Generalitat de Catalunya and a short-term fellowship from the Federation of European Biochemical Societies.

§§ To whom correspondence should be addressed: Tel: 46-(0)8-164150; Fax: 46-(0)8-152350; E-mail: Britt-Marie.Sjoberg@molbio.su.se.

[1] The abbreviations used are: RNR, ribonucleotide reductase; apoR2(F), R2 proteins lacking a metal site; DTT, dithiothreitol; Fe-R2F, R2F protein reconstituted with iron; IPTG, isopropyl-1-thio-β-D-galactopyranoside; metR2(F), R2 protein with a metal site but lacking a tyrosyl radical; Mn-R2(F), R2 protein purified from bacteria grown in the presence of manganese or manganese-reconstituted apoR2; PCR, polymerase chain reaction; PAGE, polyacrylamide gel electrophoresis.

THE JOURNAL OF BIOLOGICAL CHEMISTRY
Vol. 274, No. 26, Issue of June 25, pp. 18252–18260, 1999

Printed in U.S.A.

The NAD(P)H:Flavin Oxidoreductase from *Escherichia coli*

EVIDENCE FOR A NEW MODE OF BINDING FOR REDUCED PYRIDINE NUCLEOTIDES*

(Received for publication, December 14, 1998, and in revised form, March 6, 1999)

Vincent Nivière‡§, Franck Fieschi¶, Jean-Luc Décout‡, and Marc Fontecave‡

From the ‡Laboratoire de Chimie et Biochimie des Centres Rédox Biologiques, DBMS-CEA/CNRS/Université J. Fourier, Batiment K, 17 Avenue des Martyrs, 38054 Grenoble, Cedex 9, France and ¶Institut de Biologie Structurale, CEA/CNRS/Université J. Fourier, 41 Avenue des Martyrs, 38027 Grenoble Cedex 1, France

The NAD(P)H:flavin oxidoreductase from *Escherichia coli*, named Fre, is a monomer of 26.2 kDa that catalyzes the reduction of free flavins using NADPH or NADH as electron donor. The enzyme does not contain any prosthetic group but accommodates both the reduced pyridine nucleotide and the flavin in a ternary complex prior to oxidoreduction. The specificity of the flavin reductase for the pyridine nucleotide was studied by steady-state kinetics using a variety of NADP analogs. Both the nicotinamide ring and the adenosine part of the substrate molecule have been found to be important for binding to the polypeptide chain. However, in the case of NADPH, the 2′-phosphate group destabilized almost completely the interaction with the adenosine moiety. Moreover, NADPH and NMNH are very good substrates for the flavin reductase, and we have shown that both these molecules bind to the enzyme almost exclusively by the nicotinamide ring. This provides evidence that the flavin reductase exhibits a unique mode for recognition of the reduced pyridine nucleotide. In addition, we have shown that the flavin reductase selectively transfers the pro-R hydrogen from the C-4 position of the nicotinamide ring and is therefore classified as an A-side-specific enzyme.

Flavin reductases are enzymes defined by their ability to catalyze the reduction of free flavins (riboflavin, FMN, or FAD) by using reduced pyridine nucleotides, NADPH, or NADH (1). The products of these enzyme activities, protein-free reduced flavins, were suggested to have important biological functions as electron transfer mediators, even though the real physiological significance of these mediators has so far not been fully appreciated. In fact, *in vitro*, free reduced flavins can reduce ferric complexes or iron proteins very efficiently, and it has been suggested that flavin reductases could play a key role in: iron metabolism (1, 2), activation of ribonucleotide reductase (3, 4), and reduction of methemoglobin (5, 6). There is also indirect evidence for their function in bioluminescence (7, 8) and oxygen reduction (9). Recently, flavin reductases have been found to be associated with oxygenases involved in the desulfurization process of fossil fuels (10) and antibiotic biosynthesis (11–13).

Up to now, two major classes of flavin reductases have been characterized. Class I enzymes do not contain any flavin prosthetic group and cannot be defined as flavoproteins (3, 14), whereas class II enzymes are canonical flavoproteins (15–17). These two classes also exhibit different enzymatic mechanisms for flavin reduction. Class I enzymes use a sequential mechanism (14), whereas class II use a Ping-Pong mechanism, as a consequence of having a redox cofactor bound to the polypeptide chain (17, 18).

The prototype for class I flavin reductases is an enzyme, named Fre,[1] which was initially discovered in *Escherichia coli* as a component of a multienzymatic system involved in the activation of ribonucleotide reductase, a key enzyme in DNA biosynthesis (3, 4). Fre consists of a single polypeptide chain of 233 amino acids, with a molecular mass of 26,212 Da (19). It uses an electron donor, which can be either NADPH or NADH, and riboflavin (Rf) is the best substrate (3, 14). Steady-state kinetic studies have shown that Fre functions through an ordered mechanism, with NADPH binding first and riboflavin being the second substrate (14). Product order release has also been determined, with reduced flavin being the first product to be released and $NADP^+$ the second (14).

Although Fre is not a flavoprotein, several lines of evidence suggested that Fre belongs to a large family of flavoenzymes of which spinach ferredoxin-$NADP^+$ reductase (FNR) is the structural prototype (20). Despite very low global sequence similarity, Fre contains a sequence motif of four amino acids, $R^{46}PFS^{49}$, similar to the $R^{93}LYS^{96}$ region of spinach FNR. In the FNR family, these conserved residues are involved in the interaction between the protein and the flavin isoalloxazine ring (20). In spinach FNR, Ser-96 has been proposed to make a hydrogen bond to the N-5 position of the FAD cofactor (20) and was found to be essential for activity (21). Site-directed mutagenesis experiments allowed us to demonstrate that Ser-49 of Fre (corresponding to Ser-96 of spinach FNR) is indeed involved in flavin binding, and that it is also essential for activity (22). These results were the first to support the structural relationship between Fre and the members of the FNR family.

This was further confirmed by characterization of reaction intermediates that are formed during the catalytic cycle of Fre (23). For the flavoenzymes of the FNR family, rapid kinetic studies have demonstrated the occurrence of two distinct intermediates species during the catalytic cycle, identified as charge transfer complexes between pyridine nucleotide and the flavin cofactor (24–26). Similarly, in the case of Fre, the same

* The costs of publication of this article were defrayed in part by the payment of page charges. This article must therefore be hereby marked "*advertisement*" in accordance with 18 U.S.C. Section 1734 solely to indicate this fact.

§ To whom correspondence should be addressed. Tel.: 33-4-76-88-91-09; Fax: 33-4-76-88-91-24; E-mail: niviere@cbcrb.ceng.cea.fr.

[1] The abbreviations used are: Fre, NAD(P)H:flavin oxidoreductase; FNR, ferredoxin-$NADP^+$ reductase; PDR, phthalate dioxygenase reductase; Rf, riboflavin; AMP, adenosine 5′-monophosphate; 2′,5′-ADP, 2′-phosphoadenosine 5′-phosphate; ADP-ribose, adenosine 5′-diphosphoribose; ATP-ribose, 2′-phosphoadenosine 5′-diphosphoribose; NMNH, β-nicotinamide mononucleotide reduced form; 3-acetyl-NADH, 3-acetylpyridine adenine dinucleotide reduced form; thio-NADH, thionicotinamide adenine dinucleotide reduced form; v_i, initial velocity; v_m, maximal velocity; $K_{m(app)}$, apparent Michaelis constant; e, enzyme concentration; ϕ_o, ϕ_A, ϕ_B, ϕ_{AB}, kinetic parameters defined by Dalziel (30).

THE JOURNAL OF BIOLOGICAL CHEMISTRY
Vol. 271, No. 28, Issue of July 12, pp. 16656–16661, 1996

Printed in U.S.A.

Is the NAD(P)H:Flavin Oxidoreductase from *Escherichia coli* a Member of the Ferredoxin-NADP$^+$ Reductase Family?

EVIDENCE FOR THE CATALYTIC ROLE OF SERINE 49 RESIDUE*

(Received for publication, February 6, 1996, and in revised form, March 26, 1996)

Vincent Nivière, Franck Fieschi, Jean-Luc Décout, and Marc Fontecave‡

From the Laboratoire d'Etudes Dynamiques et Structurales de la Sélectivité, UMR C5616, CNRS, Université Joseph Fourier, BP 53X, 38041 Grenoble Cedex 9, France

The NAD(P)H:flavin oxidoreductase from *Escherichia coli*, Fre, is a monomer of 26.1 kDa which catalyzes the reduction of free flavins by NADPH or NADH. The flavin reductase Fre is the prototype of a new class of flavin reductases able to transfer electrons with no prosthetic group. It has been suggested that the flavin reductase could belong to the ferredoxin-NADP$^+$ reductase (FNR) family, on the basis of limited sequence homologies. A sequence, conserved within the ferredoxin-NADP$^+$ reductase family and present in the flavin reductase, is important for recognition of the isoalloxazine ring. Within this sequence, we have mutated serine 49 of the flavin reductase into alanine or threonine. k_{cat} value of the S49A mutant was 35-fold lower than k_{cat} of the wild-type enzyme. Determination of real K_d values for NADPH and lumichrome, a flavin analog, showed that recognition of the flavin is strongly affected by the S49A mutation, whereas affinity for the nicotinamide cofactor is only weakly modified. This suggests that serine 49 is involved in the binding of the isoalloxazine ring. Moreover, the K_d value for 5-deazariboflavin, in which the N-5 position of the isoalloxazine ring has been changed to a carbon atom, is not affected by the serine 49 to alanine mutation. This is consistent with the concept that the N-5 position is the main site for serine 49-flavin interaction. In the ferredoxin-NADP$^+$ reductase family, the equivalent serine residue, which has been shown to be essential for activity, is hydrogen-bonded to the N-5 of the FAD cofactor. Taken together, these data provide the first experimental support to the hypothesis that the flavin reductase Fre may belong to the ferredoxin-NADP$^+$ reductase family.

The NAD(P)H:flavin oxidoreductase (or flavin reductase) from *Escherichia coli*, also named Fre, is the prototype of a group of enzymes, the flavin reductases, which are defined by their ability to catalyze the reduction of free flavins, riboflavin, flavin mononucleotide (FMN), or flavin adenine dinucleotide (FAD) by reduced pyridine nucleotides, NADPH or NADH (1, 2). The physiological importance of such enzymes is still unclear, even though there is indirect evidence for their function, at least in prokaryotes, in bioluminescence (3, 4), ferric reduction (5), oxygen reduction (6), antibiotic synthesis (7, 8), and activation of ribonucleotide reductase (1), the enzyme responsible for the biosynthesis of the deoxyribonucleotides. Flavin reductase activities have been detected also in eukaryotic cells (9), one of them is better know as a methemoglobin reductase (10).

Since very little is known as far as the structure and the catalytic mechanism of these enzymes are concerned, the flavin reductase from *E. coli* has become the focus of recent efforts to unravel its biochemistry. The corresponding *fre* gene has been cloned, sequenced, and overexpressed (11, 12). This now allows the preparation of large amounts of pure protein, in particular for crystallographic studies. The flavin reductase consists of a single polypeptide chain of 232 amino acids, with a molecular mass of 26,111 Da, and does not contain any prosthetic group. The catalysis of the reaction is made possible through the existence of a site which can probably accommodate both reduced pyridine nucleotide and the flavin substrate (1, 12).

In a previous work (12), we demonstrated, by using a variety of synthetic flavin analogs acting either as substrates or as inhibitors, that recognition of the flavin by the polypeptide chain occurs exclusively through the isoalloxazine ring. The 1′-ribityl side chain is not significantly involved in the flavin-protein interaction.

We undertook this work in order to identify important residues for substrate binding and catalysis and to understand the structural basis for the interaction between the polypeptide chain and the flavin. While this has been studied extensively in the case of flavoproteins, such an investigation on flavin reductases, which bind flavins less specifically and less tightly, should provide new insights to the general understanding of the protein-flavin interaction.

Thiol reagents, iodoacetate and *N*-ethylmaleimide, were found to inhibit the flavin reductase activity (1, 13). In a previous work, the three cysteine residues of the flavin reductase were mutated into serine residues, but none of these mutations affected activity. Cysteine residues are thus not involved in catalysis and substrate binding, but two of them, cysteine 5 and cysteine 214, were suggested to reside in close proximity to the flavin site (13).

On the basis of sequence homologies, it has been proposed that the flavin reductase could belong to a class of flavoprotein enzymes which includes ferredoxin-NADP$^+$ reductase (FNR),[1] cytochrome P-450 reductase, cytochrome b_5 reductase, nitrate reductase, phthalate dioxygenase reductase, sulfite reductase and others (14). Four members of this family have been structurally characterized (15–19).

Although the overall sequence similarity is below significance, the flavin reductase contains a sequence of four amino acids, starting from arginine 46 and ending with serine 49, which is present, highly conserved, within the whole FNR

* The costs of publication of this article were defrayed in part by the payment of page charges. This article must therefore be hereby marked "*advertisement*" in accordance with 18 U.S.C. Section 1734 solely to indicate this fact.

‡ To whom correspondence should be addressed. Tel.: 33-76-51-44-67; Fax: 33-76-51-43-82.

[1] The abbreviations used are: FNR, ferredoxin-NADP$^+$ reductase; Rf, riboflavin.

Vol. 179, No. 1, 1991
August 30, 1991

BIOCHEMICAL AND BIOPHYSICAL RESEARCH COMMUNICATIONS
Pages 442-448

INACTIVATION OF RIBONUCLEOTIDE REDUCTASE BY NITRIC OXIDE

Michel LEPOIVRE[1,*], Franck FIESCHI[1], Jacques COVES[2], Lars THELANDER[3], Marc FONTECAVE[2]

[1]URA CNRS 1116, Bât 432, Université Paris-Sud, 91405 ORSAY, France

[2]Laboratoire d'Etudes Dynamiques et Structurales de la Sélectivité, Université Joseph Fourier, BP 53X, 38041 GRENOBLE Cedex, France

[3]Department of Medical Biochemistry and Biophysics, University of Umeå, S-90187 Umeå, Sweden

Received June 20, 1991

SUMMARY: Ribonucleotide reductase has been demonstrated to be inhibited by NO synthase product(s). The experiments reported here show that nitric oxide generated from sodium nitroprusside, S-nitrosoglutathione and the sydnonimine SIN-1 inhibits ribonucleotide reductase activity present in cytosolic extracts of TA3 mammary tumor cells. Stable derivatives of these nitric oxide donors were either inactive or much less inhibitory. EPR experiments show that the tyrosyl radical of the small subunit of E. Coli or mammalian ribonucleotide reductase is efficiently scavenged by these NO donors.

The extracellular cytotoxicity of activated murine macrophages against tumor cells requires the expression of a NO synthase activity that is responsible for the controlled production of nitric oxide NO and citrulline from L-arginine (1-3). A specific pattern of metabolic perturbations in the tumor target cell characterizes this L-arginine-dependent cytotoxicity, including intracellular iron release, inhibition of mitochondrial functions and inhibition of DNA synthesis (4, for review). There is some evidence that nitric oxide itself is a mediator of the cytotoxic process since incubation of tumor cells with authentic NO gas reproduced the same pattern of biochemical alterations (2,3). The detection of nitrosyl-iron-sulfur complexes after induction of NO synthesis in cytotoxic macrophages (5,6) provided a molecular basis for the L-arginine-dependent mitochondrial dysfunction targeted at the level of electron-transfer 4Fe-4S enzymes (4). On the other hand, the mechanism of inhibition of DNA synthesis is unknown. Recent experiments have established that ribonucleotide reductase

*To whom correspondence should be addressed.

0006-291X/91 $1.50